



**Effect of Cation Substitutions in an Ionomer
Glass Composition on the Setting Reaction and
Properties of the Resulting Glass Ionomer
Cements**

By

Mitra A. M. P. Kashani

A thesis submitted to the University of Birmingham for the
degree of DOCTOR OF PHILOSOPHY

**School of Metallurgy and Materials
University of Birmingham
April 2013**

UNIVERSITY OF
BIRMINGHAM

University of Birmingham Research Archive

e-theses repository

This unpublished thesis/dissertation is copyright of the author and/or third parties. The intellectual property rights of the author or third parties in respect of this work are as defined by The Copyright Designs and Patents Act 1988 or as modified by any successor legislation.

Any use made of information contained in this thesis/dissertation must be in accordance with that legislation and must be properly acknowledged. Further distribution or reproduction in any format is prohibited without the permission of the copyright holder.

Abstract

This study investigated the effect of Ba²⁺ and Sr²⁺ substitutions for Ca²⁺ in an ionomer glass composition 4.5SiO₂-3Al₂O₃-1.5P₂O₅-3CaO-2CaF₂ on the setting reaction and properties of the resulting glass ionomer cements (GICs).

Experimental GICs (Ca-GIC, Ca-Sr-GIC and Ca-Ba-GIC) were characterized via various techniques: Diametral tensile strength, compressive strength, flexural strength, Vickers hardness and nano-indentation measurements were conducted at different time points during setting. Real time Fourier transform infrared (FTIR) spectroscopy was used to study the effect of the glass composition on cement setting reactions. A resistance to penetration method evaluated the cement setting time. Additionally, the wear resistance of the experimental GIC was measured by a ball-on-flat wear test. Furthermore, fluoride (F⁻) release and the antimicrobial behaviour of cements were investigated.

The compressive, diametral and flexural strength of the cements in which Ca²⁺ was substituted by Sr²⁺ and Ba²⁺ were both statistically significantly higher than the unsubstituted control at 1 hour after setting ($P < 0.001$). FTIR results confirmed that enhanced metal salt crosslinking occurred in the ion substituted materials, especially from 1 to 60 minutes. Therefore, it can be concluded that replacing Ca²⁺ with larger cations (Sr²⁺ and Ba²⁺) affects the setting reaction and resulting mechanical properties in the short term.

All three experimental GICs inhibited growth of *Streptococcus mutans* over a period of 48 hours. The F⁻ release analysis showed that there was less F⁻ release in artificial saliva (AS) than in deionized water over 40 days.

Summary

Glass ionomer cements (GICs) have retained their status as dental restorative materials in the market for the last 40 years. However, often their clinical application was limited by their low mechanical strength in comparison to amalgam restorative materials, and therefore much research was focused on the improvement of their clinical behavior. This resulted in the development of diverse restorative dental materials, with enhanced properties.

In the present study, strontium and barium cations were substituted for calcium in an experimental glass composition: $4.5\text{SiO}_2\text{-}3\text{Al}_2\text{O}_3\text{-}1.5\text{P}_2\text{O}_5\text{-}3\text{CaO}\text{-}2\text{CaF}_2$, and the influence on the glass structure and physical properties were studied. The aim of this study is a systematic investigation of the effect of cation substitution (strontium and barium) for calcium in the glass composition on the properties of the three resulting experimental GICs, namely; Ca-GIC, Ca-Sr-GIC and Ca-Ba-GIC, via a range of characterization techniques. Diametral tensile strength (DTS), compressive strength (CS), flexural strength (FS), Vickers hardness (HV) and nano-indentation measurements were conducted at different time points during setting. Real time Fourier transform infrared (FTIR) spectroscopy was used to study the effect of the glass composition on the setting reaction of cements. A resistance to penetration method was conducted to evaluate the cement setting time. Additionally, the wear resistance of the experimental GIC was measured by a ball-on-flat wear test. Furthermore, the fluoride (F^-) release and the antimicrobial behaviour of cements were investigated.

An acid-base neutralisation process occurred for all three cement compositions, following the chemical setting mechanism of cements by real time FTIR spectroscopy. Ca-Ba-GIC exhibited the highest metal salt development over 1 hour.

From the FTIR spectra the metal salt crosslinking development over 60 minutes for all experimental GICs was obtained. Ca-Ba-GIC with the biggest substituted ion radius exhibited 35% crosslinking followed by Ca-Sr-GIC and Ca-GIC with 24% and 14%, respectively.

Higher powder content resulted in a shorter setting time. A P/L ratio of 3:1 was ideal with the cements setting in approximately four minutes. The setting time for the experimental GICs with a P/L ratio of 3:1 was approximately half the setting time of the GICs with a P/L ratio of 2:1.

Compared to other commercially available GICs, the 3 experimental GICs used in this work exhibited less F^- release. The fluoride release analysis showed that there was less F^- release in artificial saliva (AS) than in deionized water over 40 days. After exposing the mature GICs to a fluoride source, the fluoride concentration was higher the longer the specimens were exposed to fluoride solution.

All three experimental GICs exhibited inhibition of growth of *Streptococcus mutans* (*S. mutans*) over a period of 48 hours.

Vickers hardness (HV) illustrated that all three GIC compositions increased in hardness over 30 days.

All experimental GICs exhibited an increase in strength over one month. Substitution of barium (ionic radius of 0.135 nm) for calcium (ionic radius of 0.1 nm) in the glass composition resulted in an increase of non-bridging oxygens (NBOs), and therefore in the formation of an expanded glass network that led to a weaker glass network with weak bond strengths. The development of NBOs in the glass component of the GIC had an effect on the diffusion process of ions upon acid attack. Ca-Ba-GIC exhibited the highest strength in all mechanical tests at 1 hour. This high strength is

correlated with the high degree of ionic crosslinking in the cement matrix, hence a high amount of cations diffused from the glass network into the aqueous phase.

From the obtained results in this project, it can be concluded that substituting bigger cations proportionally to smaller cations will have an effect on the setting reaction and the resulting mechanical properties of the cements.

Acknowledgments

First I would like to thank Dr Artemis Stamboulis for her time, support, motivation and discussions during my PhD. Danke schoen Artemis.

I owe appreciation to Dr Mark Webber and his staff for their support and assistance.

I am thankful to Dr Mike Jenkins during my PhD.

Also, thanks to Dr James Bowen for his time, personal, technical and scientific support.

I also would like to thank John Wedderburn, Dr Stephen Baker and Frank Bridgestone for their advice, scientific support and for their trouble.

I also would like to express my gratitude to Steve Hopkins, who assisted in correcting my grammar. Thank you for laughing at my language and correcting me.

I would like to express my appreciation to Dr Herbert Allen Kordan, who gave up his time to go through and discuss my work.

I also would like to express my deep gratitude for Dr Rachel Sammons, who gave up her time to discuss and dealt with the viva corrections.

I would like to thank my sister, Dr Mona Kashani, for her continuous support and dentistry knowledge during my PhD time.

Most of all I owe appreciation to my parents for all their support through out this work.

List of Figures

FIGURE 1-1: THE CONTINUUM OF WHITE RESTORATIVE DENTAL MATERIALS SINCE 1972.	3
FIGURE 1-2: POSSIBLE CEMENT COMPONENTS.	6
FIGURE 1-3: SCHEMATIC REPRESENTATION OF THE SETTING REACTION OF THE GLASS IONOMER CEMENTS (INFORMATION FROM CULBERTSON).	11
FIGURE 1-4: SCHEMATIC ILLUSTRATION OF COPOLYMERS WITH (A) ACRYLIC ACID AND ITACONIC ACID AND (B) ACRYLIC ACID AND MALEIC ACID [HOSODA].	16
FIGURE 1-5: SCHEMATIC ILLUSTRATION OF CALCIUM FLUORIDE IN THE GLASS STRUCTURE. F ⁻ CREATES NBFs, BY SURROGATING THE BOS AND C ²⁺ CREATES NBO BY CHARGE BALANCING THE AL ₃ O ₄ ⁻ [DE BARRA AND HILL].	20
FIGURE 2-1: TOOLS FOR THE PREPARATION OF GIC SAMPLES.	41
FIGURE 2-2: CHEMICAL STRUCTURES OF (A) LA-ALC AND (B) LA-ALC-F [LEI <i>ET AL.</i>].	44
FIGURE 2-3: MTT PLATE CONTAINING GIC SPECIMENS ALLOWING SAMPLING AT DIFFERENT TIME POINTS WITH 150 µL SUSPENSION. (T ₁ = 10 MIN, T ₂ = 3 HOURS, T ₃ = 24 HOURS, T ₄ = 48 HOURS; NC = NO CEMENT, CG = CA-GIC, SG = CA-SR-GIC, BG = CA-BA-GIC, C = CONTROL).	46
FIGURE 2-4: DILUTION SERIES (UP TO 10 ⁻⁶) FOLLOWED BY PLATE COUNT METHOD TO DETERMINE VIABLE MICROORGANISM NUMBERS ON THE AGAR PLATES FOR ALL THREE GIC COMPOSITIONS.	46
FIGURE 2-5: EXAMPLE OF AN INOCULATED CB AGAR PLATE, DIVIDED INTO THREE QUADRANTS AND CONTAINING THREE EVENLY SPACED DROPS OF DILUTED SAMPLES AT THE TIME POINT T ₁ = 10 MIN FOR ALL THREE GIC COMPOSITIONS.	47
FIGURE 2-6: DETERMINATION OF THE SETTING TIME THROUGH THE RESISTANCE OF PENETRATION METHOD; (A) MATERIAL IS NOT SET YET, (B) MATERIAL IS SET [JOHN F. MCCABE].	48
FIGURE 2-7: HUMIDITY CHAMBER USED TO MIMIC THE HUMAN ORAL CONDITION (ADVANCED HEALTHCARE LTD, KENT).	49

FIGURE 2-8: THE NEEDLE INDENTER AND THE METAL BLOCK IN THE HUMIDITY CHAMBER. (A) NEEDLE INDENTER IN THE HUMIDITY CHAMBER; (B) EMPTY METAL BLOCK MOULD; (C) METAL BLOCK MOULD COVERED WITH AN ALUMINUM FOIL AND FILLED WITH GIC; (D) NEEDLE INDENTER WITH A FLAT END.	50
FIGURE 2-9: VICKERS HARDNESS TESTING BY INDENT PENETRATION VIA A DIAMOND TIP (SEM IMAGE KASHANI).	51
FIGURE 2-10: SCANNING ELECTRON MICROSCOPE IMAGES OF (A) BERKOVICH PYRAMIDAL INDENTER AND (B) BERKOVICH INDENTATION INTO STEEL [JAMES BOWEN].	52
FIGURE 2-11: A TYPICAL SCHEMATIC DIAGRAM OF FORCE-DISPLACEMENT CURVE DURING NANO-INDENTATION EXPERIMENT [TOWLER <i>ET AL.</i>].	53
FIGURE 2-12: SCHEMATIC ILLUSTRATION OF THE UNLOADING PROCESS WITH THE PERMANENT DISPLACEMENT, CAUSED BY PLASTIC DEFORMATION [OLIVER AND PHARR].	54
FIGURE 2-13: RECIPROCATING (BALL-ON-FLAT) SLIDING TEST WAS CARRIED OUT IN DEIONIZED WATER USING A MACHINE WITH A MOTOR-DRIVEN STAGE THAT OSCILLATES A FLAT SPECIMEN BENEATH A FIXED BALL.	55
FIGURE 2-14: WEAR SCARS, RESULTING FROM THE SLIDING MOTIONS OF THE ALUMINA BALL.	56
FIGURE 2-15: (A) TEFLON SPLIT MOULD FOR COMPRESSIVE STRENGTH (CS) MEASUREMENTS CAPABLE OF HOLDING 4 SAMPLES; (B) TEFLON SPLIT MOULD FOR DIAMETRAL TENSILE STRENGTH (DTS) MEASUREMENTS CAPABLE OF HOLDING 8 SAMPLES; (C) TEFLON SPLIT MOULD FOR FLEXURAL STRENGTH (FS) MEASUREMENTS CAPABLE OF HOLDING 1 SAMPLE.	57
FIGURE 2-16: ILLUSTRATION OF THE AXIAL FORCE APPLIED THROUGH AN INSTRON ON THE CYLINDRICAL CS SPECIMEN. THERE IS NO SIGNIFICANT DIFFERENCE BETWEEN DTS AND CS TESTING OR PROCEDURE, BUT THE SHAPE AND APPLIED FORCES IN THE SPECIMEN DO DIFFER.	59
FIGURE 2-17: A UNIFORM TENSILE STRESS WAS APPLIED ONTO THE CIRCULAR DTS SPECIMEN WITH A CROSSHEAD SPEED OF 1 MM MIN ⁻¹ AND A 1 KN LOAD CELL.	60
FIGURE 2-18: THREE POINT BENDING TESTING.	60

FIGURE 3-1: FTIR SPECTRA OF THE THREE GLASS COMPOSITIONS (CA-GLASS (100%), CA-SR-GLASS (75%) AND CA-BA-GLASS (75%)).	62
FIGURE 3-2: FTIR SPECTRUM OF 40% AQUEOUS SOLUTION OF POLY (ACRYLIC ACID) ACID.	64
FIGURE 3-3: REAL TIME ATR-FTIR ANALYSIS OF THE SETTING REACTION OF CA-GIC AT DIFFERENT TIME INTERVALS FOR 60 MINUTES.	67
FIGURE 3-4: REAL TIME ATR-FTIR ANALYSIS OF THE SETTING REACTION OF CA-GIC AT 1 MINUTE, 30 MINUTES AND 60 MINUTES AFTER MIXING.	67
FIGURE 3-5: REAL TIME ATR-FTIR ANALYSIS OF CA-GIC AT DIFFERENT TIME INTERVALS FOR 60 MINUTES AT WAVE NUMBERS 2500 – 4000 CM^{-1} .	70
FIGURE 3-6: REAL TIME ATR-FTIR ANALYSIS OF THE SETTING REACTION OF CA-GIC AT 1 MINUTE, 30 MINUTES AND 60 MINUTES AFTER MIXING AT WAVE NUMBERS 2500 – 4000 CM^{-1} .	71
FIGURE 3-7: REAL TIME ATR-FTIR ANALYSIS OF CA-GIC AT DIFFERENT TIME INTERVALS FOR 60 MINUTES AT WAVE NUMBERS 700 – 1350 CM^{-1} .	72
FIGURE 3-8: REAL TIME ATR-FTIR ANALYSIS OF THE SETTING REACTION OF CA-GIC AT 1 MINUTE, 30 MINUTES AND 60 MINUTES AFTER MIXING AT WAVE NUMBERS 700 – 1350 CM^{-1} .	72
FIGURE 3-9: REAL TIME ATR-FTIR ANALYSIS OF CA-GIC AT DIFFERENT TIME INTERVALS FOR 60 MINUTES AT WAVE NUMBERS 1350 – 1750 CM^{-1} .	74
FIGURE 3-10: REAL TIME ATR-FTIR ANALYSIS OF THE SETTING REACTION OF CA-GIC AT 1 MINUTE, 30 MINUTES AND 60 MINUTES AFTER MIXING AT WAVE NUMBERS 1350 – 1750 CM^{-1} .	74
FIGURE 3-11: REAL TIME ATR-FTIR ANALYSIS OF THE SETTING REACTION CA-SR-GIC AT DIFFERENT TIME INTERVALS FOR 60 MINUTES.	76
FIGURE 3-12: REAL TIME ATR-FTIR ANALYSIS OF THE SETTING REACTION OF CA-SR-GIC AT 1 MINUTE, 30 MINUTES AND 60 MINUTES AFTER MIXING.	77
FIGURE 3-13: REAL TIME ATR-FTIR ANALYSIS OF CA-SR-GIC AT DIFFERENT TIME INTERVALS FOR 60 MINUTES AT WAVE NUMBERS 2500 – 4000 CM^{-1} .	79
FIGURE 3-14: REAL TIME ATR-FTIR ANALYSIS OF THE SETTING REACTION OF CA-SR-GIC AT 1 MINUTE, 30 MINUTES AND 60 MINUTES AFTER MIXING AT WAVE NUMBERS 2500 – 4000 CM^{-1} .	80

FIGURE 3-15: REAL TIME ATR-FTIR ANALYSIS OF CA-SR-GIC AT DIFFERENT TIME INTERVALS FOR 60 MINUTES AT WAVE NUMBERS 700 – 1350 CM ⁻¹ .	81
FIGURE 3-16: REAL TIME ATR-FTIR ANALYSIS OF THE SETTING REACTION OF CA-SR-GIC AT 1 MINUTE, 30 MINUTES AND 60 MINUTES AFTER MIXING AT WAVE NUMBERS 700 – 1350 CM ⁻¹ .	82
FIGURE 3-17: REAL TIME ATR-FTIR ANALYSIS OF CA-SR-GIC AT DIFFERENT TIME INTERVALS FOR 60 MINUTES AT WAVE NUMBERS 1350 – 1750 CM ⁻¹ .	83
FIGURE 3-18: REAL TIME ATR-FTIR ANALYSIS OF THE SETTING REACTION OF CA-SR-GIC AT 1 MINUTE, 30 MINUTES AND 60 MINUTES AFTER MIXING AT WAVE NUMBERS 1350 – 1750 CM ⁻¹ .	84
FIGURE 3-19: REAL TIME ATR-FTIR ANALYSIS OF THE SETTING REACTION OF CA-BA-GIC AT DIFFERENT TIME INTERVALS FOR 60 MINUTES.	86
FIGURE 3-20: REAL TIME ATR-FTIR ANALYSIS OF THE SETTING REACTION OF CA-BA-GIC AT 1 MINUTE, 30 MINUTES AND 60 MINUTES AFTER MIXING.	87
FIGURE 3-21: REAL TIME ATR-FTIR ANALYSIS OF CA-BA-GIC AT DIFFERENT TIME INTERVALS FOR 60 MINUTES AT WAVE NUMBERS 2500 – 4000 CM ⁻¹ .	89
FIGURE 3-22: REAL TIME ATR-FTIR ANALYSIS OF THE SETTING REACTION OF CA-BA-GIC AT 1 MINUTE, 30 MINUTES AND 60 MINUTES AFTER MIXING AT WAVE NUMBERS 2500 – 4000 CM ⁻¹ .	90
FIGURE 3-23: REAL TIME ATR-FTIR ANALYSIS OF CA-BA-GIC AT DIFFERENT TIME INTERVALS FOR 60 MINUTES AT WAVE NUMBERS 700 – 1350 CM ⁻¹ .	90
FIGURE 3-24: REAL TIME ATR-FTIR ANALYSIS OF THE SETTING REACTION OF CA-BA-GIC AT 1 MINUTE, 30 MINUTES AND 60 MINUTES AFTER MIXING AT WAVE NUMBERS 700 – 1350 CM ⁻¹ .	91
FIGURE 3-25: REAL TIME ATR-FTIR ANALYSIS OF THE SETTING REACTION OF CA-BA-GIC AT DIFFERENT TIME INTERVALS FOR 60 MINUTES AT WAVE NUMBERS 1350 – 1750 CM ⁻¹ .	93
FIGURE 3-26: REAL TIME ATR-FTIR ANALYSIS OF THE SETTING REACTION OF CA-BA-GIC AT 1 MINUTE, 30 MINUTES AND 60 MINUTES AFTER MIXING AT WAVE NUMBERS 1350 – 1750 CM ⁻¹ .	94
FIGURE 3-27: CUMULATIVE FLUORIDE RELEASE IN DEIONIZED WATER AT DIFFERENT TIME INTERVALS OVER 40 DAYS (($P_{CA-GIC TO CA-SR-GIC} = 0.46$), ($P_{CA-GIC TO CA-BA-GIC} < 0.001$) AND ($P_{CA-SR-GIC TO CA-BA-GIC} < 0.001$)).	96

FIGURE 3-28: CUMULATIVE FLUORIDE RELEASE IN ARTIFICIAL SALIVA AT DIFFERENT TIME INTERVALS OVER 40 DAYS (($P_{CA-GIC TO CA-SR-GIC} = 0.08$), ($P_{CA-GIC TO CA-BA-GIC} = 0.09$) AND ($P_{CA-SR-GIC TO CA-BA-GIC} < 0.001$)).	96
FIGURE 3-29: CUMULATIVE FLUORIDE RELEASE IN DEIONIZED WATER FROM A MATURE CA-GIC AFTER EXPOSURE TO A FLUORIDE CONTAINING MOUTHWASH AT DIFFERENT TIME INTERVALS OVER 24 HOURS (P VALUES ARE SHOWN IN TABLE 3-7).	98
FIGURE 3-30: CUMULATIVE FLUORIDE RELEASE IN DEIONIZED WATER FROM A MATURE CA-SR-GIC AFTER EXPOSURE TO A FLUORIDE CONTAINING MOUTHWASH AT DIFFERENT TIME INTERVALS OVER 24 HOURS (P VALUES ARE SHOWN IN TABLE 3-7).	99
FIGURE 3-31: CUMULATIVE FLUORIDE RELEASE IN DEIONIZED WATER FROM A MATURE CA-BA-GIC AFTER EXPOSURE TO A FLUORIDE CONTAINING MOUTHWASH AT DIFFERENT TIME INTERVALS OVER 24 HOURS (P VALUES ARE SHOWN IN TABLE 3-7).	99
FIGURE 3-32: CUMULATIVE FLUORIDE RELEASE IN AS FROM A MATURE CA-GIC AFTER EXPOSURE TO A FLUORIDE CONTAINING MOUTHWASH AT DIFFERENT TIME INTERVALS OVER 24 HOURS (P VALUES ARE SHOWN IN TABLE 3-7).	100
FIGURE 3-33: CUMULATIVE FLUORIDE RELEASE IN AS FROM A MATURE CA-SR-GIC AFTER EXPOSURE TO A FLUORIDE CONTAINING MOUTHWASH AT DIFFERENT TIME INTERVALS OVER 24 HOURS (P VALUES ARE SHOWN IN TABLE 3-7).	100
FIGURE 3-34: CUMULATIVE FLUORIDE RELEASE IN AS FROM A MATURE CA-BA-GIC AFTER EXPOSURE TO A FLUORIDE CONTAINING MOUTHWASH AT DIFFERENT TIME INTERVALS OVER 24 HOURS (P VALUES ARE SHOWN IN TABLE 3-7).	101
FIGURE 3-35: THE AVERAGE NUMBER OF VIABLE BACTERIA (CFU PER ML) FOR ALL THREE GIC COMPOSITIONS AND ONE CEMENT FREE SAMPLE (AS CONTROL) AT 4 DIFFERENT TIME POINTS. ASTERISKS INDICATE VALUES STATISTICALLY SIGNIFICANTLY DIFFERENT TO THE CEMENT FREE CONTROL (P VALUES ARE SHOWN IN TABLE 3-8).	102
FIGURE 3-36: A COMPARISON OF SETTING TIME AT DIFFERENT P/L RATIOS (P VALUES ARE SHOWN IN TABLE 3-10).	104

FIGURE 3-37: MEAN MICRO-HV AND STANDARD DEVIATION OF THE EXPERIMENTAL GIC ($P_{1\text{HOUR}} \& P_{1\text{MONTH}} > 0.01$).	105
FIGURE 3-38: MEAN NANO-INDENTATION AND STANDARD DEVIATION OF THE THREE EXPERIMENTAL GICS (P VALUES ARE SHOWN IN TABLE 3-11).	106
FIGURE 3-39: MEAN REDUCED MODULUS CALCULATION FROM THE NANO-INDENTATION AND STANDARD DEVIATION OF THE THREE EXPERIMENTAL GICS (P VALUES ARE SHOWN IN TABLE 3-11).	108
FIGURE 3-40: FORCE-DISPLACEMENT CURVE OF THE THREE GIC COMPOSITIONS USING A BERKOVICH INDENTER.	108
FIGURE 3-41: CREEP RESPONSE AT A MAXIMUM LOAD OF 300 NM.	109
FIGURE 3-42: WEAR RESULTS OF THE THREE GICS COMPOSITIONS (P VALUES ARE SHOWN IN TABLE 3-12).	110
FIGURE 3-43: MEAN COMPRESSIVE STRENGTH OF SR AND BA CONTAINING GICS WITH P/L=3:1 AT 1 HOUR, 1 DAY, 1 WEEK AND 1 MONTH AGEING TIME (P VALUES ARE SHOWN IN TABLE 3-13).	111
FIGURE 3-44: MEAN COMPRESSIVE STRENGTH OF CA, SR AND BA CONTAINING GICS WITH P/L=2:1 AT 1 HOUR, 1 DAY, 1 WEEK AND 1 MONTH AGEING TIME (P VALUES ARE SHOWN IN TABLE 3-13).	112
FIGURE 3-45: MEAN DIAMETRAL TENSILE STRENGTH OF SR AND BA CONTAINING GICS WITH P/L=3:1 AT 1 HOUR, 1 DAY, 1 WEEK AND 1 MONTH AGEING TIME (P VALUES ARE SHOWN IN TABLE 3-14).	113
FIGURE 3-46: MEAN DIAMETRAL TENSILE STRENGTH OF CA CONTAINING GICS WITH P/L=2:1 AT 1 HOUR, 1 DAY, 1 WEEK AND 1 MONTH AGEING TIME.	115
FIGURE 3-47: MEAN FLEXURAL STRENGTH OF SR AND BA CONTAINING GICS WITH P/L=3:1 AT 1 HOUR, 1 DAY, 1 WEEK AND 1 MONTH AGEING TIME (P ARE SHOWN IN TABLE 3-15).	116
FIGURE 3-48: MEAN FLEXURAL STRENGTH OF CA CONTAINING GICS WITH P/L=2:1 AT 1 HOUR, 1 DAY, 1 WEEK AND 1 MONTH AGEING TIME.	116

FIGURE 3-49: MEAN MODULUS OF ELASTICITY FROM COMPRESSIVE STRENGTH OF SR AND BA CONTAINING GICS WITH P/L=3:1 AT 1 HOUR, 1 DAY, 1 WEEK AND 1 MONTH AGEING TIME (<i>P</i> VALUES ARE SHOWN IN TABLE 3-16).	118
FIGURE 3-50: MEAN MODULUS OF ELASTICITY FROM COMPRESSIVE STRENGTH OF CA, SR AND BA CONTAINING GICS WITH P/L=2:1 AT 1 HOUR, 1 DAY, 1 WEEK AND 1 MONTH AGEING TIME (<i>P</i> IS SHOWN IN TABLE 3-16).	119
FIGURE 3-51: MEAN MODULUS OF ELASTICITY FROM DIAMETRAL TENSILE STRENGTH OF SR AND BA CONTAINING GICS WITH P/L=3:1 AT 1 HOUR, 1 DAY, 1 WEEK AND 1 MONTH AGEING TIME (<i>P</i> IS SHOWN IN TABLE 3-17).	119
FIGURE 3-52: MEAN MODULUS OF ELASTICITY FROM DIAMETRAL TENSILE STRENGTH OF CA CONTAINING GICS WITH P/L=2:1 AT 1 HOUR, 1 DAY, 1 WEEK AND 1 MONTH AGEING TIME.	120
FIGURE 3-53: MEAN MODULUS OF ELASTICITY FROM FLEXURAL STRENGTH OF SR AND BA CONTAINING GICS WITH P/L=3:1 AT 1 HOUR, 1 DAY, 1 WEEK AND 1 MONTH AGEING TIME (<i>P</i> IS SHOWN IN TABLE 3-18).	121
FIGURE 3-54 MEAN MODULUS OF ELASTICITY FROM FLEXURAL STRENGTH OF CA CONTAINING GICS WITH P/L=2:1 AT 1 HOUR, 1 DAY, 1 WEEK AND 1 MONTH AGEING TIME.	122

List of Tables

TABLE 1-1: CONCISE SUMMARY OF AVAILABLE LITERATURE REGARDING GIC CHARACTERISATION.	30
TABLE 2-1: MOLAR COMPOSITION OF BARIUM AND STRONTIUM SUBSTITUTED ALUMINO-SILICATE GLASSES.	39
TABLE 2-2: POWDER/LIQUID RATIO OF THE RESULTING GICS.	40
TABLE 2-3: THE INGREDIENTS OF EACH 50 G OF AQUEOUS SOLUTION OF GLANDOSANE® (ARTIFICIAL SALIVA).	42
TABLE 3-1: FTIR PEAK ASSIGNMENT IN THE THREE GLASS COMPOSITIONS.	63
TABLE 3-2: FTIR PEAK ASSIGNMENT IN 40% AQUEOUS SOLUTION OF PAA.	64
TABLE 3-3: FTIR PEAK ASSIGNMENT IN THE SETTING REACTION OF GLASS IONOMER CEMENTS.	65
TABLE 3-4: RATIO OF CHANGE IN THE INTENSITY PLOTTED OVER TIME FOR CA-GIC, WITH THE ASSOCIATED PEAK ASSIGNMENTS.	69
TABLE 3-5: RATIO OF CHANGE IN INTENSITY PLOTTED OVER TIME FOR CA-SR-GIC, WITH THE ASSOCIATED PEAK ASSIGNMENTS.	78
TABLE 3-6: RATIO OF CHANGE IN INTENSITY PLOTTED OVER TIME FOR CA-BA-GIC, WITH THE ASSOCIATED PEAK ASSIGNMENTS.	88
TABLE 3-7: ANALYSIS BY THE PAIRED TWO SAMPLE T-TEST IN DEIONIZED WATER AND AS OF THE MATURE GIC COMPOSITIONS AT DIFFERENT TIME POINTS AFTER BEING EXPOSED FOR 1 MINUTE, 10 MINUTES, 1 HOUR, 6 HOURS AND 12 HOURS TO A F ⁻ ION CONTAINING MOUTHWASH.	98
TABLE 3-8: ANALYSIS BY THE PAIRED TWO SAMPLE T-TEST OF THE ANTIMICROBIAL EFFECTIVENESS OF THE THREE EXPERIMENTAL GIC COMPOSITIONS.	102
TABLE 3-9: SETTING TIME OF THE RESULTING GICS WITH DIFFERENT POWDER/LIQUID RATIOS.	103
TABLE 3-10: ANALYSIS BY THE T-TEST OF THE SETTING TIME OF THE THREE EXPERIMENTAL GIC COMPOSITIONS AT DIFFERENT P/L RATIOS (2:1 AND 3:1).	104
TABLE 3-11: ANALYSIS BY THE PAIRED TWO SAMPLE T-TEST OF THE NAN-INDENTATION AND REDUCED MODULUS OF THE THREE EXPERIMENTAL GIC COMPOSITIONS.	107

TABLE 3-12: ANALYSIS BY THE TWO SAMPLE T-TEST OF THE WEAR VOLUME AND WEAR DEPTH OF THE THREE EXPERIMENTAL GIC COMPOSITIONS.	110
TABLE 3-13: ANALYSIS BY THE PAIRED TWO SAMPLE T-TEST OF THE CS OF THE THREE EXPERIMENTAL GIC COMPOSITIONS AT DIFFERENT AGEING TIMES WITH DIFFERENT P/L RATIOS.	113
TABLE 3-14: ANALYSIS BY THE PAIRED TWO SAMPLE T-TEST OF THE DTS OF CA-SR-GIC WITH CA-BA-GIC COMPOSITIONS AT DIFFERENT AGEING TIMES.	115
TABLE 3-15: ANALYSIS BY THE PAIRED TWO SAMPLE T-TEST OF THE FS OF CA-SR-GIC WITH CA-BA-GIC COMPOSITIONS AT DIFFERENT AGEING TIMES.	117
TABLE 3-16: ANALYSIS BY THE PAIRED TWO SAMPLE T-TEST OF THE CS OF THE THREE EXPERIMENTAL GIC COMPOSITIONS AT DIFFERENT AGEING TIMES WITH DIFFERENT P/L RATIOS.	118
TABLE 3-17: ANALYSIS BY THE PAIRED TWO SAMPLE T-TEST OF MODULUS OF ELASTICITY FROM DTS OF CA-SR-GIC WITH CA-BA-GIC COMPOSITIONS AT DIFFERENT AGEING TIMES.	120
TABLE 3-18: ANALYSIS BY THE PAIRED TWO SAMPLE T-TEST OF THE MODULUS OF ELASTICITY FROM FS OF CA-SR-GIC WITH CA-BA-GIC COMPOSITIONS AT DIFFERENT AGEING TIMES.	121
TABLE 4-1: PERCENTAGE RATIO OF POLYCARBOXYLATE SALT DEVELOPMENT AND THE SILICA GEL FORMATION OVER 60 MINUTES FOR EACH GIC COMPOSITION.	132

List of Abbreviations

ADA	American Dental Association
AET	Antimicrobial Efficacy Test
ART	Atraumatic restorative treatment
ASPA	Aluminosilicate polyacrylic acid
AS	Artificial saliva
ATR	Attenuated Total Reflectance
B.C.	Before Christ
BHI	Brain-heart infusion
BLGC	The Laboratory of the Government Chemist
BO	Bridging oxygen
C-GIC	Conventional glass ionomer cement
CB	Columbia Blood
CFU	Colony forming units
CS	Compressive strength
DCL	Degree of crosslinking
DF	Dilution factors
DTGS	Deuterated triglycine sulfate
DTS	Diametral tensile strength
E_r	Reduced modulus
ESEM	Environmental scanning electron microscopy

ESPE	European Society for Paediatric Endocrinology
FAP	Fluorohydroxyapatite
FT	Flexural toughness
FTIR	Fourier Transform Infrared
GIC	Glass ionomer cement
GPC	Glass polyalkenoate cement
HAP	Hydroxyapatite
HEMA	2-Hydroxyethyl methacrylate
HV	Vickers hardness
ICP-MS	Inductively coupled plasma mass spectrometry
IR	InfraRed
ISO	International Organization for Standardization
KBr	Potassium bromide
KH	Knoop hardness
KHN	Knoop hardness number
La-ALC	Lanthanum/alizarin complexone
La-ALC-F	Fluoro-lanthanum/alizarin complexone
MAS-NMR	Magic angle spinning nuclear magnetic resonance
Mw	Molecular weight
NB	Non-bridging
NBO	Non-bridging oxygen

NBF	Non-bridging fluoride
OD	Optical density
PAA	Poly (acrylic acid)
PE	Polyethylene
P/L	Powder/liquid
PMMA	Poly (methyl methacrylate)
PPM	Parts per million
PS	Particle size
PSD	Particle size distribution
Ra	Roughness
RM-GIC	Resin modified glass ionomer cement
RT	Room temperature
SEM	Scanning electron magnification
SIMS	Secondary ion mass spectrometry
<i>S. gordonii</i>	<i>Streptococcus gordonii</i>
<i>S. mitis</i>	<i>Streptococcus mitis</i>
<i>S. mutans</i>	<i>Streptococcus mutans</i>
<i>S. sanguinis</i>	<i>Streptococcus sanguinis</i>
TA	Tartaric acid
TEM	Transmission electron microscopy
T _g	Glass transition temperature
UHMWPE	Ultra high molecular weight polyethylene

WHN

Woxen hardness numbers

List of chemical abbreviations

Silver	Ag
Alumina (aluminium oxide)	Al ₂ O ₃
Aluminium	Al ³⁺
Aluminium oxide	Al ₂ O ₃
Aluminium trifluoride	AlF ₃
Barium	Ba ²⁺
Calcium	Ca ²⁺
Calcium carbonate	CaCO ₃
Calcium fluoride	CaF ₂
Calcium oxide	CaO
Carboxylate anions	COOH ⁻
Cryolite	Na ₃ AlF ₆
Fluoride/fluorine	F ⁻
Fluoride glass	SiO ₂ -Al ₂ O ₃ -CaF ₂
Fluorite	CaF ₂
Hydrogen fluoride	HF
Hydron	H ⁺
Hydroxide ion	OH ⁻
Magnesium	Mg ²⁺

Oxide glass	$\text{SiO}_2\text{-Al}_2\text{O}_3\text{-CaO}$
Phosphorus	PO_4^{3-}
Phosphorus pentoxide	P_2O_5
Poly (acrylic acid)	$(\text{C}_3\text{H}_4\text{O}_2)_n$
Potassium oxide	K_2O
Quartz/Silicon dioxide	SiO_2
Silicon	Si^{4+}
Silicon dioxide/quartz	SiO_2
Silver oxide	Ag_2O
Sodium	Na^+
Sodium fluoride	NaF
Sodium oxide	Na_2O
Strontium	Sr^{2+}
Strontium carbonate	SrCO_3
Strontium fluoride	SrF_2
Titanium	Ti^{4+}
Zinc	Zn^{2+}

Contents

Abstract.....	I
Summary.....	II
Acknowledgments.....	V
List of Figures.....	VI
List of Tables.....	XIII
List of Abbreviations.....	XV
List of chemical abbreviations.....	XIX
1 Literature review.....	1
1.1 Introduction.....	1
1.2 Continuum and classification of restorative materials.....	2
1.3 The development of dental restorative materials.....	4
1.4 The chemistry of GICs.....	10
1.5 Glass ionomer cements (GICs).....	12
1.6 GIC compositions.....	12
1.6.1 The ion leachable glass powder.....	13
1.6.2 Polyacrylic acid (PAA).....	14
1.7 Glass compositions to form GICs.....	16
1.7.1 Aluminosilicate glasses.....	16
1.7.2 Aluminoborate glasses.....	17
1.7.3 Zinc silicate glasses.....	18

1.8	Factors which can influence the properties of the resulting GIC	18
1.8.1	Al ₂ O ₃ /SiO ₂ ratio in the glass component	18
1.8.2	Phosphorus in the glass component.....	19
1.8.3	Fluoride in the glass component.....	19
1.8.4	Na ⁺ in the glass component	21
1.8.5	Decrease of glass reactivity	22
1.8.5.1	Heat treatment	22
1.8.5.2	Acid washing.....	23
1.8.6	Glass particle size (PS) and distribution	24
1.9	Fluoride release and recharge ability	25
1.10	Antimicrobial effectiveness.....	27
1.11	Experimental methods for GIC characterisation	28
1.12	Aims and objectives	37
2	Materials and methods.....	39
2.1	Materials.....	39
2.1.1	Poly (acrylic acid) (PAA).....	40
2.1.2	Preparation of glass ionomer cements (GICs).....	40
2.2	Methods	41
2.2.1	Fourier Transform Infrared (FTIR) Spectroscopy.....	41
2.2.2	Fluoride release of GICs in artificial saliva and deionized water	42
2.2.3	Antimicrobial Efficacy Test (AET)	44
2.2.4	Calculation of cement setting time	47

2.2.5	Vickers Hardness (HV) of glass ionomer cements.....	50
2.2.6	Nano-indentation	51
2.2.7	Reciprocating ball-on-flat wear test.....	55
2.2.8	Mechanical properties of prepared GICs	56
2.2.9	Mechanical testing	58
2.2.9.1	Compressive strength (CS).....	58
2.2.9.2	Diametral tensile strength (DTS).....	59
2.2.9.3	Flexural strength (FS)	60
2.2.9.4	Modulus of Elasticity (E-modulus).....	61
3	Results.....	62
3.1	Fourier transform infrared (FTIR) spectroscopy study.....	62
3.1.1	FTIR spectroscopy study of the ion leachable glass powder	62
3.1.2	FTIR spectroscopy study of the PAA solution.....	63
3.1.3	FTIR spectroscopy study of cement setting reaction	64
3.1.3.1	FTIR spectroscopy study of calcium cement setting reaction.....	66
3.1.3.2	FTIR spectroscopy study of strontium substituted cement setting reaction 75	
3.1.3.3	FTIR spectroscopy study of barium substituted cement setting reaction 85	
3.2	Fluoride release of GICs in artificial saliva and deionized water	95
3.3	Antimicrobial effectiveness of glass ionomer cements	101
3.4	Calculation of cement setting time.....	103

3.5	Vickers Hardness (HV).....	104
3.6	Nano-indentation.....	106
3.7	Wear behavior of glass ionomer cements.....	109
3.8	Mechanical properties of cements.....	111
3.8.1	Compressive strength (CS).....	111
3.8.2	Diametral tensile strength (DTS).....	113
3.8.3	Flexural strength (FS).....	115
3.8.4	Modulus of Elasticity.....	117
4	Discussion.....	124
4.1	FTIR.....	124
4.2	Fluoride release of GICs in artificial saliva and deionized water.....	133
4.3	Antimicrobial effectiveness of glass ionomer cements.....	139
4.4	Calculation of cement setting time.....	142
4.5	Vickers Hardness.....	146
4.6	Nano-indentation.....	150
4.7	Wear behavior of glass ionomer cements.....	152
4.8	Mechanical testing.....	154
5	Conclusions.....	162
5.1	FTIR.....	162
5.2	Fluoride release of GICs in deionized water and AS.....	163
5.3	Antimicrobial effectiveness of glass ionomer cements.....	163
5.4	Calculation of cement setting time.....	164

5.5	Vickers hardness.....	164
5.6	Nano-indentation.....	164
5.7	Wear behaviour of GICs.....	164
5.8	Mechanical properties of GICs.....	165
6	Future work.....	167
7	References.....	169

1 Literature review

In a society where the most people are concerned about their cosmetic appearance, the first choice for a dental filling material is one that resembles the natural tooth in appearance and function and lasts the life-time of the patient

Dental practitioners have at their disposal a wide variety of dental filling materials. The choice of the correct material, possessing the appropriate properties for each application, thereby ensuring good long-term clinical performance, is dependent upon the detailed knowledge of the dental practitioner¹. A highly desirable property of a restorative dental material is that it be aesthetically attractive and white. A general disappointment with the clinical performance of 'white' restorative materials encouraged scientists to continue to seek improvements. This led to extensive research into the creation of a dental restorative material that is visually attractive and fulfils the desired property requirements, to withstand mastication forces. The research presented in this work is an attempt towards realisation of the above ideal.

1.1 Introduction

Dentistry can be traced back through millennia, to as early as 3000 B.C. The modern day dentist can now choose from a broad variety of restorative materials, which mimic the tooth substance.

In the 18th century, all medical specialities, including primitive dentistry, were practised by surgeons. Goldsmiths and metal turners began to manufacture dental prosthesis out of ivory, ox, sea cow and preferably hippopotamus teeth because of its delayed discolouration properties in the mouth when used as a prosthesis. In the 18th century the first dental schools opened and the dental profession started to modernize and evolve. In the 19th century dentistry made significant advances in

sophistication. Moving forward, the 19th – 20th century witnessed the mass production of dental items such as toothpaste, tooth brushes and floss. Furthermore, a peak in the production of dental instruments occurred².

Whilst previously, dental treatment had resembled a wrestling match, treatment now began to resemble modern dentistry. The first power drill (hand piece) was introduced in 1872. After the discovery of X-rays by Roentgen in 1895³, dentists were able to identify inflammation/infection through X-ray images and with appropriate instruments treatment strategies were developed. Thus the fundamentals for modern odontology were laid⁴.

1.2 Continuum and classification of restorative materials

In the middle of the 19th century amalgam was one of the first restorative dental materials used by dental practitioners. In the first half of the 19th century dental cements developed from being merely luting and lining materials to being employed as more aesthetic restorative materials⁴. Subsequently several white restorative dental materials, shown in Figure 1-1, became available. Glass ionomer cements, white restorative materials, are formed from an acidic polymer solution and a basic glass powder. When these two components are mixed together they undergo an acid-base reaction. The resulting material is cement, which consists of glass filler particles imbedded in a metal polyacrylate matrix⁵.

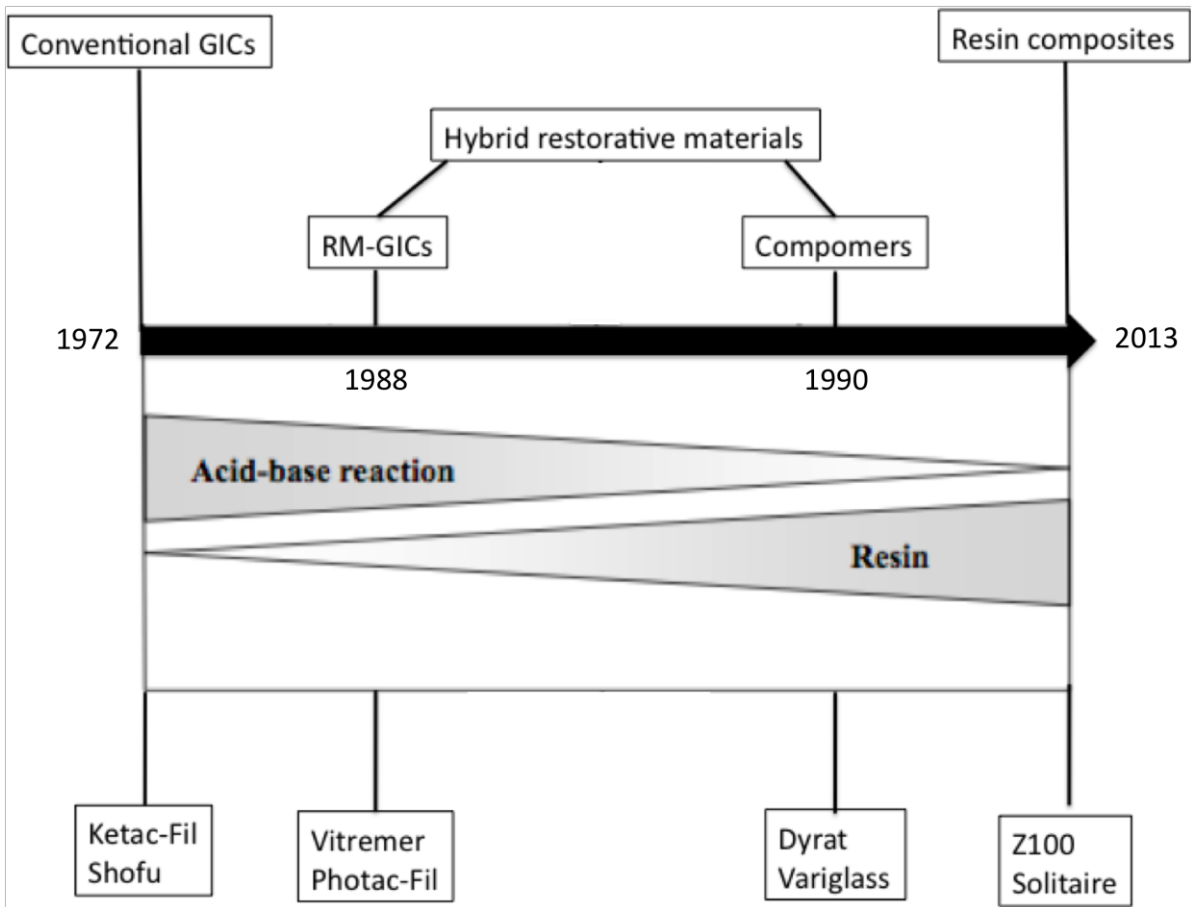


Figure 1-1: The continuum of white restorative dental materials since 1972⁶.

GICs can be categorized as restorative dental cements, including liner/base materials or luting materials, cavity bases and buildups, as well as root canal fillings⁷. GICs, when deployed as restorative materials, can be characterized as metal-modified, resin-modified, self-hardening and partially light-hardening. GICs as luting materials are self-hardening and a number of them are modified with resin⁸. Variation in the particle size (PS) and powder to liquid (P/L) ratio can lead to several physico-mechanical properties and corresponding clinical applications. The traditional classification of GICs is as follows:

Type I	Luting and bonding cements (PS ca. 13 – 19 μm and P/L ratio ca. 1.5:1)
--------	---

Type II	Restorative cement (PS ca. 50 µm and P/L ratio ca. 3:1)
	<ul style="list-style-type: none"> • Restorative aesthetic • Restorative reinforced
Type III	Lining or case cement ⁹ .

Regarding the newer classification of GICs according to their physical and chemical properties, 3 further types have been added over the years:

Type IV	Fissure sealants
Type V	Orthodontic cements
Type VI	Core build up ¹⁰ .

1.3 The development of dental restorative materials

The use of dental materials to fill cavities can be dated back to the Chinese in the 7th century. Taveau, in France (1816), developed, by mixing silver coins and mercury, the first dental amalgam. This entailed several problems such as expansion after replacement and mercury poisoning¹. In the 1890's the amalgam composition was altered and dentists, including in the United States, began using it as dental filling material. However, amalgam, with its positive aspects, such as being an inexpensive dental material, durable and easy to manipulate, also possessed two negative aspects; first, mercury poisoning (causing neurodegenerative disease, and birth defects, in the event of long term exposure, and its dubious aesthetic appearance, silver in colour. In the future the use of dental amalgam will continue to decline, because of environmental restrictions (mercury release) and the aesthetic issue. The development of more durable and technique insensitive restorative materials will further rise¹.

The cements used daily in modern dentistry are largely derived from investigations made in the first half of the 19th century. Sorel¹¹ presented the first dental restorative cement, zinc oxychloride, in 1855. In 1879 Pierce¹² largely replaced the previous zinc oxychloride with zinc oxide-phosphate cements. These cements exhibited lower pulp irritation and greater durability. The modern zinc phosphate cements were established by the work of Ames¹³ and Fleck¹⁴ around the turn of the 1900's. At the same time, around 1875, Pierce and Flagg originated the zinc oxide eugenol cement, which soon became in demand because of its anodyne effect. By the end of the 19th century these cements were used as adhesives, temporary restoratives and cavity bases. Silicate cement, a more aesthetic restorative material, developed by Fletcher in 1873, was not popular until Steenbock¹⁵ in 1904 modified the previous version. In 1908 Shoenbeck¹⁶ developed the first silicate cement with the addition of fluoride.

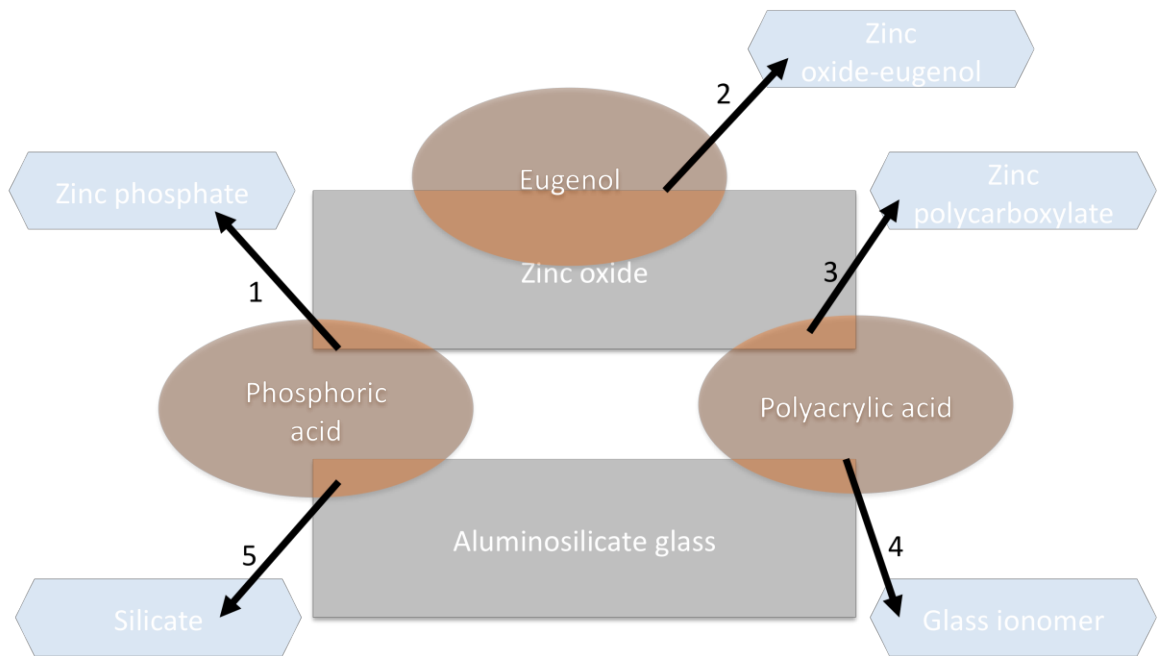
At the beginning of the 1900's three main categories of cement had come into existence:

- Zinc oxide-eugenol cements by Pierce¹² and Flagg (1875)
- Zinc phosphate cements by Ames¹³ (1892) and Fleck¹⁴ (1902)
- Silicate cements by Schoenbeck¹⁶ (1908).

All these three types of cement remained unmodified for the next 50 years. Nevertheless, cement was still in great need of improvement.

Putting together different components with zinc containing glass ceramic, silicate cement powder mixtures were investigated for many years. The British Laboratory of the Government Chemists (BLGC) tried to enhance the properties of silicate cements, zinc polycarboxylate cements and zinc phosphate cements. The intention was to combine the desirable features of the two the silicate cements (translucency

and F⁻ release) with the polycarboxylate cements (adherence chemically to tooth substance and not irritating the pulpa)^{17,18}. At BLGC, Alan Wilson and Brian Kent¹⁸ tried to resolve why dental cements were almost unworkable, set sluggishly and were hydrolytically unstable. Figure 1-2 illustrates the different types of cements and their components.



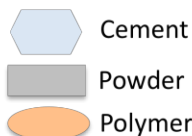
- | | | |
|-------------------------------------|---|---|
| 1: Zinc phosphate cement | = Phosphoric acid + Zinc oxide powder |  |
| 2: Zinc oxide-eugenol cement | = Eugenol + Zinc oxide powder | |
| 3: Zinc polycarboxylate | = Polyacrylic acid + Zinc oxide powder | |
| 4: Glass ionomer cement | = Polyacrylic acid + Aluminosilicate glass powder | |
| 5: Silicate cement | = Phosphoric acid + Aluminosilicate glass powder | |

Figure 1-2: Possible cement components¹⁰.

They observed that the setting reaction in these materials results from a neutralization reaction involving the inorganic (alkaline) glass powder and organic (acidic) polymer, which forms a polysalt matrix. The cause of the problem was the reduced sensitivity of the glass component opposite the acidic polymer. To promote the reactivity of the glass, its basic oxide ratio had to be increased; thus, the alkalinity of the glass would increase and this would improve the sensitivity of the glass component towards the acidic polymer^{1,19,20}.

In 1972 Wilson and Kent¹⁸ made the first commercial available GIC, with the trade name aluminosilicate polyacrylate-I (ASPA-I). Since, this cement required 20 minutes to harden, and was not aesthetically pleasing because its high fluoride content gave it an opaque appearance, ASPA-I was clinically not fit for purpose. However, in 1972 Wilson and McLean⁹ reformulated the cement by adding tartaric acid (TA) accelerators and by changing aluminium oxide to silicon dioxide in the silicate glass. TA is a reaction controlling stabilizer. It extends the substance's working time (by complexing with Al^{3+} and Ca^{2+} cations to form tartaric aluminium and tartaric calcium), enables the use of glasses containing reduced fluoride and further strengthens and hardens the cement. This cement was named ASPA-II^{21,22}.

The conventional GIC (C-GIC) is provided as fine glass particles and a polyacid solution. If polyacid comes as a suspension, it has a tendency to gel with time, because of an increase in intermolecular hydrogen bonds^{10,23}. As a consequence, the cement paste is more difficult to process. A small amount of methanol was added to the polyacrylic acid (PAA) in order to stop the flexible PAA chains forming intermolecular hydrogen bonds. This improved cement was called ASPA-III^{17,19,24}.

From 1979 to 1980 dental cements, also called water mixed or water hardened cements, were distinguished from previous products by their improved shelf life and mechanical properties²⁵. The trend was towards using PAA not in solution form but in powder state. The PAA was mixed with either H_2O or TA. This was the key to reducing the risk of high viscosity in the early stages of mixing^{17,18,24}.

The improved GIC was successfully used in low stress bearing areas. However, the fact that GIC has poor mechanical properties remained a problem²⁶. Low tensile strength of 7 – 14 MPa made GIC virtually impossible to use in molar areas, where high stress is present. To enlarge the field of application, scientists had to enhance

the mechanical properties of GIC^{27,28}. Massler *et al.*²⁹ described how amalgam powder was mixed with zinc phosphate cement in 1957. In 1962 Mahler and Armen³⁰ proved that by adding amalgam particles to the zinc phosphate powder solubility improved in the new restorative cement, in comparison with the original cement. These restoratives are termed admixtures. Difficulty in achieving a homogenous mixture was a major disadvantage. The amalgam particles were not well incorporated in the resulting GIC, resulting in accelerated erosion and enhanced wear. The incorporation of metal particles in GIC is contraindicated for big fillings in the maxillary and mandibular molar, due to enhanced wear and fatigue fracture³⁰.

In 1987 ESPE launched the initial cermet¹⁰ (ceramic + metal) called Ketac-Silver® on the market. McLean and Gasser's³¹ intention was to improve the properties of the material. The aluminosilicate glass particles were coated with silver (Ag), which resulted in a lower coefficient of friction due to abrasion resistance. Ketac-Silver® uses pure Ag powder, which is fused to 3.5 µm ion leachable calcium aluminium fluorosilicate glass powder. But unfortunately after a period of time, the Ag particles in the material formed Ag₂O, which caused a discolouration of the tooth. Cermet ionomer cements have higher flexural strength (FS) compared to C-GIC, but are still not sufficiently powerful to replace amalgam alloys³².

In 1988 Antonucci *et al.*³³ introduced the first light cured resin-modified glass ionomer cement (RM-GIC). This material combines the best properties of composite resins and glass ionomers; it has a cariostatic property because of its fluoride release, low thermal expansion and the hydrophilic qualities of the C-GICs. The RM-GICs have improved fracture toughness (FT), are wear resistant and easier to polish in comparison to the original GICs¹⁰. To describe it simply, the C-GIC is mixed with a little amount of resin such as 2-hydroxyethyl methacrylate (HEMA) in the polymeric

solution³⁴. The first commercial light cured GIC, Vitrebond, was developed by Mitra³⁵ in 1989. This modified cement has two setting mechanisms: a light initiated polymerisation reaction and a glass ionomer acid-base reaction. In 1991 a modified resin was developed by Mitra³⁶ which was able to polymerize without light. RM-GICs possess the advantages of both C-GIC and resin composites, though, disadvantages remain such as setting shrinkage and limited depth of curing¹⁰.

In 1995 a highly viscous GIC was introduced³⁷. This GIC is used mainly in third world countries where instruments and equipment are in short supply and filling is mostly functional for atraumatic restorative treatment (ART) procedures. Non-dental professionals are able to restore the tooth merely by excavating the caries using hand instruments and fill the resultant hole with GIC. The mechanical properties of the highly viscous C-GIC is improved through higher powder and liquid ratios^{38,39}.

Further GICs were developed in order to enhance their ease of handling in practice. GICs with adequate P/L ratios were launched to ensure a higher degree of dosing consistency and the corresponding consistent mechanical properties^{11,40}.

Around 1990 Dentsply released a new restorative dental product, compomer (Dyract)⁴¹. Compomers are fluoride containing resin composites and are also known as polyacid-modified resin composites. Compomers became popular because of their aesthetic characteristics, which resemble resin composites. These compomers lacked the capability to adhere to the tooth substance and release lower levels of F⁻ ions. However, there are some disadvantages as the amount of fluoride which this product releases is limited and additionally there is its inability to recharge fluoride^{41,42}.

1.4 The chemistry of GICs

The setting reaction of GICs has been extensively studied via a number of analytical methods including solid state Magic angle spinning nuclear magnetic resonance (MAS-NMR) spectroscopy^{43,44}, Raman spectroscopy^{45,46}, Fourier transform infrared spectroscopy (FTIR)^{47,48,49}, pH change⁵⁰ and electron probe microanalysis⁵¹.

C-GICs are produced by a neutralization reaction (acid-base) involving the alkali, finely powdered fluoroaluminosilicate glass particles and an aqueous acrylic acid or co-polymers^{22,52,53,54}.

The acid-base setting reaction starts once the acrylic acid groups of PAA (C₃H₄O₂)_n (which dissociate to form acrylic anions COO⁻ and hydron H⁺) are mixed with the ion leachable glass powder. The hydrons (H⁺) attack the surface of the inorganic glass structure, causing disintegration of the glass structure. The protons initially attack the Ca²⁺ abundant part, due to its higher alkaline content, followed by the Al³⁺ site of the alkali glass^{55,56}. The continuous attack on the ion leachable glass structure causes the release of Ca²⁺, Al³⁺, Mg²⁺ and F⁻ amongst others, depending on the glass content. These ions enter the aqueous phase of the cement and form complexes with the anions of the carboxylates (COO⁻) to form metal polysalts linking the polyacid chains, resulting in the development of silica hydrogel (Si-OH) on the exterior of the glass particles linking the cement matrix and the glass particles. The general reaction may be simplified as:



The outer layer of the basic glass powder is attacked by the carboxylic acid, but the glass core persists and presents as filler in the GIC matrix⁵⁷. An endless network is shaped by the released ions from the ion leachable glass. However, the two main

cations which are released from the alkali glass (which have an important role in both the polysalt matrix formation and the correspondent resulting mechanical properties of GIC) are calcium (Ca^{2+}) and aluminium (Al^{3+}) cations. The degree to which the formation of the polysalt matrix is advanced is determined by the vulnerability of the glass structure and the ingredients of the inorganic glass^{52,53,54,56}.

The incorporation of the bi-valent Ca^{2+} ions and tri-valent Al^{3+} ions into the preformed matrix with additional PO_4^{3-} and F^- anions forms a hard, crosslinked, ceramic like cement and results in the formation of a three-dimensional water-insoluble calcium- and aluminium-carboxylate gel^{56,57,58}.

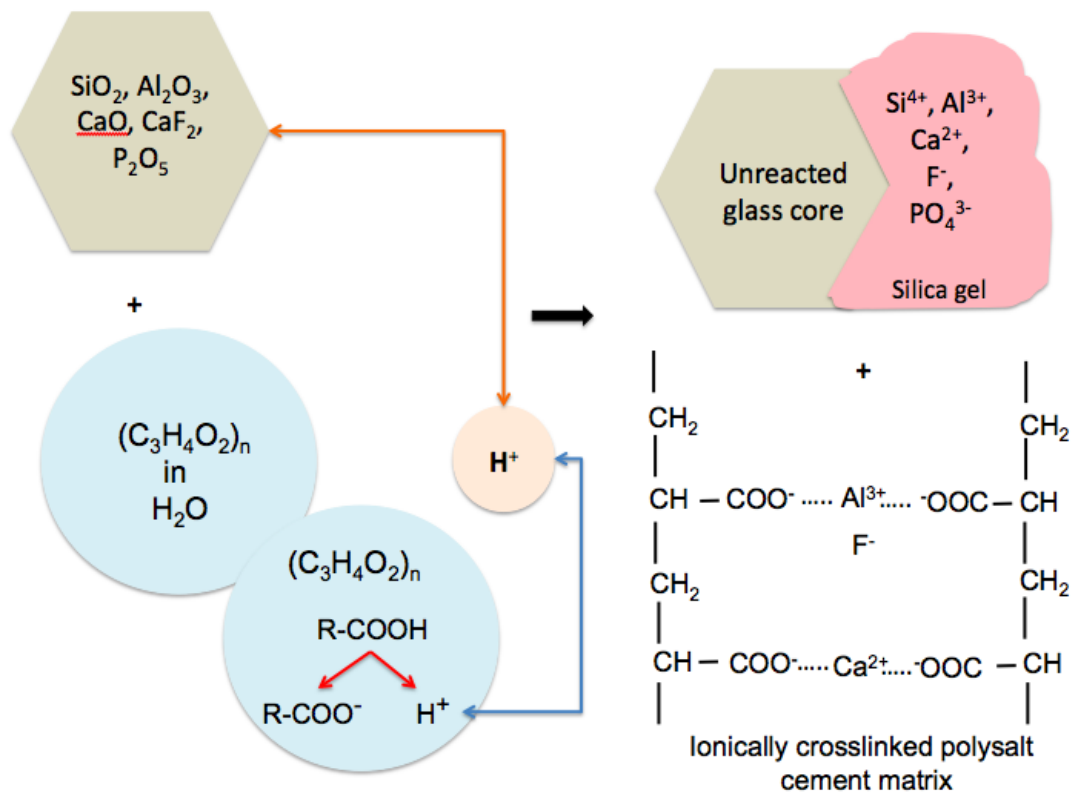


Figure 1-3: Schematic representation of the setting reaction of the glass ionomer cements (information from Culbertson²⁰).

Hatton and Brook⁵¹ demonstrated with transmission electron microscopy (TEM) sections, which were examined with X-ray analysis, that in the polysalt matrix, ions such as Na^+ , P^{3-} and Si^{4+} are available throughout the cement structure. Wasson and Nicholson^{59,60} investigated the inorganic network based on Si^{4+} and P^{3-} and its water

solubility. They suggested that the inorganic network, which adds to the insolubility of the cement, causes the increased CS. Hill *et al.*^{61,62} reported that the Mw of the polymer, defines the strength of the resulting GIC with its flexural toughness (FT). Another factor which increases the CS of the resulting GIC, is the addition of F⁻. It can increase the CS of a 1 day old GIC up to 200 MPa, whereas a GIC without the addition of F⁻ exhibits just up to 100 MPa⁵⁷. F⁻ although present, is not involved in the polysalt matrix, and reacts with the ions to form F⁻ complexes. These F⁻ complexes delay the reaction of the cations, which help create metal carboxylates. These increase the ability to react and retard the gelation but lengthen working time⁶³. Other factors which could influence the setting reaction of the GICs are listed below:

- I. Ratio of bound to unbound water molecules⁵⁹,
- II. P/L ratio^{64,65,66},
- III. Glass composition^{67,68,69},
- IV. Mixing time/mixing temperature⁷⁰,
- V. Glass PS⁷¹,
- VI. Mw of the polymer^{62,72,73},
- VII. Concentration of the polymer⁷⁴.

1.5 Glass ionomer cements (GICs)

The International Organization for Standardization (ISO)⁷⁵ has adopted the term glass polyalkenoate cement (GPC) which is usually known as glass ionomer cement (GIC).

1.6 GIC compositions

GICs are composed of two essential elements: the ion leachable glass powder, which is based on a calcium fluoroaluminosilicate glass composition, and the acidic polymer solution, which is made out of a water-soluble polymer⁵.

1.6.1 The ion leachable glass powder

Generally, the ion leachable fluoroaluminosilicate glass powder is produced by the fusion method or melt quench route⁷⁶ of several inorganic chemicals, (such as quartz (SiO_2), alumina (also called aluminium oxide Al_2O_3), cryolite (Na_3AlF_6), fluorite (CaF_2), aluminium trifluoride (AlF_3) and aluminium) as listed in Table 3-1. The American Society for Testing and Materials (ASTM)⁷⁷ has defined glass as “an inorganic product of fusion which had cooled to rigid condition without crystallizing.”

The glass network consists of a random silica network Si-O-Si. The assemblies of individual SiO_4 tetrahedra (simplest possible glass) are cross-linked at the corners to build a chain and are immune to acid attack, because of their electroneutrality⁷⁸.

Zachariasen⁷⁸ proposed a theory regarding the glass network whereby he divided the glass network constituents into three groups:

1. network formers (Si^{4+} , PO_4^{3-}),
2. network modifiers (Ca^{2+} , Sr^{2+} , Ba^{2+} , Na^+) and
3. intermediates (Al^{3+} , Ti^{4+})⁷⁸.

By introducing network modifiers in the glass structure, such as Na^+ , Ca^{2+} , Sr^{2+} and Ba^{2+} , the Si-O-Si bonds break, leading to a surplus negative charge thus forming non-bridging oxygens (NBOs) in the cement matrix. Generally, all oxygens in the glass structure are bridging oxygens (BOs). By adding other compounds such as CaO and Na_2O (network modifiers) in the glass composition NBOs can be formed.

Lowenstein⁷⁹ suggested the centre of one tetrahedron, which is linked by one oxygen bridge to a second tetrahedron, can be engaged by Al^{3+} , while the other centre must be engaged by Si^{4+} or different small ion of four or more electrovalence. Since Al^{3+} is an intermediate, it is able to act as a network modifier and network former⁷⁸. The

inclusion of Al^{3+} , as a network former, in the tetrahedra changes the behaviour of the glass and leaves a surplus negative charge on the structure (AlO_4^-). The network has now a surplus of negative charge, which has to be balanced out by introducing a network modifier to maintain electroneutrality. The substitution of Si^{4+} by Al^{3+} ions in the glass happens only upon the ratio limit 1. However, the glasses used to form GICs have to fulfil several requirements, such as the $\text{Al}^{3+}/\text{Si}^{4+}$ ratio. The ratio of Al^{3+} to Si^{4+} in the glass is critical, and must exceed 1.2:1 by mass (equivalent to 1:1 by mole ratio) for the glass to be able to form cement⁸⁰.

A glass network consisting of NBOs and Al sites renders these glasses more vulnerable towards acid attack. Generally, Si^{4+} ions have greater field strength, whereas the polarity of BOs (Si-O-Si) is quite low. In contrast, Al^{3+} ions (Si-O-Al) have weaker field strength, because of NBOs, but their polarity is higher regarding complexing with other cations⁶⁸.

In general, creating more NBO in the glass structure weakens the general glass network⁶⁹, increases susceptibility of the glass to acid attack⁶⁷, and decreases the glass transition temperature (T_g)^{81,82}.

1.6.2 Polyacrylic acid (PAA)

PAA use as an acidic water-soluble polymer to form cements has several favourable properties:

- PAA is capable of linking to Ca^{2+} and H^+ ions with organic polymers (collagen).
- PAA has very low toxicity,
- appropriate physical properties and

- has the ability to adhere to the tooth substance⁸³.

In 1969 the first commercially available zinc polycarboxylate cement, named Durelon®, was launched from European Society for Paediatric Endocrinology (ESPE), in which zinc oxide powder with PAA was mixed^{11,84}.

Generally, the main ingredient of the acidic polymer is H₂O. Because of its high water content, it is prone to dehydration¹¹.

Initially, PAA was used as a 50% aqueous solution to form cement, but these cements required a lengthy period (10 – 30 minutes) to set. Furthermore, the aqueous solution started to increase in viscosity (gelation) after 10 weeks of storage²². McLean and Wilson²³ found that the gelation of the polymeric solution results from the hydrogen bonding among the polyacid chains. To manage these difficulties, the copolymers of acrylic acid, itaconic acid, maleic acid and fumaric acid were introduced to enhance its storage life. The higher degree of carboxyl groups (COOH) in these copolymers enhances the reactivity of the acidic polymer. Figure 1-4 presents a schematic illustration of the copolymers of acrylic acid and itaconic acid (Figure 1-4 a) and maleic acid (Figure 1-4 b). Furthermore, the addition of TA in the polyacid has a desirable effect on the handling properties of the cement and its setting rate²⁰.

Generally, increasing the Mw⁷³ or the concentration⁷⁴ of the PAA enhances the mechanical properties of the resulting GIC. Handling properties however are compromised⁷². The Mw and the concentration ratio of the PAA can reduce the gelation, but only to a certain degree. In order to ensure appropriate resulting mechanical properties without neglecting the handling properties, it is possible to either use higher powder content to constant liquid volume or incorporate vacuum- or freeze dried PAA powder in anhydrous glass ionomers or water-hardened cements²⁵.

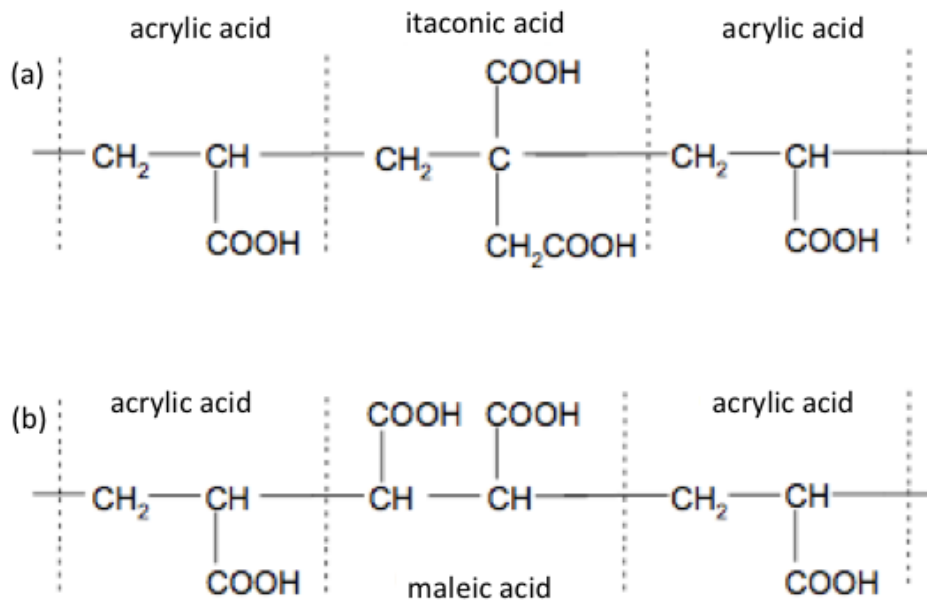


Figure 1-4: Schematic illustration of copolymers with (a) acrylic acid and itaconic acid and (b) acrylic acid and maleic acid [Hosoda⁸⁵].

1.7 Glass compositions to form GICs

Various glasses have been investigated as cement developers. Three main glasses have emerged.

1.7.1 Aluminosilicate glasses

Oxide ($\text{SiO}_2\text{-Al}_2\text{O}_3\text{-CaO}$) and fluoride ($\text{SiO}_2\text{-Al}_2\text{O}_3\text{-CaF}_2$) glasses were investigated by Wilson and Kent^{18,86}.

Oxide glasses exhibited a typical random glass network structure composed of AlO_4 and SiO_4 bridges⁷⁸. Introducing Al^{3+} as a network former into the glass structure, resulted in four-fold coordination $[\text{AlO}_4^-]$ with a surplus negative charge. The negative surplus charge in turn was compromised with network modifiers⁷⁹.

In fluoride glasses, the chemical compound calcium oxide (CaO) was substituted for calcium fluoride (CaF_2), resulting in non-bridging fluorides (NBFs) instead of NBOs, as was the case with CaO . These fluoride glasses were observed to be stronger and

had a shorter setting time because of the incorporation of fluoride in the glass structure⁸⁷.

Several other new derivatives of aluminosilicate glasses were investigated and developed where new compositional ingredients, such as NaF, P₂O₅, K₂O, were added to the original oxide and/or fluoride glasses^{44,88}.

Present time (2013), the glass component to form GICs is mainly aluminosilicate glass, whereas the addition of other compositional ingredients can vary¹⁰.

The ability of these glasses to form cement was observed to be dependent on the Al₂O₃/SiO₂ ratio (Al³⁺:Si⁴⁺ > 1.2:1 mass ratio; equivalent to 1:1 by mole ratio⁸⁰), the sodium (Na⁺) content⁸⁹ and the glass network connectivity (BO to NBO ratio)⁹⁰.

1.7.2 Aluminoborate glasses

Aluminoborate glasses have the general composition Al₂O₃-B₂O₃-ZnO-ZnF₂ and Neve *et al.*^{91,92} suggested that the aluminoborate glasses absorb more water than the aluminosilicate glasses. Generally, water hardening cements coming in contact with moisture absorb water and this acts as a plasticizer⁹³. Neve *et al.*⁹² investigated the mechanical properties and storage time as well as the P/L ratio in the aluminoborate glasses. They reported that the CS (< ca. 60 MPa at 1 h with further reduction with ageing time) of aluminoborate cements was poor and may have been related to the slow development of ionic crosslinking in the cement matrix. However, DTS (5 – 8 MPa at 1 h) exhibited more representative values. Furthermore, the aluminoborate glasses were significantly affected by their powder content. An increase in strength was observed if powder content was increased by constant liquid volume whereas, increased B₂O₃ content in the glass powder raised the dissolution rate of the aluminoborate glasses⁹⁴.

1.7.3 Zinc silicate glasses

Zinc silicate glasses with the composition of CaO-ZnO-SiO₂ and/or Al₂O₃-ZnO-SiO₂ have Zn²⁺ as the main participant. Zn²⁺, as with Al³⁺, is an intermediate and serves as both network modifier and network former⁷⁸. In zinc silicate glasses, no aluminium is present, therefore the cement forming abilities of the glass are not dependent on the Si/Al ratio. In these glasses, low Si mole fraction and high ZnO provide the ability to form cements. The addition of Zn²⁺ has several biological advantages; it enhances the bone formation and mineralization⁹⁵ and it is recognized as an antibacterial agent⁹⁶. However, cements made of zinc silicate glass component exhibit poor mechanical properties in comparison to the cements with aluminosilicate glass component⁹⁰.

1.8 Factors which can influence the properties of the resulting GIC

1.8.1 Al₂O₃/SiO₂ ratio in the glass component

The Al₂O₃:SiO₂ ratio determines the reactivity of the glass in an acidic solution and the extent of leaching of the ions from the glass structure. Wilson *et al.*⁸⁰ investigated the cement forming abilities of several ion-leachable glass systems. They suggested that the key criterion which controls the setting rate of the cement is the Al₂O₃:SiO₂ ratio which also determines vulnerability of the glass towards acid attack. Moreover, vulnerability of the glass to acid attack increases if Si⁴⁺ is substituted by Al³⁺, which results in a higher polarizability of Al-O-Si bridges in the glass structure when attacked by H⁺. Furthermore, Wilson *et al.*⁸⁰ concluded that the BO to NBO ratio is as important as the Al/Si ratio in determining the cement formation abilities. Introducing Al³⁺ in the glass structure as network formers may lead to the susceptibility of the glass towards acid attack by creating a higher degree of NBOs⁶⁷.

1.8.2 Phosphorus in the glass component

PO_4^{3-} ions in the aqueous phase might interfere with the setting reaction by complexing with other cations (Al^{3+} or Ca^{2+}), which affects the setting time and properties of the resulting cement⁹⁷. High amounts of phosphorus prevent the development of the metal salt ionic crosslinking, which is responsible for the strength of the resulting cement⁹⁷.

Griffin and Hill⁹⁷ investigated the function of PO_4^{3-} in the glass composition $(4.5-2x)\text{SiO}_2-3.0\text{Al}_2\text{O}_3-(3.0-x)\text{CaO}-(1.5+x)\text{P}_2\text{O}_5-2.0\text{CaF}_2$, where P_2O_5 was substituted for CaO and SiO_2 . The Al/P ratio in these glasses was kept > 1 . The CS of the resulting cement over a 1 month period was observed. Griffin and Hill⁹⁷ evaluated the CS values of low formulation cements ($x=0$) with a maximum of 121.8 ± 4.5 MPa. They found that the incorporation of PO_4^{3-} in the glass structure and the resulting cement showed a high degree of plasticity before failure. The plasticity of the cement decreased, while the strength increased with ageing. A high amount of phosphorus in the glass component reduces the CS and the E-modulus of the resulting cement, whereas adding a low amount of phosphorus in the glass component can extend the setting and working time, resulting in improved strength of the resulting cement. Ray⁹⁸ reported that the solubility of phosphate glasses is dependent on the double bonded oxygen connected to phosphorus. Generally, the Al/P ratio is kept < 1 , to avoid the double bonded oxygen-phosphorus complexes resulting in hydrolysis.

1.8.3 Fluoride in the glass component

Wilson and McLean⁹⁹ summarised the findings of other research regarding the SiO_2 - Al_2O_3 - CaO - CaF_2 glasses which reported that an increase in F^- content or CaF_2 content in these glasses resulted in the glass being too reactive to form cement.

Generally, CaF_2 is known to be an influential network modifier and by introducing it in the glass component the network structure of the glass weakens, hence leading to the creation of NBOs or even non-bridging fluorines (NBFs)¹⁰⁰ as illustrated in Figure 1-5.

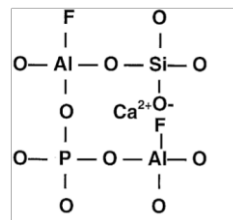


Figure 1-5: Schematic illustration of calcium fluoride in the glass structure. F^- creates NBFs, by surrogating the BOs and Ca^{2+} creates NBO by charge balancing the AlO_4^- [De Barra and Hill¹⁰⁰].

In general, disruption of the glass network resulted in a decrease in glass transition temperature (T_g)^{81,82}. De Barra and Hill¹⁰⁰ investigating the influence of CaF_2 (Ca^{2+} and F^- ions) on the glass composition $1.5\text{SiO}_2\text{-}0.5\text{P}_2\text{O}_5\text{-Al}_2\text{O}_3\text{-CaO-XCaF}_2$. De Barra and Hill¹⁰⁰ observed a weakened glass network associated with the inclusion of F^- in the glass structure and a reduction in the T_g . The cement setting time (CS with E-Modulus) was, evaluated during which a reduction in setting time was observed. This was interpreted as being a result of glass structure disturbance coupled with increased cement viscosity. Thus, an increase in glass reactivity in the form of higher cation diffusion in the aqueous phase and higher degree of polysalt ionic crosslinking was observed to be associated with increased CaF_2 content, increase CS value and a corresponding E-Modulus increase¹⁰⁰.

Since, high F^- content is present in the glass component of the modern day GICs¹⁰¹, F^- provides several important characteristics to GICs. The presence of F^- ions reduces the index of refraction of the glass, making it translucent and F^- is known to have a cariostatic effect, when released in the oral environment^{102,103}.

Griffin and Hill⁶³ investigated the glass T_g in the following glass compositions $4.5\text{SiO}_2\text{-}3.0\text{Al}_2\text{O}_3\text{-}1.5\text{P}_2\text{O}_5\text{-}(5\text{-}x)\text{CaO-xCaF}_2$. They reported that, with increased F^- in the glass composition, a considerable reduction in the T_g was seen. This was explained by the addition of F^- ions weakening the glass structure by replacing the BOs in the glass matrix with NBF, resulting in higher reactivity of the glass. Substituting the BOs in the glass structure with NBFs results in a decrease in T_g . The setting time and handling time of the cement paste decreases with additional F^- ions whereas, the strength values and E-modulus of the resulting cement increases⁶³.

1.8.4 Na^+ in the glass component

Investigating the decomposition of single component glass powder containing Na^+ as the main cation, Crisp and Wilson⁵² found that Na^+ was mobile and replaced H^+ from the carboxylate group $(\text{RCOO})_n$ when the powder was under acid attack. They suggested that Na^+ in the glass component could combine with the carboxylate group $(\text{RCOO})_n$ in the PAA to form sodium carboxylate (COONa) thereby preventing the formation of metal carboxylates.

Kent *et al.*¹⁰⁴ investigating the Na^+ and Ca^{2+} effect in multicomponent glasses, stated that the higher the Na^+ content in these glasses the greater the susceptibility of the glass component towards the acid attack, resulting in a faster setting time in comparison with Ca^{2+} . Furthermore, they reported that a high content of Na^+ in the glass would result in the solubility of the glass surface in an aqueous state.

De Barra and Hill¹⁰⁵ investigated the substitution of Na^+ for Ca^{2+} in two series of glass compositions based on $\text{PSiO}_2\text{-}Q\text{Al}_2\text{O}_3\text{-}0.75\text{P}_2\text{O}_5\text{-}(1\text{-}z)\text{CaO-xCaF}_2\text{-}Z\text{Na}_2\text{O}$ with a high F^- content ($x = 0.75$) and a low F^- content ($x = 0.5$) and monitored the effect on the resulting properties of the cement. The presence of Na^+ in the high F^- content glass

had minimal effect on the resulting cement properties, compared with the dominant influence exerted by the high F^- content. In contrast, in the low F^- content glass, Na^+ had the greater influence on the resulting mechanical properties of the cement, and a significant decrease in the E-modulus was observed. Whereas, in the low F^- content glass with decreased Na^+ content (with low $z_{(Na^+)}$ content), the E-Modulus, fracture strength and toughness also decreased, the CS values were not affected. This was explained by the Na^+ ions complexing with the carboxylate anions and disturbing the ionic crosslinking in the resulting cement matrix. However, in a low F^- content glass with increased Na^+ content (with high $z_{(Na^+)}$ content), the CS values were markedly affected. De Berra and Hill¹⁰⁵ stated that the decrease in the CS values could be an indication that such high degrees of ionic crosslinking exist that this has a reverse effect on the properties of the cement and it becomes brittle. De Barra and Hill¹⁰⁵ suggested that additional investigation was needed to ascertain the influence of Na^+ on the resulting mechanical properties.

1.8.5 Decrease of glass reactivity

Two processes employed for controlling glass reactivity and diffusion of ions into the cement matrix are heat treatment and acid washing.

1.8.5.1 Heat treatment

Preheating the glass powder before mixing with other constituents was observed to improve both the handling properties and the strength of the resultant cement. Brune¹⁰⁶ investigating the effect of preheated aluminosilicate glass powder on the properties of the cement, reported a 10% enhancement of the CS values when the glass powder was preheated at 100°C before the addition of polymeric solution.

Neve *et al.*¹⁰⁷ in their investigation on the consequence of heat treatment on the aluminoborate glass component to form GICs, concluded that the reactivity of the glass towards acid attack was reduced after having heat treated the glass component. Also, the handling characteristics, such as mixing and packing in the mould were improved and the CS values also increased when the glass component was preheated before the addition of acidic solution.

1.8.5.2 Acid washing

Acid washing the glass component of the GIC before the addition of acidic solution delayed the leaching of the ions from the glass structure into the cement matrix. This delay of the ionic crosslinking in the cement matrix, and hence the delay of cation diffusion from the glass structure into the aqueous phase, resulted in an increase in the setting and working time¹⁰⁸.

In their desire to have a direct measurement of the acid degradability of the glass component of the GICs, De Maeyer *et al.*⁶⁷ examined the reactivity of untreated fluoroaluminosilicate glasses towards a dilute acetic acid solution. Acid-washing the glass component resulted in partial ion leaching of the surface of the glass particles, when the treated glass was introduced to the acidic solution, the initial ion leaching process decreased, hence no ions were available on the outer surface of the glass particles. After the initial delay, both the untreated and treated glass behaved in similar manner. De Maeyer *et al.*⁶⁷ stated that treating the glass component with acidic solution was an effective way to adjust the initial ion release, and extend the handling and setting time of the cement.

1.8.6 Glass particle size (PS) and distribution

As well as the reactivity of the glass, glass particle size (PS) can influence the speed of reaction. The smaller the PS of the glass powder, the bigger the surface area, leading to an increase in the chemical kinetics, thus an increase in the speed of reaction⁸. Furthermore, if higher amounts of glass particle are available, which is the source of ions, a higher amount of ions can diffuse from the glass structure into the aqueous form to crosslink with carboxylate anions¹⁰⁹.

The combination of reduced glass PS with a high amount of glass powder content would result in a decreased working time. Generally, the glass PS and the distribution of glass powder content have a considerable influence on the resulting properties of the cement. It is well known that the mean PS in C-GICs are larger than other restorative materials⁸.

The role of PS and size distribution of the glass component in GICs regarding the handling, setting time, clinical handling and the CS of the resulting cement were investigated by Prentice *et al.*¹¹⁰. An improvement in CS with a decrease in PS and corresponding increase of surface area was observed and, at low P/L ratio, the working time was extended, due to the ions diffusing out of the glass matrix into the aqueous phase to form ionic crosslinking. In this case, the acid-base reaction was dominant. An increase in the surface area of the glass particles resulted in higher ion diffusion in the aqueous phase, thus reducing the working time. At higher P/L ratio, the handling of the paste was better than the rate of reaction, although there was a decrease in the working time. In this case the acid-base reaction was in the background and the paste viscosity was in the foreground¹¹⁰.

1.9 Fluoride release and recharge ability

One of the major characteristics of F^- is its anticariogenic action. A number of studies analysed the F^- release from restorative dental materials, such as GICs^{103,111,112,113,114,115,116,117,118,119,120}. Whilst it is believed that the release of F^- ions in the oral environment has a beneficial cariostatic effect^{103,121}, to date the precise amount of F^- ions required to inhibit caries remains unknown¹¹¹.

Several processes are involved in the cariostatic effect of F^- in the oral environment. Firstly, a decrease in tooth mineralisation, coupled with an increase in tooth remineralisation take place¹²², and secondly, the benefits for both hygiene as a result of the repression of microbial growth in the presence of F^- ions^{102,121}.

The F^- release of GICs has been divided into two stages¹¹⁶. First, is the short term (up to 24 hours) discharge of F^- ions on the surface of the restorative material into the oral environment, followed by a long-term release, via a diffusion process from the inner cement¹¹⁶. Several authors have reported that the maximum release of F^- occurs in the first 48 hours, followed by a rapid decline to a modest, residual level which endures up to a few years F^- release^{115,118}.

Generally, several factors can influence the F^- ion release into the oral environment. These factors may consist of storage media, such as deionized/distilled water and artificial saliva (AS)¹²⁶, plaque formation¹²³, the pH¹²⁴ and the F^- ion source (glass component¹²⁵ of the GIC).

In vitro experiments demonstrated that the F^- release in AS was not as high as in deionised or distilled water. This was related to similar ion distribution, as between AS, saliva and GIC, which caused a low diffusion gradient. Conversely, the dissimilar ion distribution, as between deionized water and GIC, caused a higher diffusion gradient¹²⁶.

Plaque formation can hinder the F⁻ ion release, or even the formation of saliva set down on the tooth structure and after ca. 10 minutes can hinder or delay the F⁻ ion release. A reduction of pH in the oral environment can cause dissolution of the restorative material, resulting in a higher F⁻ ion release¹²⁶.

Furthermore, GICs possess the ability to recharge F⁻ ions. This recharge ability of the restorative material is dependent on permeability and frequent exposure to the F⁻ source¹²⁷.

The recharge ability of the restorative materials if exposed to a F⁻ source is believed to be superficial, since the recharge occurs rapidly¹²⁸.

It is well known that the ionic crosslinking in the cement matrix progresses over a few years and is responsible for the increasing strength of the restorative material. Therefore, permeability of the restorative materials plays a very important role of the resultant cement properties and the F⁻ ion release. The diffusion of F⁻ ions from a mature cement matrix is further reduced because of the tight crosslinked cement structure¹²⁹. Air voids and cracks facilitate the diffusion process, but might decrease the strength of the restorative material¹²⁰.

Fluoride not only has an effect on the de- and re-mineralisation of the tooth structure, but also affects the physiology of microbial cells, including *Streptococci*^{130,131}. Hydrogen fluoride (HF) is formed easily under acidic condition ($H^+ + F^- \leftrightarrow HF$). The bacteria cell membrane has a higher permeability to HF, therefore HF enters into the bacterial cell easily. In the cytoplasm HF dissociates into H⁺ and F⁻ ions which causes the bacterial cell to become more alkaline than the exterior environment¹³². The presence of intracellular F⁻ ions inhibits glycolytic enzymes, resulting in a decrease of acid (H⁺) production. The cytoplasmic pH increases with the presence of F⁻ ions in the cytoplasm, decreasing the acid production and the acid tolerance of

the *Streptococcus mutans* (*S. mutans*)¹³⁰. The presence of F⁻ ions also inhibits the plasma membrane H⁺-ATPase's (H⁺ is one of the substrates as well as one of the products), hence excreted H⁺ are brought back into the bacteria cell, causing a decrease of the H⁺ excretion from the bacteria cell^{133,134,135}.

1.10 Antimicrobial effectiveness

S. mutans are Gram-positive, anaerobic, spherical bacteria and are the major cause of tooth decay. Of all the oral streptococci, *S. mutans* are thought to develop and promote the most caries¹³⁶. Mainly the *Streptococcus* genus nourish on food debris in the oral cavity. *S. mutans* are acidogenic; they attach to the enamel and metabolize sucrose to lactic acid that is released into the resultant meshwork¹³⁷. The tooth pellicle is generally colonized by early colonizers. Co-aggregation contributes to sequential binding and colonization (including *Streptococcus mitis* (*S. mitis*), *Streptococcus gordonii* (*S. gordonii*) and *Streptococcus sanguinis* (*S. sanguinis*)). The acidic environment favours demineralisation of the dental material. The dental substance is composed of 98% hydroxyapatite (HAP) crystals (Ca₅(PO₄)₃OH)¹³⁸. After digesting sucrose the microorganisms secrete, a sticky polymer of sucrose that cannot be removed solely by saliva. The acidic environment makes the hard and highly mineralized enamel susceptible to caries. The acid in the plaque causes demineralization of the outer mineral structure and progresses into the inner dental substance (dentin), finally resulting in decaying of the tooth structure and the formation of a cavity¹³⁶.

Respective *in vitro* studies and *in vivo* studies established the inhibitory effect of fluoride on bacterial growth^{123,139,140,141}. Because of the porous matrix of the tooth the F⁻ ions may become incorporated in the matrix¹⁴². This makes the tooth matrix become more resistant to the acidic environment (formation of fluorohydroxyapatite

(FAP)) and impeded dissolution of the tooth structure. F^- ions with an ionic radius of 1.36 nm replace OH^- ions (ionic radius of 1.40 nm) of the HAP matrix, resulting in the formation of the more resistant FAP¹⁴³. The acidic environment causes a reduction in pH and release of Ca^{2+} and PO_4^{3-} ions into the oral cavity; this was illustrated through *in vivo* and *in vitro* experiments^{144,145}. During the demineralization, the F^- ions complex to CaF_2 crystals, which position themselves on and penetrate into the tooth structure during the remineralization¹⁴⁴. However, it is still unclear as the precise level of fluoride concentration that is needed to have an antimicrobial effect and suppress the dissolution of the tooth structure by lactic acid¹¹⁵.

1.11 Experimental methods for GIC characterisation

Several experimental methods were used to characterize the mechanical properties of the resulting restorative dental materials:

- compressive strength (CS),
- diametral tensile strength (DTS),
- flexural strength (FS),
- Vickers hardness (HV),
- nano-indentation and
- wear rate (WR).

The first three methods were conducted according to the British Standards (BS) ISO 9917-1:2007^{75,146} and the last three methods give information about the outer surface characteristics of GICs.

CS measurements are an important indication for mastication forces¹⁴⁷. The British Standards Institution adopted the DTS¹⁴⁶, as it is not feasible to determine the tensile

strength of brittle materials. In the DTS testing, the specimens are placed across the diameter, while in CS the specimens are placed vertically on the Instron plate¹⁴⁸. Generally, the tensile strength of brittle materials is significantly lower than their compressive strength. Prosser *et al.*¹⁰⁹ suggested that FS measurements (or three point bending tests) are more convenient and reliable to evaluate the tensile strength of a brittle material. Various studies have reported CS and DTS data^{6,27,149}, whereas FS data are rarely reported^{70,109,150}.

Generally, the hardness of a material gives an indication of its wear resistance¹⁵¹. The nano-indentation was performed, which gives an indication of the hardness and the creep characteristics of the restorative material^{152,153}.

Table 1-1 gives a concise summary of the existing literature regarding the above mentioned testing procedures. GICs have been investigated since 1970¹⁸, a wide spectrum of research was conducted, therefore the literature was restricted to the above mentioned test procedures regarding GICs. Additional explanation of the literature is given in the relevant chapters of this work.

Table 1-1: Concise summary of available literature regarding GIC characterisation.

Author (ref)	Performed experiments	GIC material Type (P/L ratio)	Sample dimensions (mm) (amount of samples; time of testing)	Paper content	Strength values		
Yap et al. ³⁹	Micro-indentation	GIC 1: Beautiful <i>Giomer</i> GIC 2: Dyract Extra <i>COM</i> GIC 3: Fuji II LC <i>RM-GIC</i> GIC 4: Fuji IX GP Fast <i>HV-GIC</i>	3L x 3W x 2D (n=7; 30d).	Microindentation with several commercial GICs over 30 days.	GIC	Hardness (MPa)	Modulus (GPa)
					GIC 1	712.45±37.46	110.81±4.7
					GIC 2	539.16±57.17	95.5±7.35
					GIC 3	475.03±69.72	106.5±9.61
					GIC 4	549.36±104.93	125.32±26.47
Xu & Burgess ¹⁵⁴	CS, fluoride release	GIC 1: Fuji IX <i>HV-GIC</i> GIC 2: Miracle Mix <i>C-GIC</i> GIC 3: Ketac-Molar Aplicap <i>C-GIC</i> GIC 4: Ketac-Silver Aplicap <i>MR-GIC</i> GIC 5: Vitremer <i>RM-GIC</i> GIC 6: Photac-Fil Aplicap <i>RM-GIC</i> GIC 7: Fuji II LC <i>RM-GIC</i> GIC 8: Compoglass <i>COM</i> GIC 9: F2000 <i>COM</i> GIC 10: Dyract AP <i>COM</i> GIC 11: Hytac <i>COM</i> GIC 12: Ariston pHc <i>CP</i> GIC 13: Surefil <i>CP</i> GIC 14: Solitaire <i>CP</i> GIC 15: Teric Ceram <i>CP</i>	CS: 4Ø x 9H (n=10; 21d).	CS and fluoride release of different GICs.	GIC	CS (MPa)	
					GIC 1	117±22	
					GIC 2	127±7.1	
					GIC 3	168±14	
					GIC 4	184±14	
					GIC 5	150±12	
					GIC 6	154±18	
					GIC 7	166±11	
					GIC 8	227±11	
					GIC 9	231±18	
					GIC 10	262±16	
					GIC 11	254±20	
					GIC 12	285±18	
					GIC 13	290±45	
					GIC 14	265±22	
					GIC 15	286±26	

Author (ref)	Performed experiments	GIC material Type (P/L ratio)	Sample dimensions (mm) (amount of samples; time of testing)	Paper content	Strength values					
Mitra & Kedrowski 147	CS, FS, DTS	GIC 1: Fuji II C-GIC (HM) GIC 2: Fuji Cap II C-GIC (EN) GIC 3: Fuji II LC RM-GIC GIC 4: Miracle Mix MR-GIC GIC 5: Ketac-Fil C-GIC GIC 6: Ketac-Silver MR-GIC GIC 7: VariGlass VLC RM-GIC GIC 8: Vitremer Tri-cure RM-GIC	CS: 4Ø x 8H (n=ns; 1d, 1w, 3m, 6m, 1y). DTS: 4Ø x 2H (n=ns; 1d, 1w, 3m, 6m, 1y). FS: 25L x 2D x 2W (n=ns; 1d).	Long-term mechanical properties	GIC	CS 1d (MPa)	CS 1y (MPa)	FS 1d (MPa)	DTS 1d (MPa)	DTS 1y (MPa)
					GIC 1	210±23	219±23	14.2±1.2	16.3±0.9	18.5±2.2
					GIC 2	156±21	220±16	20.5±2.5	7.9±1.6	16.1±1
					GIC 3	203±12	209±10	56.6±3.8	40.7±0.5	40±1.1
					GIC 4	128±3	167±16	10.6±1.3	7.0±0.9	10.2±0.7
					GIC 5	172±6	213±21	12.2±2.2	15.4±1.7	20.3±2.1
					GIC 6.	170±4	219±27	26±2.1	14.1±1.4	16.5±1.5
					GIC 7	190±9	173±3	20.3±3.8	25.9±1.1	27.8±0.7
					GIC 8	229±5	253±5	61.7±4.1	40.9±2.6	46.3±2.5
Xie <i>et al.</i> ²⁷	FS, CS, DTS, KHN, WR	GIC 1: Ketac-Bond C-GIC (3/1) GIC 2: α-Silver MR-GIC (4.2/1) GIC 3: α-Fill (2.7/1) GIC 4: Ketac-Silver MR-GIC (EN) GIC 5: Ketac-Fil (3.2/1) GIC 6: Ketac-Molar (3.1/1) GIC 7: Fuji II (2.7/1) GIC 8: Vitremer (2.5/1) GIC 9: Fuji II LC (3.2/1) GIC 10: Photac-Fil (3.2/1)	CS: 4Ø x 8L (n=6; 1w). DTS: 4Ø x 2L (n=6; 1w). KHN, WR: 3.5Ø x 5L (n=9; 1w). FS: 2W x 2D x 25L (n=7; 1w).	Mechanical properties explained via microstructure.	GIC	FS (MPa)	CS (MPa)	DTS (MPa)	KHN (kg mm⁻²)	WR (µm/rev)
					GIC 1	11.1±1.1	225.7±7.3	20±0.8	108.5±5.2	1.0734±0.130
					GIC 2	31.4±3.4	176±6.5	18.7±0.9	45.36±1.12	0.6894±0.059
					GIC 3	26.8±3.1	196.5±8.3	18.2±1	87.34±9.52	1.1018±0.069
					GIC 4	22.9±1.9	211.8±3.2	22.1±1.3	29.74±3.08	1.1001±0.097
					GIC 5	22.6±2.5	251.2±10	25.5±0.6	176.8±12.8	0.7983±0.030
					GIC 6	21.2±3.1	301.3±10.1	23.8±1.1	108.4±5.8	0.8557±0.049
					GIC 7	26.1±3.9	202±10	20.1±0.6	83.15±8.2	0.8140±0.072
					GIC 8	82.1±3.3	265.3±7.5	47.5±0.9	66.4±6.89	0.9446±0.066
					GIC 9	71.1±3.6	306.2±6.8	44.4±1.1	84.56±6.58	1.4270±0.046
					GIC 10	74.4±5.1	243.5±7.9	37.9±1.7	63.6±7.28	1.0968±0.077

Author (ref)	Performed experiments	GIC material Type (P/L ratio)	Sample dimensions (mm) (amount of samples; time of testing)	Paper content	Strength values				
Nomoto & McCabe ⁶⁴	CS	KC: Ketac-Cem (1/1) KM: Ketac-Molar (1/2)	CS: 4Ø x 6H (n=20; 1d).	Different mixing methods (HM, shaking and rotating) effect on CS.	GIC		CS (MPa)		
					KC (HM)		194.1±19.8		
					KC Aplicap (shaking)		112.4±27.5		
					KC Aplicap (rotating)		91.8±33.5		
					KC Maxicap (shaking)		119.3±19.9		
					KC Maxicap (rotating)		120.4±25.4		
					KM (HM)		219.1±23.7		
					KM Aplicap (shaking)		222.4±22.6		
KM Aplicap (rotating)		222.4±22.6							
Behr et al. ⁷¹	HV, WR, FS	GIC 1: Harvard ZOPC (1.8/1.5) GIC 2: Durelon CC (1/1) GIC 3: Ketac Cem C-GIC (6.26/1) GIC 4: Merron Plus RM-GIC (2/1)	HV: 2W x 2D x 25L (n=8; 24h). WR: 50,000cycles (n=12; 24h). FS: 2W x 2D x 25L (n=8; 24h).	Cement properties change with P/L ratio and mixing method.	GIC		VH (MPa)	Wear (µm)	FS (MPa)
					GIC 1		37.3±7	154.2±22	-----
					GIC 2		12.5±2.6	112.8±23	----
					GIC 3		113±3.4	31±2.4	-----
					GIC 4		31.6±1.1	194±7	53.2±1.8
Ellakuria et al. ¹⁵⁵	HV	GIC 1: Ketac-Fil Aplicap C-GIC GIC 2: Ketac-Molar C-GIC GIC 3: Ketac-Silver MR-GIC GIC 4: Vitremer RM-GIC GIC 5: Photac-Fil Aplicap RM-GIC GIC 6: Fuji II LC RM-GIC	HV: 5Ø x 4L (n=45; 1d, 7d, 15d, 1m, 3m, 6m, 12m).	HV measurements after 1 year storage in water	GIC		HV 1d (MPa)	HV 7d (MPa)	HV 1m (MPa)
					GIC 1		823.8±75.1	990.49±59.04	1177±33.25
					GIC 2		814±100.3	980.7±58.25	1177±31.38
					GIC 3		647.3±12.85	657.1±10	696.3±11.77
					GIC 4		411.9±47.47	735.5±14.61	735.5±15
					GIC 5		519.8±15.4	559±13.73	568.8±14.61
					GIC 6		460.9±16.57	480.5±15.69	500.2±16.67

Author (ref)	Performed experiments	GIC material Type (P/L ratio)	Sample dimensions (mm) (amount of samples; time of testing)	Paper content	Strength values			
					GIC	SR (μm)	VH (MPa)	
Gladys et al. ⁶	SR, HV,	GIC 1: Silux Plus CP GIC 2: Z100 CP GIC 3: Dyract COM GIC 4: Fuji II LC RM-GIC (EN) GIC 5: Fuji II LC RM-GIC (HM) GIC 6: Geristore CP GIC 7: Ionosit-Fil RM-GIC GIC 8: Photac-Fil RM-GIC GIC 9: Variglass RM-GIC GIC 10: Vitremer RM-GIC GIC 11: HIFI Master Palette (Shofu) C-GIC GIC 12: Ketac-Fil C-GIC	SR & HV: 5 \emptyset x 5H (n=8; 1m).	Physico-mechanical characterisation of GICs.	GIC	SR (μm)	VH (MPa)	
					GIC 1	0.02 \pm 0	539 \pm 49	
					GIC 2	0.02 \pm 0	1187 \pm 39	
					GIC 3	0.1 \pm 0.05	638 \pm 49	
					GIC 4	0.33 \pm 0.07	981 \pm 78	
					GIC 5	0.35 \pm 0.05	1207 \pm 108	
					GIC 6	0.41 \pm 0.3	422 \pm 49	
					GIC 7	0.09 \pm 0.01	1128 \pm 137	
					GIC 8	0.84 \pm 0.39	824 \pm 127	
					GIC 9	0.12 \pm 0	1,295 \pm 137	
					GIC 10	0.25 \pm 0.06	863 \pm 69	
					GIC 11	0.52 \pm 0.1	1020 \pm 137	
					GIC 12	0.29 \pm 0.04	1138 \pm 461	
Prosser et al. ⁹³	FS	GIC 1: Experimental glass G200 + PAA (13,900 mm) GIC 2: Experimental glass G200 + PAA (56,000 mm)	FS: 25L x 3D x 3W (n=6; 1d).	Effect of experimental glass composition on FS with different polymers.	GIC	FS (MPa)		
					GIC 1	9.7 \pm 2.3		
					GIC 2	20.4 \pm 5.8		
Gee et al. ¹⁵⁶	Wear	GIC 1: Ketac-Fil Aplicap C-GIC GIC 2: Fuji Cap II C-GIC GIC 3: Chemfil Superior C-GIC GIC 4: Shofu High Dense MR-GIC GIC 5: Ketac-Silver MR-GIC GIC 6: Photac-Fil Aplicap RM-GIC GIC 7: Fuji II LC Capsule RM-GIC GIC 8: Vitremer RM-GIC	20,000 cycles (n=10; 8h, 1w, 2w, 4m, 1y).	Wear measurements over 1 year period.	GIC	Wear 8h (μm)	Wear 1w (μm)	Wear 1y (μm)
					GIC 1	125	91	37
					GIC 2	128	104	57
					GIC 3	128	97	53
					GIC 4	116	57	27
					GIC 5	95	89	52
					GIC 6	522	350	152
					GIC 7	308	202	138
					GIC 8	211	135	82

Author (ref)	Perfor med experi ments	GIC material Type (P/L ratio)	Sample dimensions (mm) (amount of samples; time of testing)	Paper content	Strength values				
					GIC	CS 1h (MPa)	CS 1d (MPa)	CS 7d (MPa)	CS 30d (MPa)
Matsuya <i>et al.</i> ¹⁵⁷	CS, FTIR	GIC 1: Tokuso Ionomer C-GIC (1.9) GIC 2: Fuji I C-GIC (1.8) GIC 3: Livcarbo ZPCC (2) GIC 4: Experimental glass powder (1.9)	CS: 4Ø x 6L (n=4-8; 1h, 2h, 4h, 8h, 1d, 7d, 30d).	CS over 30 days.	GIC	CS 1h (MPa)	CS 1d (MPa)	CS 7d (MPa)	CS 30d (MPa)
					GIC 1	ca. 90	ca. 120	ca. 150	ca. 180
					GIC 2	ca. 120	ca. 170	ca. 180	ca. 200
					GIC 3	ca. 50	ca. 55	ca. 60	ca. 55
					GIC 4	ca. 45	ca. 70	ca. 80	ca. 95
Tang & Xu ¹⁵⁸	CS	Experimental glass powder + TA+ acrylic acid/Itaconic acid	CS: (1d, 1w, 1m, 2m, 4m)	CS at different time points in different storage medium (water, air, oil).	CS 1d (MPa) Water 37±1°C	CS 1m (MPa) Water 37±1°C	CS 1d (MPa) Air 37±1°C	CS 1m (MPa) Air 37±1°C	
					125.6±6.3	177±38.2	238.8±21.2	212.4±30.3	
Fleming <i>et al.</i> ¹⁵⁹	CS, ST	GIC 1: ChemFil (7.4/1) GIC 2: ChemFil (6.66/1) GIC 3: ChemFil (5.92/1) GIC 4: ChemFil (3.7/1)	CS: 6Ø x 4H (n=20; 24h). ST (n=3).	Comparing CS at 24h with different powder content at a constant polymer volume	GIC	CS (MPa)	ST (min)		
					ChF1	102.1±23.1	2.5±0.03		
					ChF2	93.7±22.9	2.8±0.3		
					ChF3	82.6±18.5	3.1±0.06		
					ChF4	55.7±17.2	3.5±0.01		
Towler <i>et al.</i> ¹⁶⁰	Nano-indentation	Fuji IX HV-GIC	2Ø x 2L (n=8; 7.5h).	Nano-indentation measurements of Fuji IX chemically and ultrasonically cured.	GIC	Hardness (mean) (GPa)	Hardness (max) (GPa)	Hardness (min) (GPa)	
					Fuji IX Chemically cured	0.176	0.386	0.022	
					Fuji IX Ultrasonically cured	2.62	4.45	1.04	
Pearson & Atkins ⁷⁰	FS	GIC 1: Chemfil II GIC 2: Opusfil GIC 3: Rexodent GIC 4: Ketac Fil C-GIC GIC 5: Ketac-Silver MR-GIC	FS: 25L x 2D x 2W (n=5; 1h, 3h, 6h, 1d, 2d, 4d, 5d, 6d, 7d, 3m).	FS over 3 months.	GIC	FS 1h (MPa)	FS 1d (MPa)	FS 7d (MPa)	
					GIC 1	30.8±9.1	29±9	36.3±10.4	
					GIC 2	15±1.7	36.3±7	46.9±23	
					GIC 3	16.1±6.7	39.1±6.7	69.8±22.6	
					GIC 4	14.8±3.5	29.1±1.7	29.5±2.5	
					GIC 5	12.8±4.6	30±5.3	27.7±6.3	

Author (ref)	Performed experiments	GIC material Type (P/L ratio)	Sample dimensions (mm) (amount of samples; time of testing)	Paper content	Strength values						
Bonifacio <i>et al.</i> ¹⁶¹	CS,FS, KH	GIC 1: Riva Self cure HV-GIC GIC 2: Fuji IX HV-GIC GIC 3: Hi Dense HV-GIC GIC 4: Vitro Molar HV-GIC GIC 5: Maxxion R HV-GIC GIC 6: Ketac Molar Easymix HV-GIC	FS: 25L x 2D x 2W (n=10; 24h in paraffin). CS: 4Ø x 6H (n=10; 1h, 1d, 7d). KH: 8Ø x 4H (n=2; 24h in paraffin).	Comparison of mechanical properties of GICs used in ART.	GIC	CS 1d (MPa)	FS 1d (MPa)	KH 1d			
					GIC 1	126.5±18.5	23.9±10.7	38.7±12.9			
					GIC 2	166.7±31.3	33.3±6.1	68.7±10.9			
					GIC 3	159.2±26.7	33.3±3.9	55.8±11.5			
					GIC 4	135.7±48.3	19.2±4.0	37.0±5.5			
					GIC 5	130.3±23.2	29.5±3.6	50.4±5.3			
					GIC 6	177.8±28.2	34.5±7.2	73.8±9.4			
Kleverlaan <i>et al.</i> ¹⁶²	CS	GIC 1: Fuji IX FAST GIC 2: Fuji IX HV-GIC GIC 3: Ketac Molar Quick GIC 4: Ketac Molar	CS: 3.15Ø x 5H (n=8; 15m, 1h, 1d, 28d).	Comparison of external applied 'command' set application (SC, UC and HC) on the mechanical properties.	GIC 1	CS 15m (MPa)	CS 1h (MPa)	CS 1d (MPa)	CS 28d (MPa)		
					SC 23°C	53.3±5.5	83.9±9.5	155.7±37.0	194.4±27.4		
					UC	88.1±2.9	120.8±10.2	188.8±14.2	218.3±32.3		
					HC 70°C	122.1±18.7	127.2±9.8	193.3±26.8	240.1±15.9		
Bresciani <i>et al.</i> ¹⁴⁸	DTS, CS	GIC 1: Bioglass R C-GIC (3/1) GIC 2: Vitro Molar C-GIC (3/1) GIC 3: Fuji IX HV-GIC (3.6/1)	DTS: 6Ø x 3H (n=5; 1h, 1d, 7d). CS: 6Ø x 12H (n=5; 1h, 1d, 7d).	Comparison of CS and DTS at different time points with different GICs.	GIC	CS 1h (MPa)	CS 1d (MPa)	CS 1w (MPa)	DTS 1h (MPa)	DTS 1d (MPa)	DTS 1w (MPa)
					GIC 1	42.3±6.83	83.39±16.6	95.67±15.27	5.54±0.529	6.58±0.808	8.74±1.396
					GIC 2	70.26±6.05	125.67±6.95	148.03±17.8	8.27±0.475	9.43±0.822	10.76±3.072
					GIC 3	99.51±7.91	147.93±18.18	155.47±9.02	7.24±0.699	11.96±1.514	13.72±2.834

Author (ref)	Performed experiments	GIC material Type (P/L ratio)	Sample dimensions (mm) (amount of samples; time of testing)	Paper content	Strength values						
					GIC	CS 1h (MPa)	CS 12m (MPa)	DTS 1h (MPa)	DTS 12m (MPa)	FS 1h (MPa)	FS 12 m (MPa)
Cattani-Lorente <i>et al.</i> ¹⁴⁹	CS, DTS, FS	GIC 1: Chemfil II (EN) GIC 2: Chemfil II (HM) GIC 3: Ketac-Fil Aplicap C-GIC (EN) GIC 4: GC Fuji II GIC 5: Ketac-silver RM-GIC (EN)	CS: 4Ø x 6L (n=3-4; 24h, 2m, 6m, 12m). DTS: 4Ø x 6L (n=3-4; 24h, 2m, 6m, 12m). FS: 25L x 2D x 2W (n=2-6; 24h, 2m, 6m, 12m).	CS, DTS and FS over 12 month storage in water.	GIC	CS 1h (MPa)	CS 12m (MPa)	DTS 1h (MPa)	DTS 12m (MPa)	FS 1h (MPa)	FS 12 m (MPa)
					GIC 1	197.5±12.4	138±18.8	12.2±3.8	6.1±0.4	9.2±4.2	17.3±5.5
					GIC 2	134.4±37.3	163±13	10.8±2.8	10.2±4.2	25±5.7	5.2±0.6
					GIC 3	152.4±10.6	150.4±19.5	14±4	11.8±3.6	10.3±3.6	9.4±3.3
					GIC 4	158.9±14.1	127.2±38.3	8.7±2	7.4±0.9	3.5±0.6	3.7±1.9
					GIC 5	112.6±26.1	142.9±8.7	12.9±2	11.7±2	6.9±0.5	12.8±2.4
Crisp <i>et al.</i> ²¹	CS, WIN, WHN	GIC 1: ASPA II (2/1) GIC 2: ASPA III (3/1) GIC 3: ASPA IV (3.5/1) GIC 4: Durelon (3/1) GIC 5: Super Syntrex (4/1)	WHN, WI: 20Ø x 1.5W (n=3; 15min, 1d, 1m, 1y). CS: 6Ø x 12L (n=ns; 15min, 1d, 1m, 1y).	Long-term hardness and CS.	GIC	WIN (WHN*) 1d (N/mm ²)	WIN (WHN*) 1y (N/mm ²)	CS 1d (N/mm ²)	CS 1y (N/mm ²)		
					GIC 1	90 ¹ (160*)	67 (290*)	-----	-----		
					GIC 2	77 (220*)	74 (240*)	130	225		
					GIC 3	65 (310*)	66 (300*)	170	230		
					GIC 4	122 (87*)	73 (240*)	-----	-----		
					GIC 5	50 (520*)	46 (610*)	-----	-----		

ART: atraumatic restorative treatment; **CC:** carboxylate cement; **C-GIC:** conventional GIC; **COM:** compomer; **CP:** composite; **CS:** compressive strength; **d:** day; **D:** depth; **DTS:** diametral tensile strength; **EN:** Encapsulate; **FS:** Flexural strength; **FTIR:** Fourier transform infrared; **h:** hours; **H:** height; **HC:** heat source; **HV-GIC:** high viscous GIC; **HM:** hand mixing; **HV:** Vickers hardness; **KH:** Knoop microhardness; **L:** length; **m:** month; **min:** minutes; **MR-GIC:** metal reinforced GIC; **mm:** molar mass; **n:** number of specimens; **ns:** not specified; **PAA:** poly acrylic acid; **PMRC:** polyacid-modified resin composite; **ref:** reference; **RM-GIC:** Resin modified GIC; **SC:** **ST:** standard curing; setting time; **SR:** surface roughness; **UC:** ultrasonic excitation; **w:** week; **WHN:** woxen hardness number; **W:** width; **WIN:** wallace indentation number; **WR:** Wear rate; **y:** year; **ZPCC:** zinc polycarboxylate cement; **ZOPC:** zinc oxide phosphate cement; **Ø:** diameter; **±** standard deviations.

1.12 Aims and objectives

GICs are versatile materials and are indicated for different clinical applications; however, their inferior mechanical strength limits their clinical usage. The primary aim of this project was to study the change in the mechanical strength and setting properties by substituting bigger cations for smaller cations. Furthermore, there is some evidence that Sr^{2+} has an antibacterial effect^{117,200} and this would be advantageous for clinical application. Substituting the bigger Ba^{2+} and Sr^{2+} cations for the smaller Ca^{2+} cation alters the original glass structure through the formation of non-bridging oxygens (NBOs)¹⁶³. These NBOs in turn affect the cation diffusion process in these glasses upon acid attack. The effect barium (Ba^{2+}) and strontium (Sr^{2+}) substitutions for calcium (Ca^{2+}) may have on the setting reaction and other properties of the resultant glass ionomer cements was studied. The Ba^{2+} and Sr^{2+} substitution were performed on glass composition $4.5\text{SiO}_2\text{-}3\text{Al}_2\text{O}_3\text{-}1.5\text{P}_2\text{O}_5\text{-}3\text{CaO}\text{-}2\text{CaF}_2$, the substitutions being accomplished using a known melt quench route. Ba^{2+} and Sr^{2+} were introduced into the Ca-glass structure as substitutes for Ca^{2+} on a molar basis of 75% barium and 75% strontium.

In this project, the effect of the disturbance in the glass component of the experimental GICs was observed. Furthermore, the effect of the disturbance in the glass component upon the properties of the resulting cement was interpreted as outlined below.

1. The acid-base neutralisation process over 60 minutes for all three GIC compositions was observed with a real time FTIR.
2. The setting time of the three experimental GICs at different P/L ratios (2:1 and 3:1) was evaluated using a resistance to penetration test method.
3. The fluoride release experiment was divided into two stages. In the first stage, the fluoride release in AS and deionized water of the three experimental

GICs over 40 days was observed. During the second stage of the experiment, the specimens after 40 days of fluoride release were exposed in a commercial fluoride solution and the fluoride release was measured again at different time intervals up to 24 hours.

4. The antimicrobial effect of the three GIC compositions at different time intervals up to 48 hours was observed.
5. The surface characteristics of the experimental GICs was observed by three different methods:
 - a. Vickers hardness (HV); the mean hardness value for a total of 9 indents at 1 hour and 1 month after mixing was measured and calculated.
 - b. Nano-indentation; the mean hardness and reduced modulus value for a total of 108 indents at 1 hour, 1 day, 1 week and 1 month after mixing was measured and calculated.
 - c. Reciprocating ball-on-flat; the wear behaviour of the three GIC compositions was measured 1 day after mixing. The wear volume was calculated via three wear scars across the specimens.
6. Three mechanical testings were conducted:
 - a. diametral tensile strength (DTS),
 - b. compressive strength (CS) and
 - c. flexural strength (FS)

at 1 hour, 1 day, 1 week and 1 month after mixing. The mean value of 15 measurements for each time point of the test methods was calculated. Furthermore, the compressive, tensile and flexural E-modulus was calculated from the relevant stress-strain curves.

2 Materials and methods

The calcium base glass composition used in this work is $4.5\text{SiO}_2\text{-}3\text{Al}_2\text{O}_3\text{-}1.5\text{P}_2\text{O}_5\text{-}3\text{CaO}\text{-}2\text{CaF}_2$. Barium and strontium were introduced into the glass structure by substituting calcium in the molar amount of 75% as shown in Table 2-1¹⁶³. The glass powders were produced by a well-known melt quench route⁷⁶, as described in detail by Wang and Stamboulis¹⁶³.

Table 2-1: Molar composition of barium and strontium substituted aluminosilicate glasses.

Glass ID	Particle size (μm)	SiO_2	Al_2O_3	P_2O_5	CaO	CaF_2	BaO	BaF_2	SrO	SrF_2
Ca-Glass (100%)	7.90 ± 0.13	4.5	3	1.5	3	2	0	0	0	0
Ca-Sr-Glass (75%)	8.87 ± 0.22	4.5	3	1.5	0	1.25	0	0	3	0.75
Ca-Ba-Glass (75%)	7.80 ± 0.42	4.5	3	1.5	0	1.25	3	0.75	0	0

All oxide powders were supplied from Sigma Aldrich and their grade was puriss. The oxide powders used for glass making were silicon dioxide (SiO_2), aluminium oxide (Al_2O_3), phosphorus pentoxide (P_2O_5), calcium carbonate (CaCO_3), calcium fluoride (CaF_2), strontium carbonate (SrCO_3), strontium fluoride (SrF_2), and barium fluoride (BaF_2). The different batches with the desired oxide compositions were mixed by hand and melted in a conventional furnace (Elite Thermal Systems Ltd, Leicestershire) at 1475°C for 1 h. The glass melt was then quenched directly into deionized water to avoid any phase separation and crystallization and glass frit was formed. The glass frit was ground using a TEMA mill, (TEMA (Machinery) Limited, Germany) for 10 min to obtain a fine glass powder. The powder was finally sieved to obtain less than $45 \mu\text{m}$ glass particles.

2.1 Materials

40 wt% of aqueous poly (acrylic acid) (PAA) ($\text{C}_3\text{H}_4\text{O}_2$)_n solution was supplied by Advanced Healthcare Ltd, Tonbridge, UK. Ca-Glass, Ca-Sr-Glass and Ca-Ba-Glass

experimental glass powders were made by the melt quench route developed at the University of Birmingham¹⁶³. The powder/liquid (P/L) ratio was kept at 2:1 for Ca-GIC and 3:1 for Ca-Sr-GIC and Ca-Ba-GIC (Table 2-2).

2.1.1 Poly (acrylic acid) (PAA)

A 40wt% PAA aqueous solution was supplied by Advanced Healthcare Ltd, Tonbridge (Mw \approx 60,000 according to the manufacturer). The solution was kept in the fridge for further usage.

2.1.2 Preparation of glass ionomer cements (GICs)

Three groups of experimental cements Ca-GIC, Ca-Sr-GIC and Ca-Ba-GIC were prepared by hand mixing at the adequate powder to liquid ratio shown in Table 2-2. Initially, all three GIC compositions were mixed with a P/L ratio of 3:1. In the case of Ca-GIC, however, the P/L ratio of 3:1 was not appropriate as the viscosity of the paste was too high for homogeneous mixing. Therefore, a lower P/L of 2:1 (Table 2-2) was used.

Table 2-2: Powder/liquid ratio of the resulting GICs.

Cement Specimen	Liquid [weight%]	Experimental glass powder	Experimental glass	P/L ratio
Ca-GIC	PAA [40w%]	Ca 100%	Ca-Glass	2:1
Ca-Sr-GIC	PAA [40w%]	Ca 25%, Sr 75%	Ca-Sr-Glass	3:1
Ca-Ba-GIC	PAA [40w%]	Ca 25%, Ba 75%	Ca-Ba-Glass	3:1

Figure 2-1 illustrates the tools used to prepare GIC samples. GICs were prepared by hand mixing the experimental glass powder (Ca-Glass, Ca-Sr-Glass and Ca-Ba-Glass) and the PAA solution on a poly (methyl methacrylate) (PMMA) mixing plate using a polyethylene (PE) spatula (SciLabware Ltd, Staffordshire) at RT (Figure 2-1). After complete mixing of the glass powder and the polymeric solution, which should not exceed 60 s, the formed cement paste was mechanically packed in the mould

and kept in place with a G-clamp. The samples in the mould were allowed to set for 60 minutes at RT and were taken out of the mould and placed in deionized water in glass containers in a water-bath (Thermo Fisher Scientific Inc., Waltham, United States) kept at $37 \pm 1^\circ\text{C}$. The specimens with non-uniform ends, defects or visually apparent pores were disposed of.

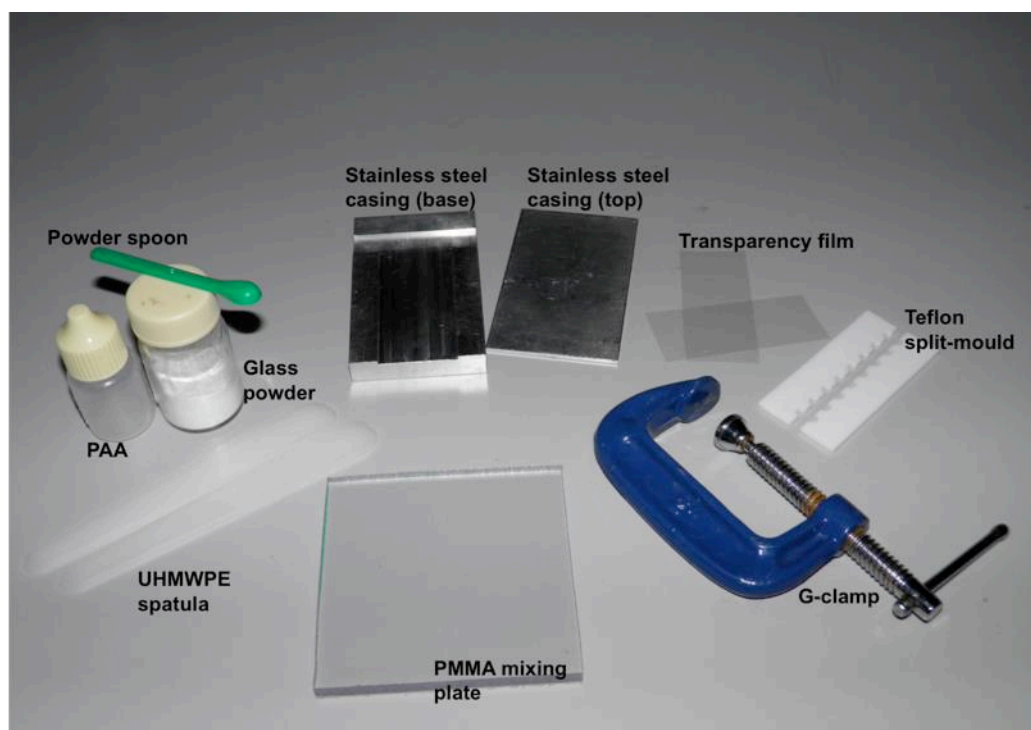


Figure 2-1: Tools for the preparation of GIC samples.

2.2 Methods

2.2.1 Fourier Transform Infrared (FTIR) Spectroscopy

Attenuated Total Reflectance (ATR) attachment of a Nicolet FTIR Spectrometer (Magna-IR 860) was used to collect high-quality real time spectra for Ca-GIC, Ca-Sr-GIC and Ca-Ba-GIC (Table 2-2) over the duration of 60 minutes to investigate and follow the chemical setting reaction of GIC. A deuterated triglycine sulfate (DTGS) detector in a mid-infrared frequency range ($700 - 4000 \text{ cm}^{-1}$) with a resolution of 4 cm^{-1} and conducting 100 scans over 60 minutes was used. An IR source in Transmission E.P.S mode having a velocity of 0.6329 m/s^2 was used to collect the

spectra. The background noise was subtracted from all measurements. The glass powder and polymeric solution as described in Table 2-2 were mixed and quickly loaded on a brass ring of 10 mm diameter positioned centrally on the Golden Gate. The first spectrum was recorded within 1 minute of the initial mixing. A rubber ring was positioned around the Golden Gate and then deionized water was added inside the rubber ring until the sample on the Golden Gate was covered, in order to prevent dislocation and to mimic the humid oral environment. In addition, FTIR spectra of the three glass compositions (Table 2-1) and the PAA were collected. To ensure further examination in the lower region for the glass compositions, below 1200 cm^{-1} , potassium bromide (KBr) disks were prepared by mixing 2 mg of the glass powder (Table 2-1) with 200 mg of KBr powder.

2.2.2 Fluoride release of GICs in artificial saliva and deionized water

Disc-shaped specimens (4 ± 0.1 mm in diameter and 2 ± 0.1 mm in height) of each composition were formed in a Teflon split mould and immersed individually in PE test tubes (Sigma-Aldrich, UK) containing either 4 ml deionized water or 4 ml of a commercial synthetic saliva (Glandosane®, Stada Arzneimittel AG, Hannover, Germany). The composition is shown in Table 2-3.

Table 2-3: The ingredients of each 50 g of aqueous solution of Glandosane® (artificial saliva).

Artificial saliva Ingredients	Concentration in 50 g of artificial saliva	Artificial saliva Ingredients	Concentration in 50 g of artificial saliva
Carboxymethylcellulose sodium	0.5 g	Magnesium chloride (6 H ₂ O)	0.0026 g
Calcium chloride (2 H ₂ O)	0.0073 g	Potassium monohydrogen phosphate	0.0171 g
Sodium chloride	0.0422 g	Sorbic acid	0.025 g
Potassium chloride	0.06 g	Sodium benzoate	0.0295 g
Sorbitol	1.5 g		

The test tubes were then placed in a water-bath (Thermo Fisher Scientific Inc., Waltham, United States) at $37 \pm 1^\circ\text{C}$ and kept for 40 days. The experiment was divided into two stages. During the first stage the fluoride release was measured in deionized water or synthetic saliva over different time periods up to 40 days. During the second stage of the experiment, the specimens after 40 days of fluoride release were exposed in a commercial fluoride solution (Colgate® FluoriGard, Guilford, United Kingdom) for 1 min, 10 min, 1 hour, 6 hours and 12 hours before the fluoride release was measured again at different time intervals up to 24 hours.

The main ingredients of Colgate® FluoriGard Fluoride mouthwash solution are: Aqua, Glycerin, Propylene Glycol, Sorbitol, Sodium Phosphate, Poloxamer 407, Sodium Benzoate, Disodium Phosphate, Aroma, Cetylpyridinium Chloride, Sodium Fluoride, Sodium Saccharin, Cinnamal, CI 19140, and CI 42053. The mouthwash solution contained 225 ppm sodium fluoride. The amount of fluoride release was expressed in parts per million (ppm). The results of ion release are presented as mean cumulative fluoride release of each GIC group (Ca-GIC, Ca-Sr-GIC and Ca-Ba-GIC) in AS and deionized water, respectively. The fluoride release was measured using a single beam photometer Nanocolor 500D (Macherey-Nagel GmbH & Co KG, Dueren, Germany). A tungsten lamp was used as the light source and a silicon photodiode was used as the detector. The photometric accuracy was $\pm 1\%$. The measuring range for the fluoride photometer was from 0.1 to 2.0 mg F^- and the wavelength ranged from 340 to 860 nm (± 2 nm). Fluoride was detected at a wavelength of 620 nm. The reaction mechanism was based on a colourimetric determination of fluoride (lanthanum/alizarin complexone, La-ALC). The molecular structure of La-ALC is illustrated in Figure 2-2 (a). The red coloured La-ALC turns to a purple coloured solution after the water molecules replaced by F^- ions (Fluoro-lanthanum/alizarin complexone, La-ALC-F) as shown in Figure 2-2 (b)¹⁶⁴.

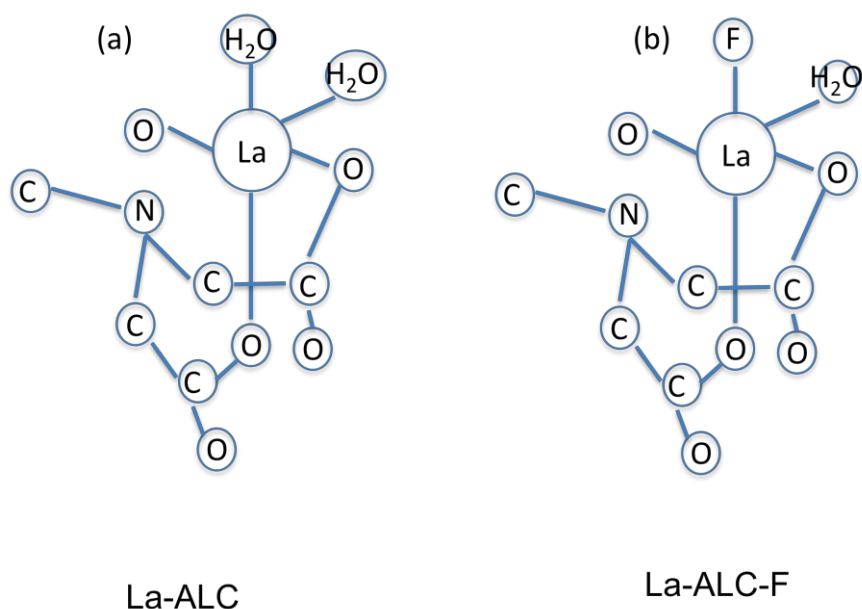


Figure 2-2: Chemical structures of (a) La-ALC and (b) La-ALC-F [Lei *et al.*¹⁶⁴].

2.2.3 Antimicrobial Efficacy Test (AET)

Cultures of *Streptococcus mutans* NTCC10449 (*S. mutans*) were used throughout this work. A freeze-dried ampoule from the NCTC was broken open and the bacterial pellet revived by re-suspending in 500 μ l of Brain-heart infusion (BHI) broth and incubating at 37°C with 5% CO₂ overnight. BHI broth (Oxoid, U.K) was prepared by adding 18.5 g of BHI powder to 500 ml of deionized water and autoclaving the broth to sterilise. As a solid culture media, Columbia agar (Oxoid, U.K) with 5% v/v defibrinated sheep blood (CB) agar was used for cultivation of *S. mutans*. 39 g of powdered agar was added to 1 l of deionized water and dissolved. The dissolved medium was sterilized by autoclaving at 121°C for 90 minutes.

From a freshly inoculated plate the cells were harvested using a sterile plastic loop and resuspended into 5 ml of sterile BHI containing 20% v/v glycerol. 1 ml aliquots were then stored at -80°C to act as starter cultures for experiments. These starter cultures were used daily to inoculate 5 ml of fresh BHI broth and incubated (24 hours) as above. Growth was monitored using culture absorbance, measured optically by a spectrophotometer (Jenway, UK). Bacterial suspensions were

transferred into 1 ml cuvettes (Geneflow, UK), and a light beam was scattered by the cells while passing through the cuvette to determine the optical density (OD). The OD at 600 nm (OD_{600}) of the *S. mutans* was measured and then adjusted with fresh broth to ca. 0.25 ± 0.01 in 1 ml. The original bacterial suspension, adjusted to $\sim 1 \times 10^8$ cfu/ml, was added to the specimens. 150 μ l aliquots of these adjusted suspensions were then transferred into 96 well microtitre trays (MTT) to allow susceptibility testing (Figure 2-3). To measure the antimicrobial effect of the three GIC compositions over time, four specific time points were chosen; 10 min, 3 hours, 1 day (24 hours) and 2 days (48 hours). Figure 2-3 displays duplicate GIC specimens (4 ± 0.1 mm in diameter and 2 ± 0.1 mm in height) that were used in a MTT with 150 μ l duplicate cultures. All experiments were repeated at different time points. The number of viable microorganisms present at each time point was then determined. In order to count viable cells, 20 μ l of the test suspension was serially diluted ten fold six times (10^{-6}) with BHI broth and three 20 μ l spots plated onto CB plates and incubated for each dilution. For dilutions where individual colonies could be counted, the average number of viable colony forming units (CFUs) per ml of original suspension was calculated (Figure 2-4).

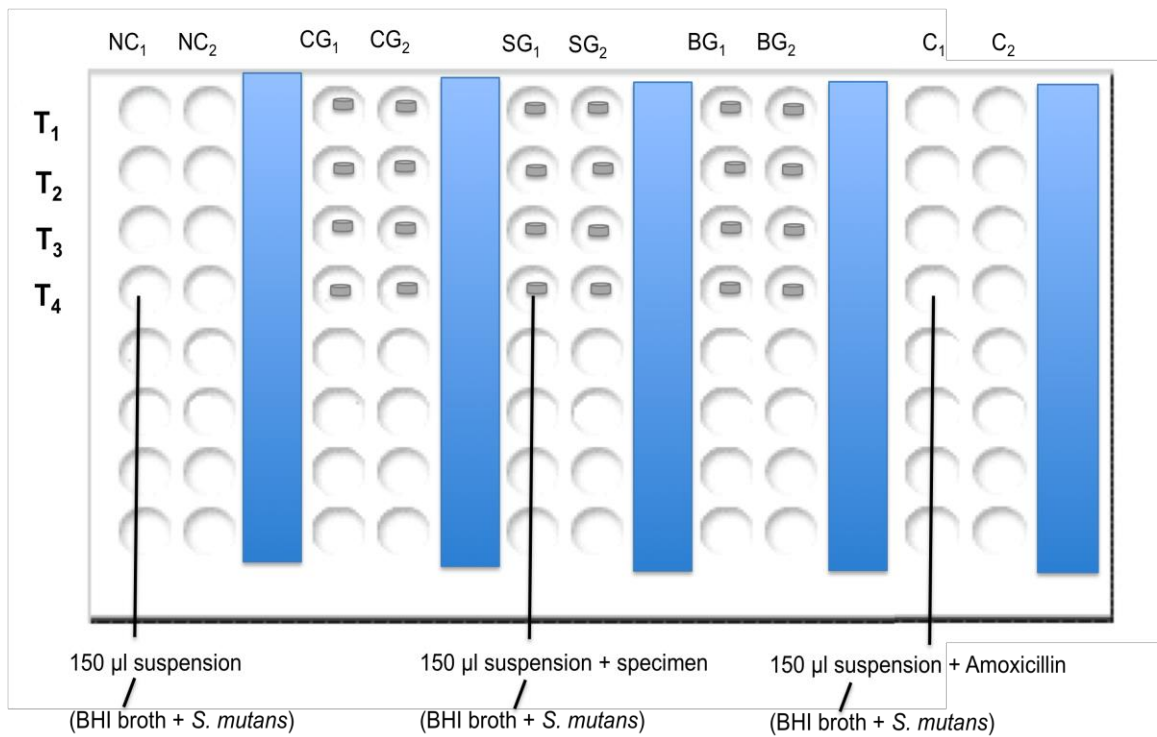


Figure 2-3: MTT plate containing GIC specimens allowing sampling at different time points with 150 µl suspension. (T₁ = 10 min, T₂ = 3 hours, T₃ = 24 hours, T₄ = 48 hours; NC = No cement, CG = Ca-GIC, SG = Ca-Sr-GIC, BG = Ca-Ba-GIC, C = Control).

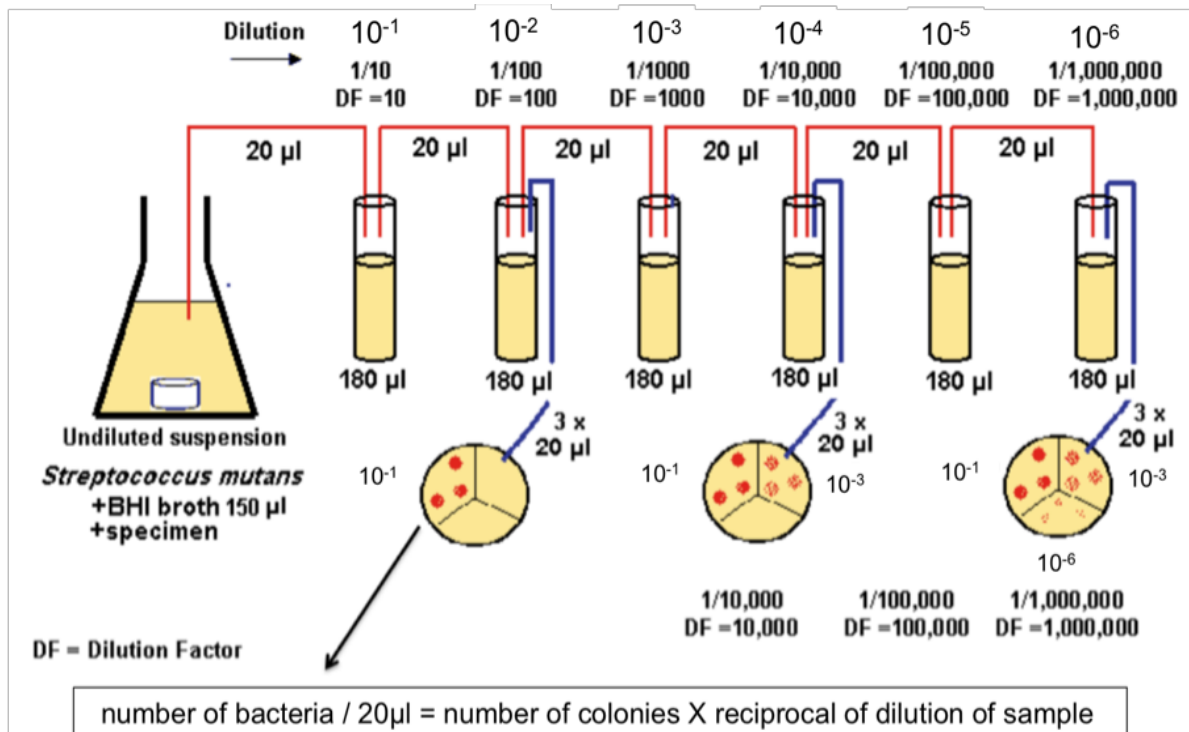


Figure 2-4: Dilution series (up to 10⁻⁶) followed by plate count method to determine viable microorganism numbers on the agar plates for all three GIC compositions.

A series of dilutions was plated on a CB agar plate, which was previously divided into three quadrants with different Dilution factors (DFs), such as 10^{-2} , 10^{-4} and 10^{-6} (Figure 2-4). Three 20 μ l spots from each corresponding DF were evenly spaced in the associated quadrant of the CB agar plates and incubated for 24 hours as before. After 24 hours the amount of CFUs are counted and recorded. All dilutions were plated in triplicate to give results.

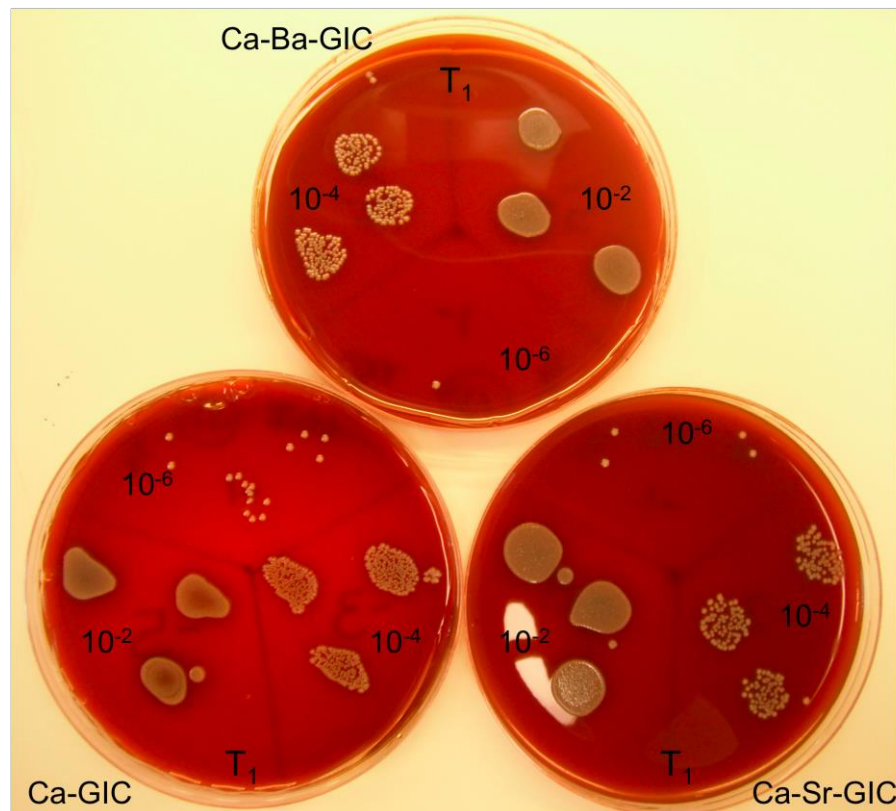


Figure 2-5: Example of an inoculated CB agar plate, divided into three quadrants and containing three evenly spaced drops of diluted samples at the time point $T_1 = 10$ min for all three GIC compositions.

2.2.4 Calculation of cement setting time

The setting time of the cements was calculated using a resistance to penetration test method. This test has been used widely in the dental industry and is in accordance with the British Standard ISO 9917-1:2007(E) for water-based cements⁷⁵. The repeatability of the method is high. The method is based on the assumption that as the material sets, it will resist penetration (Figure 2-6). In Figure 2-6 (a) the probe tip penetrates into the cement, indicating that the cement is not set yet. If the cement

resists the penetration of the probe tip, as demonstrated in Figure 2-6 (b), it suggests that the cement is set.

The viscosity of the resulting GIC is monitored as a function of the setting time, while a fixed working time of 30 s (or maximum 60 s) is assumed. It should be mentioned that the evaluation of the setting time depends on the weight and the tip diameter of the probe²⁰⁶.

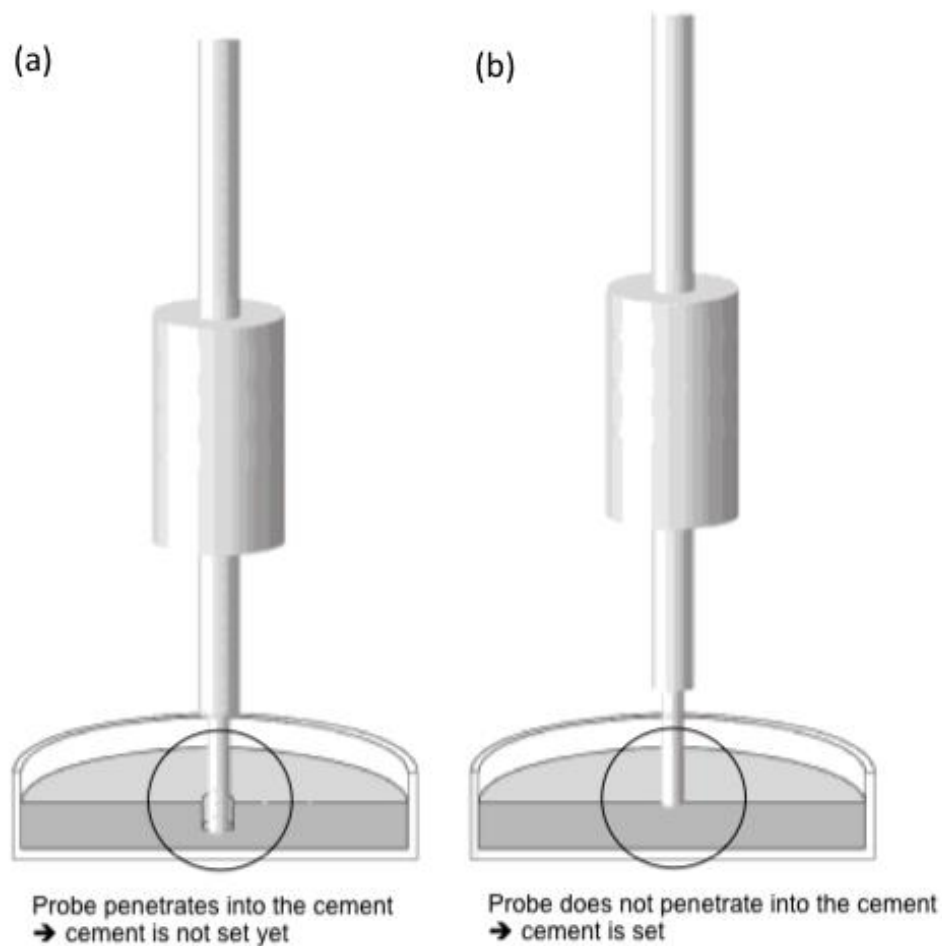


Figure 2-6: Determination of the setting time through the resistance of penetration method; (a) material is not set yet, (b) material is set [John F. McCabe²⁰⁶].

The measurements were performed in a humidity chamber (to mimic the humid environment of the human mouth) illustrated in Figure 2-7, with a temperature of $37 \pm 1^\circ\text{C}$ and a controlled humidity of at least 90%.

A needle as indenter (Figure 2-8 (d)) with a flat end ($\text{Ø } 1.0 \pm 0.1 \text{ mm}$) and a weight of $400 \pm 5 \text{ g}$, was positioned vertically in the chamber (Figure 2-8 (a)). GICs with different P/L ratios were mixed in a time interval of 30 to 60 s and transferred into a metal block mould ($8 \times 75 \times 100 \pm 0.15 \text{ mm}$) (Figure 2-8 (b)), which was covered with aluminum foil (Figure 2-8 (c)). After an additional 60 s time period the metal block mould (Figure 2-8 (c)) was placed in the humidity chamber (Figure 2-8 (a)). The needle was rested on the cement and remained there for 5 s. This procedure was repeated every 30 s, after moving the metal block (Figure 2-8 (c)) until the flat needle did not leave an indent on the surface of the set cement. Three measurements for each composition (Ca-GIC, Ca-Sr-GIC and Ca-Ba-GIC) with two different P/L ratios (2:1, 3:1) were performed and the mean setting time was calculated.



Figure 2-7: Humidity chamber used to mimic the human oral condition (Advanced Healthcare Ltd, Kent).

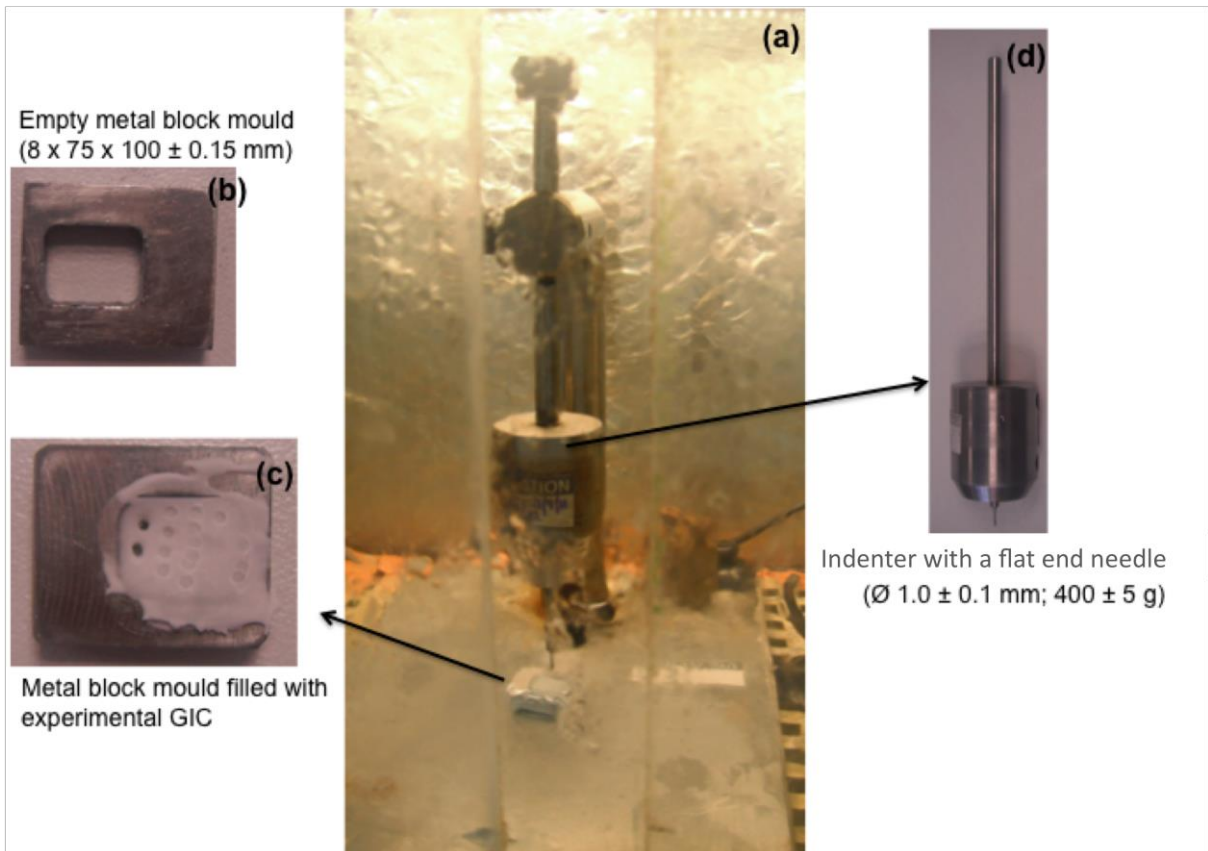


Figure 2-8: The needle indenter and the metal block in the humidity chamber. (a) Needle indenter in the humidity chamber; (b) empty metal block mould; (c) metal block mould covered with an aluminum foil and filled with GIC; (d) needle indenter with a flat end.

2.2.5 Vickers Hardness (HV) of glass ionomer cements

The specimens for the HV experiment were tested in accordance with ASTM standard C1327-08¹⁶⁵. A micro-indenter hardness (MVK-H1 Mitutoyo, UK) with an integrated optical microscope was used to measure the hardness of the specimens with a load of 1 kg for 10 s. The surface of the specimens was wet-ground with 800 and 1200-grit silicon carbide discs prior to testing. Three specimens (4 ± 0.1 mm diameter by 2 ± 0.1 mm height) for each GIC composition at 1 h and 1 month were prepared and tested. Figure 2-9 illustrates an indentation shape that is used for HV; it has a pyramid shape with a square base and an angle of 136° between opposite faces.

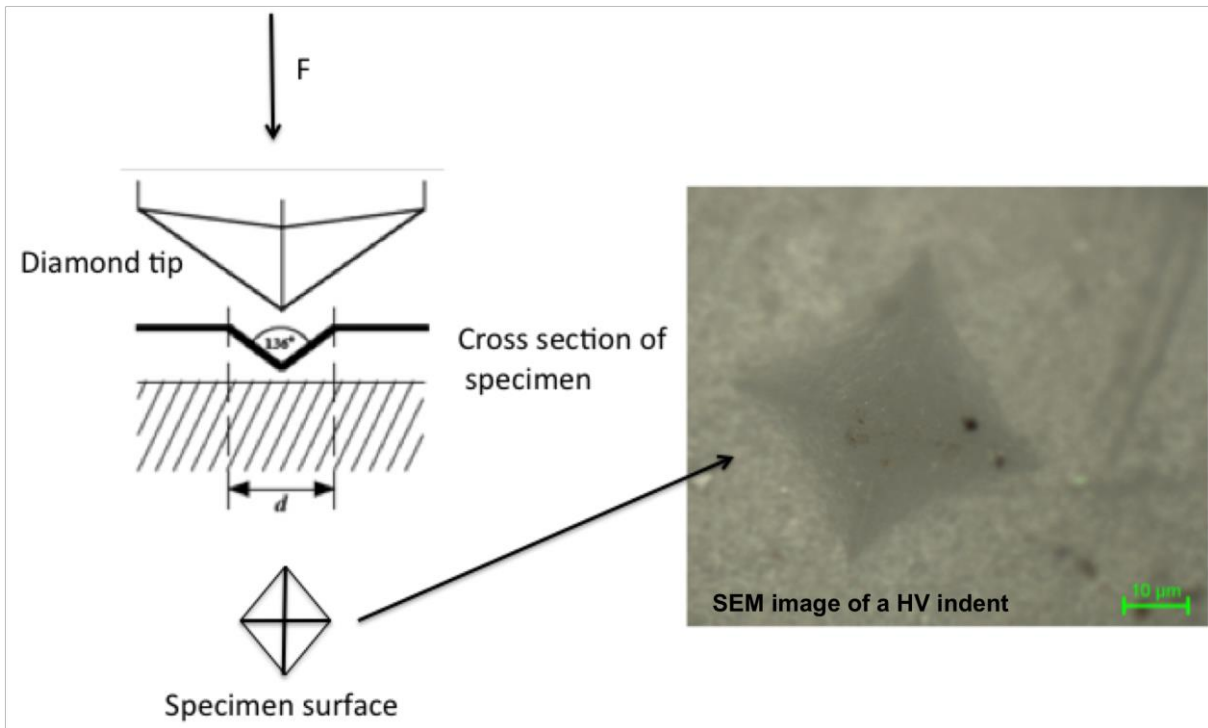


Figure 2-9: Vickers hardness testing by indent penetration via a diamond tip (SEM image Kashani).

On each specimen 3 indents were applied; the mean hardness value for a total of 9 indents at each test period was calculated according to Equation 2-1¹⁶⁵:

Equation 2-1

$$HV = \frac{2F \times \sin(136^\circ/2)}{d^2}$$

where F is the applied load on the specimen and d is the diagonal length of the diamond impression on the specimen. The HV results in this study were expressed in MPa.

2.2.6 Nano-indentation

Nano-indentation testing of a material consists of applying a compressive normal load onto the surface of a sample, via an indenter tip. The indenter tip is usually made of diamond, or is diamond-coated. Diamond exhibits a very high elastic modulus of 1,140 GPa and a hardness of ca. 200 GPa¹⁶⁶. The diamond indenter tip in the experiments performed here is a Berkovich pyramidal indenter, exhibiting a

sharp, three sided symmetric shape (Figure 2-10). The load range employed during nano-indentation testing is in the order of 0.1 – 500 mN.

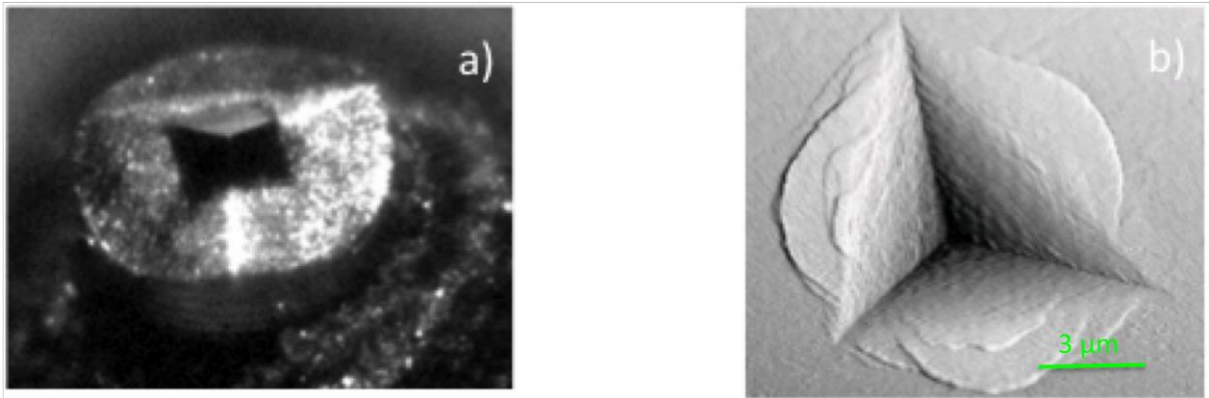


Figure 2-10: Scanning electron microscope images of (a) Berkovich pyramidal indenter and (b) Berkovich indentation into steel [James Bowen¹⁶⁶].

The nano-indentation experiment was carried out using a NanoTest (MicroMaterials, UK). A load of 300 mN was applied at a loading rate of 15 mN/s. The 300 mN load was held for 30 seconds, before retraction of the indenter, once again at 15 mN/s. Three samples were measured for each GIC composition (Ca-GIC, Ca-Sr-GIC, and Ca-Ba-GIC) at each time scale (1 hour, 1 day, 1 week, and 1 month). Each sample was indented 36 times and mean hardness and reduced modulus values were calculated. Figure 2-11 illustrates a typical indentation curve, with a characteristic loading and unloading pathway.

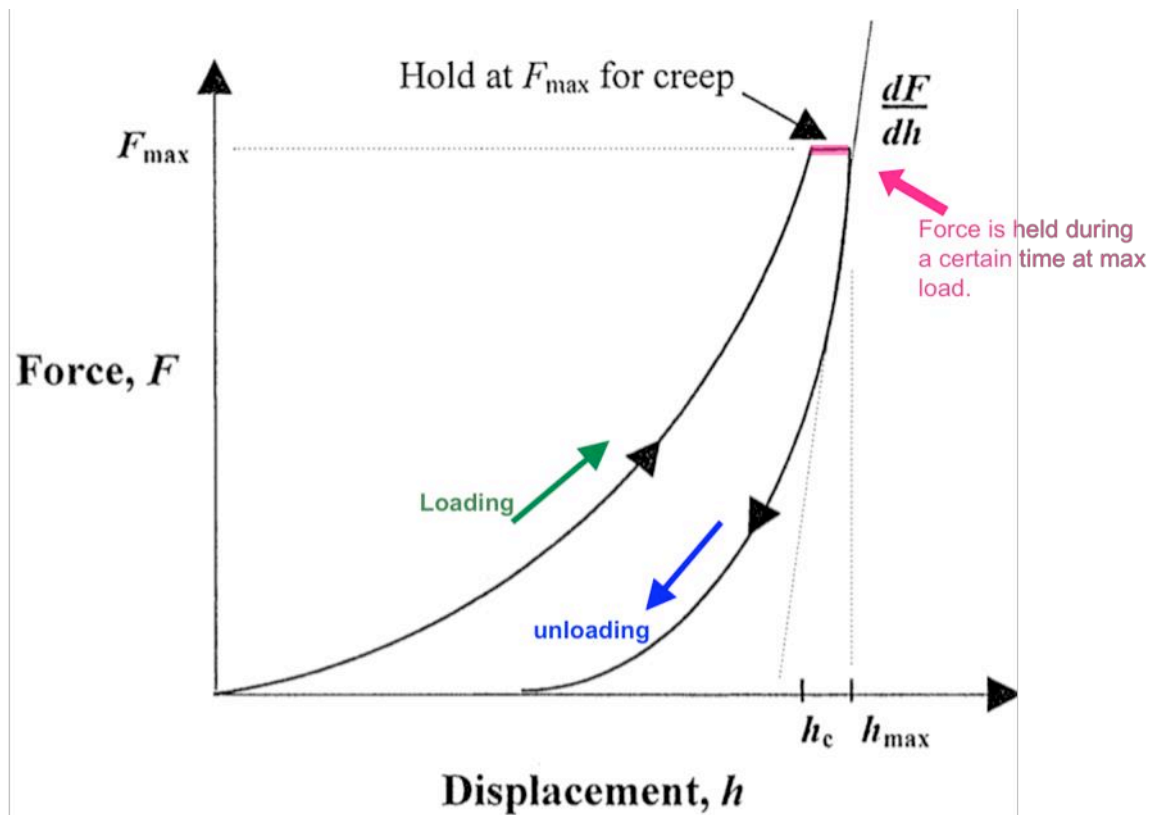


Figure 2-11: A typical schematic diagram of force-displacement curve during nano-indentation experiment [Towler *et al.*¹⁶⁰].

The hardness is defined as the mean contact pressure of a material and is calculated according to Equation 2-2¹⁶⁰:

Equation 2-2

$$H = \frac{P}{A}$$

where H is the hardness of the specimen, P is the applied pressure and A is the contact area.

Creep measurements were taken, when the applied force at a constant maximum value, (in this case 300 mN), is maintained (for 30 seconds) and the change in depth of the indenter as a function of time is measured (Figure 2-11)¹⁶⁰.

During the loading phase that is illustrated in Figure 2-11, the nano-indenter head is forced into the surface of the material. During this phase the elastic and plastic deformations are occurring. However, during the unloading phase just the elastic

displacement is recovered (Figure 2-12). Figure 2-12 illustrates the unloading process of the nano-indentation. The final depth (h_f) is caused by the plastic deformation, while the elastic displacement is recovered (Figure 2-12)¹⁶⁷.

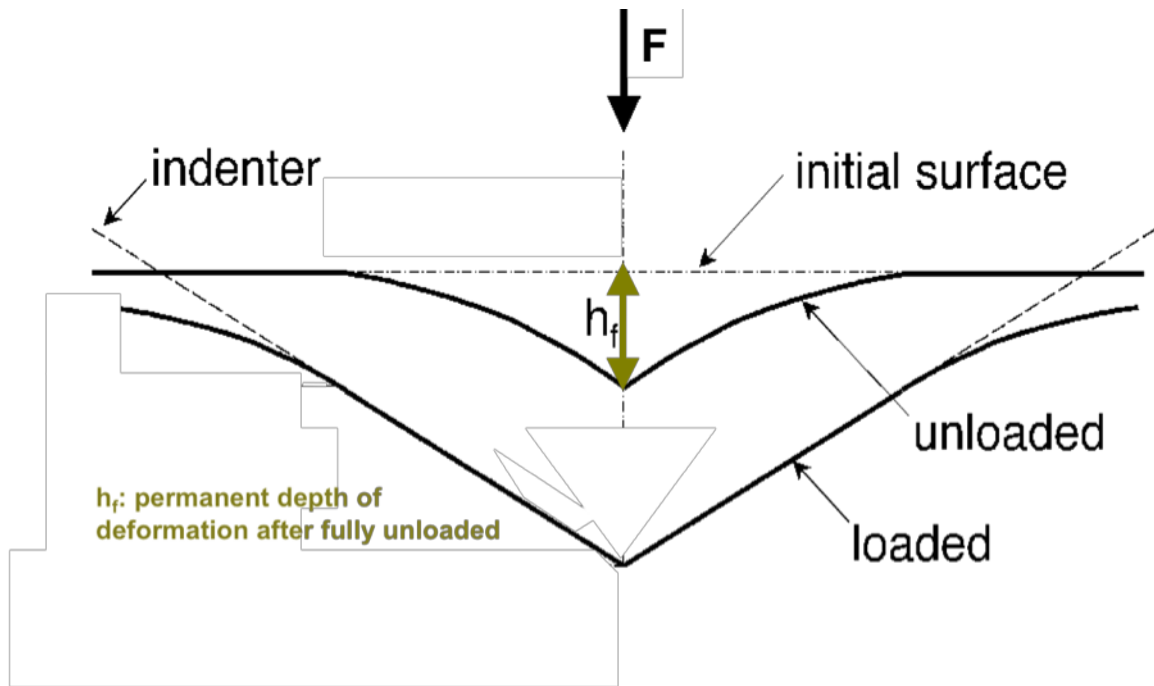


Figure 2-12: Schematic illustration of the unloading process with the permanent displacement, caused by plastic deformation [Oliver and Pharr¹⁶⁷].

The reduced modulus (E_r) is calculated from the slope of the unloading curve, based on Equation 2-3¹⁶⁰:

Equation 2-3

$$E_r = \left(\frac{dP}{dh}\right) \times \left(\frac{1}{2 \times h_p}\right) \times \left(\frac{1}{\beta}\right) \times \left(\frac{\pi}{24.5}\right)^{0.5}$$

where E_r is the reduced modulus of the specimen, dP/dh is the slope of unloading curve, h_p is the penetration depth, π is a mathematical constant equal to 3.14 and $\beta_{\text{Berkovich pyramidal indenter}}$ is the geometry correction factor and equal to 1.034¹⁶⁸.

2.2.7 Reciprocating ball-on-flat wear test

Wear is the material's loss of a surface caused by mechanical action¹⁵¹. However, in dentistry it can also include chemical interaction.

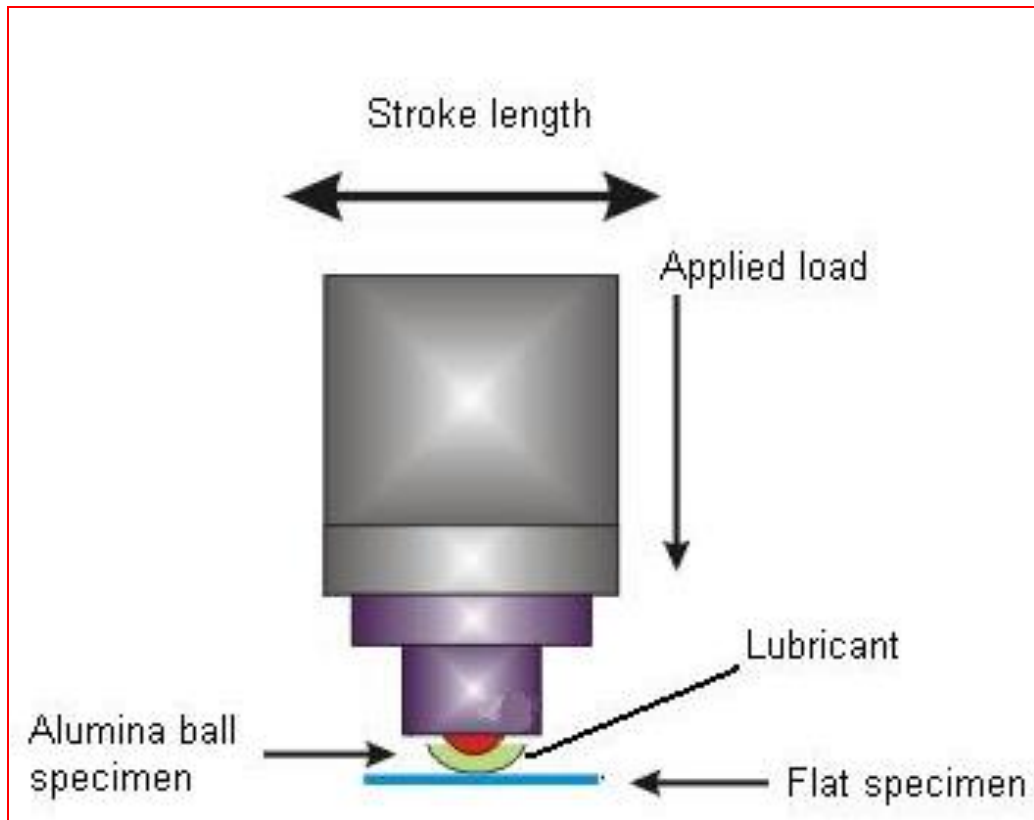


Figure 2-13: Reciprocating (ball-on-flat) sliding test was carried out in deionized water using a machine with a motor-driven stage that oscillates a flat specimen beneath a fixed ball.

Figure 2-13 illustrates the schematic arrangement for a reciprocating ball-on-flat test machine. For the reciprocating experiment, one specimen of each composition (Ca-GIC, Sr-Ca-GIC, Ba-Ca-GIC) with 25 ± 0.1 mm of length, 10 ± 0.1 mm of width and 2 ± 0.1 mm height were prepared and tested in accordance with ASTM standard G133-05¹⁶⁹. The sliding test was carried out in deionized water at RT, using a machine with a motor-driven stage that oscillates a flat specimen beneath a fixed alumina ball. The alumina ball (Spheric Trafalger Limited, Sussex) with a diameter of 12.5 mm and an average surface roughness (Ra) of about $0.01 \mu\text{m}$ was used. The alumina ball was carefully washed with acetone and deionized water before each experiment. A load of 20 nN with an average sliding speed of 1 m/s ($1 \text{ Hz} \times$

60 cycles) and a sliding distance of 6 mm was used. The specimens were wet-ground with 800 and 1200-grit silicon carbide paper at RT using water as lubricant. Figure 2-14 indicates the three wear scars across the specimens which resulted from the sliding motions. The three wear scar profiles were measured by a surface Ra measuring stylus profilometer (Surf-corder, Mitutoyo, UK). The wear scar area was calculated using Microcal Origin version 6.0 analytical software (Northampton, MA USA) by integrating the area across the wear scar profile measured by a stylus profilometer, and then multiplying by the circumference length of the track.

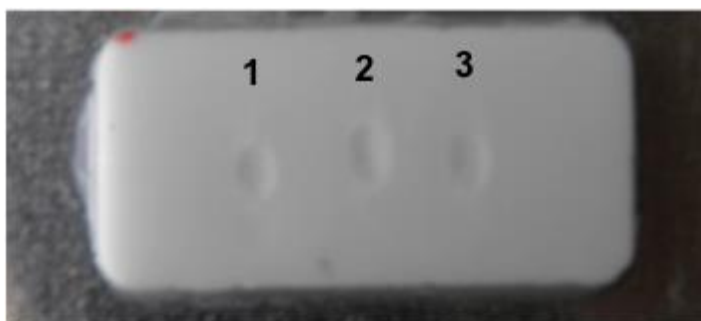


Figure 2-14: Wear scars, resulting from the sliding motions of the alumina ball.

2.2.8 Mechanical properties of prepared GICs

The requirements for dental GICs regarding environmental factors and the test methods are determined by the American Dental Association¹⁷⁰ (ADA) specification number 66 (1989) and the British Standards ISO 9917-1:2007 for Dentistry⁷⁵. Diametral tensile strength (DTS), compressive strength (CS) and flexural strength (FS) were conducted according to the British Standards ISO 9917-1:2007^{75,146}. Figure 2-15 illustrates the Teflon split moulds (Direct Plastics Limited, Sheffield), used for the preparation of the samples for compressive strength measurements (Figure 2-15 (a): four cylindrical samples of 4 ± 0.1 mm of diameter and 6 ± 0.1 mm of thickness), diametral tensile strength measurements (Figure 2-15 (b): eight circular samples with 4 ± 0.1 mm of diameter and 2 ± 0.1 mm of thickness) and flexural

strength measurements (Figure 2-15 (c): one sample with dimensions of 25 ± 0.1 mm of length, 2.0 ± 0.1 mm of thickness and 2.0 ± 0.1 mm of width).

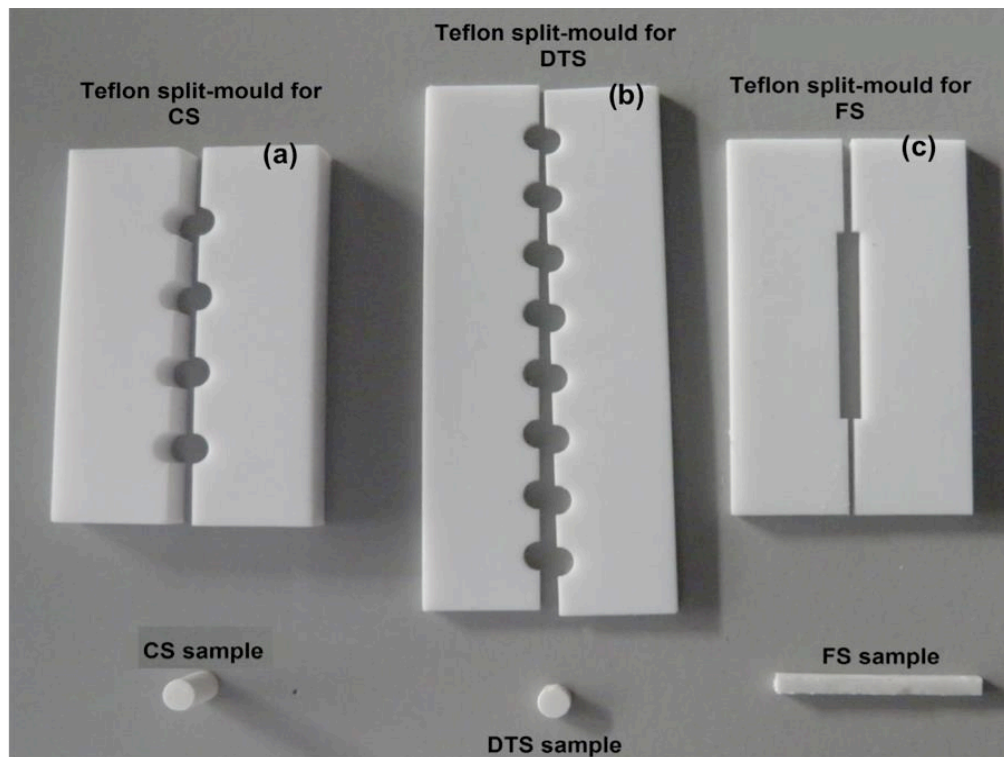


Figure 2-15: (a) Teflon split mould for compressive strength (CS) measurements capable of holding 4 samples; (b) Teflon split mould for diametral tensile strength (DTS) measurements capable of holding 8 samples; (c) Teflon split mould for flexural strength (FS) measurements capable of holding 1 sample.

The cements were prepared according to P/L ratio mentioned in Table 2-2. All cements were prepared by hand mixing at RT using an ultra high molecular weight polyethylene (UHMWPE) (SciLabware Ltd, Staffordshire) spatula and a PMMA mixing plate in order to avoid contamination (Figure 2-1). A transparent film (Lloyd Paton Ltd, Cardiff) was placed in the groove of the base of the stainless steel casing. The Teflon split mould was placed over the transparent film. The GIC paste was then packed into the split moulds. A second transparent film was placed on the top of the split mould and a stainless steel cover was placed over the transparent film and was secured by a G-clamp. The samples were left to set in the air and at RT for 60 minutes. The glass powders (Figure 2-1) were left overnight in an oven in order to protect them from environmental humidity and the polymer was kept in a fridge.

The samples were then removed from the moulds and stored in a sealed glass container in deionized water and were stored in a water-bath maintained at $37 \pm 1.0^\circ\text{C}$. Testing the samples was then conducted at specific time periods of 1 hour, 1 day, 1 week and 1 month. For each time period and test 15 samples were measured for statistical purposes.

2.2.9 Mechanical testing

For the mechanical testing of the GIC samples a screw-driven Instron mechanical testing machine Model 1195, Instron Corporation, High Wycombe) was used.

2.2.9.1 Compressive strength (CS)

CS testing was carried out according to BS 6039:4¹⁴⁶. The crosshead speed was 1 mm min⁻¹ and the load cell used was 5 kN. The CS measurement is shown in Figure 2-16. CS was calculated according to the following Equation 2-4²²⁹:

Equation 2-4

$$CS = \frac{4 \times P}{\pi \times d^2}$$

where P is the maximum applied load at the specimen, π is a mathematical constant equal to 3.14 and d is the diameter of the cylindrical sample and the CS units were given in MPa.

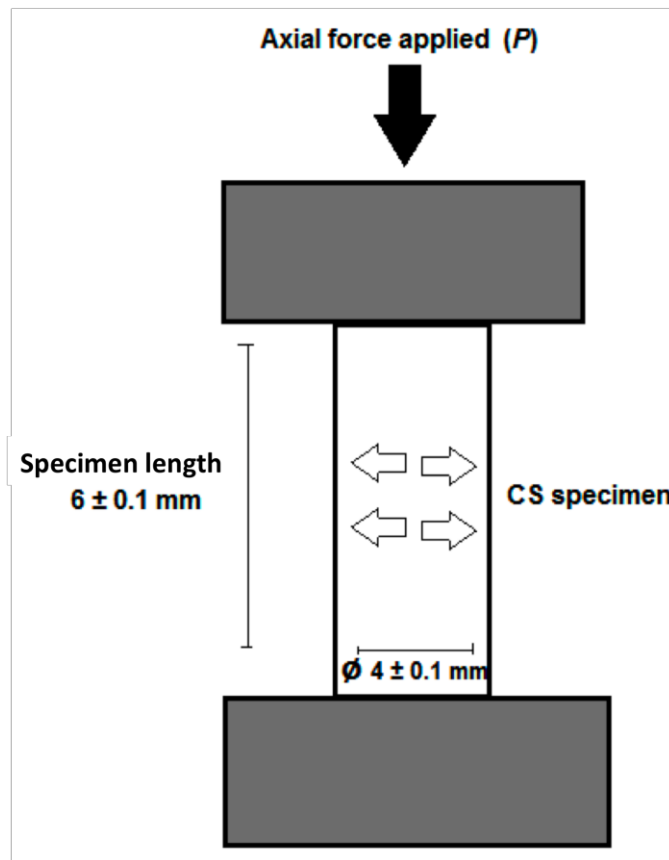


Figure 2-16: Illustration of the axial force applied through an Instron on the cylindrical CS specimen. There is no significant difference between DTS and CS testing or procedure, but the shape and applied forces in the specimen do differ.

2.2.9.2 Diametral tensile strength (DTS)

The DTS testing was performed according to BS 6039:4¹⁴⁶. The crosshead speed was 1 mm min⁻¹ and the load cell used was 1 kN. The DTS measurement is illustrated in Figure 2-17. DTS was calculated according to the following Equation 2-5²²⁹:

$$DTS = \frac{2 \times P}{\pi \times D \times T}$$

Equation 2-5

where P is the maximum applied load, π is a mathematical constant equal to 3.14, D is the diameter of the circular specimen and T is the thickness of the circular specimen. The DTS values were expressed in MPa.

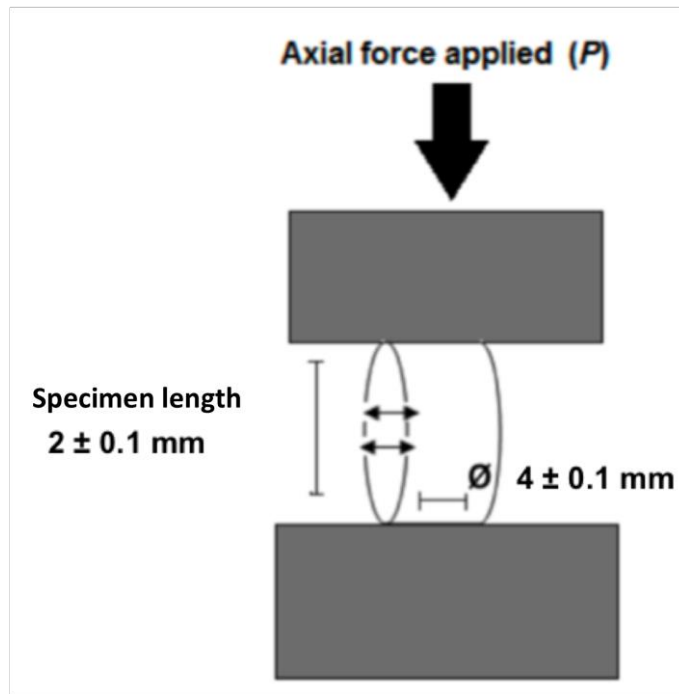


Figure 2-17: A uniform tensile stress was applied onto the circular DTS specimen with a crosshead speed of 1 mm min^{-1} and a 1 kN load cell.

2.2.9.3 Flexural strength (FS)

The FS testing was carried out according to BS 6039:4¹⁴⁶. The crosshead speed was 1 mm min^{-1} and the load cell was 1 kN. A description of the measurement is presented in Figure 2-18.

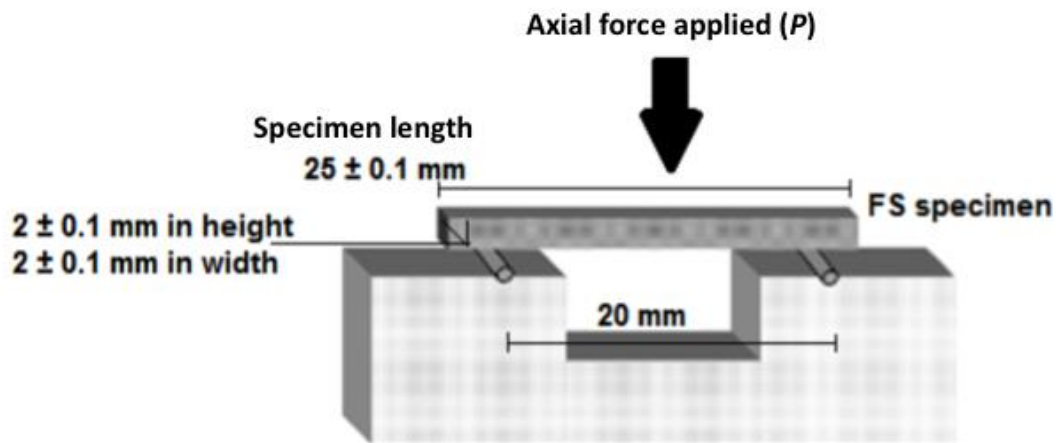


Figure 2-18: Three point bending testing.

The FS was calculated according to the following Equation 2-6⁷⁰:

$$FS = \frac{3 \times F \times I}{2 \times b \times h^2}$$

Equation 2-6

where F is the ultimate load at specimen's fracture, π is a mathematical constant equal to 3.14, I is the distance between the two supports, b is the specimen width, and h is the specimen thickness. The FS values in this work were expressed in MPa.

2.2.9.4 Modulus of Elasticity (E-modulus)

The modulus of elasticity can be obtained from the slope of the elastic region of the stress-strain curve. The compressive, tensile and flexural E-modulus were calculated from the relevant stress-strain curves according to the Equation 2-7:

$$E = \frac{\sigma}{\varepsilon} = \frac{\Delta F \times L_0}{A_0 \times \Delta L}$$

Equation 2-7

where σ is the compressive, tensile or flexural stress, ε is the strain, ΔF is the average compressive, tensile or flexural load applied to the specimen, L_0 is the original length of the specimen, A_0 is the original cross-sectional area of the specimen and ΔL is the distance of the deformation of the specimen. The E-modulus in this work was expressed in MPa.

3 Results

3.1 Fourier transform infrared (FTIR) spectroscopy study

In this chapter, FTIR spectra from the individual GIC compositions (ion leachable glass powder and the PAA solution) and the setting reaction were collected. The spectra with major peak position assignments are provided in Figure 3-1 to Figure 3-26 and Table 3-1 to Table 3-3.

3.1.1 FTIR spectroscopy study of the ion leachable glass powder

FTIR spectra were collected for the three glass compositions (Table 2-1), Ca-Glass, Ca-Sr-Glass and Ca-Ba-Glass. The spectra with major peak position assignments are provided in Table 3-1. Additionally, the description of the main peaks is presented in Figure 3-1. Ca-Glass is used as reference and is compared with Ca-Sr-Glass and Ca-Ba-Glass (Table 2-1).

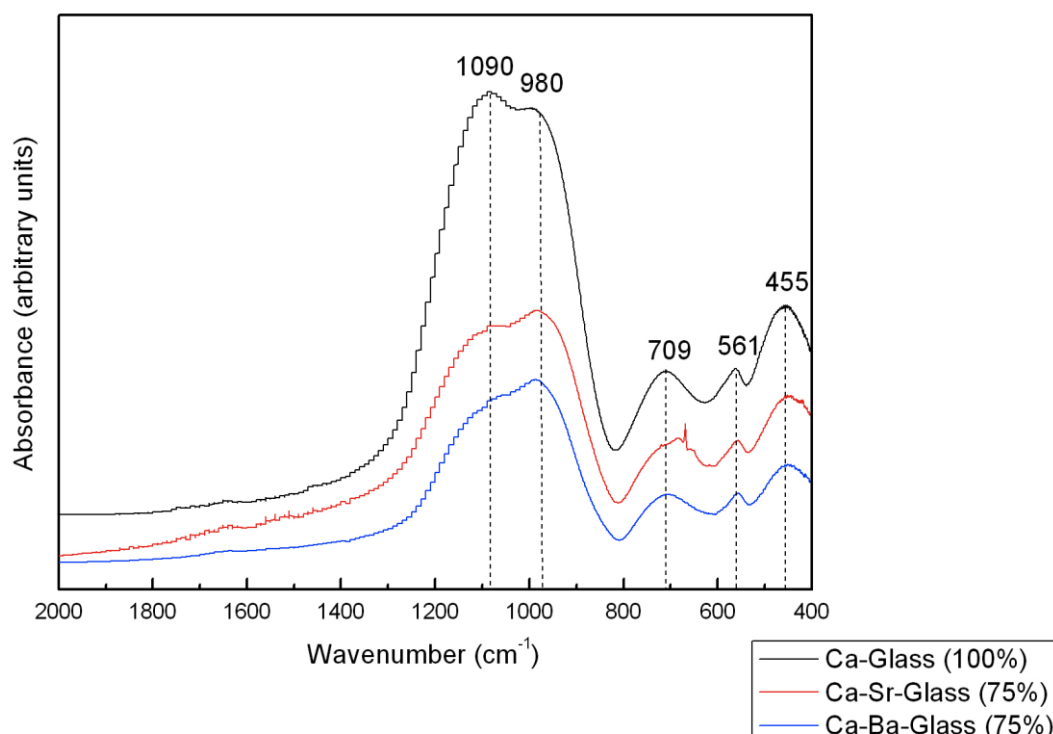


Figure 3-1: FTIR spectra of the three glass compositions (Ca-Glass (100%), Ca-Sr-Glass (75%) and Ca-Ba-Glass (75%)).

Figure 3-1 illustrates the FTIR spectra of the three glass compositions with the associated peak assignments. The FTIR spectra show an intensive and characteristic broad band from 800 to 1400 cm^{-1} which exhibits two apparent peaks at 1090 cm^{-1} and 980 cm^{-1} . These peaks are associated with Si-O stretching vibrations and P-O bonds. The number of BO of SiO_4 varies dependent upon the location of its stretching vibrations. A peak at 709 cm^{-1} is associated with the stretching vibrations of Al-O bonds. A narrow peak at 561 cm^{-1} is associated with P-O bending vibrations and Si-O-Al stretching vibrations. The last main peak at 455 cm^{-1} is associated with Si-O-Si stretching vibrations^{171,172,173}.

All the peaks and their associated interpretations for the three glass compositions are summarized and listed below in Table 3-1.

Table 3-1: FTIR peak assignment in the three glass compositions.

Wave number (cm^{-1})	Assignment	Reference
400 – 530	Si-O-Si vibrations	Stoch and Stroda ¹⁷¹
530 – 620	P-O bending and Si-O-Al linkages	Huang and Behrman ¹⁷²
620 – 800	Al-O stretching (four fold coordination)	Stamboulis <i>et al.</i> ¹⁷⁴
800 – 1300	Symmetric and asymmetric stretching of Si-O	Clayden <i>et al.</i> ¹⁷⁵
800 – 1400	Si-O stretching (Q3 & Q4) and Si-O-[NBO] and P-O bonds	MacDonald <i>et al.</i> ¹⁷⁶ Serra <i>et al.</i> ¹⁷⁷

3.1.2 FTIR spectroscopy study of the PAA solution

FTIR spectra for the 40% aqueous solution of PAA were collected. The spectra with major peak position assignments are provided in Figure 3-2. Additionally, the description of the main peaks is presented in Table 3-2. The spectrum of PAA presents several absorption peaks and is presented in Figure 3-2.

A pronounced absorption peak at 1710 cm^{-1} is associated with carbonyl stretching (C=O) vibrations of PAA^{46,188}.

A broad and noticeable absorption band around 3350 cm^{-1} is due to inter- and intralayer H-bonded O-H stretching vibrations^{56,179,180}.

A medium peak at 1462 cm^{-1} is associated with C-H scissor vibrations of the PAA and monomers⁴⁶.

A peak at 1240 cm^{-1} is attributed to C-O stretching vibrations of the PAA⁴⁶.

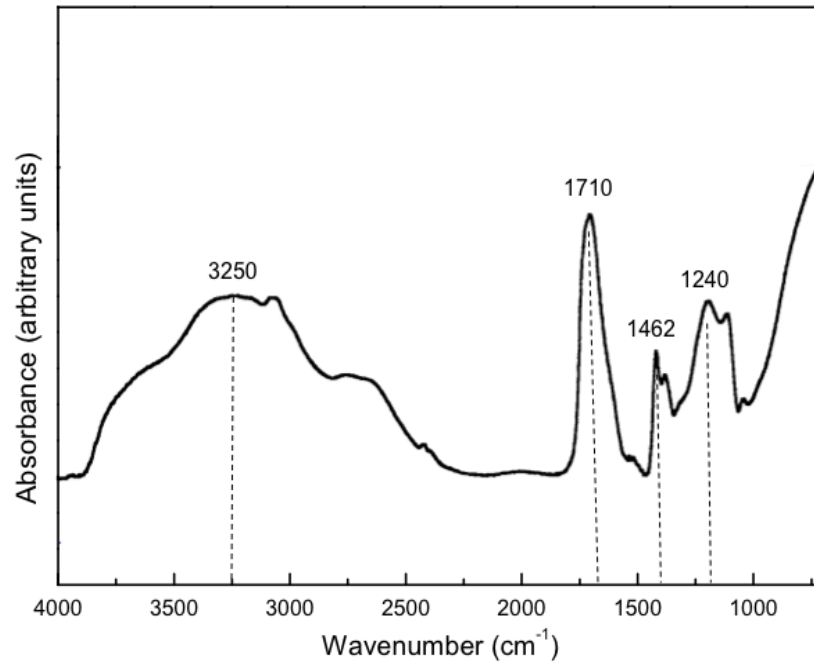


Figure 3-2: FTIR spectrum of 40% aqueous solution of poly (acrylic acid) acid.

Table 3-2: FTIR peak assignment in 40% aqueous solution of PAA.

Wave number (cm ⁻¹)	Assignment	Reference
1720	C=O stretching of PAA	Young <i>et al.</i> ^{46,188}
1452	C-H scissoring of PAA and monomers	Young <i>et al.</i> ⁴⁶
1370	C-H bending of PAA and monomers	Young <i>et al.</i> ⁴⁶
1249	C-O stretching of PAA	Young <i>et al.</i> ⁴⁶
3500	Inter- and intralayer H-bonded O-H stretching vibrations	Gao and Heimann ¹⁷⁹ Billingham <i>et al.</i> ¹⁸⁰ Barry <i>et al.</i> ⁵⁶

3.1.3 FTIR spectroscopy study of cement setting reaction

In order to characterise and follow the chemical setting reactions of the three GIC compositions (Table 2-2) real time FTIR spectra were collected over a 60 minute

period. However, as mentioned in Chapter 2.2.1, the sample was kept on the Golden Gate and covered with deionized water for 60 minutes to avoid dehydration and to mimic the oral environment as closely as possible.

Three GIC compositions, Ca-GIC, Ca-Sr-GIC and Ca-Ba-GIC (Table 2-2), were used in this study, with the Ca-GIC as the control reference. For each composition a 2D and 3D spectrum from 700 to 4000 cm^{-1} is illustrated. Furthermore, in order to be able to follow the acid-base neutralisation of the three GIC compositions, they were subdivided into three sections. The first section from 2500 – 4000 cm^{-1} , the second section from 700 – 1350 cm^{-1} and the last section from 1350 – 1750 cm^{-1} . The 3D figures from the three sections demonstrate substantial changes in the spectra over a period of 60 minutes whereas the 2D figures from the corresponding sections illustrate the changes between 1 minute, 30 minutes and 60 minutes after mixing. This 2D illustration makes it simple to distinguish between changes in the absorbance intensity.

All the peaks for all the three GIC compositions and their associated interpretations for the GIC setting reaction are illustrated in Table 3-3. Additionally, from the 2D figures of each glass composition, a ratio of the change in intensity against time (1 minute, 30 minutes and 60 minutes) was obtained and is presented in Table 3-4 to Table 3-6.

Table 3-3: FTIR peak assignment in the setting reaction of glass ionomer cements.

Wave number (cm^{-1})	Assignment	Reference
Near 730	Symmetric stretching of Si-O	Efimov ¹⁸¹ Miller and Lakshmi ¹⁸²
730 – 800	Symmetric stretching of Si-O	Farmer <i>et al.</i> ¹⁷⁸

1000 – 1200	Asymmetric stretching of Si-O (Glass)	Efimov ¹⁸¹
900 – 1200	GIC setting	Matsuya <i>et al.</i> ¹⁸³ Matsuya <i>et al.</i> ¹⁵⁷
1018 – 1073	Asymmetric stretching of Si-O	Efimov ¹⁸¹
400 – 850	Amorphous silica	De Maeyer <i>et al.</i> ¹⁸⁵
Near 1640	Bending vibration of water	Davis and Tamosava ¹⁸⁴
950 – 1640	Silica gel is formed upon acid degradation; Si-OH ~ 950 cm ⁻¹	De Maeyer <i>et al.</i> ¹⁸⁵
1720	C=O stretching of PAA	Young <i>et al.</i> ⁴⁶
1700	Stretching of carboxylic acid groups	Young <i>et al.</i> ⁴⁶
1550	C=O asymmetric stretching of calcium polyacrylate	Nicholson ⁵⁷
1410	C=O symmetric stretching of calcium polyacrylate	Nicholson ⁵⁷
1559	C=O asymmetric stretching of aluminium polyacrylate	Nicholson ⁵⁷
1460	C=O symmetric stretching of aluminium polyacrylate	Nicholson ⁵⁷
1635	O-H stretching of monomers	Young <i>et al.</i> ⁴⁶
1640	C=C stretching of monomers	Young <i>et al.</i> ⁴⁶
3500	Inter- and intralayer H-bonded O-H stretching vibrations	Gao and Heimann ¹⁷⁹ Billingham <i>et al.</i> ¹⁸⁰ Barry <i>et al.</i> ⁵⁶
1050	Formation of silicic acid	Matsuya <i>et al.</i> ¹⁵⁷

3.1.3.1 FTIR spectroscopy study of calcium cement setting reaction

Figure 3-19 illustrates the 3D real time FTIR series of the setting reaction for Ca-GIC over a period of 60 minutes. Several absorption bands with changes in the spectra over time in Figure 3-3 can be observed. Additionally, Figure 3-4 illustrates the changes in intensity at 1 minute, 30 minutes and 60 minutes after mixing.

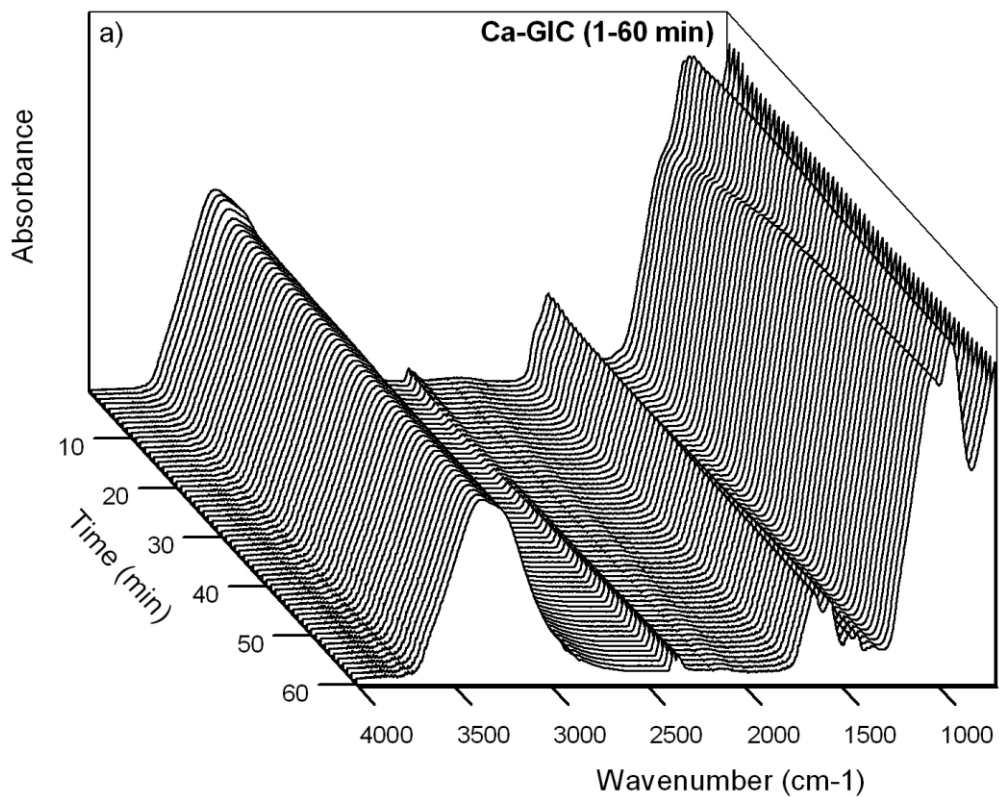


Figure 3-3: Real time ATR-FTIR analysis of the setting reaction of Ca-GIC at different time intervals for 60 minutes.

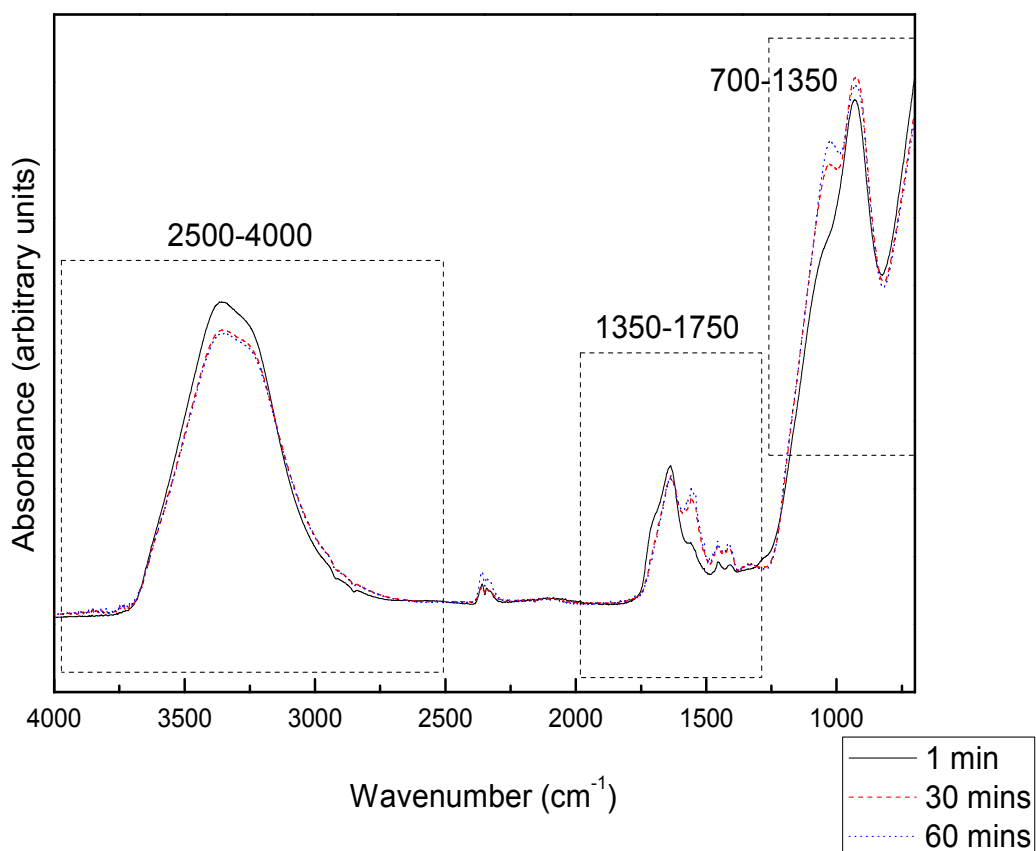


Figure 3-4: Real time ATR-FTIR analysis of the setting reaction of Ca-GIC at 1 minute, 30 minutes and 60 minutes after mixing.

Table 3-4 illustrates the ratio of the change in the intensity over time from the 2D figures. Percentage changes in the intensity from 1 minute to 30 minutes (A/B), from 1 minute to 60 minutes (A/C) and from 30 minutes to 60 minutes (B/C) were obtained.

Table 3-4: Ratio of change in the intensity plotted over time for Ca-GIC, with the associated peak assignments.

Glass composition	Ratio A/B (%)	Ratio A/C (%)	Ratio B/C (%)	Wave number (cm ⁻¹)	Figure	Peak number	Assignment	Reference
Ca-GIC	9	9	0	3300	3D: Figure 3-5 2D: Figure 3-6	-----	Inter- and intralayer H-bonded O-H stretching vibrations	Gao and Heimann ¹⁷⁹ Billingham <i>et al.</i> ¹⁸⁰ Barry <i>et al.</i> ⁵⁶
	11	11	0	1411	3D: Figure 3-9 2D: Figure 3-10	1	Symmetric C=O stretching of Ca-polycarboxylate	Nicholson ⁵⁷
	11	11	0	1454	3D: Figure 3-9 2D: Figure 3-10	2	Symmetric C=O stretching of Al-polycarboxylate	Nicholson ⁵⁷
	23	26	4	1558	3D: Figure 3-9 2D: Figure 3-10	3	Asymmetric C=O stretching of Ca-polycarboxylate	Nicholson ⁵⁷
	7	7	0	1638	3D: Figure 3-9 2D: Figure 3-10	4	Asymmetric C=O stretching of Al-polycarboxylate	Nicholson ⁵⁷
	47	47	0	1705	3D: Figure 3-9 2D: Figure 3-10	5	Stretching of carboxylic acid groups	Young <i>et al.</i> ⁴⁶
	2	4	1	927	2D: Figure 3-7 3D: Figure 3-8	2	Si-O in glass powder	Matsuya <i>et al.</i> ¹⁵⁷
	13	16	4	1023	2D: Figure 3-7 3D: Figure 3-8	3	Formation of silica gel	Matsuya <i>et al.</i> ¹⁵⁷

A/B: 1 minute/30 minutes; A/C: 1 minute/60 minutes; B/C: 30 minutes/60 minutes.

The development of the Ca-GIC over 60 minutes in the wave number range from 2500 – 4000 cm^{-1} can be observed in Figure 3-5 and Figure 3-6.

Figure 3-5 illustrates a characteristic band for Ca-GIC composition that ranges from 3691 – 2790 cm^{-1} , which is due to inter- and intralayer H-bonded O-H stretching vibrations^{56,179,180}.

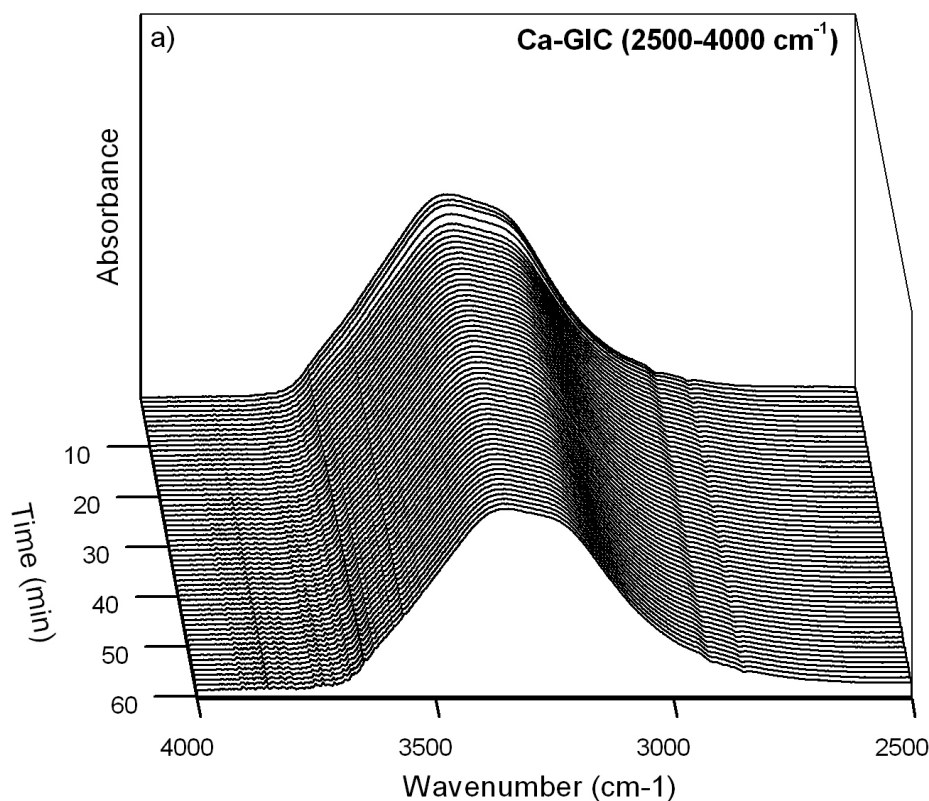


Figure 3-5: Real time ATR-FTIR analysis of Ca-GIC at different time intervals for 60 minutes at wave numbers 2500 – 4000 cm^{-1} .

The intensity of the inter- and intralayer H-bonded O-H stretching vibrations decreases from 1 minute to 30 minutes (Figure 3-6) by approximately 9%. No further changes can be observed from 30 minutes to 60 minutes.

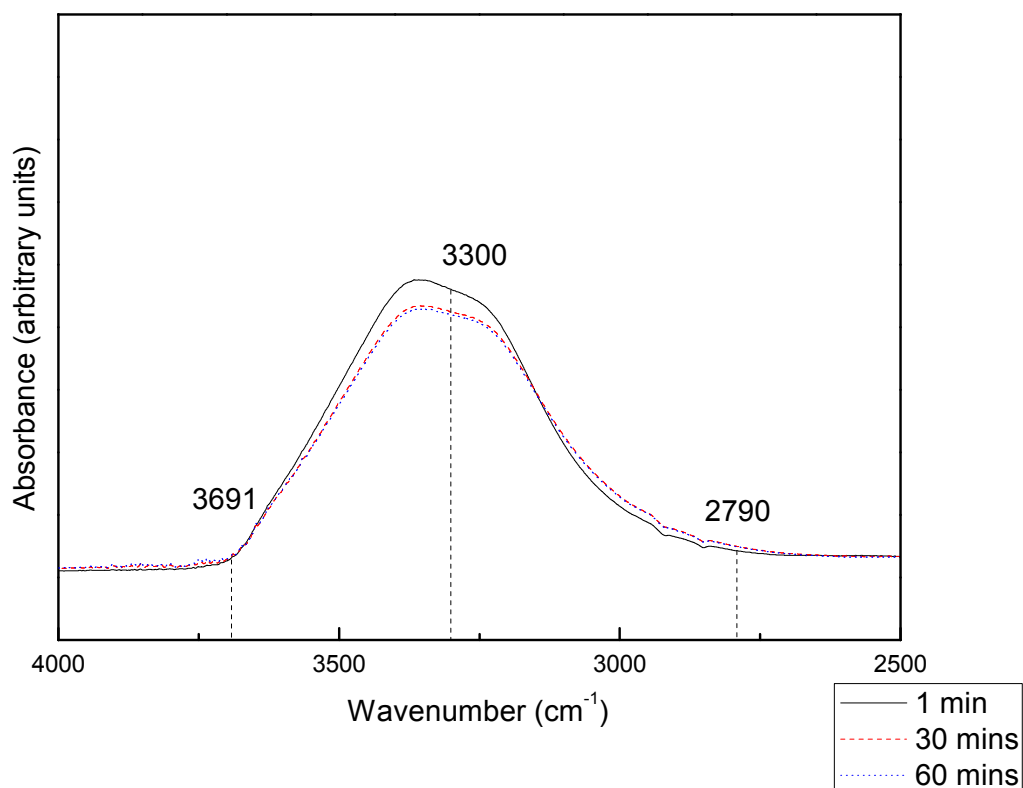


Figure 3-6: Real time ATR-FTIR analysis of the setting reaction of Ca-GIC at 1 minute, 30 minutes and 60 minutes after mixing at wave numbers 2500 – 4000 cm^{-1} .

The development of the Ca-GIC during 60 minutes in the wave number range from 700 to 1350 cm^{-1} is presented in Figure 3-7 and Figure 3-8.

Figure 3-7 No 1 illustrates a strong absorbance band in the FTIR spectra of Ca-GIC at ca. 700 cm^{-1} . The main peak at ca. 700 cm^{-1} is attributed to the symmetric stretching of Si-O^{178,181,182}. Figure 3-8 No 1 presents a decrease in intensity from 1 minute to 30 minutes, but no changes from 30 minutes to 60 minutes.

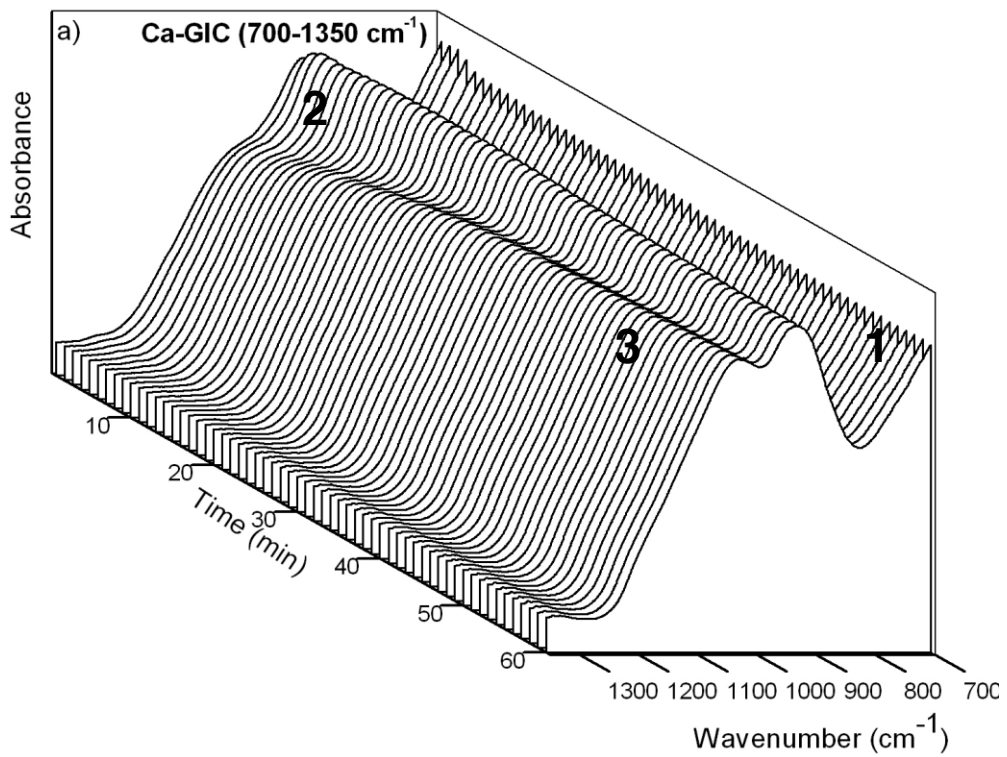


Figure 3-7: Real time ATR-FTIR analysis of Ca-GIC at different time intervals for 60 minutes at wave numbers 700 – 1350 cm^{-1} .

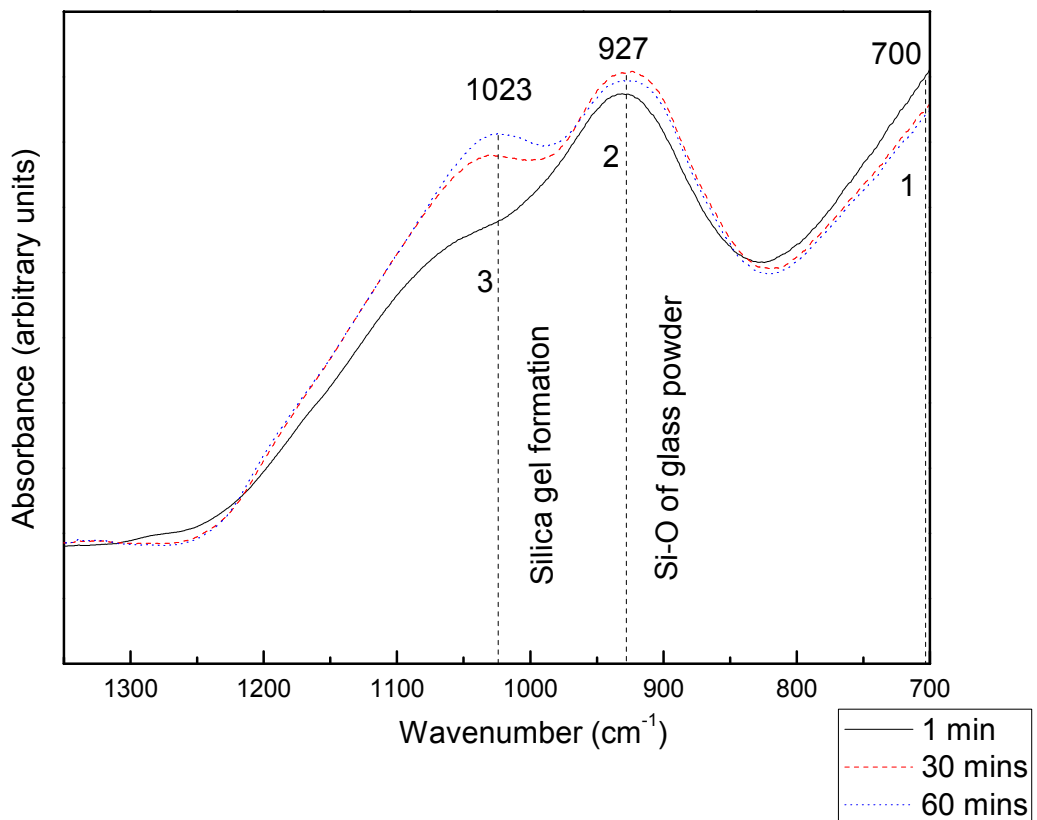


Figure 3-8: Real time ATR-FTIR analysis of the setting reaction of Ca-GIC at 1 minute, 30 minutes and 60 minutes after mixing at wave numbers 700 – 1350 cm^{-1} .

A noticeable band appears at 927 cm^{-1} for Ca-GIC (Figure 3-7 No 2). An increase in intensity (Figure 3-8 No 2) is apparent from 3 minutes (Figure 3-7 No 2) to 30 minutes for Ca-GIC. Between 30 to 60 minutes the peak at 927 cm^{-1} (Figure 3-8 No 2) reduces slightly in intensity, while still retaining a greater intensity than at the 1 minute mark. Peaks in the region $900 - 1200\text{ cm}^{-1}$ are attributed to the setting reaction of GIC^{157,183}.

A broad, shallow peak rises noticeably at 1023 cm^{-1} (Figure 3-8 No 3) after ca. 15 minutes (Figure 3-7 No 3) to 30 minutes (around 13 %) and continues to increase up to 60 minutes (Figure 3-8 No 3). Absorptions around $1000 - 1200\text{ cm}^{-1}$ are attributed to the asymmetric stretching of Si-O¹⁸¹. Peaks in the range $950 - 1640\text{ cm}^{-1}$ are an indication for silica gel formation upon acid degradation of the glass powder¹⁸⁵.

The development of the Ca-GIC over 60 minutes in the wave number range from 1350 to 1750 cm^{-1} can be observed in Figure 3-9 and Figure 3-10.

Figure 3-9 presents absorption peaks at 1411 cm^{-1} and 1454 cm^{-1} (Figure 3-9 No 1 & No 2) for Ca-GIC. These two peaks are due to the C=O symmetric stretching and the formation of calcium and aluminium salts⁵⁷. The calcium polyacrylate peak at 1411 cm^{-1} (Figure 3-10 No 1) slightly increases in intensity after ca. 5 minutes (Figure 3-9 No 1) and continues to increase up to 30 minutes (11%). There is no change in intensity from 30 minutes to 60 minutes (Figure 3-10 No 1). The aluminium polyacrylate peak at 1454 cm^{-1} (Figure 3-9 No 2) exhibits the same development (Figure 3-10 No 2) as the calcium polyacrylate peak (Figure 3-10 No 1).

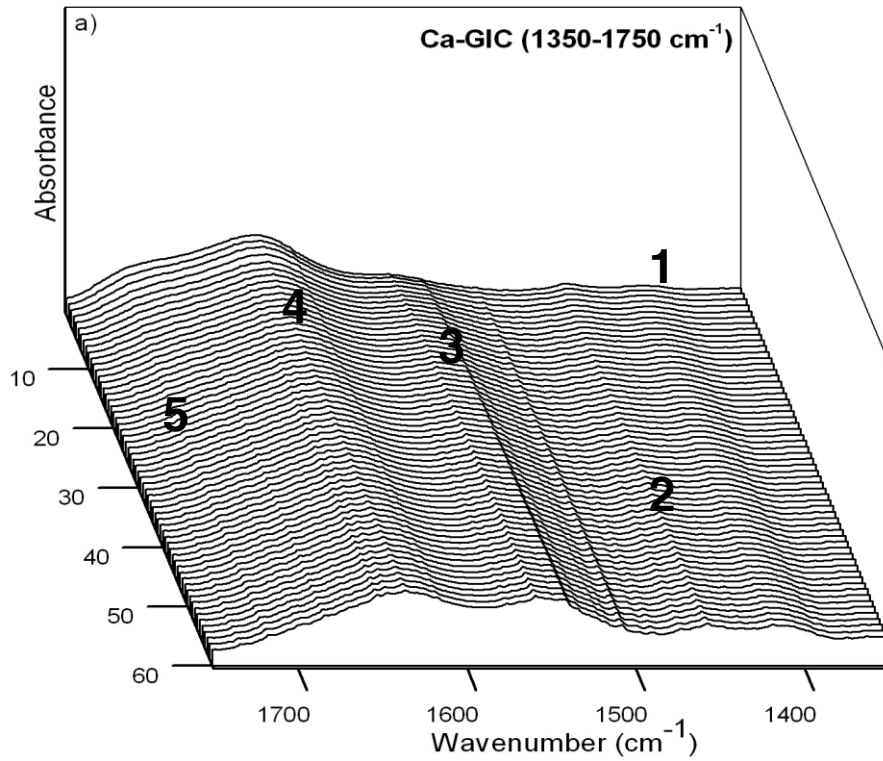


Figure 3-9: Real time ATR-FTIR analysis of Ca-GIC at different time intervals for 60 minutes at wave numbers 1350 – 1750 cm⁻¹.

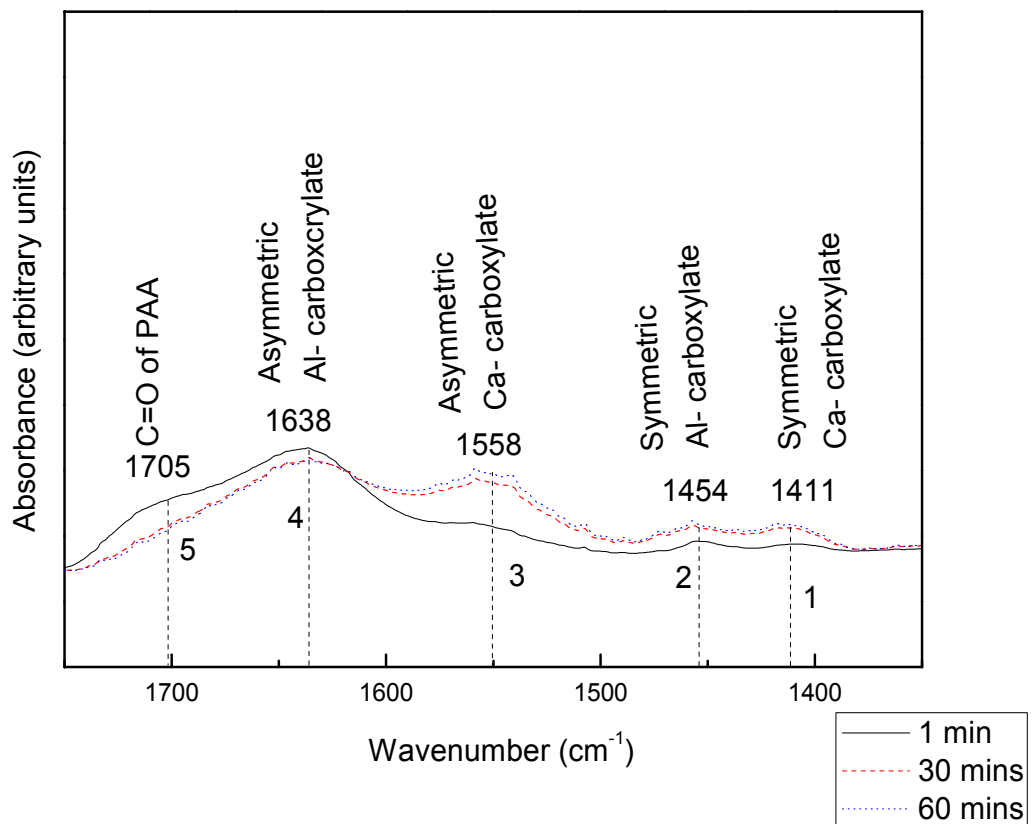


Figure 3-10: Real time ATR-FTIR analysis of the setting reaction of Ca-GIC at 1 minute, 30 minutes and 60 minutes after mixing at wave numbers 1350 – 1750 cm⁻¹.

A broad peak with low intensity became more narrow and increased in intensity around 26% at 1550 cm^{-1} over 60 minutes (Figure 3-9 No 3 and Figure 3-10 No 3). The intensity increased after ca. 2 minutes (Figure 3-9 No 3) for Ca-GIC. There is a significant increase from 2 minutes to 30 minutes followed by a further but slight increase from 30 to 60 minutes (Figure 3-10 No 3). Peaks at 1550 cm^{-1} are associated with C=O asymmetric stretching of calcium polyacrylate^{47,57}.

A broad peak at 1638 cm^{-1} (Figure 3-9 No 4) decreased in intensity over 60 minutes (Figure 3-10 No 4). However, there is no change in intensity from 30 minutes to 60 minutes (Figure 3-10 No 4). Peaks near wave number 1640 cm^{-1} (Figure 3-9 No 4 and Figure 3-10 No 4) are associated with the bending vibrations of water¹⁸⁴. Furthermore, peaks around 1600 cm^{-1} are associated with C=O asymmetric stretching of Al-polycarboxylates⁵⁷.

A peak in the wavelength 1705 cm^{-1} (Figure 3-9 No 5) is almost invisible. Peaks at 1705 cm^{-1} are associated with stretching of carboxylic acid groups⁴⁶. A decrease in intensity from 1 minute to 30 minutes is observed (Figure 3-10 No 5), but no changes from 30 minutes to 60 minutes (Figure 3-10 No 5).

All the peaks for all the three GIC compositions and their associated interpretations for the GIC setting reaction are illustrated in Table 3-3 and Table 3-4.

3.1.3.2 FTIR spectroscopy study of strontium substituted cement setting reaction

Figure 3-11 illustrates the 3D real time FTIR series of the setting reaction for strontium substituted GIC over a period of 60 minutes.

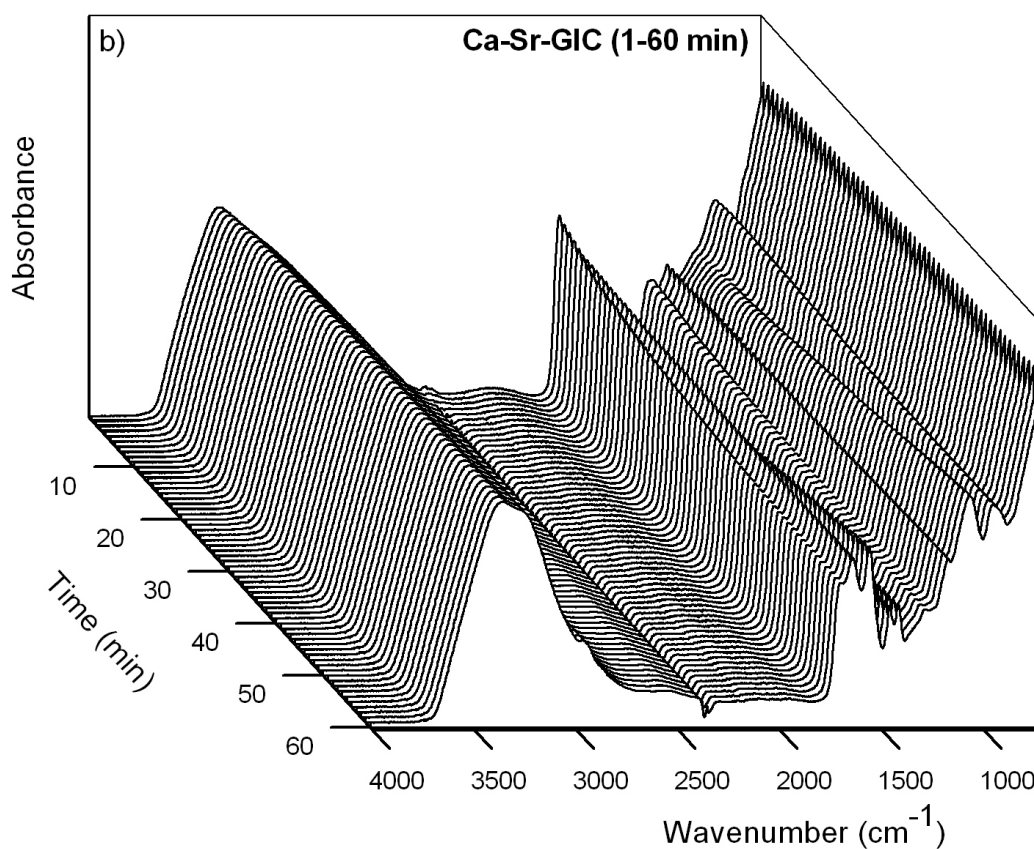


Figure 3-11: Real time ATR-FTIR analysis of the setting reaction Ca-Sr-GIC at different time intervals for 60 minutes.

Several absorption bands with changes in the spectra over time in Figure 3-11 can be observed. Additionally, Figure 3-12 presents the changes in the intensity at 1 minute, 30 minutes and 60 minutes after mixing.

The FTIR spectrum of Ca-GIC shown in Figure 3-3 exhibits fewer peaks in the range from 700 to 1350 cm⁻¹, in comparison to Ca-Sr-GIC, shown in Figure 3-11. Additionally, more fluctuations in intensity in the spectrum of Ca-Sr-GIC (Figure 3-12) can be observed in comparison to the spectrum of Ca-GIC illustrated in Figure 3-4.

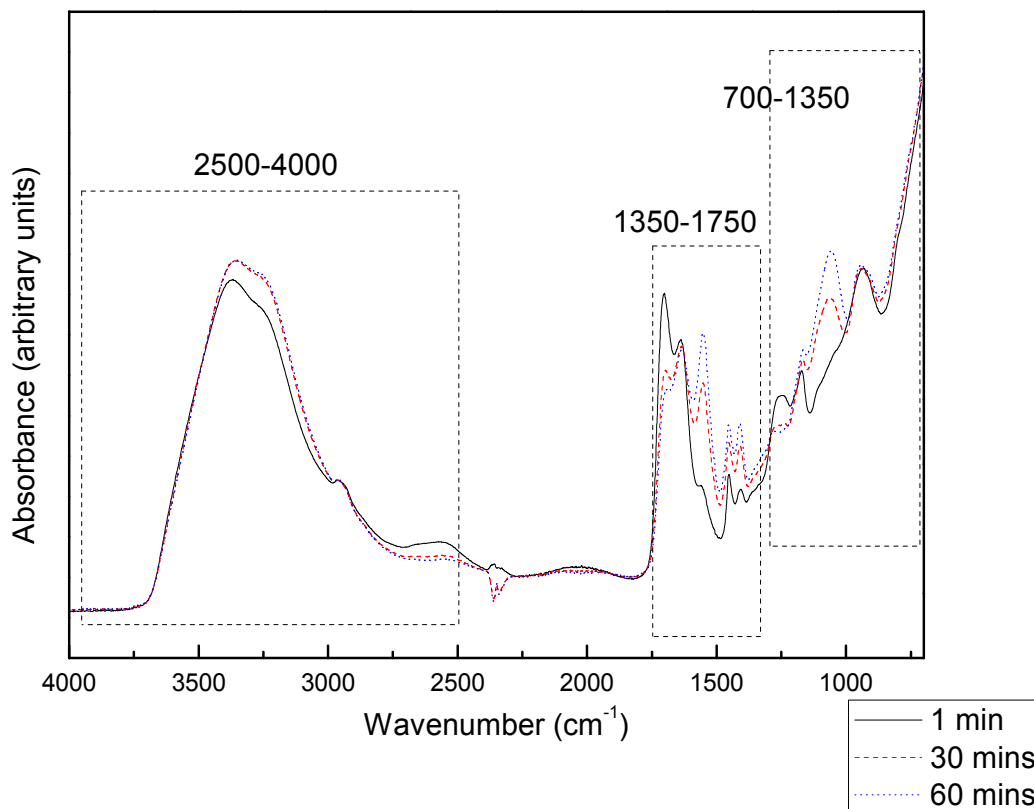


Figure 3-12: Real time ATR-FTIR analysis of the setting reaction of Ca-Sr-GIC at 1 minute, 30 minutes and 60 minutes after mixing.

Table 3-5 illustrates the ratio of the change in the intensity over time from the 2D figures. Percentage changes in the intensity from 1 minute to 30 minutes (A/B), from 1 minute to 60 minutes (A/C) and from 30 minutes to 60 minutes (B/C) were obtained.

Table 3-5: Ratio of change in intensity plotted over time for Ca-Sr-GIC, with the associated peak assignments.

Glass composition	Ratio A/B (%)	Ratio A/C (%)	Ratio B/C (%)	Wave number (cm ⁻¹)	Figure	Peak number	Assignment	Reference
Ca-Sr-GIC	9	9	0	3300	3D: Figure 3-13 2D: Figure 3-14	-----	Inter- and intralayer H-bonded O-H stretching vibrations	Gao and Heimann ¹⁷⁹ Billingham <i>et al.</i> ¹⁸⁰ Barry <i>et al.</i> ⁵⁶
	22	28	7	1409	3D: Figure 3-17 2D: Figure 3-18	1	Symmetric C=O stretching of Ca-polycarboxylate	Nicholson ⁵⁷
	19	21	4	1452	3D: Figure 3-17 2D: Figure 3-18	2	Symmetric C=O stretching of Al-polycarboxylate	Nicholson ⁵⁷
	39	44	7	1550	3D: Figure 3-17 2D: Figure 3-18	3	Asymmetric C=O stretching of Ca-polycarboxylate	Nicholson ⁵⁷
	2	2	0	1636	3D: Figure 3-17 2D: Figure 3-18	4	Asymmetric C=O stretching of Al-polycarboxylate	Nicholson ⁵⁷
	32	41	7	1703	3D: Figure 3-17 2D: Figure 3-18	5	Stretching of carboxylic acid groups	Young <i>et al.</i> ⁴⁶
	0	0	0	939	3D: Figure 3-15 2D: Figure 3-16	2	Si-O in glass powder	Matsuya <i>et al.</i> ¹⁵⁷
	18	18	0	1063	3D: Figure 3-15 2D: Figure 3-16	3	Formation of silica gel	Matsuya <i>et al.</i> ¹⁵⁷

A/B: 1 minute/30 minutes; A/C: 1 minute/60 minutes; B/C: 30 minutes/60 minutes.

The development of the Ca-Sr-GIC during 60 minutes in the wave number range from 2500 to 4000 cm^{-1} can be observed in Figure 3-13 and Figure 3-14.

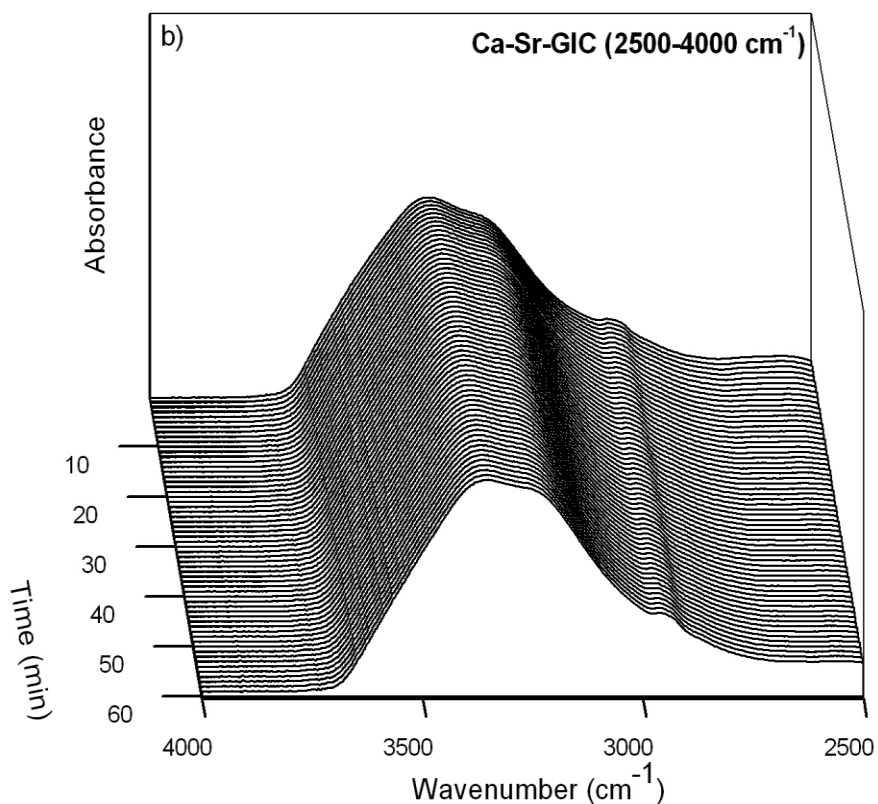


Figure 3-13: Real time ATR-FTIR analysis of Ca-Sr-GIC at different time intervals for 60 minutes at wave numbers 2500 – 4000 cm^{-1} .

Figure 3-13 illustrates a characteristic band for Ca-Sr-GIC composition that ranges from 3719 to 2753 cm^{-1} , which is due to inter- and intralayer H-bonded O-H stretching vibrations^{56,179,180}. This is similar to Ca-GIC shown in Figure 3-5.

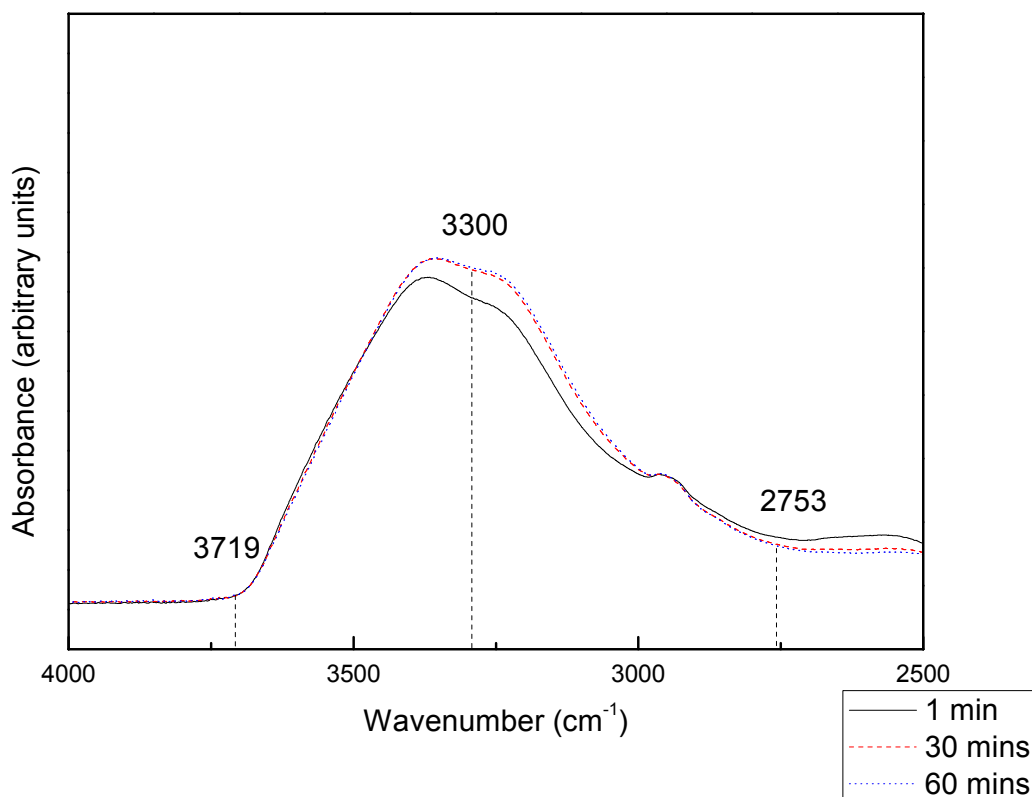


Figure 3-14: Real time ATR-FTIR analysis of the setting reaction of Ca-Sr-GIC at 1 minute, 30 minutes and 60 minutes after mixing at wave numbers 2500 – 4000 cm^{-1} .

The intensity of the characteristic band of Ca-Sr-GIC (Figure 3-14) is in marked contrast to Ca-GIC (Figure 3-6). The Ca-Sr-GIC's intensity increases over 30 minutes. But, no further changes can be observed from 30 minutes to 60 minutes for Ca-Sr-GIC (Figure 3-14), consistent with the observations for Ca-GIC (Figure 3-6). However, while Ca-Sr-GIC (Figure 3-14) increases overall in intensity from 1 minute to 60 minutes, Ca-GIC (Figure 3-6) in contrast decreases overall from 1 minute to 60 minutes.

The development of the Ca-Sr-GIC over 60 minutes in the wave number range from 700 to 1350 cm^{-1} can be observed in Figure 3-15 and Figure 3-16.

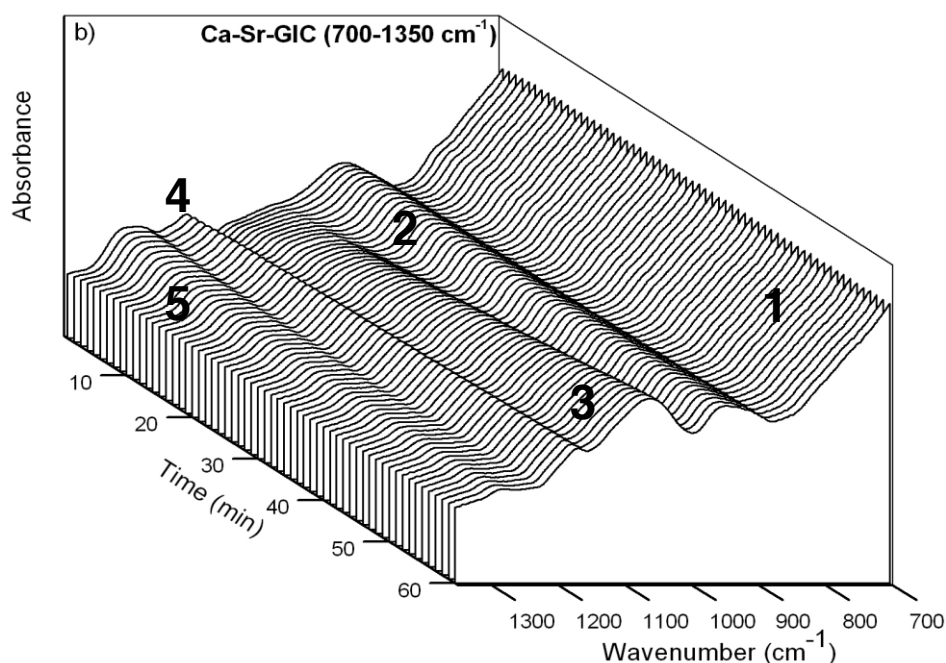


Figure 3-15: Real time ATR-FTIR analysis of Ca-Sr-GIC at different time intervals for 60 minutes at wave numbers 700 – 1350 cm^{-1} .

Figure 3-15 No 1 illustrates a strong absorbance band in the FTIR spectra of strontium substituted GIC at ca. 700 cm^{-1} . The peak at ca. 700 cm^{-1} is attributed to the symmetric stretching of Si-O^{178,181,182}.

An increase in intensity for Ca-Sr-GIC (Figure 3-16 No 1) was observed, whereas for Ca-GIC (Figure 3-8 No 1) a decrease was observed.

A noticeable band appears at 939 cm^{-1} for Ca-Sr-GIC (Figure 3-15 No 2). Peaks in the region $900 - 1200 \text{ cm}^{-1}$ are attributed to the setting reaction of GIC^{157,183}. Almost no change in the intensity for Ca-Sr-GIC (Figure 3-16 No 2) is apparent, whereas for Ca-GIC (Figure 3-8 No 2) a slight increase in the intensity was observed over a time period of 60 minutes. The increase in the intensity for Ca-Sr-GIC (Figure 3-15 No 2) occurs after ca. 5 minutes, ca. 2 minutes later than with in Ca-GIC (Figure 3-7 No 2).

A new peak rises at 1063 cm^{-1} for Ca-Sr-GIC (Figure 3-15 No 3) at ca. 10 minutes and keeps markedly increasing in intensity up to 30 minutes (Figure 3-16 No 3) followed by a further noticeable increase up to 60 minutes. This is similar to Ca-GIC (Figure 3-8 No 3). Absorptions around $1000 - 1200 \text{ cm}^{-1}$ and $1018 - 1073 \text{ cm}^{-1}$ are attributed to the asymmetric stretching of Si-O¹⁸¹.

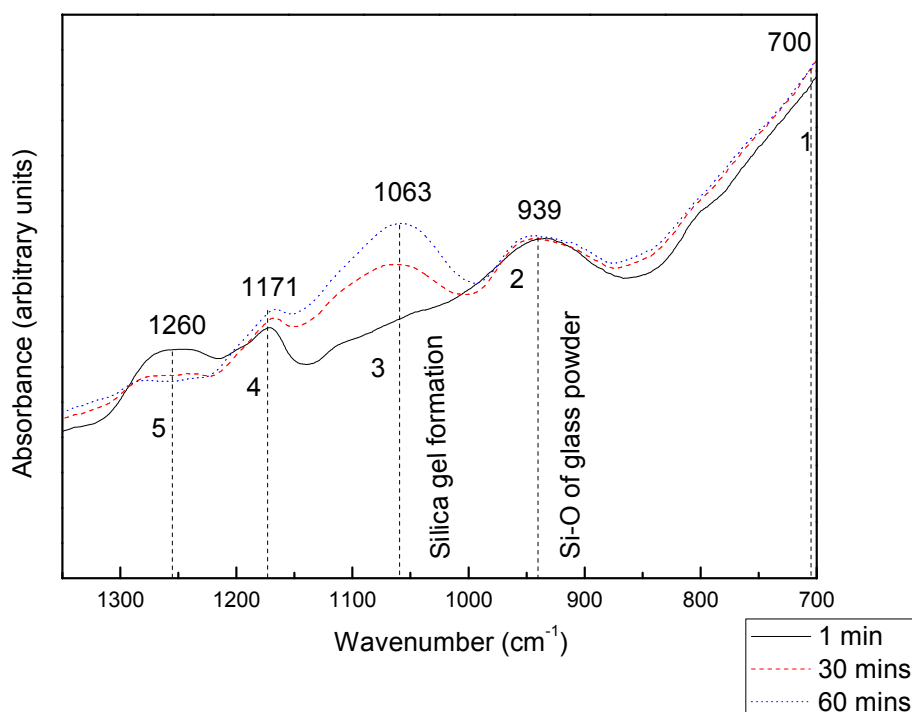


Figure 3-16: Real time ATR-FTIR analysis of the setting reaction of Ca-Sr-GIC at 1 minute, 30 minutes and 60 minutes after mixing at wave numbers 700 – 1350 cm^{-1} .

A shallow, narrow peak at 1171 cm^{-1} for Ca-Sr-GIC (Figure 3-15 No 4) broadens and increases marginally in intensity (Figure 3-16 No 4) during 60 minutes. Peaks in the range from $950 - 1640 \text{ cm}^{-1}$ are an indication for silica gel formation upon acid degradation of the glass powder¹⁸⁵.

A broad peak at 1260 cm^{-1} for Ca-Sr-GIC (Figure 3-15 No 5) reduces noticeably in intensity from 1 minute to 30 minutes followed by a slight decrease from 30 minutes to 60 minutes (Figure 3-16 No 5). This peak broadens until the point of invisibility (Figure 3-15 No 5). Absorptions around $1000 - 1200 \text{ cm}^{-1}$ are attributed to asymmetric stretching of Si-O¹⁸¹.

In contrast, peaks in the wave number frequency 1171 cm^{-1} and 1260 cm^{-1} do not exist for Ca-GIC (Figure 3-7 and Figure 3-8).

The development of the Ca-Sr-GIC over 60 minutes in the wave number range from 1350 to 1750 cm^{-1} is illustrated in Figure 3-17 and Figure 3-18.

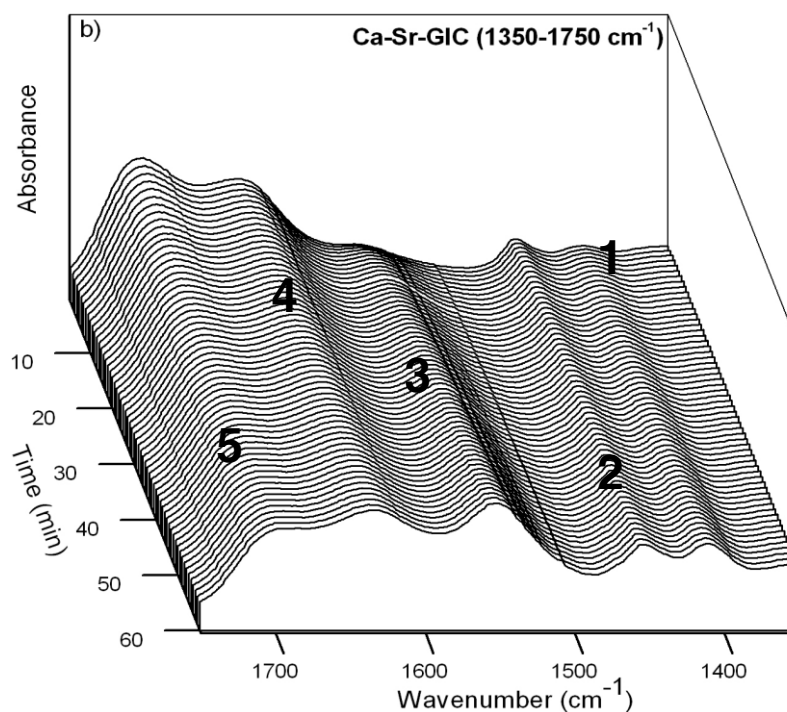


Figure 3-17: Real time ATR-FTIR analysis of Ca-Sr-GIC at different time intervals for 60 minutes at wave numbers 1350 – 1750 cm⁻¹.

Ca-Sr-GIC (Figure 3-17 No 1 & No 2) exhibits absorption peaks at 1407 cm⁻¹ and 1451 cm⁻¹. These peaks are due to the C=O symmetric stretching and formation of calcium and aluminium salts⁵⁷ and are more noticeable for Ca-Sr-GIC (Figure 3-17 No 1 & No 2) and much higher in intensity (Figure 3-18 No 1 & No 2) in comparison with Ca-GIC (Figure 3-9 and Figure 3-10 No 1 & No 2).

The calcium polyacrylate (at 1407 cm⁻¹) peak for Ca-Sr-GIC increases in intensity (Figure 3-18 No 1) just after ca. 3 minutes (Figure 3-17 No 1), whereas the intensity started to increase for Ca-GIC (Figure 3-9 No 1) after ca. 5 minutes.

For the calcium polyacrylate (at 1407 cm⁻¹) and the aluminium polyacrylate (at 1451 cm⁻¹) a noticeable increase in intensity (Figure 3-18 No 1 & No 2) from 1 minute (Figure 3-17 No 1 & No 2) to 30 minutes was observed, followed by a further increase up to 60 minutes (Figure 3-18 No 1 & No 2). In contrast, from 30 minutes to 60 minutes for Ca-GIC (Figure 3-10 No 1 & No 2) no change in intensity for calcium and aluminium polyacrylate peaks was observed.

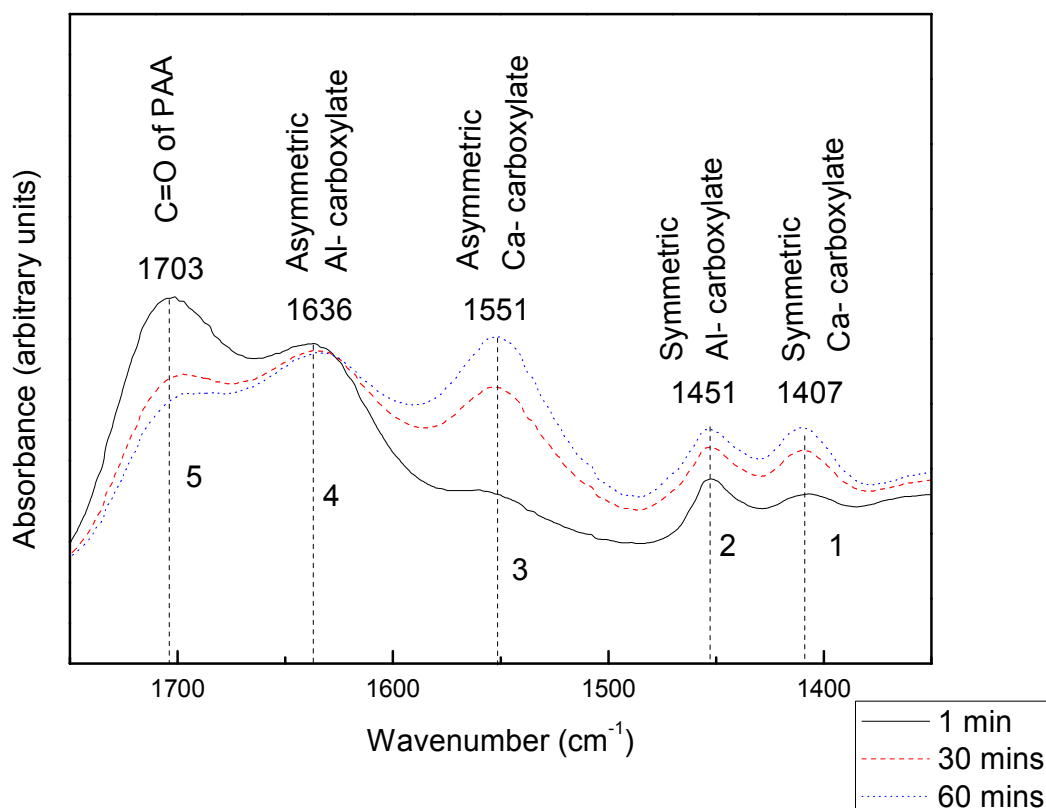


Figure 3-18: Real time ATR-FTIR analysis of the setting reaction of Ca-Sr-GIC at 1 minute, 30 minutes and 60 minutes after mixing at wave numbers 1350 – 1750 cm^{-1} .

A broad peak at 1551 cm^{-1} for Ca-Sr-GIC (Figure 3-17 No 3 and Figure 3-18 No 3) initially with low intensity thereafter became more narrow and increased noticeably in intensity from 1 minute to 60 minutes (Figure 3-18 No 3). Peaks at 1550 cm^{-1} are associated with C=O asymmetric stretching of calcium polyacrylate^{47,57}. The increase of the asymmetric stretching vibration of calcium polyacrylate for Ca-GIC (Figure 3-10 No 3) is consistent with Ca-Sr-GIC (Figure 3-18 No 3). In contrast, only a marginal increase in intensity from 30 minutes to 60 minutes was observed for Ca-GIC (Figure 3-10 No 3), whereas for Ca-Sr-GIC (Figure 3-18 No 3) a marked increase was observed.

A broad peak at 1636 cm^{-1} for Ca-Sr-GIC (Figure 3-18 No 4) decreased slightly in intensity and became narrower from 1 minute to 60 minutes. Peaks near wave number 1640 cm^{-1} (Figure 3-18 No 4) are associated with the bending vibrations of water¹⁸⁴. Furthermore, peaks around 1600 cm^{-1} are associated with C=O asymmetric

stretching of Al-polycarboxylates⁵⁷. This is similar to Ca-GIC (Figure 3-10 No 4).

A narrow peak at 1703 cm^{-1} for Ca-Sr-GIC (Figure 3-17 No 5 and Figure 3-18 No 5) is associated with stretching of carboxylic acid groups⁴⁶, which decreased noticeably in intensity presenting shallow shoulders on a broad COO^- salt peak in the first 10 minutes (Figure 3-17 No 5) up to 30 minutes, followed by a slight decrease from 30 minutes to 60 minutes (Figure 3-18 No 5). In contrast, a broad peak for Ca-GIC (Figure 3-10 No 5) was present 1 minute after mixing, whereas for Ca-Sr-GIC a narrow peak was present at 1 minute (Figure 3-18 No 5). From 30 minutes to 60 minutes for Ca-GIC (Figure 3-10 No 5) no further decrease was observed in contrast with Ca-Sr-GIC (Figure 3-18 No 5). Furthermore, there was a decrease in intensity from 1 minute to 60 minutes for Ca-GIC (Figure 3-10 No 5), which was less pronounced as for Ca-Sr-GIC (Figure 3-18 No 5).

All the peaks for all the three GIC compositions and their associated interpretations for the GIC setting reaction are illustrated in Table 3-3 and Table 3-5.

3.1.3.3 FTIR spectroscopy study of barium substituted cement setting reaction

Figure 3-19 illustrates the 3D real time FTIR series of the setting reaction for barium substituted GIC (Ca-Ba-GIC) during 60 minutes.

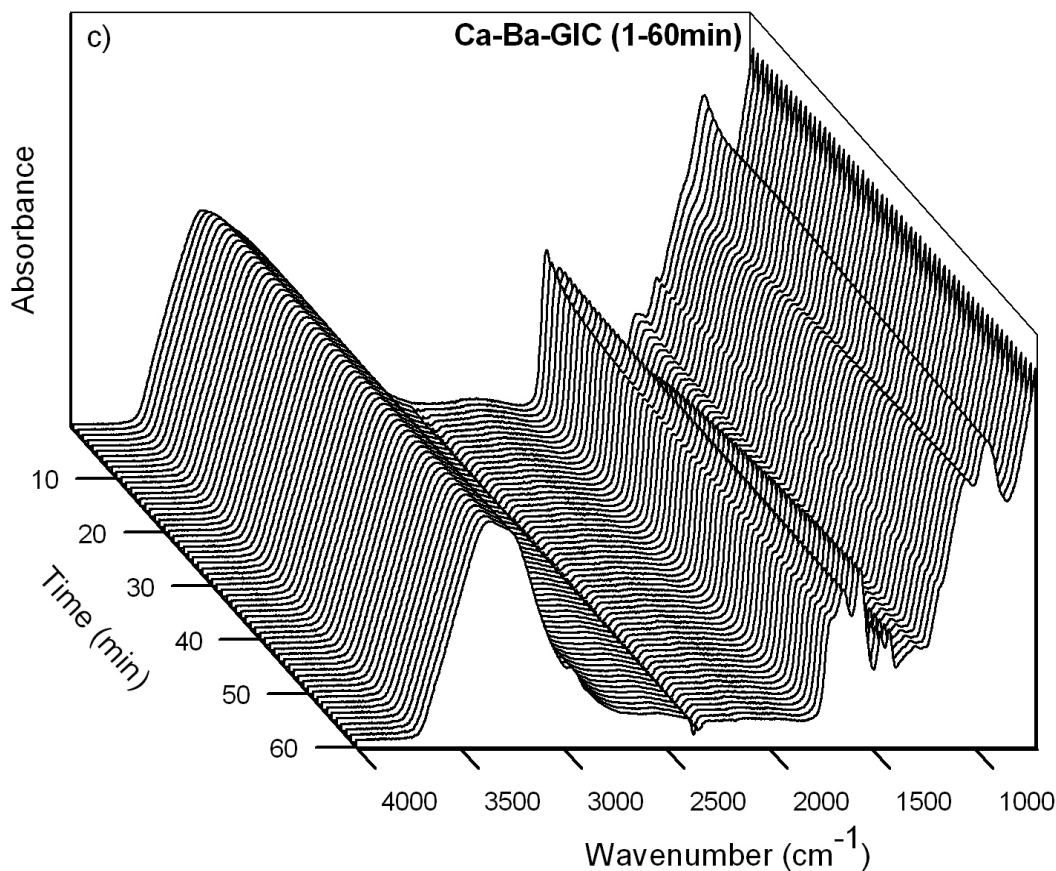


Figure 3-19: Real time ATR-FTIR analysis of the setting reaction of Ca-Ba-GIC at different time intervals for 60 minutes.

Several absorption bands with changes in the spectra over time in Figure 3-19 can be observed. Additionally, Figure 3-20 presents the changes in the intensity at 1 minute, 30 minutes and 60 minutes after mixing.

Comparing all three spectra for the three GIC compositions, Ca-Sr-GIC (Figure 3-11) and Ca-Ba-GIC (Figure 3-19) show similarities in course of curvature. In contrast, the FTIR spectrum of Ca-GIC shown in Figure 3-3 exhibits fewer peaks. Furthermore, more fluctuations in intensity in the spectra of Ca-Sr-GIC (Figure 3-12) and Ca-Ba-GIC (Figure 3-20) can be observed in comparison to the spectrum of Ca-GIC shown in Figure 3-4.

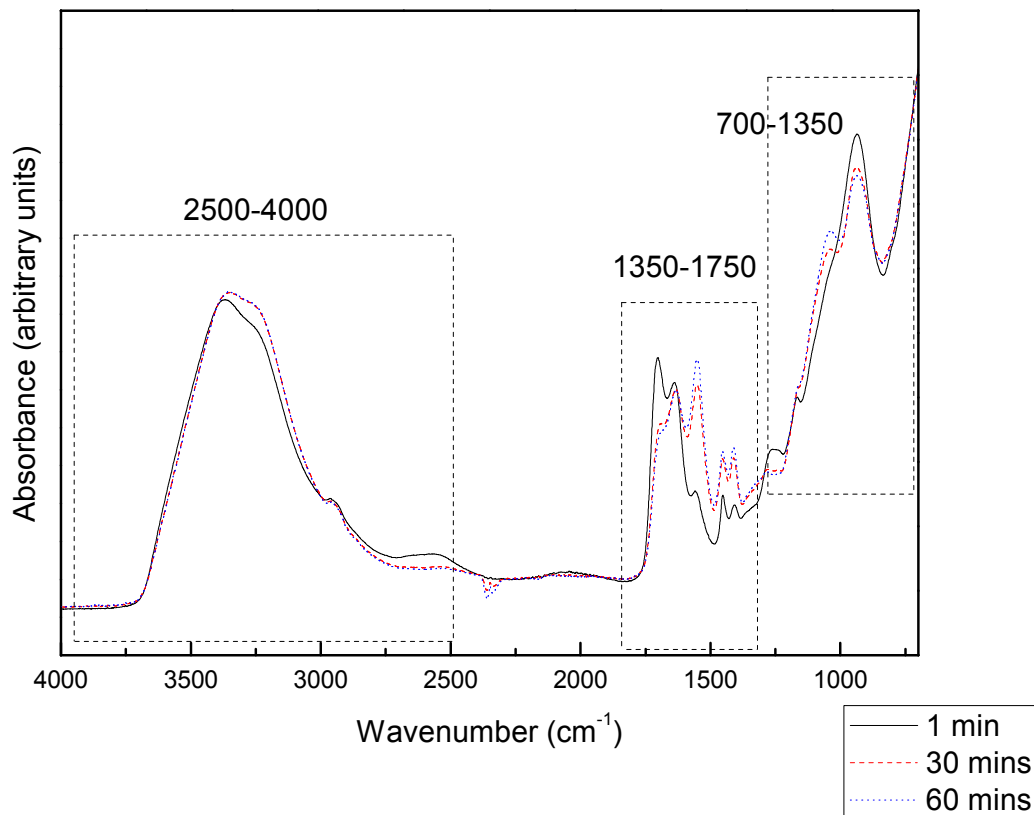


Figure 3-20: Real time ATR-FTIR analysis of the setting reaction of Ca-Ba-GIC at 1 minute, 30 minutes and 60 minutes after mixing.

Table 3-6 illustrates the ratio of the change in the intensity over time from the 2D figures. Percentage changes in the intensity from 1 minute to 30 minutes (A/B), from 1 minute to 60 minutes (A/C) and from 30 minutes to 60 minutes (B/C) were obtained.

Table 3-6: Ratio of change in intensity plotted over time for Ca-Ba-GIC, with the associated peak assignments.

Glass composition	Ratio A/B (%)	Ratio A/C (%)	Ratio B/C (%)	Wave number (cm ⁻¹)	Figure	Peak number	Assignment	Reference
Ca-Ba-GIC	7	7	0	3300	3D: Figure 3-21 2D: Figure 3-22	-----	Inter- and intralayer H-bonded O-H stretching vibrations	Gao and Heimann ¹⁷⁹ Billingham <i>et al.</i> ¹⁸⁰ Barry <i>et al.</i> ⁵⁶
	28	39	8	1409	3D: Figure 3-25 2D: Figure 3-26	1	Symmetric C=O stretching of Ca-polycarboxylate	Nicholson ⁵⁷
	21	30	12	1452	3D: Figure 3-25 2D: Figure 3-26	2	Symmetric C=O stretching of Al-polycarboxylate	Nicholson ⁵⁷
	13	21	9	1550	3D: Figure 3-25 2D: Figure 3-26	3	Asymmetric C=O stretching of Ca-polycarboxylate	Nicholson ⁵⁷
	37	47	16	1636	3D: Figure 3-25 2D: Figure 3-26	4	Asymmetric C=O stretching of Al-polycarboxylate	Nicholson ⁵⁷
	6	6	0	1703	3D: Figure 3-25 2D: Figure 3-26	5	Stretching of carboxylic acid groups	Young <i>et al.</i> ⁴⁶
	7	9	1	936	3D: Figure 3-25 2D: Figure 3-26	2	Si-O in glass powder	Matsuya <i>et al.</i> ¹⁵⁷
	5	5	0	1049	3D: Figure 3-23 2D: Figure 3-24	3	Formation of silica gel	Matsuya <i>et al.</i> ¹⁵⁷

A/B: 1 minute/30 minutes; A/C: 1 minute/60 minutes; B/C: 30 minutes/60 minutes.

The development of the barium substituted GIC during 60 minutes in the wave number 2500 – 4000 cm^{-1} can be observed in Figure 3-21 and Figure 3-22.

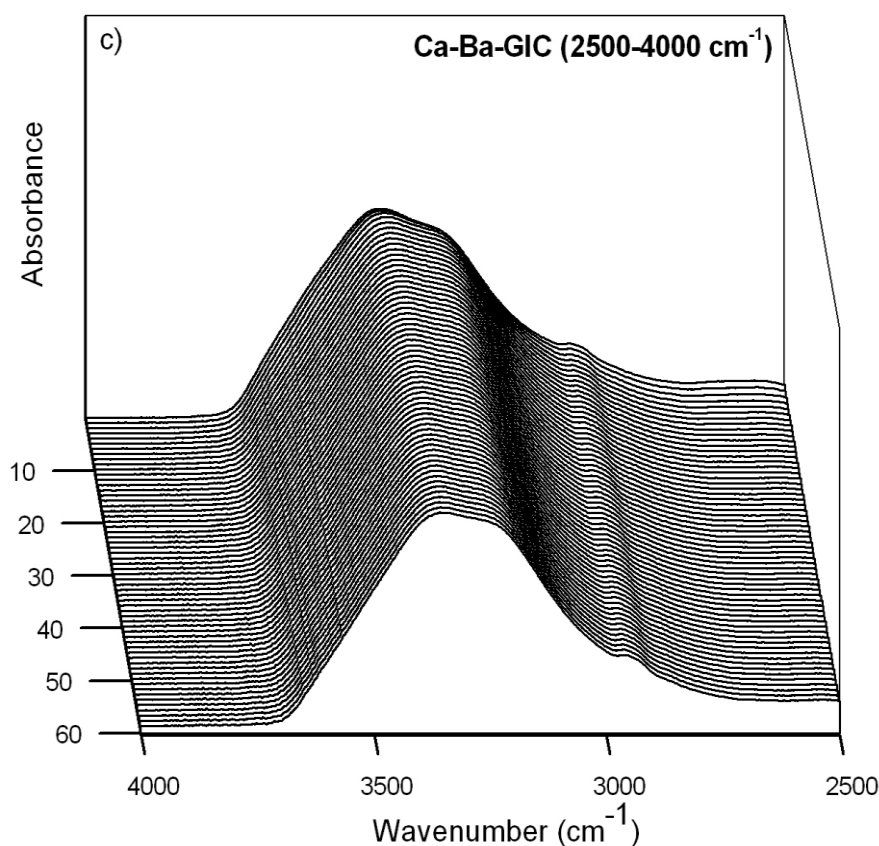


Figure 3-21: Real time ATR-FTIR analysis of Ca-Ba-GIC at different time intervals for 60 minutes at wave numbers 2500 – 4000 cm^{-1} .

Figure 3-21 illustrates a characteristic band that was apparent for all three GIC compositions. This band for Ca-Ba-GIC occurs at ca. 3729 – 2767 cm^{-1} and is due to inter- and intralayer H-bonded O-H stretching vibrations^{56,179,180}. In totality, from 1 minute to 60 minutes for Ca-Ba-GIC (Figure 3-22) and Ca-Sr-GIC (Figure 3-12) the intensity from the inter- and intralayer H-bonded O-H stretching vibrations increases to similar extent. In marked contrast, from 1 minute to 60 minutes for Ca-GIC (Figure 3-6) a decrease in intensity was observed.

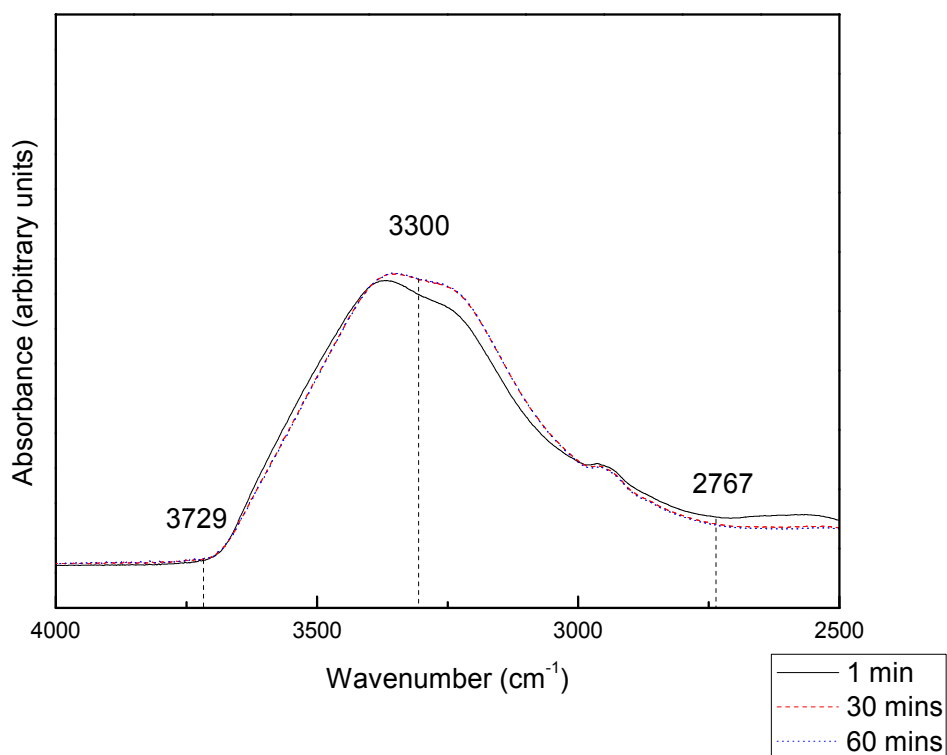


Figure 3-22: Real time ATR-FTIR analysis of the setting reaction of Ca-Ba-GIC at 1 minute, 30 minutes and 60 minutes after mixing at wave numbers 2500 – 4000 cm^{-1} .

The development of the Ca-Ba-GIC during 60 minutes in the wave number range from 700 to 1350 cm^{-1} is presented in Figure 3-22 and Figure 3-23.

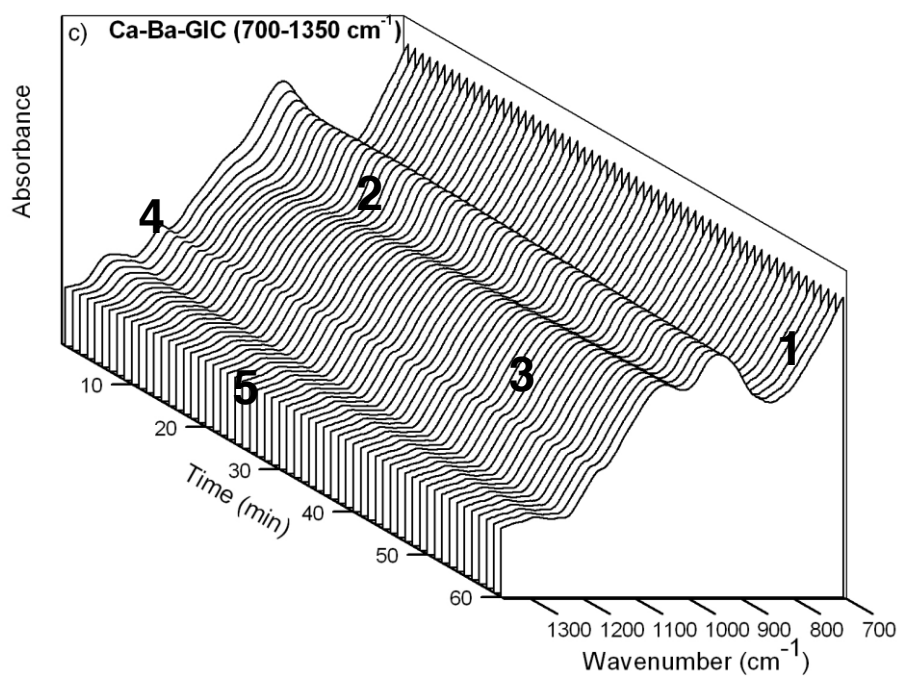


Figure 3-23: Real time ATR-FTIR analysis of Ca-Ba-GIC at different time intervals for 60 minutes at wave numbers 700 – 1350 cm^{-1} .

Figure 3-23 No 1 illustrates a strong absorbance band in the FTIR spectra of barium substituted GIC at ca. 700 cm^{-1} . This peak at ca. 700 cm^{-1} is attributed to the symmetric stretching of Si-O^{178,181,182}. Absorptions in the region $400 - 850\text{ cm}^{-1}$ are attributed to amorphous silica¹⁸⁵. During 60 minutes for Ca-Ba-GIC (Figure 3-24 No 1) there is no change in intensity. However, during 60 minutes for Ca-Sr-GIC (Figure 3-16 No 1) a marginal increase was observed and for Ca-GIC (Figure 3-8 No 1) a slight decrease was observed.

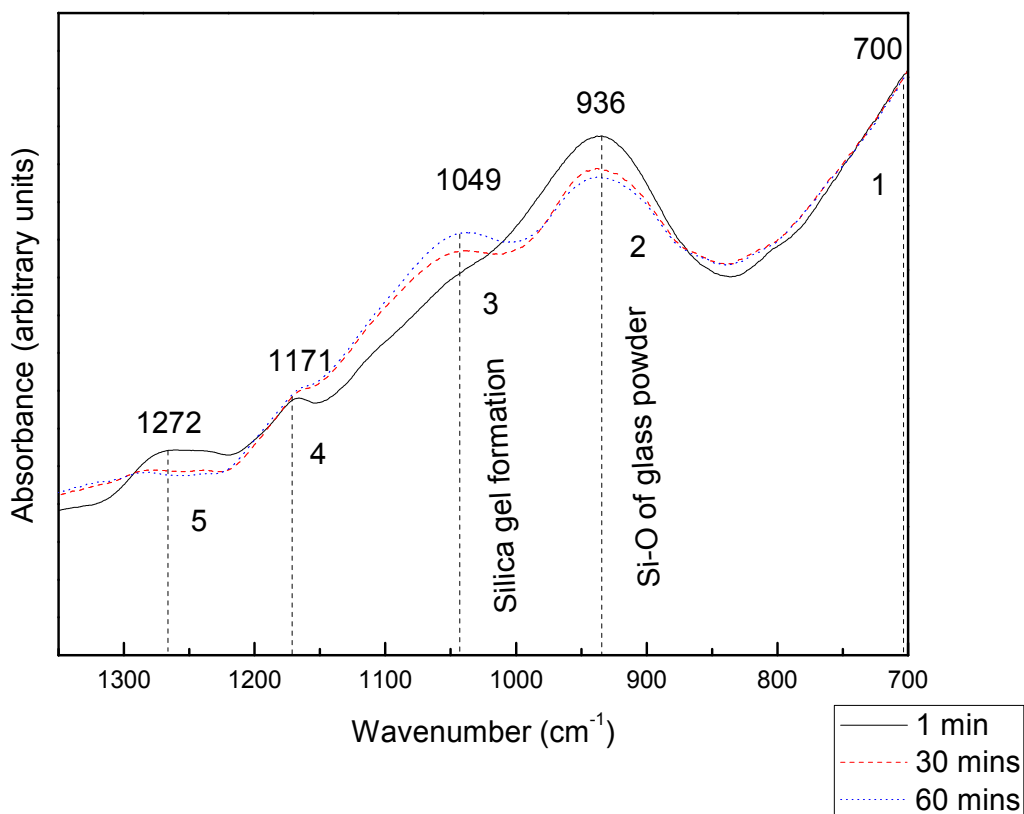


Figure 3-24: Real time ATR-FTIR analysis of the setting reaction of Ca-Ba-GIC at 1 minute, 30 minutes and 60 minutes after mixing at wave numbers $700 - 1350\text{ cm}^{-1}$.

A noticeable band appears at 936 cm^{-1} for Ca-Ba-GIC (Figure 3-23 No 2 and Figure 3-24 No 2) a noticeable decrease in intensity was observed from 1 minute to 60 minutes, followed by a marginal decrease up to 60 minutes. Peaks in the region $900 - 1200\text{ cm}^{-1}$ are attributed to the setting reaction of GIC^{157,183}. In contrast, from 1 minute to 60 minutes for Ca-Sr-GIC (Figure 3-16 No 2) almost no change in

intensity was observed, while a slight increase for Ca-GIC (Figure 3-8 No 2) was observed.

A new peak at ca. 10 minutes rises for Ca-Ba-GIC at 1049 cm^{-1} (Figure 3-23 No 3) and keeps increasing up to 60 minutes (Figure 3-24 No 3). Absorptions around $1000 - 1200\text{ cm}^{-1}$ are attributed to the asymmetric stretching of Si-O^{181} . From 1 minute to 60 minutes the most noticeable increase in intensity at this wave number is exhibited by Ca-Sr-GIC (Figure 3-16 No 3) followed by Ca-GIC (Figure 3-8 No 3) followed by Ca-Ba-GIC (Figure 3-24 No 3).

A shallow, narrow peak at 1171 cm^{-1} for Ca-Ba-GIC broadens (Figure 3-23 No 4) and increases slightly in intensity (Figure 3-24 No 4) from 1 minute to 30 minutes. From 30 minutes to 60 minutes no change was observed. Similar progress was observed for Ca-Sr-GIC (Figure 3-16 No 4), but from 30 minutes to 60 minutes a slight increase in intensity was observed, in contrast with Ca-Ba-GIC (Figure 3-24 No 4). Peaks in the range from $950 - 1640\text{ cm}^{-1}$ are an indication for silica gel formation upon acid degradation of the glass powder¹⁸⁵.

A broad peak at 1272 cm^{-1} for Ca-Ba-GIC (Figure 3-23 No 5), which reduced in intensity and broadened (Figure 3-24 No 5), was observed from 1 minute to 60 minutes. Absorptions around $1000 - 1200\text{ cm}^{-1}$ are attributed to asymmetric stretching of Si-O^{181} . Similar progress was observed for Ca-Sr-GIC (Figure 3-16 No 5). In contrast, peaks in the wave number frequency at 1171 cm^{-1} and 1272 cm^{-1} and do not occur for Ca-GIC (Figure 3-8).

The development of the Ca-Ba-GIC during 60 minutes in the wave number range from 1350 to 1750 cm^{-1} can be observed in Figure 3-25 and Figure 3-26. From 1 minute to 60 minutes both Ca-Ba-GIC and Ca-Sr-GIC show similar progress in peak development from $13500 - 1750\text{ cm}^{-1}$.

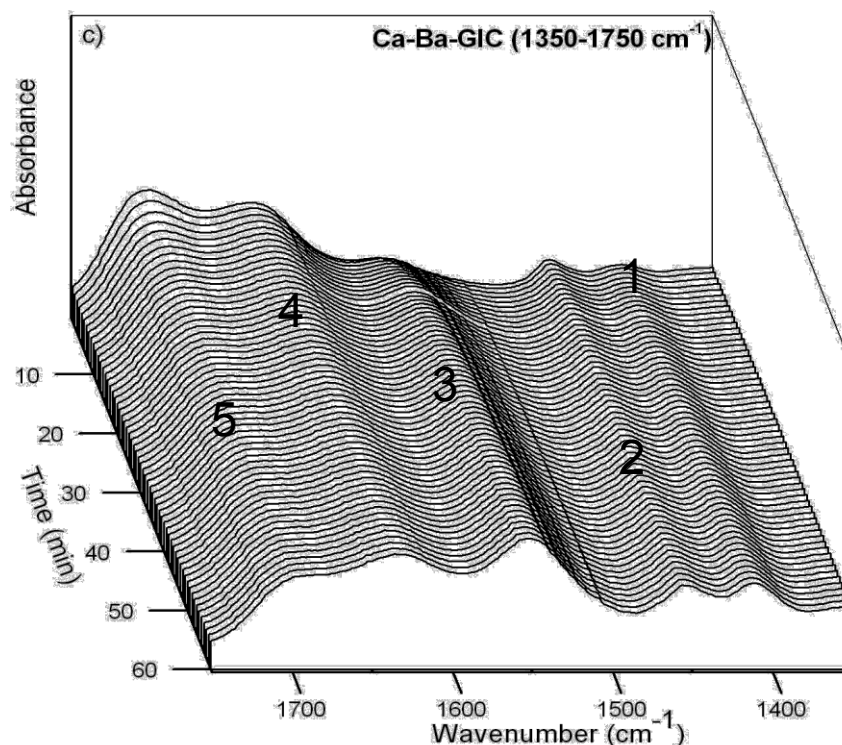


Figure 3-25: Real time ATR-FTIR analysis of the setting reaction of Ca-Ba-GIC at different time intervals for 60 minutes at wave numbers 1350 – 1750 cm^{-1} .

Absorption peaks at 1409 cm^{-1} and 1452 cm^{-1} (No 1 & No 2) for Ca-Ba-GIC are due to the C=O symmetric stretching and formation of calcium and aluminium salts⁵⁷. These peaks are more noticeable and significantly higher in intensity for Ca-Sr-GIC (Figure 3-17 No 1 & No 2) and Ca-Ba-GIC (Figure 3-25 No 1 & No 2) in contrast with Ca-GIC (Figure 3-9 No 1 & No 2). From 30 minutes to 60 minutes, for Ca-GIC (Figure 3-10 No 1 & No 2), no further increase in intensity was observed, whereas for Ca-Sr-GIC (Figure 3-18 No 1 & No 2) and Ca-Ba-GIC (Figure 3-26 No 1 & No 2) an increase in intensity was observed. However, the increase in intensity from 30 minutes to 60 minutes is more pronounced for Ca-Sr-GIC (Figure 3-18 No 1 & No 2) in comparison to Ca-Ba-GIC (Figure 3-26 No 1 & No 2).

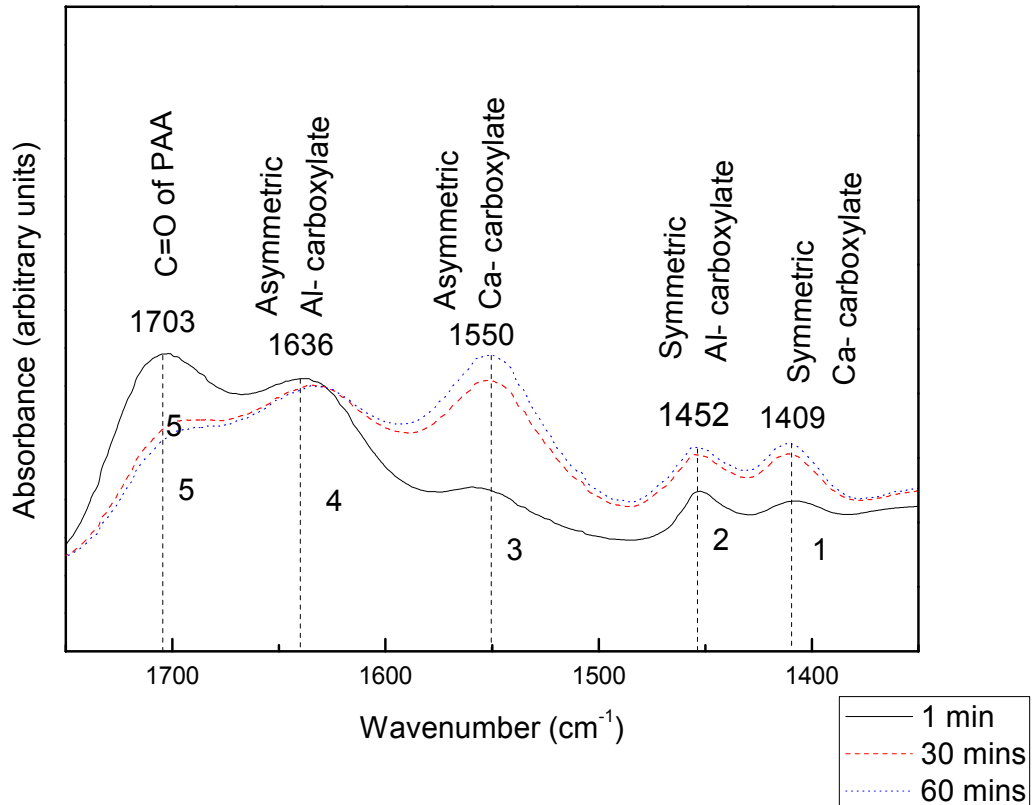


Figure 3-26: Real time ATR-FTIR analysis of the setting reaction of Ca-Ba-GIC at 1 minute, 30 minutes and 60 minutes after mixing at wave numbers 1350 – 1750 cm^{-1} .

A broad peak with low intensity at ca. 1550 cm^{-1} was apparent for all three GIC compositions. This broad peak for Ca-Ba-GIC (Figure 3-25 No 3) occurs at 1550 cm^{-1} and became narrower and noticeably increased in intensity (Figure 3-26 No 3). Peaks at 1550 cm^{-1} are associated with the C=O asymmetric stretching of calcium polyacrylate^{47,57}. From ca. 2 minutes for Ca-GIC (Figure 3-10 No 3) and ca. 5 minutes for Ca-Sr-GIC (Figure 3-18 No 3) and Ca-Ba-GIC (Figure 3-26 No 3), the intensity noticeably increases up to 60 minutes. From 1 minute to 60 minutes the most noticeable increase in intensity at this wave number is exhibited by Ca-Sr-GIC (Figure 3-18 No 3) followed by Ca-Ba-GIC (Figure 3-26 No 3) followed by Ca-GIC (Figure 3-10 No 3).

A broad peak at 1639 cm^{-1} for Ca-Ba-GIC (Figure 3-25 No 4) decreased marginally in intensity and became narrower from 1 minute to 60 minutes (Figure 3-26 No 4). Peaks near wave number 1640 cm^{-1} (Figure 3-25 No 4) are associated with the

bending vibrations of water^{184,185}. Furthermore peaks around 1600 cm⁻¹ are associated with the C=O asymmetric stretching of Al-polycarboxylates⁵⁷. Similar progress for Ca-Sr-GIC (Figure 3-18 No 4) and Ca-GIC (Figure 3-10 No 4) was observed.

A narrow peak at 1703 cm⁻¹ for Ca-Ba-GIC (Figure 3-25 No 5) is associated with the carboxylic acid groups stretching⁴⁶, which decreased noticeably in intensity (Figure 3-26 No 5) presenting shallow shoulders on a broad COO⁻ salt peak in the first 10 minutes up to 30 minutes, followed by a marginal decrease from 30 minutes to 60 minutes (Figure 3-26 No 5). Similar progress for Ca-Sr-GIC (Figure 3-18 No 5) was observed. However, from 30 minutes to 60 minutes the decrease in intensity for Ca-Ba-GIC (Figure 3-26 No 5) was not as pronounced as the decrease in intensity for Ca-Sr-GIC (Figure 3-18 No 5). In contrast, from 1 minute to 60 minutes for Ca-GIC (Figure 3-10 No 5), no change in intensity was observed in comparison with Ca-Sr-GIC (Figure 3-18 No 5) and Ca-Ba-GIC (Figure 3-26 No 5). For Ca-GIC (Figure 3-10 No 5) a peak in the wavelength around 1700 cm⁻¹ is almost invisible after 60 minutes.

All the peaks for all the three GIC compositions and their associated interpretations for the GIC setting reaction are illustrated in Table 3-3 and Table 3-6.

3.2 Fluoride release of GICs in artificial saliva and deionized water

The fluoride release experiment was divided into two stages as described in Materials and Methods Chapter 2.2.2. The results of the cumulative F⁻ release in the first 40 days at different time intervals in deionized water and AS are presented in Figure 3-27 and Figure 3-28.

Both graphs demonstrate the direct dependence of F⁻ ions release upon the release time. The cumulative F⁻ release in deionized water over 40 days (Figure 3-27) for all

three GIC compositions was increased in the order Ca-GIC > Ca-Sr-GIC > Ca-Ba-GIC. Ca-Ba-GIC reached a F⁻ release plateau after 22 days, followed by Ca-GIC after 18 days and Ca-Sr-GIC after 28 days.

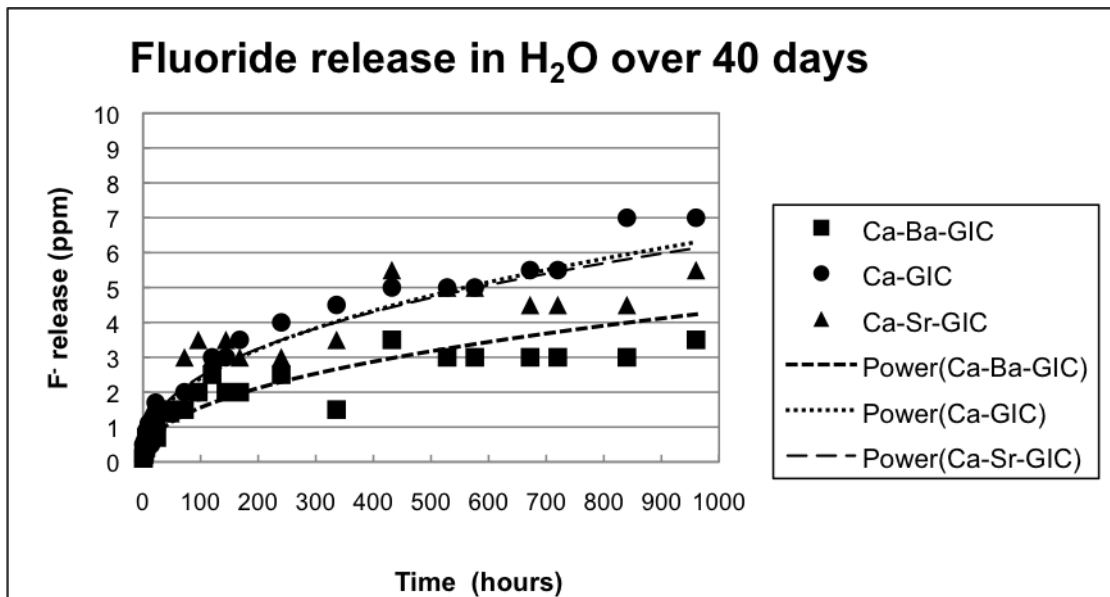


Figure 3-27: Cumulative fluoride release in deionized water at different time intervals over 40 days ($P_{Ca-GIC\ to\ Ca-Sr-GIC} = 0.46$), ($P_{Ca-GIC\ to\ Ca-Ba-GIC} < 0.001$) and ($P_{Ca-Sr-GIC\ to\ Ca-Ba-GIC} < 0.001$).

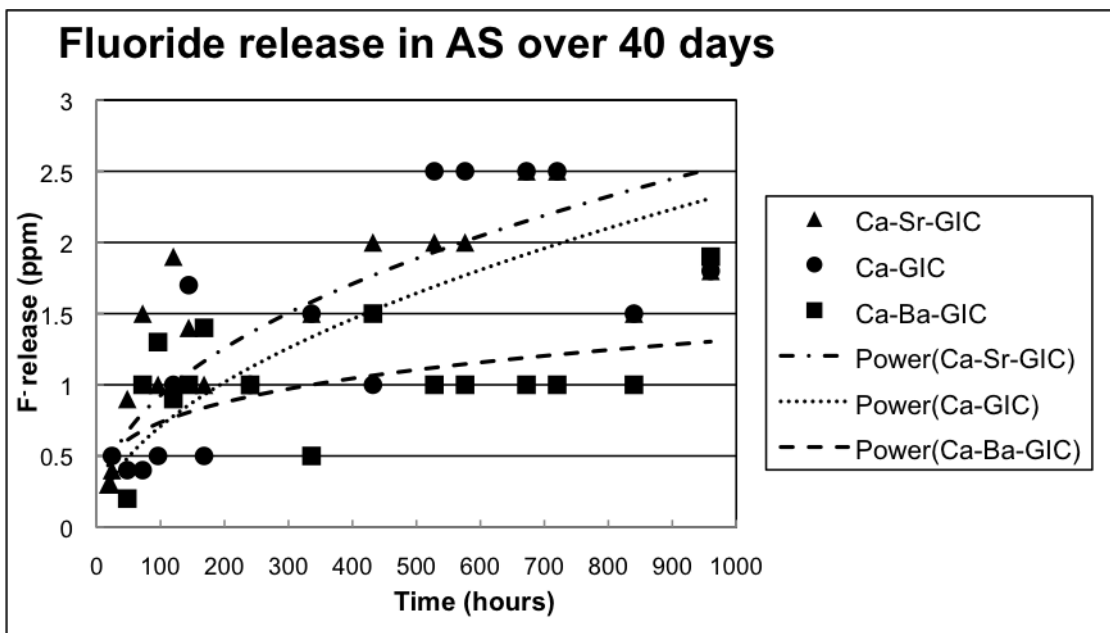


Figure 3-28: Cumulative fluoride release in artificial saliva at different time intervals over 40 days ($P_{Ca-GIC\ to\ Ca-Sr-GIC} = 0.08$), ($P_{Ca-GIC\ to\ Ca-Ba-GIC} = 0.09$) and ($P_{Ca-Sr-GIC\ to\ Ca-Ba-GIC} < 0.001$).

The paired t-test was used to compare the fluoride release data of two experimental GICs at specific time points. A total of three comparisons (1. Ca-GIC to Ca-Sr-GIC

2. Ca-GIC to Ca-Ba-GIC and 3. Ca-Sr-GIC to Ca-Ba-GIC) via the t-test were performed and illustrated below each Figure.

Analysis by the paired two sample t-test for all experimental GICs at different time points showed significant differences between Ca-Sr-GIC to Ca-Ba-GIC in deionized water and AS over 40 days ($P < 0.001$).

The F^- release in AS (Figure 3-28) for the three GIC compositions did not produce any measurable amount of F^- ions up to 24 hours, 18 hours or 48 hours for Ca-GIC, Ca-Sr-GIC and Ca-Ba-GIC, respectively. The F^- release in AS is significantly reduced and more scattered in comparison to F^- release in deionized water. However, the cumulative F^- release for all compositions was increasing in the order Ca-GIC > Ca-Sr-GIC > Ca-Ba-GIC. The F^- release plateau was reached after 18 days for Ca-Sr-GIC, followed by Ca-GIC and Ca-Ba-GIC after 22 days.

Figure 3-29 – Figure 3-31 demonstrates the F^- release in deionized water of mature GIC compositions after being exposed for 1 minute, 10 minutes, 1 hour, 6 hours and 12 hours to a F^- ion containing mouthwash. The cumulative release over 24 hours after exposure to the mouthwash increased in the order Ca-Sr-GIC > Ca-Ba-GIC > Ca-GIC.

The paired t-test compared the fluoride release of two mature experimental GICs at specific time points, after being exposed to a fluoride source, at different time intervals (from 1 minute up to 12 hours). Three comparisons (1. Ca-GIC to Ca-Sr-GIC 2. Ca-GIC to Ca-Ba-GIC and 3. Ca-Sr-GIC to Ca-Ba-GIC) at 1 minute, 10 minutes, 1 hour, 6 hours and 12 hours, via the t-test were performed and P values are shown in Table 3-7.

Table 3-7: Analysis by the paired two sample t-test in deionized water and AS of the mature GIC compositions at different time points after being exposed for 1 minute, 10 minutes, 1 hour, 6 hours and 12 hours to a F⁻ ion containing mouthwash.

Paired t-test of two GIC compositions	Time intervals in deionized H ₂ O				
	1 minutes	10 minutes	1 hour	6 hours	12 hours
Ca-GIC to Ca-Sr-GIC	<i>P</i> = 0.42	<i>P</i> = 0.23	<i>P</i> = 0.08	<i>P</i> = 0.002	<i>P</i> < 0.001
Ca-GIC to Ca-Ba-GIC	<i>P</i> = 1	<i>P</i> = 0.21	<i>P</i> = 1	<i>P</i> < 0.001	<i>P</i> < 0.001
Ca-Sr-GIC to Ca-Ba-GIC	<i>P</i> = 0.18	<i>P</i> = 0.18	<i>P</i> = 0.22	<i>P</i> = 0.019	<i>P</i> < 0.001
	Time intervals in AS				
	1 minutes	10 minutes	1 hour	6 hours	12 hours
Ca-GIC to Ca-Sr-GIC	----	----	<i>P</i> = 1	<i>P</i> = 0.5	<i>P</i> = 0.25
Ca-GIC to Ca-Ba-GIC	----	----	<i>P</i> = 0.5	<i>P</i> = 1	<i>P</i> = 0.39
Ca-Sr-GIC to Ca-Ba-GIC	----	----	<i>P</i> = 0.5	<i>P</i> = 0.5	<i>P</i> = 0.18

----: No F⁻ release; *P* > 0.01: no significant differences between the two GIC compositions present; *P* < 0.01: show significant differences between the two GIC compositions; **AS**: artificial saliva.

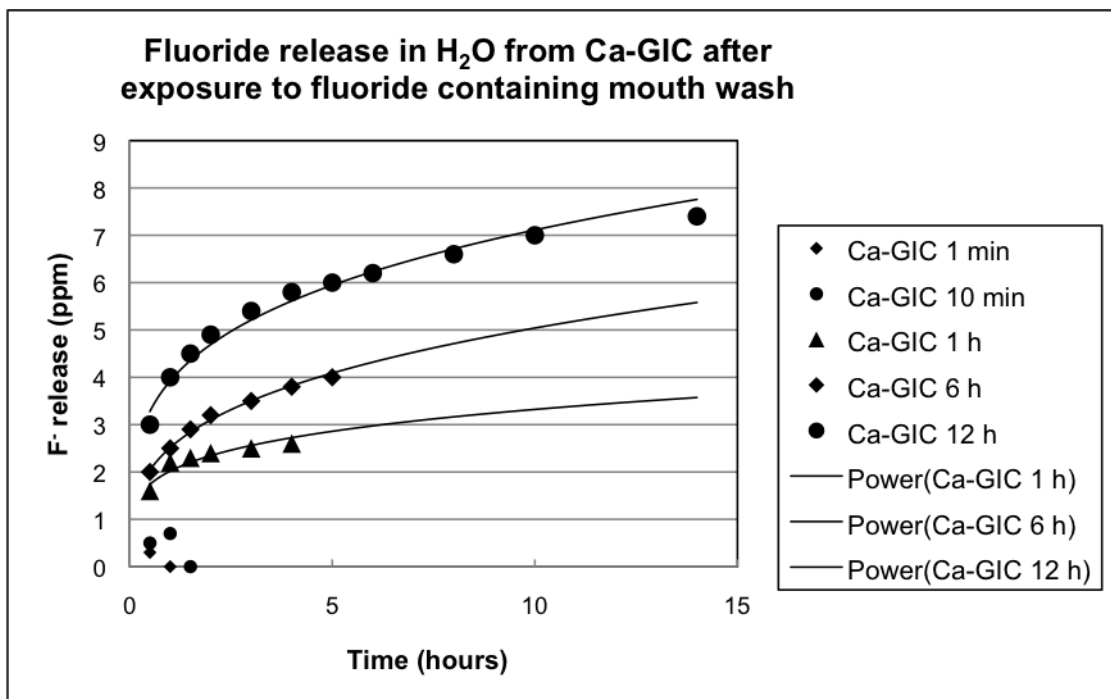


Figure 3-29: Cumulative fluoride release in deionized water from a mature Ca-GIC after exposure to a fluoride containing mouthwash at different time intervals over 24 hours (*P* values are shown in Table 3-7).

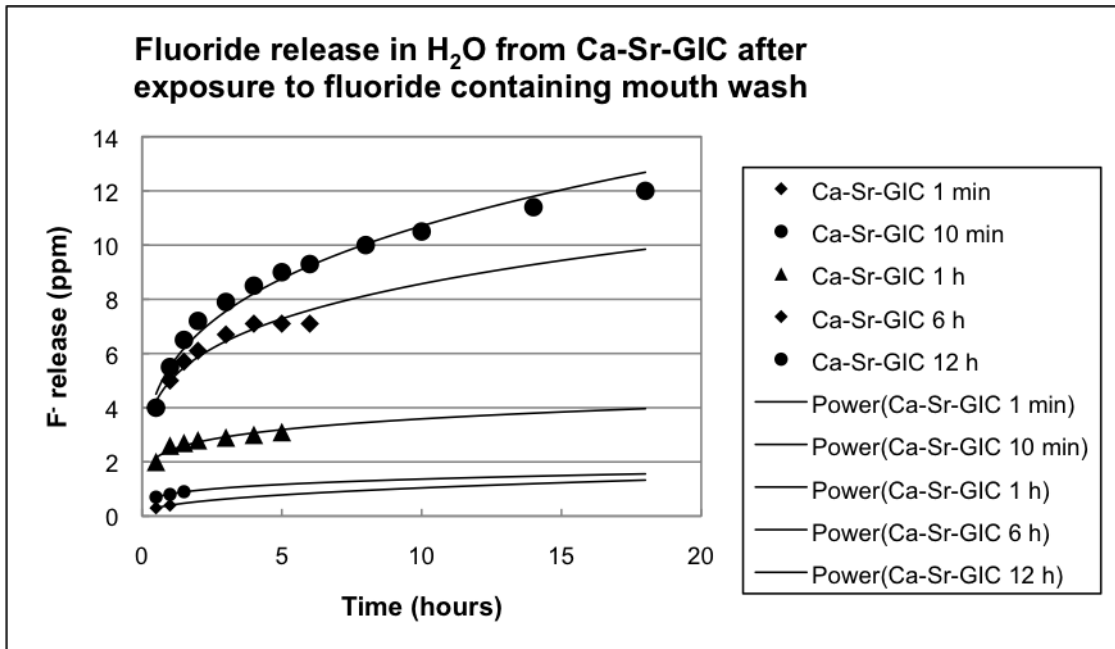


Figure 3-30: Cumulative fluoride release in deionized water from a mature Ca-Sr-GIC after exposure to a fluoride containing mouthwash at different time intervals over 24 hours (*P* values are shown in Table 3-7).

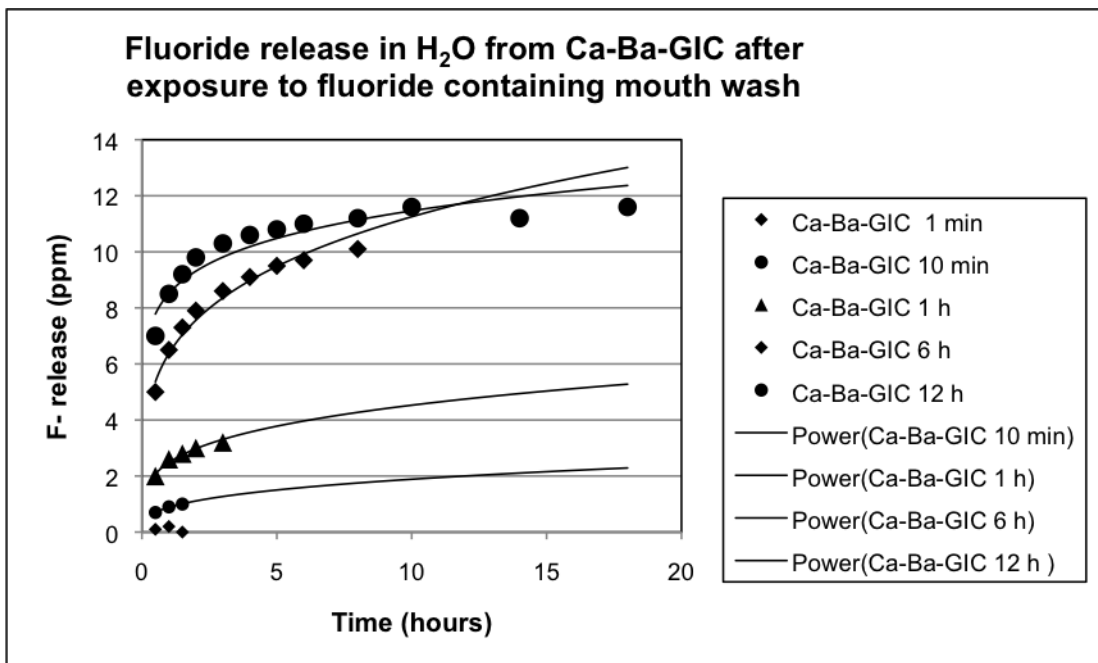


Figure 3-31: Cumulative fluoride release in deionized water from a mature Ca-Ba-GIC after exposure to a fluoride containing mouthwash at different time intervals over 24 hours (*P* values are shown in Table 3-7).

Figure 3-32 – Figure 3-34 demonstrate the F⁻ release of the three GIC compositions in AS after being exposed to a commercial available mouthwash at different time intervals over 24 hours. It was not possible to measure any F⁻ release in AS after

exposure for 1 minute and 10 minutes for the mature GICs. In case of Ca-Ba-GIC a minimal F^- release was detected first after 6 hours.

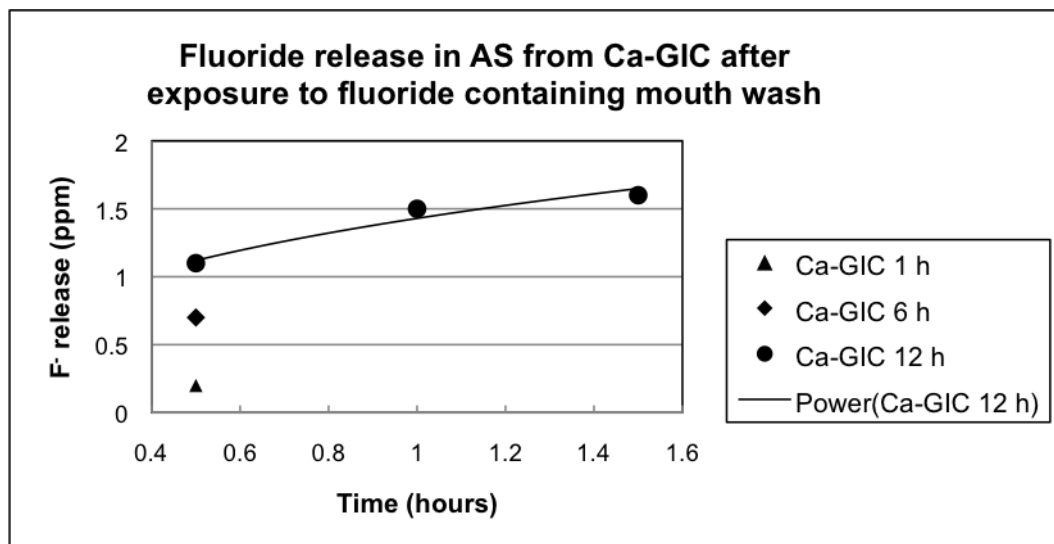


Figure 3-32: Cumulative fluoride release in AS from a mature Ca-GIC after exposure to a fluoride containing mouthwash at different time intervals over 24 hours (P values are shown in Table 3-7).

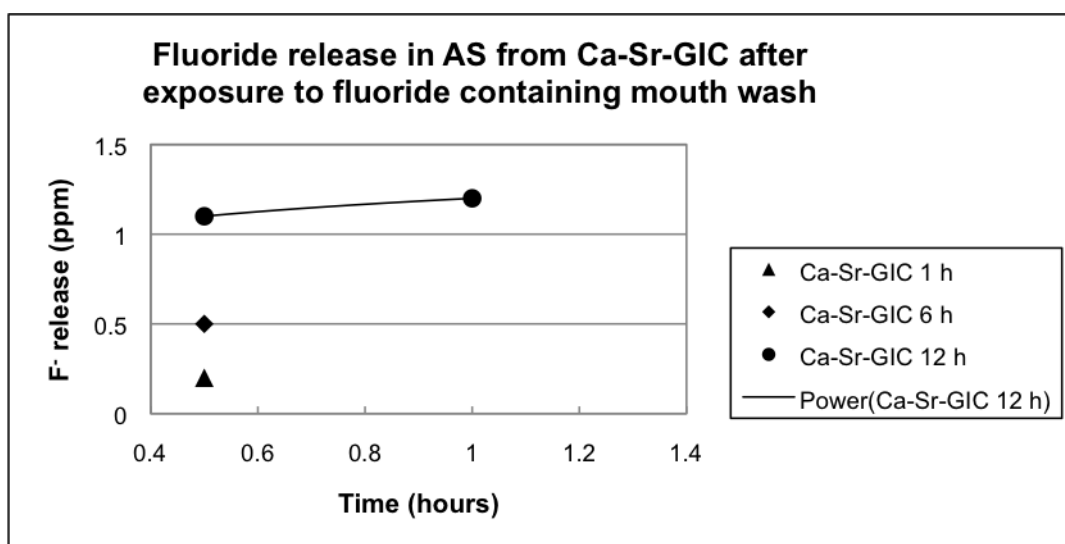


Figure 3-33: Cumulative fluoride release in AS from a mature Ca-Sr-GIC after exposure to a fluoride containing mouthwash at different time intervals over 24 hours (P values are shown in Table 3-7).

The course of progress after exposing the mature GIC to a F^- containing mouthwash and the amount of F^- released in AS is lower (23%, 11% and 12% for Ca-GIC, Ca-Sr-GIC and Ca-Ba-GIC after 12 hours exposure, respectively) in comparison to the amount of F^- released in deionized water. However, exposing the mature GIC to a F^-

containing solution for 1 minute and 10 minutes was not effective and did not produce any results.

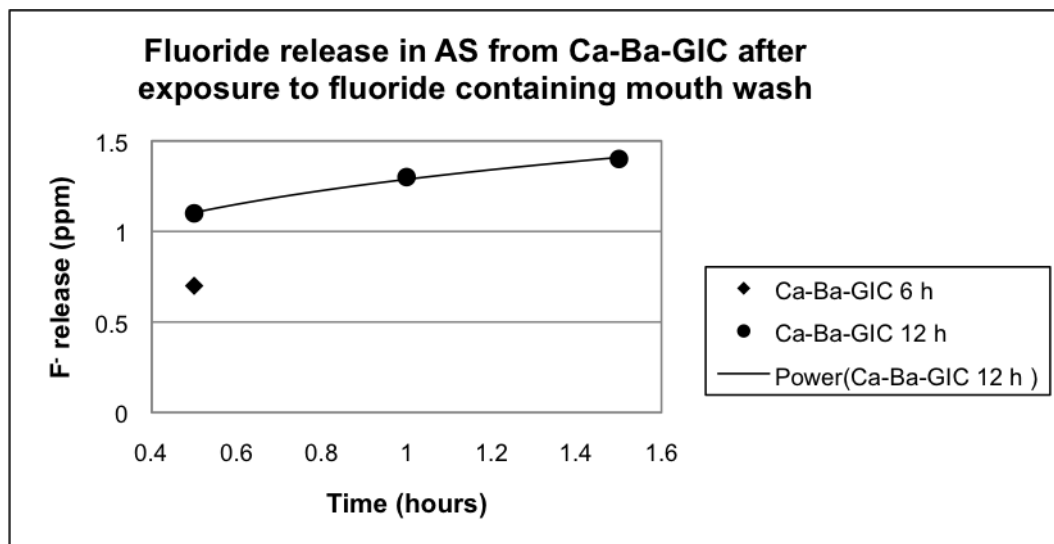


Figure 3-34: Cumulative fluoride release in AS from a mature Ca-Ba-GIC after exposure to a fluoride containing mouthwash at different time intervals over 24 hours (*P* values are shown in Table 3-7).

3.3 Antimicrobial effectiveness of glass ionomer cements

The bacteriostatic characteristic of the three GIC compositions was tested and monitored for 48 hours. *S. mutans* (NTCC No. 10449) was used for evaluation of antimicrobial activity. A direct method of measuring numbers of viable bacterial cells by plate counting as described in Materials and Methods in Chapter 2.2.3 was used to determine the number of viable bacteria remaining at each time point. In total, four time designations (10 min, 3 hours, 1 day and 2 days) were chosen to monitor the antibacterial effectiveness of the substituted GIC compositions. The antimicrobial behaviour of the three GIC compositions and a control with no cement are illustrated in Figure 3-35.

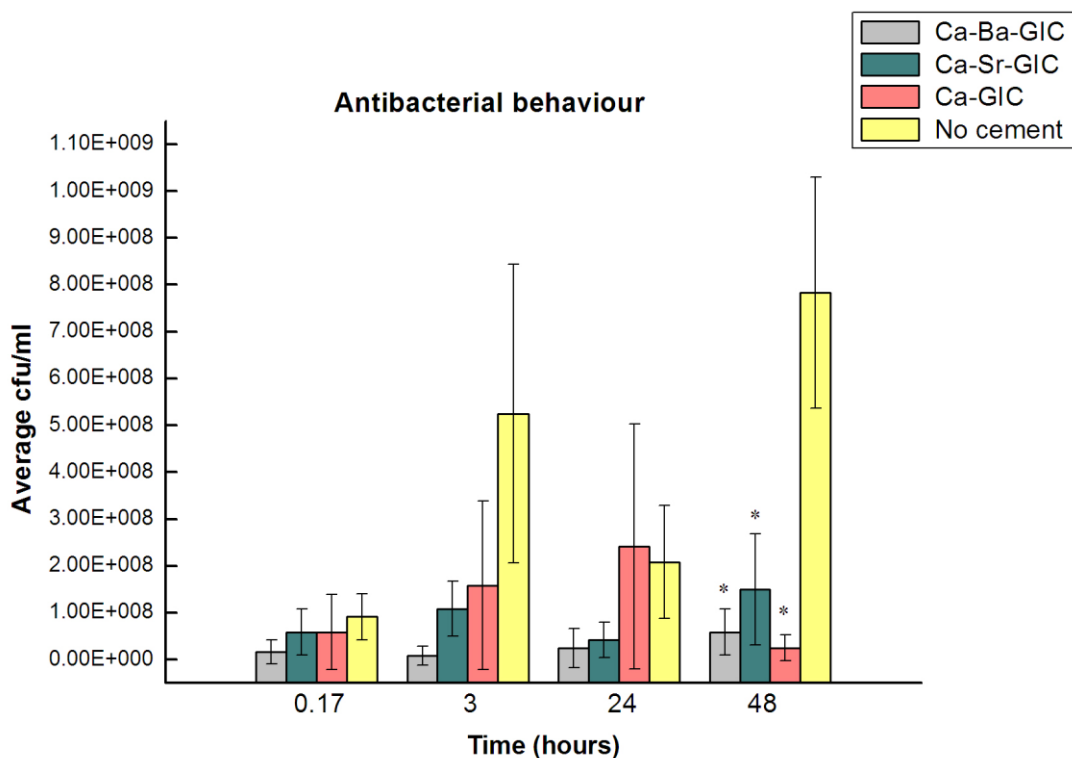


Figure 3-35: The average number of viable bacteria (cfu per ml) for all three GIC compositions and one cement free sample (as control) at 4 different time points. Asterisks indicate values statistically significantly different to the cement free control (P values are shown in Table 3-8).

As the bar chart in Figure 3-35 illustrates, all three experimental GICs exhibited an antimicrobial effect against *S. mutans* over 48 hours, with statistically significantly different results from the control without cement occurring by day 2. A total of three comparisons (1. C (control) to Ca-GIC, 2. C to Ca-Sr-GIC and 3. C to Ca-Ba-GIC) were performed via the t-test and P values are shown in Table 3-8. All experimental GICs exhibited a constant antimicrobial effect with low numbers of viable bacteria seen over the duration of the experiment.

Table 3-8: Analysis by the paired two sample t-test of the antimicrobial effectiveness of the three experimental GIC compositions.

Paired t-test of two GIC compositions	Antibacterial effectiveness
	48 hours
C to Ca-GIC	$P < 0.001$
C to Ca-Sr-GIC	$P < 0.001$
C to Ca-Ba-GIC	$P = 0.0014$

C = control (cement free sample); $P > 0.01$: no significant differences between the two GIC compositions present; $P < 0.01$: show significant differences between the two GIC compositions.

3.4 Calculation of cement setting time

The results of the setting time are shown in Table 3-9 and Figure 3-36. The latter is a comparison of the two ratios. A steady increase in the setting time of the experimental GICs with the ratio 3:1 is demonstrated (Figure 3-36).

Generally, the setting time for all three GIC compositions with a P/L ratio of 2:1 is much higher (38%, 57% and 44% for Ca-GIC, Ca-Sr-GIC and Ca-Ba-GIC, respectively) in comparison to the P/L ratio of 3:1. With increased glass powder volume and a constant amount of polymeric solution a decrease in the setting time for all three GIC compositions was observed.

Table 3-9: Setting time of the resulting GICs with different powder/liquid ratios.

Cement Specimen	Experimental glass powder	Setting time for P/L ratio 2:1 (min)	Setting time for P/L ratio 3:1 (min)
Ca-GIC	Ca 100%	9.2 ± 0.06	3.5 ± 0.1
Ca-Sr-GIC	Ca 25%, Sr 75%	7.4 ± 0.1	4.2 ± 0.08
Ca-Ba-GIC	Ca 25%, Ba 75%	8.7 ± 0.3	3.8 ± 0.3

Ca-GIC with a P/L ratio of 2:1 has the highest setting time (9.2 ± 0.06 min), while a gradual increase was also observed for the ratio 2:1 for Ca-Sr-GIC and Ca-Ba-GIC (Figure 3-36). This variation in setting time may be due to the room temperature during the experiments.

The t-test was used to compare the cement setting time of two experimental GIC compositions at different P/L ratios. A total of three comparisons (1. Ca-GIC to Ca-Sr-GIC, 2. Ca-GIC to Ca-Ba-GIC and 3. Ca-Sr-GIC to Ca-Ba-GIC) at a P/L ratio of 2:1 to 2:1 and 3:1 to 3:1 were performed via the t-test and *P* values are shown in Table 3-10.

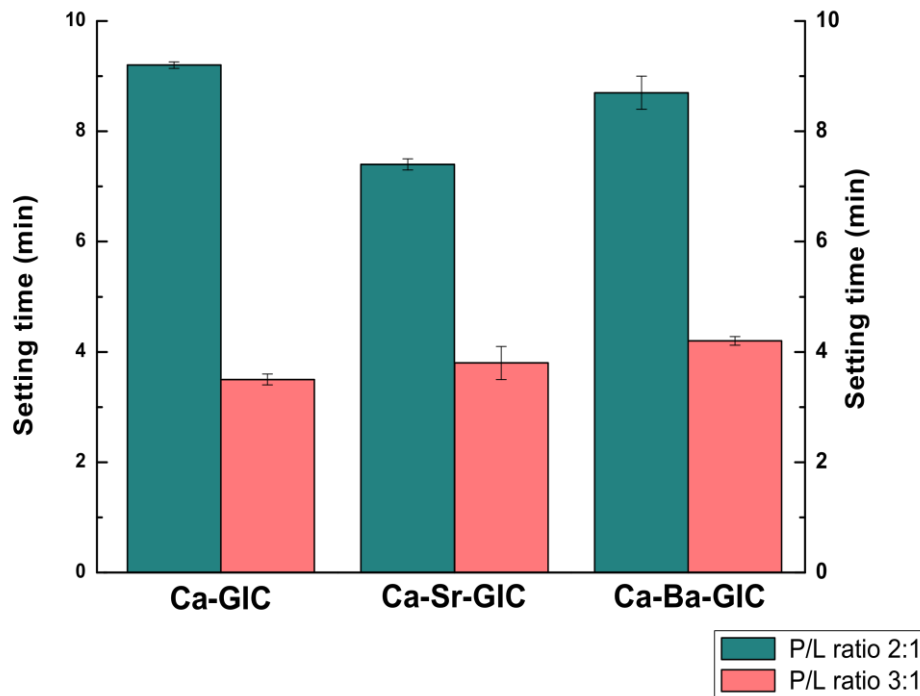


Figure 3-36: A comparison of setting time at different P/L ratios (*P* values are shown in Table 3-10).

Table 3-10: Analysis by the t-test of the setting time of the three experimental GIC compositions at different P/L ratios (2:1 and 3:1).

Paired t-test of two GIC compositions	Different P/L ratios	
	2:1 to 2:1	3:1 to 3:1
Ca-GIC to Ca-Sr-GIC	<i>P</i> = 0.001	<i>P</i> = 0.05
Ca-GIC to Ca-Ba-GIC	<i>P</i> = 0.04	<i>P</i> = 0.003
Ca-Sr-GIC to Ca-Ba-GIC	<i>P</i> = 0.01	<i>P</i> = 0.08

P > 0.01: no significant differences between the two GIC compositions present; *P* < 0.01: show significant differences between the two GIC compositions.

3.5 Vickers Hardness (HV)

The results gained from the HV are illustrated in Figure 3-37. The means and standard deviation were expressed in MPa. A total of nine indents on three specimens were applied and the mean HV for each time point (1 hour and 1 month) was calculated as described in Materials and Methods in Chapter 2.2.5.

Vickers Hardness

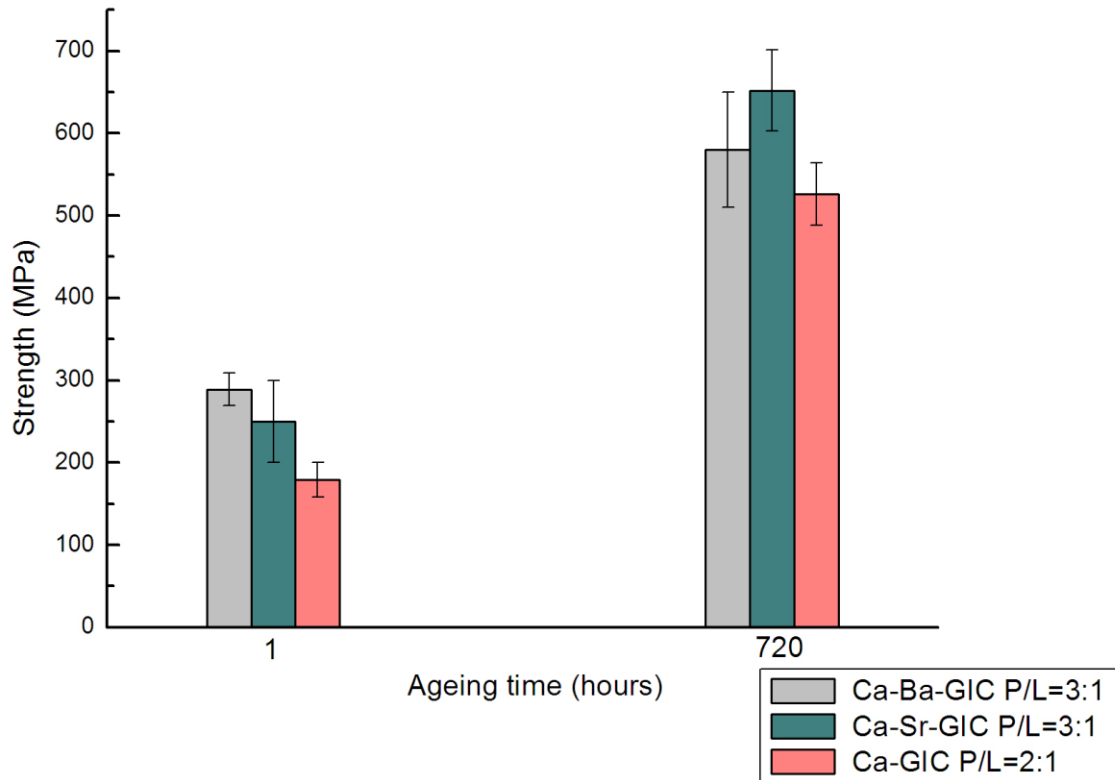


Figure 3-37: Mean micro-HV and standard deviation of the experimental GIC ($P_{1\text{hour} \& 1\text{month}} > 0.01$).

The bar chart in Figure 3-37 illustrated the microhardness of the experimental GICs, depending on ageing time. The hardness increases throughout the 1 hour to 1 month ageing time for all three GIC compositions. Ca-Ba-GIC exhibits the highest hardness at 1 hour, followed by Ca-Sr-GIC and Ca-GIC. However, Ca-Sr-GIC exhibits the highest level of hardness after 30 days, followed by Ca-Ba-GIC and Ca-GIC. The microhardness values at 30 days are almost twice that of 1 hour.

The paired t-test was used to compare the HV of two experimental GIC compositions at different time intervals (1 hour and 1 month). Three comparisons (1. Ca-GIC to Ca-Sr-GIC, 2. Ca-GIC to Ca-Ba-GIC and 3. Ca-Sr-GIC to Ca-Ba-GIC) at two time points, 1 hour and 1 month, were performed via the t-test. Analysis by the paired two sample t-test for all experimental GIC compositions at 1 hour and 1 month showed no significant differences ($P > 0.01$).

3.6 Nano-indentation

The results gained from the nano-indentation are illustrated in Figure 3-38 and the corresponding reduced modulus (E_r) is presented in Figure 3-39. The means and standard deviation are expressed in GPa.

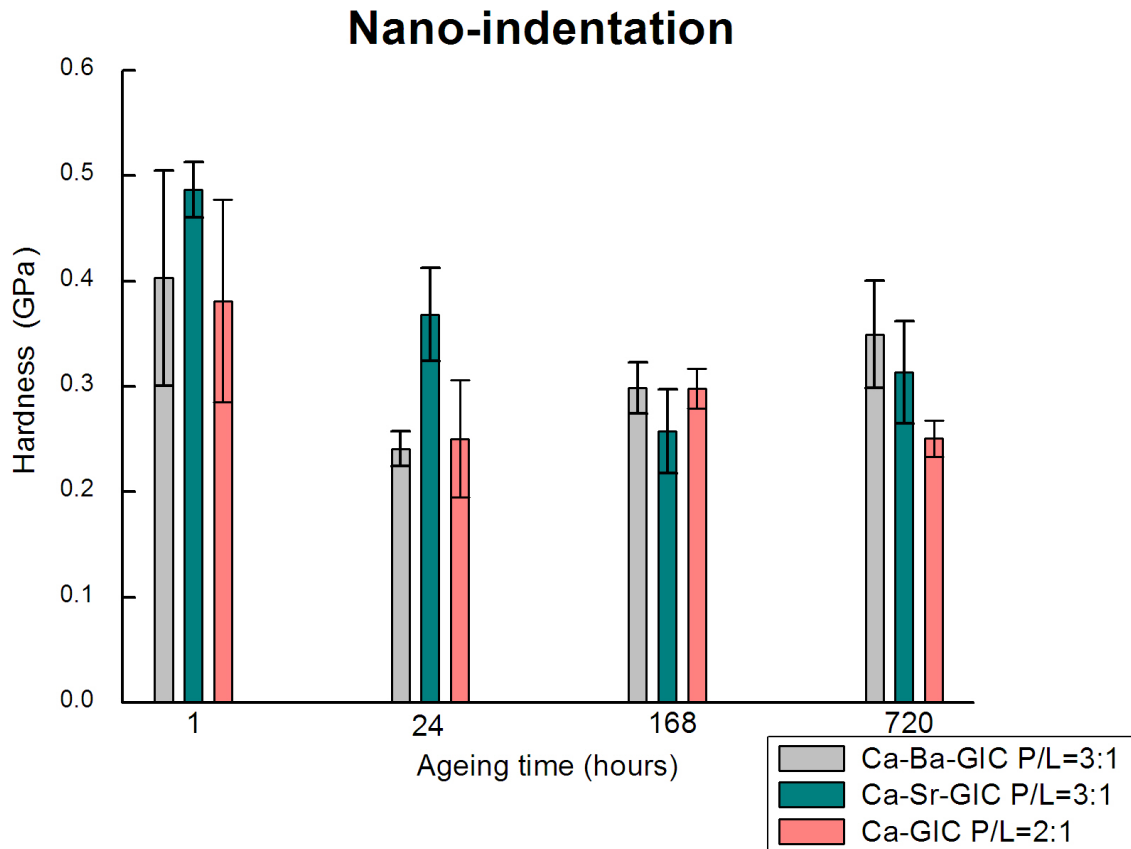


Figure 3-38: Mean nano-indentation and standard deviation of the three experimental GICs (P values are shown in Table 3-11).

The nano-indentation hardness, depending on the ageing time (Figure 3-38), slightly decreased from 1 hour to 1 month for all three GIC compositions. Ca-Ba-GIC decreased from 1 hour to 1 day but thereafter steadily increased up to 1 month. Sr substituted GIC decreased gradually up to 1 week followed by a slight increase from 1 week to 1 month. Ca-GIC fluctuated during the 1 month period. The hardness decreased from 1 hour to 1 day, followed by a minor increase from 1 day to 1 week and thereafter decreased from 1 week to 1 month. The three GIC compositions had exactly the same progress in their development for their reduced modulus (Figure 3-39) as in the nano-indentation (Figure 3-38).

The paired t-test was used to compare the nano-indentation and the reduced modulus of two experimental GIC compositions at different time intervals (1 hour, 1 day, 1 week and 1 month). Three comparisons (1. Ca-GIC to Ca-Sr-GIC, 2. Ca-GIC to Ca-Ba-GIC and 3. Ca-Sr-GIC to Ca-Ba-GIC) at each time point were performed via the t-test and P values are shown in Table 3-12. Analysis by the paired two sample t-test of the nano-indentation for all experimental GIC compositions showed no significant differences ($P > 0.01$), however, a significant difference was present at 1 day for Ca-Sr-GIC and Ca-Ba-GIC ($P = 0.004$).

Table 3-11: Analysis by the paired two sample t-test of the nan-indentation and reduced modulus of the three experimental GIC compositions.

Paired t-test of two GIC compositions	Nano-indentation			
	1 hour	1 day	1 week	1 month
Ca-GIC to Ca-Sr-GIC	$P = 1$	$P = 0.06$	$P = 0.25$	$P = 0.08$
Ca-GIC to Ca-Ba-GIC	$P = 0.71$	$P = 0.8$	$P = 1$	$P = 0.06$
Ca-Sr-GIC to Ca-Ba-GIC	$P = 0.31$	$P = 0.004$	$P = 0.08$	$P = 0.09$
	Reduced modulus			
	1 hour	1 day	1 week	1 month
Ca-GIC to Ca-Sr-GIC	$P = 0.02$	$P = 0.01$	$P = 0.85$	$P = 0.008$
Ca-GIC to Ca-Ba-GIC	$P = 0.16$	$P = 0.49$	$P = 0.009$	$P = 0.002$
Ca-Sr-GIC to Ca-Ba-GIC	$P = 0.42$	$P = 0.05$	$P = 0.07$	$P = 0.73$

$P > 0.01$: no significant differences between the two GIC compositions present; $P < 0.01$: show significant differences between the two GIC compositions.

Analysis by the paired two sample t-test, for the reduced modulus for all experimental GIC compositions showed no significant differences ($P > 0.01$); however, a significant difference was present at 1 week for Ca-GIC to Ca-Ba-GIC ($P = 0.009$) and at 1 month for Ca-GIC to Ca-Sr-GIC ($P < 0.008$) and Ca-GIC to Ca-Ba-GIC ($P < 0.002$) (Table 3-12).

Reduced modulus calculation from Nano-indentation

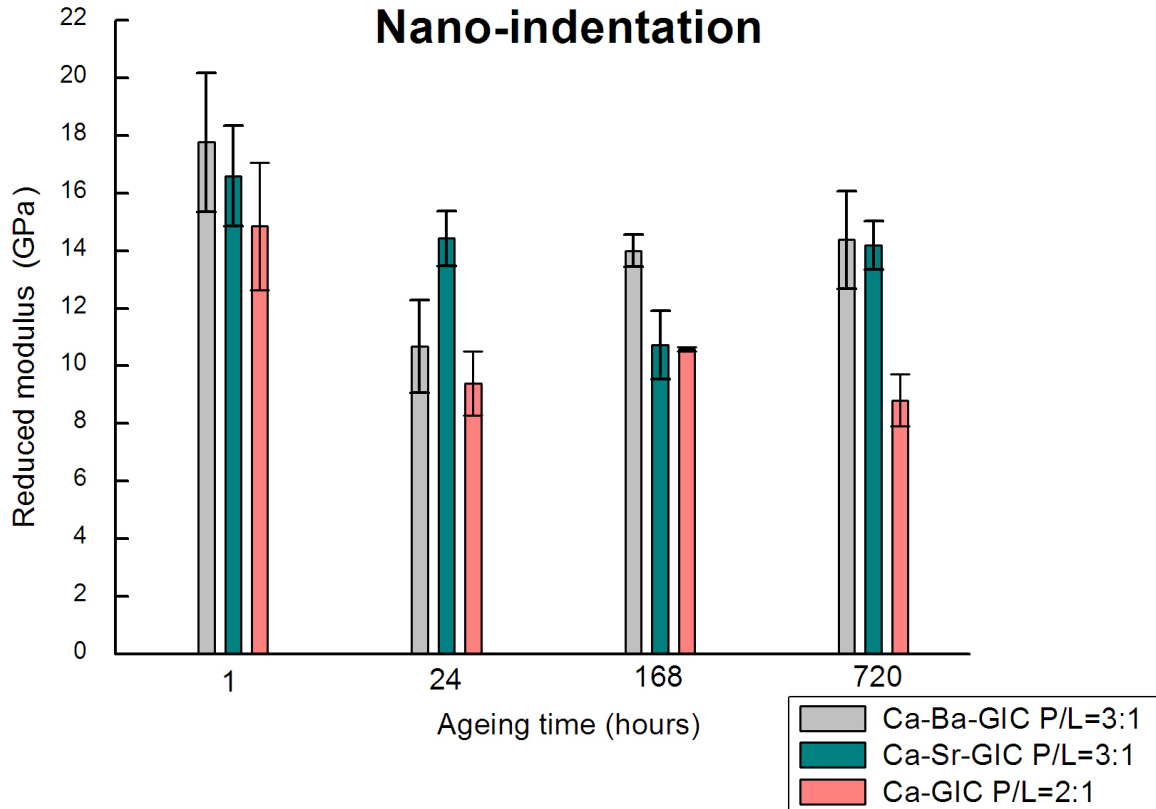


Figure 3-39: Mean reduced modulus calculation from the nano-indentation and standard deviation of the three experimental GICs (*P* values are shown in Table 3-11).

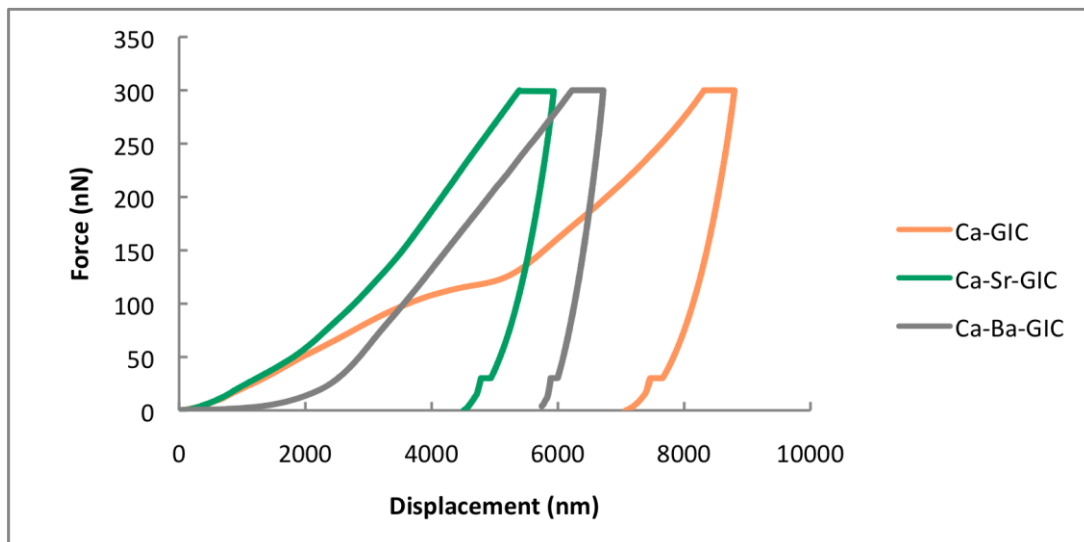


Figure 3-40: Force-displacement curve of the three GIC compositions using a Berkovich indenter.

Figure 3-40 illustrates an example of the force/displacement curve, for the three GIC compositions at 1 hour. The force/displacement result of the three experimental GICs is typical for a C-GIC. Ca-Sr-GIC exhibited the highest hardness, followed by Ca-Ba-GIC and Ca-GIC.

Figure 3-41 illustrates the creep response of the three experimental GICs. The results suggest that the mean displacement is after ca. 25 seconds for all three GIC compositions with ca. 5800 nm for Ca-Sr-GIC, ca. 6200 nm for Ca-Ba-GIC and ca. 8200 nm for Ca-GIC.

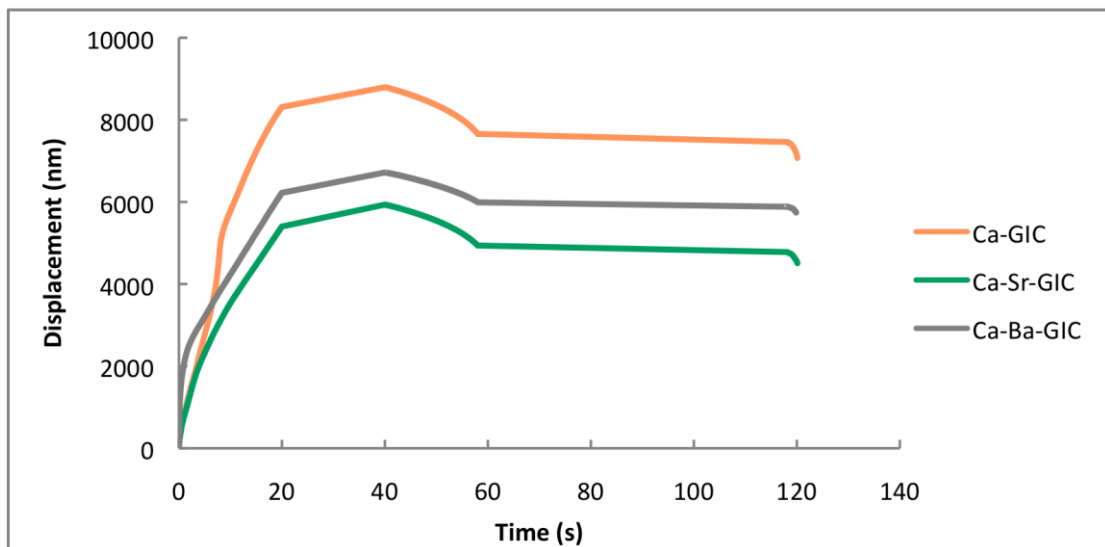


Figure 3-41: Creep response at a maximum load of 300 nm.

3.7 Wear behavior of glass ionomer cements

The wear result of all three GIC compositions after 24 hours is illustrated in Figure 3-42. Ca-Ba-GIC exhibited the least wear volume and Ca-Sr-GIC the highest wear volume. The highest wear depth caused by the alumina ball was in Ca-Sr-GIC, followed by Ca-Ba-GIC and the least wear depth was presented by Ca-GIC.

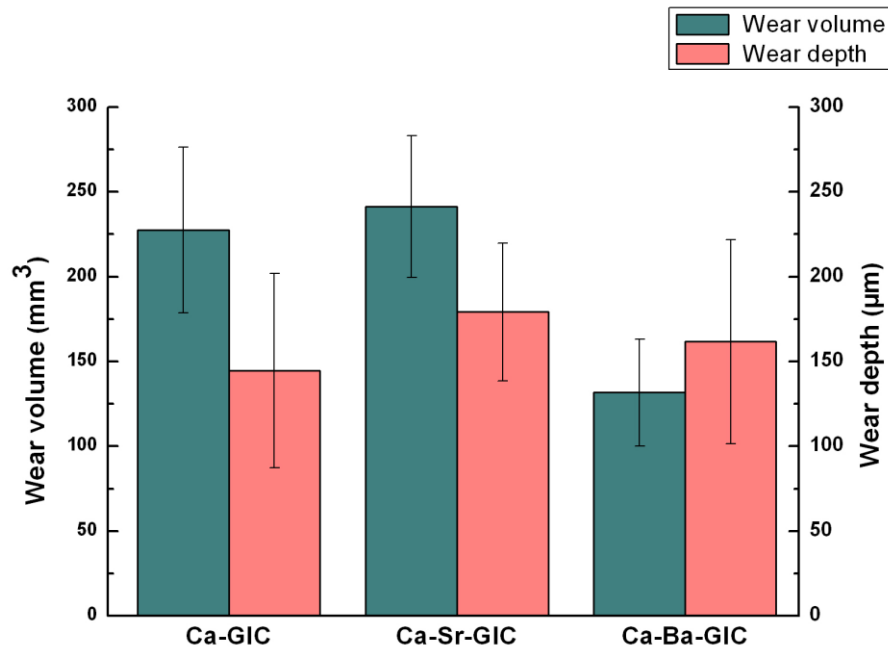


Figure 3-42: Wear results of the three GICs compositions (P values are shown in Table 3-12).

The t-test was used to compare the wear behaviour (wear volume and wear depth) of two experimental GICs. Three comparisons (1. Ca-GIC to Ca-Sr-GIC, 2. Ca-GIC to Ca-Ba-GIC and 3. Ca-Sr-GIC to Ca-Ba-GIC) for the wear volume and wear depth were performed via the t-test and P values are shown in Table 3-12. Analysis by the t-test, for the wear volume for Ca-GIC to Ca-Ba-GIC and Ca-Sr-GIC to Ca-Ba-GIC, showed significant differences ($P < 0.01$).

Table 3-12: Analysis by the two sample t-test of the wear volume and wear depth of the three experimental GIC compositions.

Paired t-test of two GIC compositions	Wear behavior	
	Wear volume	Wear depth
Ca-GIC to Ca-Sr-GIC	$P = 0.61$	$P = 0.006$
Ca-GIC to Ca-Ba-GIC	$P < 0.001$	$P = 0.04$
Ca-Sr-GIC to Ca-Ba-GIC	$P < 0.001$	$P = 0.04$

$P > 0.01$: no significant differences between the two GIC compositions present; $P < 0.01$: show significant differences between the two GIC compositions.

3.8 Mechanical properties of cements

3.8.1 Compressive strength (CS)

Figure 3-43 illustrates the CS mean values of Ca-Sr-GIC and Ca-Ba-GIC at a P/L ratio 3:1 whereas Figure 3-44 represents the mean values of Ca-GIC with a P/L ratio of 2:1 at 1 hour, 1 day, 1 week and 1 month of ageing time.

A significant increase in the mean CS values for all specimens from 1 hour to 1 month ageing times irrespective of the substitution and P/L ratio (Figure 3-43 and Figure 3-44) was observed. A steady increase in the CS values for Ca-Sr-GIC (Figure 3-43) with a P/L ratio of 3:1 was observed between 1 hour and 1 month. However, a slight decrease in strength for Ca-Ba-GIC with a P/L ratio of 3:1 was noted between 7 days and 1 month although a steady rise was noted to 7 days of ageing time.

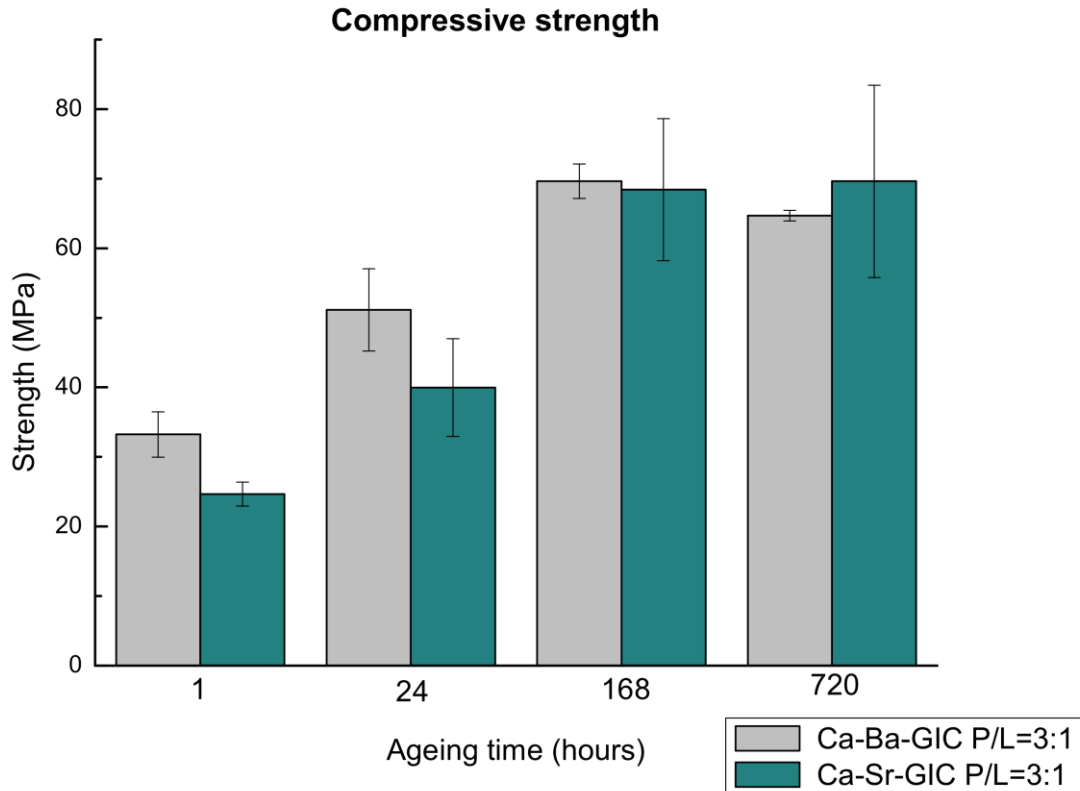


Figure 3-43: Mean compressive strength of Sr and Ba containing GICs with P/L=3:1 at 1 hour, 1 day, 1 week and 1 month ageing time (*P* values are shown in Table 3-13).

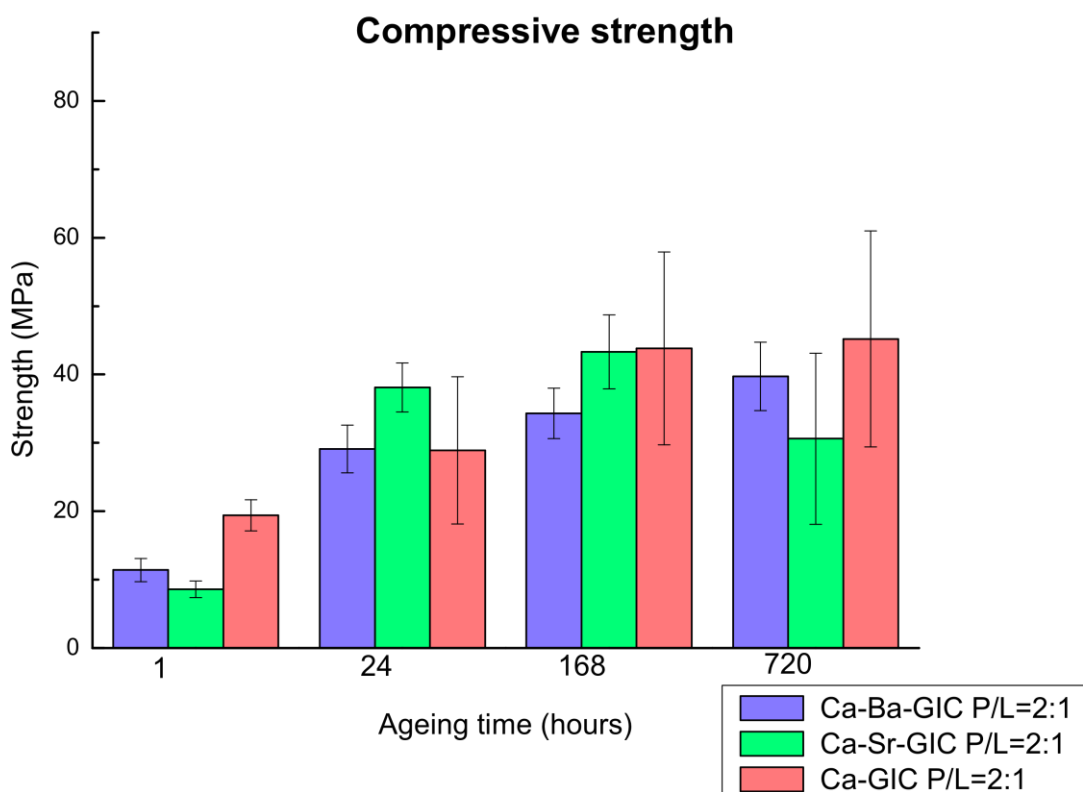


Figure 3-44: Mean compressive strength of Ca, Sr and Ba containing GICs with P/L=2:1 at 1 hour, 1 day, 1 week and 1 month ageing time (*P* values are shown in Table 3-13).

Figure 3-44 illustrates the change in mean CS against ageing time with a P/L ratio of 2:1 for all three compositions. A slight decrease (Figure 3-44) in strength for Ca-Sr-GIC (P/L ratio 2:1) was noted between 7 days and 1 month although a steady rise was thereafter noted to 7 days ageing time.

The paired t-test was used to compare the CS of two experimental GICs at different ageing times (1 hour, 1 day, 1 week and 1 month) with a P/L ratio of 2:1 and 3:1. However, a P/L of 2:1 is presentable, thus all experimental GICs at the same P/L ratio for each corresponding ageing time were compared. A total of three comparisons with a P/L ratio of 2:1 (1. Ca-GIC to Ca-Sr-GIC, 2. Ca-GIC to Ca-Ba-GIC and 3. Ca-Sr-GIC to Ca-Ba-GIC) and one comparison with a P/L ratio of 3:1 (Ca-Sr-GIC to Ca-Ba-GIC) for each ageing time were performed via the t-test and *P* values are shown in Table 3-13. Analysis by the paired two sample t-test, for the CS

for all experimental GIC compositions with a P/L ratio of 2:1 at 1 hour, showed significant differences ($P < 0.01$).

Table 3-13: Analysis by the paired two sample t-test of the CS of the three experimental GIC compositions at different ageing times with different P/L ratios.

Paired t-test of two GIC compositions	P/L ratio 3:1			
	1 hour	1 day	1 week	1 month
Ca-Sr-GIC to Ca-Ba-GIC	$P < 0.001$	$P < 0.001$	$P = 0.09$	$P = 0.003$
	P/L ratio 2:1			
Ca-GIC to Ca-Sr-GIC	$P < 0.001$	$P < 0.001$	$P = 0.29$	$P < 0.001$
Ca-GIC to Ca-Ba-GIC	$P < 0.001$	$P = 0.01$	$P < 0.001$	$P < 0.001$
Ca-Sr-GIC to Ca-Ba-GIC	$P = 0.002$	$P < 0.001$	$P < 0.001$	$P < 0.001$

$P > 0.01$: no significant differences between the two GIC compositions present; $P < 0.01$: show significant differences between the two GIC compositions.

3.8.2 Diametral tensile strength (DTS)

Figure 3-45 illustrates the DTS mean values of Ca-Sr-GIC and Ca-Ba-GIC at a P/L ratio of 3:1 whilst Figure 3-46 represents the mean values of Ca-GIC with a P/L ratio of 2:1 at 1 hour, 1 day, 1 week and 1 month ageing time.

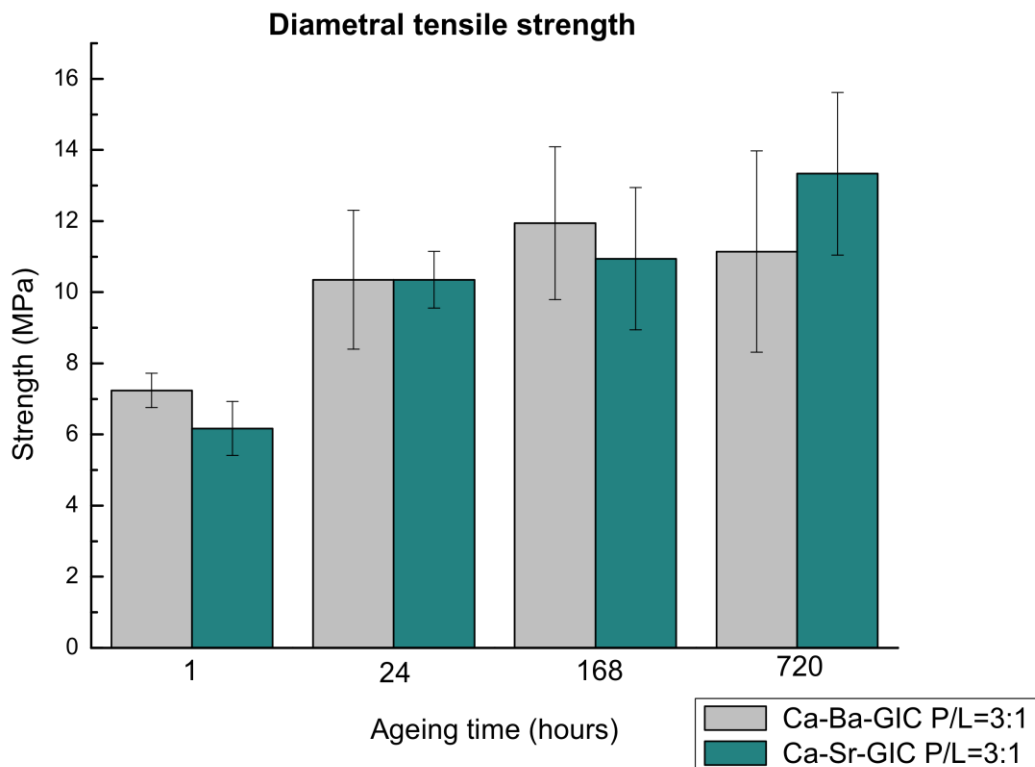


Figure 3-45: Mean diametral tensile strength of Sr and Ba containing GICs with P/L=3:1 at 1 hour, 1 day, 1 week and 1 month ageing time (P values are shown in Table 3-14).

An increase in DTS from 1 hour to 1 month ageing time was observed for all specimens. However, the highest DTS value was observed for Ca-Sr-GIC at 1 month (Figure 3-45) of ageing time, while the highest DTS values for Ca-Ba-GIC (Figure 3-45) and Ca-GIC (Figure 3-46) were reached just after one week with a minimal decrease observed thereafter.

The paired t-test was used to compare the DTS of two experimental GIC compositions at different ageing times (1 hour, 1 day, 1 week and 1 month). Ca-Sr-GIC was compared with Ca-Ba-GIC for each ageing time via the t-test and *P* values are shown in Table 3-14. Analysis by the paired two sample t-test, for the DTS for Ca-Sr-GIC to Ca-Ba-GIC at 1 hour showed significant differences ($P=0.002$).

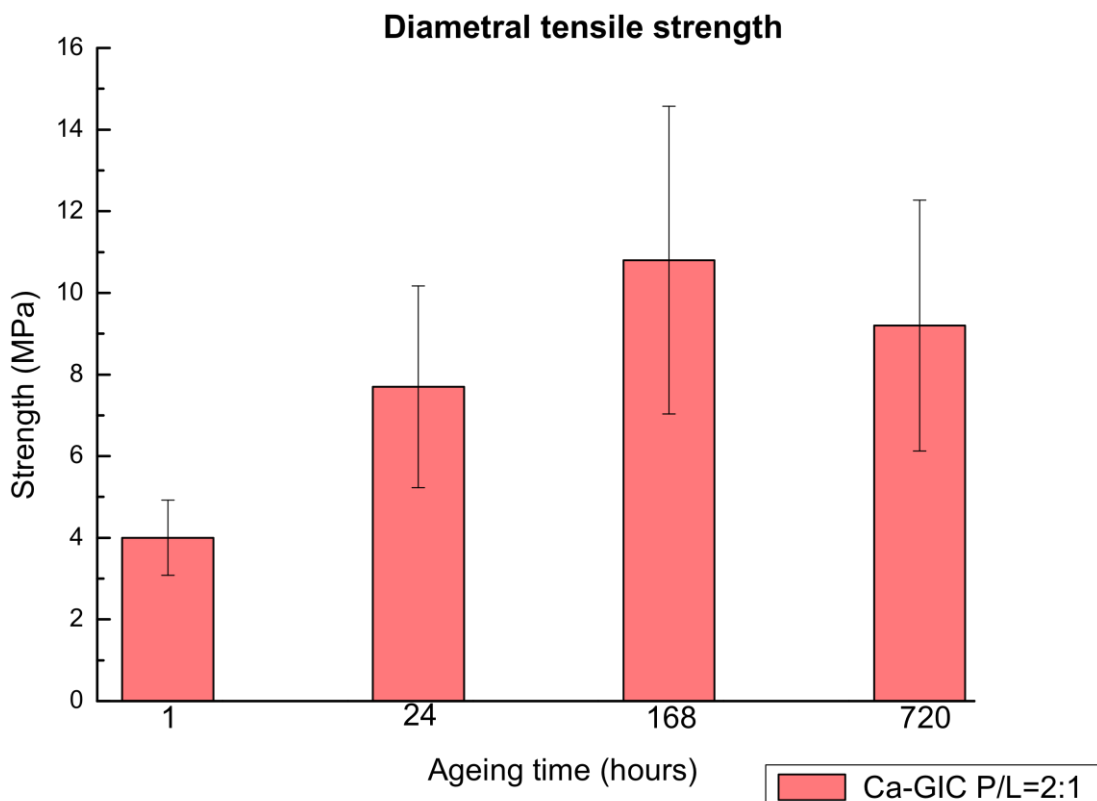


Figure 3-46: Mean diametral tensile strength of Ca containing GICs with P/L=2:1 at 1 hour, 1 day, 1 week and 1 month ageing time.

Table 3-14: Analysis by the paired two sample t-test of the DTS of Ca-Sr-GIC with Ca-Ba-GIC compositions at different ageing times.

Paired t-test of two GIC compositions	Ageing time			
	1 hour	1 day	1 week	1 month
Ca-Sr-GIC to Ca-Ba-GIC	$P = 0.002$	$P = 0.1$	$P = 0.002$	$P < 0.001$

$P > 0.01$: no significant differences between the two GIC compositions present; $P < 0.01$: show significant differences between the two GIC compositions.

3.8.3 Flexural strength (FS)

The mean FS change with ageing time for Ca-Sr-GIC and Ca-Ba-GIC with a P/L ratio of 3:1 is presented in Figure 3-47, whereas the flexural strength change with ageing time for Ca-GIC with a P/L ratio of 2:1 is illustrated in Figure 3-48.

Independent of the substitution and P/L ratio, all three GIC compositions for FS mean values (Figure 3-47 and Figure 3-48) increased from 1 hour to 1 month. However, the highest mean FS value for Ca-GIC (Figure 3-48) and Ca-Ba-GIC (Figure 3-47) was observed after 7 days and afterward a minimal decrease was seen, while the peak mean value for Ca-Sr-GIC (Figure 3-47) was apparent after 1 month.

For FS and DTS, similarities in the progression of mean strength value depending on the setting time for Ca-Ba-GIC and Ca-GIC can be observed.

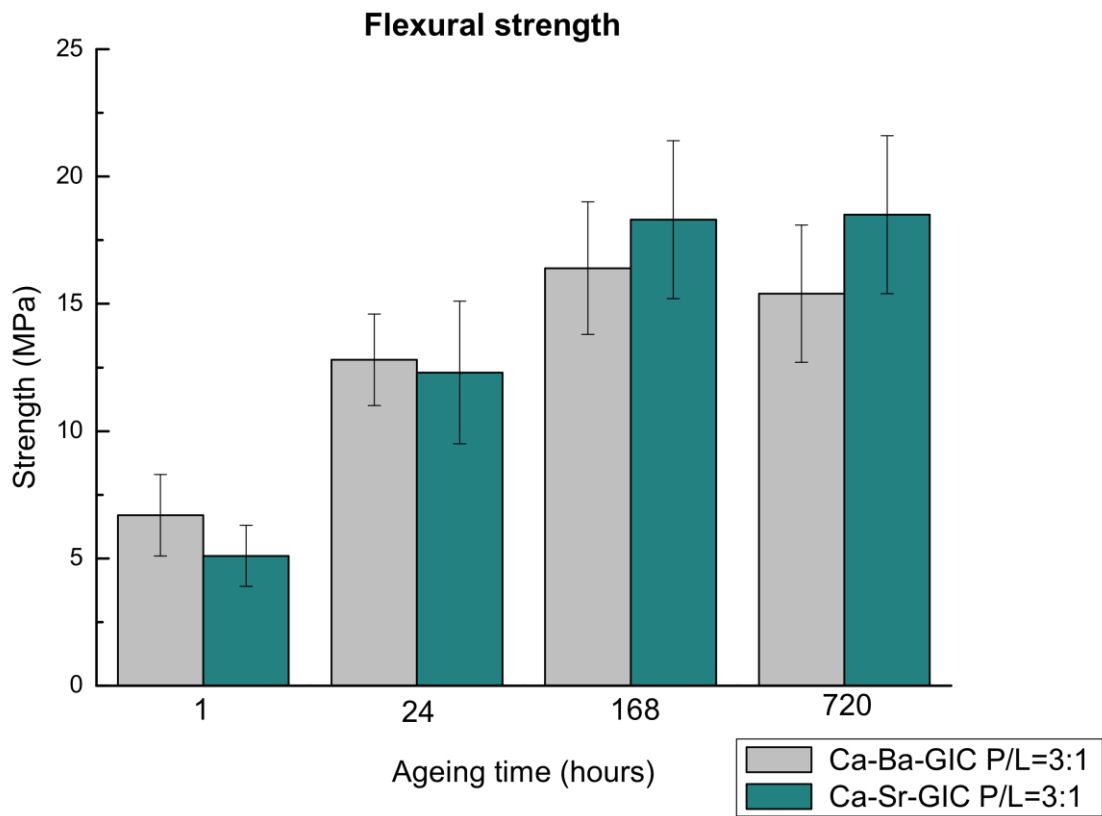


Figure 3-47: Mean flexural strength of Sr and Ba containing GICs with P/L=3:1 at 1 hour, 1 day, 1 week and 1 month ageing time (*P* are shown in Table 3-15).

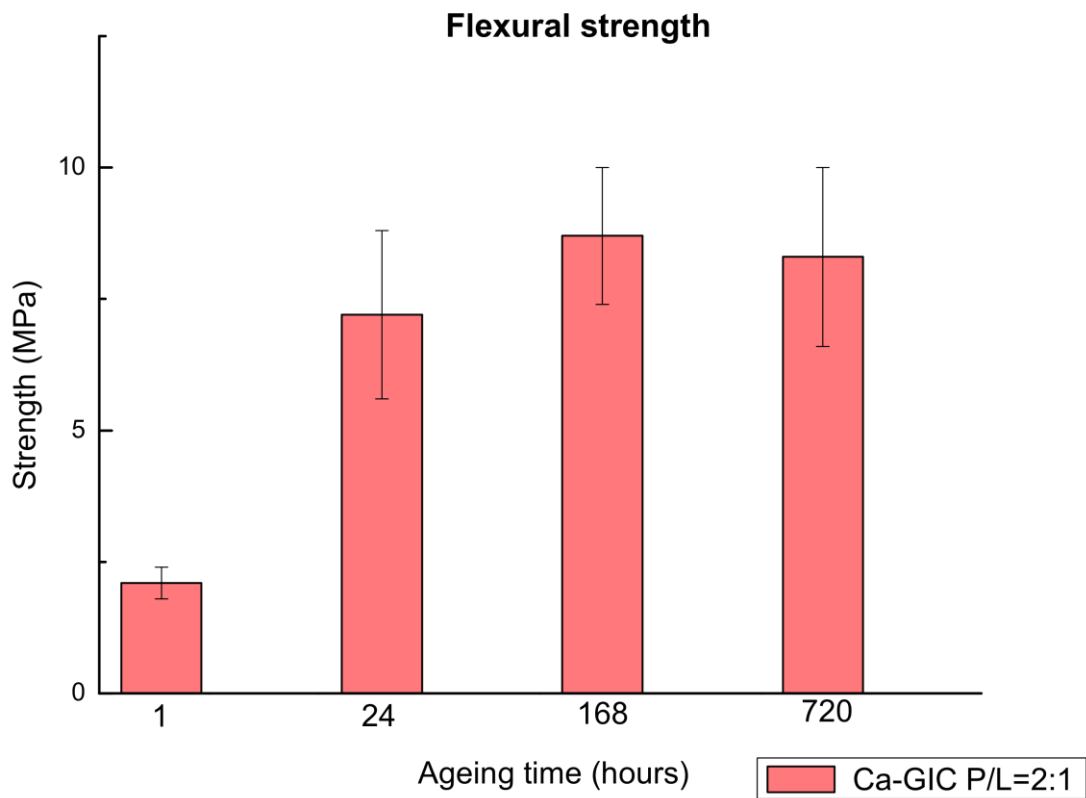


Figure 3-48: Mean flexural strength of Ca containing GICs with P/L=2:1 at 1 hour, 1 day, 1 week and 1 month ageing time.

The paired t-test was used to compare the FS of two experimental GIC compositions at different ageing times (1 hour, 1 day, 1 week and 1 month). Ca-Sr-GIC with Ca-Ba-GIC was compared for each ageing time via the t-test and *P* values are shown in Table 3-15. Analysis by the paired two sample t-test, for the FS for Ca-Sr-GIC to Ca-Ba-GIC at 1 hour showed significant differences (*P* = 0.002).

Table 3-15: Analysis by the paired two sample t-test of the FS of Ca-Sr-GIC with Ca-Ba-GIC compositions at different ageing times.

Paired t-test of two GIC compositions	Ageing time			
	1 hour	1 day	1 week	1 month
Ca-Sr-GIC to Ca-Ba-GIC	<i>P</i> = 0.002	<i>P</i> = 0.23	<i>P</i> = 0.001	<i>P</i> < 0.001

P > 0.01: no significant differences between the two GIC compositions present; *P* < 0.01: show significant differences between the two GIC compositions.

3.8.4 Modulus of Elasticity

The mean Young's modulus change against ageing time for all three compositions at a different P/L ratio (Table 2-2) is illustrated in Figure 3-51: Mean modulus of elasticity from diametral tensile strength of Sr and Ba containing GICs with P/L=3:1 at 1 hour, 1 day, 1 week and 1 month ageing time (*P* is shown in Table 3-17).

to Figure 3-54.

The paired t-test was used to compare the modulus of elasticity from the CS of two experimental GICs at different ageing time (1 hour, 1 day, 1 week and 1 month) with a P/L ratio of 2:1 and 3:1. The P/L of 2:1 is representative, because all experimental GIC compositions with the same P/L ratio for each corresponding ageing times were compared. A total of three comparisons with a P/L ratio of 2:1 (1. Ca-GIC to Ca-Sr-GIC, 2. Ca-GIC to Ca-Ba-GIC and 3. Ca-Sr-GIC to Ca-Ba-GIC) and one comparison with a P/L ratio of 3:1 (Ca-Sr-GIC to Ca-Ba-GIC) for each ageing time were performed via the t-test and *P* values are shown in Table 3-16. Analysis by the paired two sample t-test, for the modulus of elasticity from CS for all GIC compositions at 1 hour showed significant differences (*P* < 0.01).

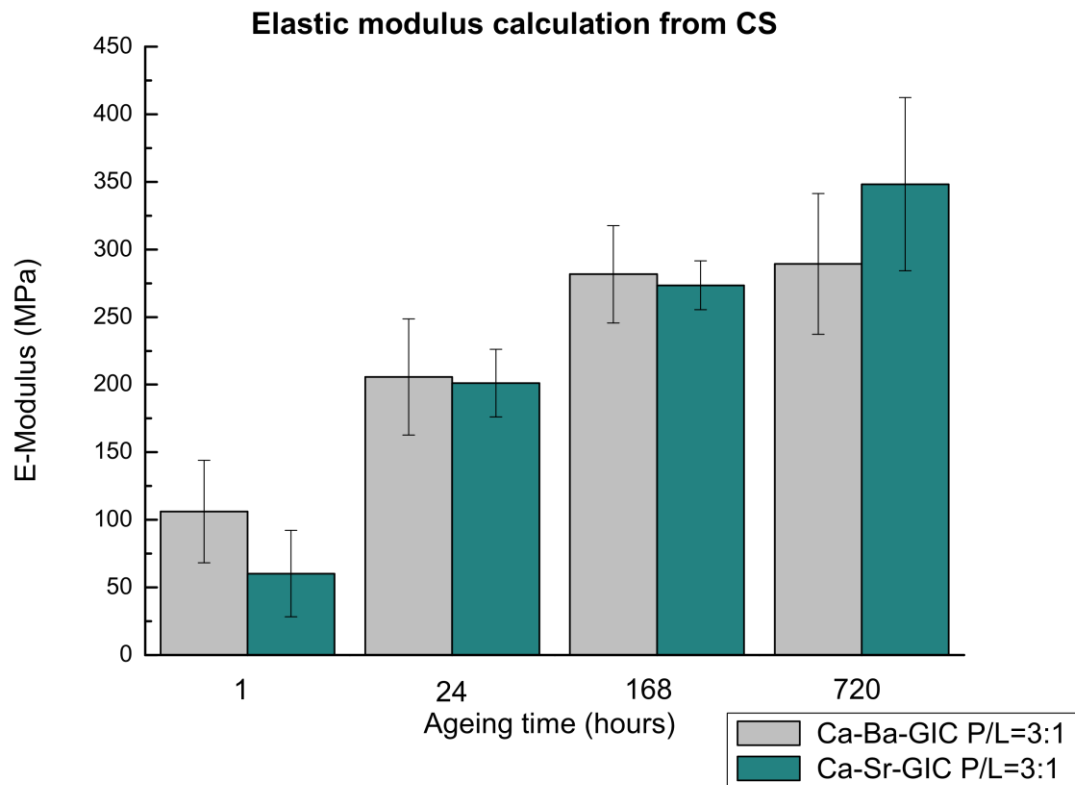


Figure 3-49: Mean modulus of elasticity from compressive strength of Sr and Ba containing GICs with P/L=3:1 at 1 hour, 1 day, 1 week and 1 month ageing time (*P* values are shown in Table 3-16).

Table 3-16: Analysis by the paired two sample t-test of the CS of the three experimental GIC compositions at different ageing times with different P/L ratios.

Paired t-test of two GIC compositions	P/L ratio 3:1			
	1 hour	1 day	1 week	1 month
Ca-Sr-GIC to Ca-Ba-GIC	<i>P</i> < 0.001	<i>P</i> = 0.24	<i>P</i> = 0.34	<i>P</i> < 0.001
	P/L ratio 2:1			
Ca-GIC to Ca-Sr-GIC	<i>P</i> < 0.001	<i>P</i> = 0.002	<i>P</i> < 0.001	<i>P</i> < 0.001
Ca-GIC to Ca-Ba-GIC	<i>P</i> < 0.001	<i>P</i> = 0.04	<i>P</i> < 0.001	<i>P</i> < 0.001
Ca-Sr-GIC to Ca-Ba-GIC	<i>P</i> < 0.001	<i>P</i> < 0.001	<i>P</i> = 0.08	<i>P</i> < 0.001

***P* > 0.01:** no significant differences between the two GIC compositions present; ***P* < 0.01:** show significant differences between the two GIC compositions.

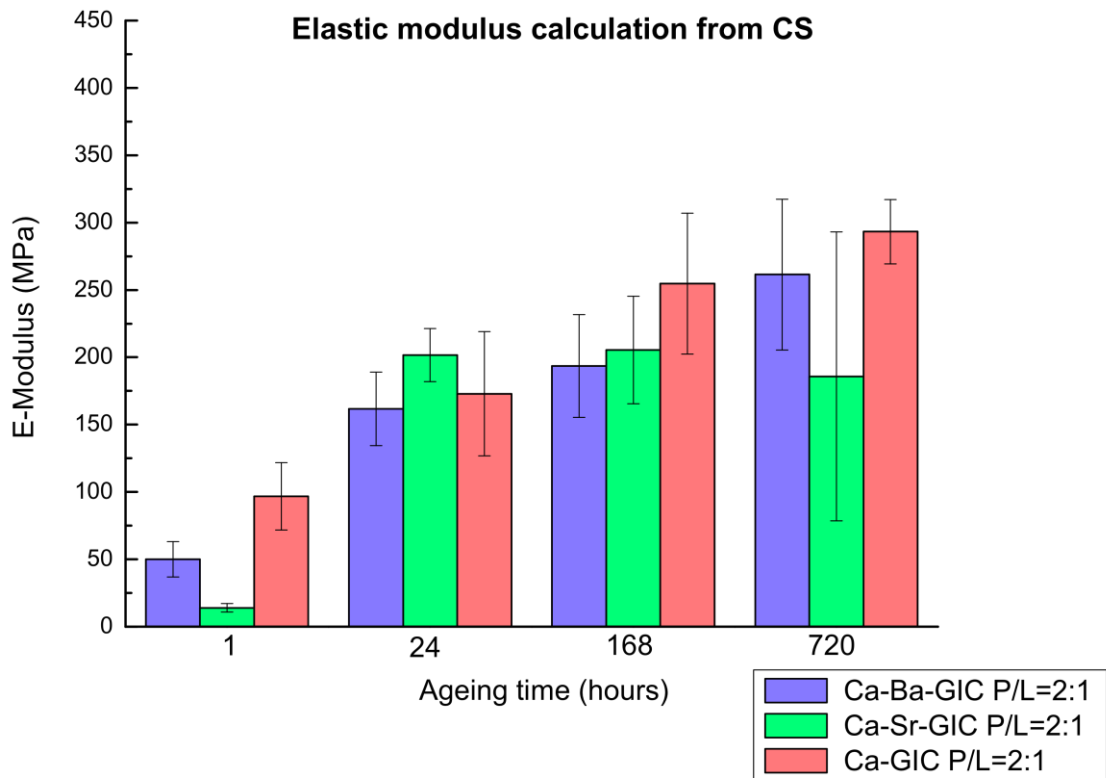


Figure 3-50: Mean modulus of elasticity from compressive strength of Ca, Sr and Ba containing GICs with P/L=2:1 at 1 hour, 1 day, 1 week and 1 month ageing time (*P* is shown in Table 3-16).

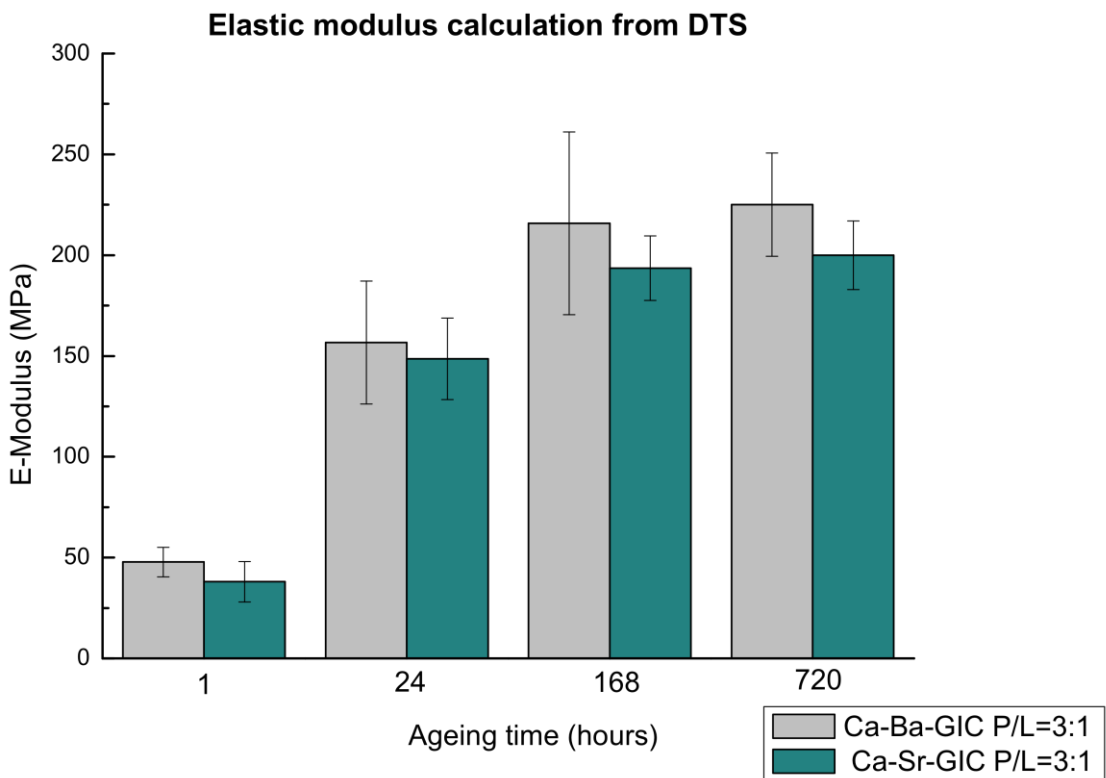


Figure 3-51: Mean modulus of elasticity from diametral tensile strength of Sr and Ba containing GICs with P/L=3:1 at 1 hour, 1 day, 1 week and 1 month ageing time (*P* is shown in Table 3-17).

The paired t-test was used to compare the modulus of elasticity from DTS of two experimental GIC compositions at different ageing time (1 hour, 1 day, 1 week and 1 month). Ca-Sr-GIC with Ca-Ba-GIC was compared for each ageing time via the t-test and *P* values are shown in Table 3-17.

Table 3-17: Analysis by the paired two sample t-test of modulus of elasticity from DTS of Ca-Sr-GIC with Ca-Ba-GIC compositions at different ageing times.

Paired t-test of two GIC compositions	Ageing time			
	1 hour	1 day	1 week	1 month
Ca-Sr-GIC to Ca-Ba-GIC	<i>P</i> = 0.04	<i>P</i> = 0.03	<i>P</i> = 0.003	<i>P</i> = 0.003

P > 0.01: no significant differences between the two GIC compositions present; *P* < 0.01: show significant differences between the two GIC compositions.

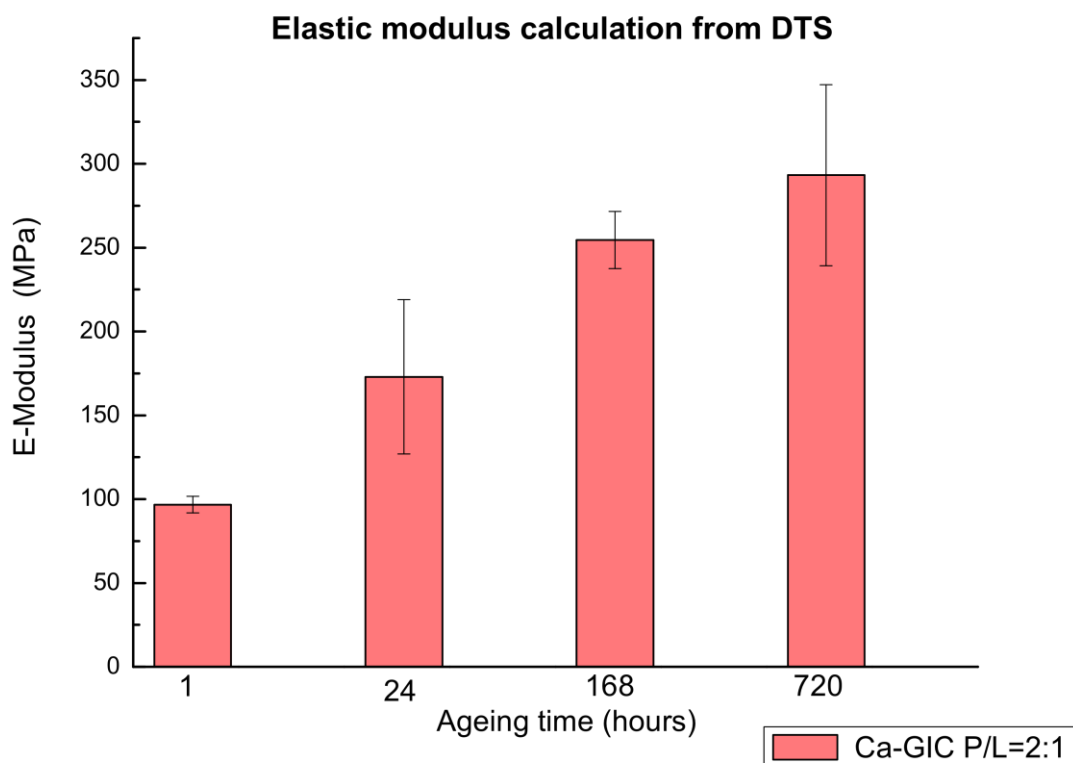


Figure 3-52: Mean modulus of elasticity from diametral tensile strength of Ca containing GICs with P/L=2:1 at 1 hour, 1 day, 1 week and 1 month ageing time.

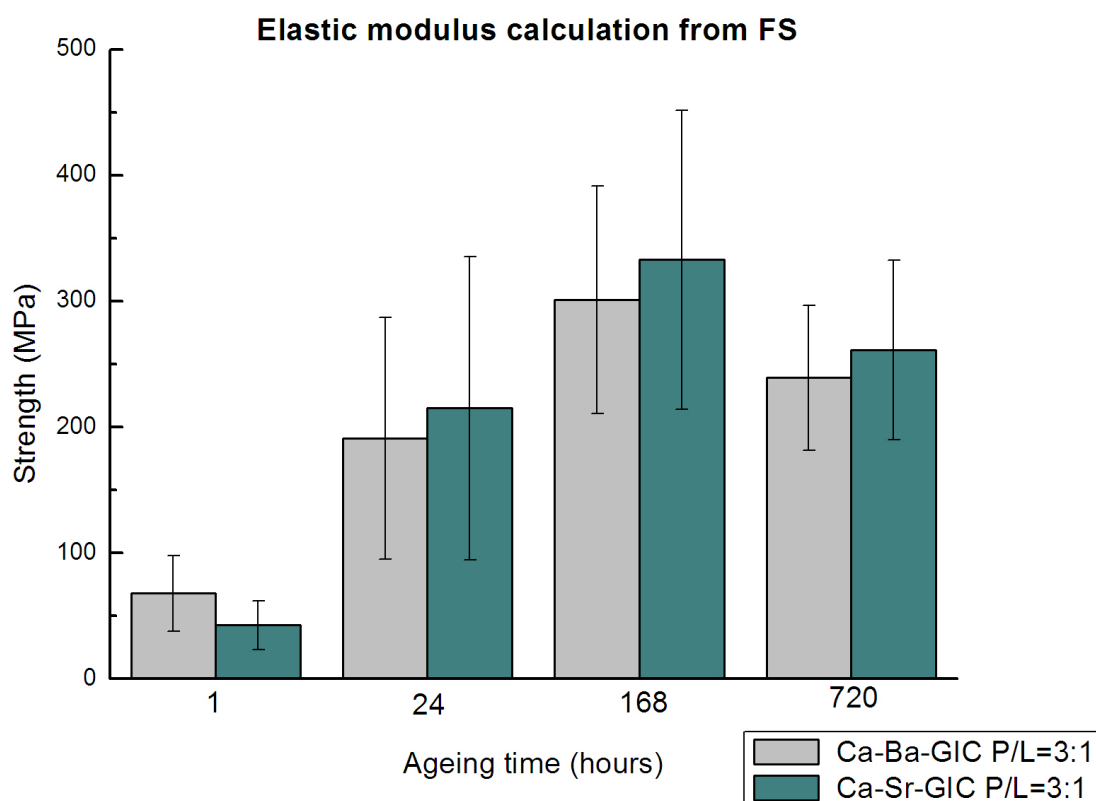


Figure 3-53: Mean modulus of elasticity from flexural strength of Sr and Ba containing GICs with P/L=3:1 at 1 hour, 1 day, 1 week and 1 month ageing time (*P* is shown in Table 3-18).

The paired t-test was used to compare the modulus of elasticity from FS of two experimental GICs at different ageing time (1 hour, 1 day, 1 week and 1 month). Ca-Sr-GIC with Ca-Ba-GIC was compared for each ageing time via the t-test and *P* values are shown in Table 3-18. Analysis by the paired two sample t-test, for the modulus of elasticity for Ca-Sr-GIC to Ca-Ba-GIC at 1 hour showed significant differences (*P* = 0.002).

Table 3-18: Analysis by the paired two sample t-test of the modulus of elasticity from FS of Ca-Sr-GIC with Ca-Ba-GIC compositions at different ageing times.

Paired t-test of two GIC compositions	Ageing time			
	1 hour	1 day	1 week	1 month
Ca-Sr-GIC to Ca-Ba-GIC	<i>P</i> = 0.002	<i>P</i> = 0.003	<i>P</i> = 0.002	<i>P</i> = 0.003

P > 0.01: no significant differences between the two GIC compositions present; *P* < 0.01: show significant differences between the two GIC compositions.

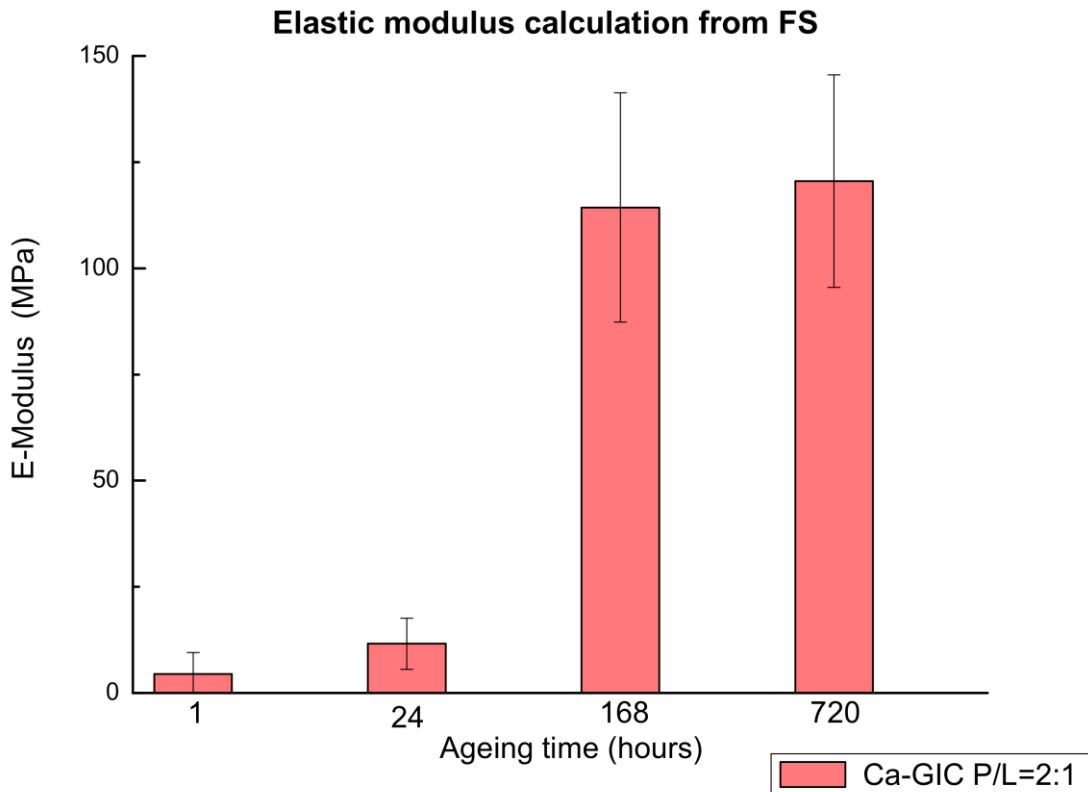


Figure 3-54 Mean modulus of elasticity from flexural strength of Ca containing GICs with P/L=2:1 at 1 hour, 1 day, 1 week and 1 month ageing time.

The mean elastic modulus for all three GIC compositions increased from 1 day to 1 month.

The Young's modulus values of Ca-GIC for DTS (Figure 3-52), CS (Figure 3-50) and FS (Figure 3-54) increased from 1 day to 1 month, however the mean elastic modulus values for FS (Figure 3-54) slightly increased up to 7 days with an abrupt rise apparent from 7 days to 1 month of ageing time.

The mean elastic modulus values for Ca-Ba-GIC with a P/L ratio of 3:1 for DTS (Figure 3-51) and CS (Figure 3-49) increased from 1 hour to 1 month. However, the mean elastic modulus for FS (Figure 3-53) increased from 1 hour to 1 week and thereafter a decrease from 1 week to 1 month was observed.

The progress for Ca-Sr-GIC with a P/L ratio of 3:1 for DTS (Figure 3-51) and CS (Figure 3-49) is identical to Ca-Ba-GIC. A steady increase from 1 hour to 1 month was observed. The mean elastic modulus for FS (Figure 3-53) decreased from

1 week to 1 month, while an increase from 1 hour to 1 week was observed. Identical progression for Ca-Sr-GIC and Ca-Ba-GIC for all three test methods with a P/L ratio of 3:1 was observed.

Ca-Ba-GIC, with a P/L ratio of 2:1 for CS (Figure 3-50), increased gradually up to 1 month, whereas Ca-Sr-GIC with a P/L ratio of 2:1 for CS (Figure 3-50) peaked after 7 days followed by a slight decrease in the mean elastic modulus up to 1 month.

4 Discussion

In this PhD work the primary aim was to investigate the effect of substituting larger cations, such as Sr^{2+} and Ba^{2+} with an ionic radius of 0.135 nm^{232} and 0.118 nm^{232} respectively, for Ca^{2+} with an ionic radius of 0.1 nm^{232} , on the resulting mechanical properties of the experimental cements.

The hypothesis was that larger cations disrupt more effectively the glass network, resulting in the formation of more NBOs. However, this disruption of the glass structure, caused by NBOs, may also lead to an expansion of the glass network that would facilitate the cation diffusion from the glass network during the formation of glass ionomer cements (acid attack and setting) especially at the early stages of setting. This should have an effect (enhanced mechanical strength) on the degree of the polysalt crosslinking and consequently on the mechanical properties of the cements.

4.1 FTIR

Aluminosilicate glasses consist of a random network of linked SiO_4 and AlO_4 tetrahedra. The glasses that are used to form GICs have to possess certain basic characteristics, such as the $\text{Al}_2\text{O}_3/\text{SiO}_2$ ratio. The $\text{Al}_2\text{O}_3/\text{SiO}_2$ ratio plays a very important role in the glass network; it determines the capacity of the glass to form cement and its corresponding resulting mechanical properties⁸⁰.

According to Zachariassen⁷⁸, Al^{3+} is an intermediate, it has the ability to act both as a network former (adapting to a four-fold coordination, five-fold coordination and six-fold coordination¹⁸⁶) and as a modifier. Substituting Al^{3+} for Si^{4+} in the glass structure, Al^{3+} has to adapt to a four-fold coordination [AlO_4^-], with a surplus of negative charge. The glass renders more alkaline and is therefore vulnerable to acid attack. The

mono- and bivalent network modifiers balance out the negative charge in the tetrahedron.

In a perfect homogeneous glass structure, the ratio of the network modifier (m) to the network former Al^{3+} ($f_{\text{Al}^{3+}}$) should be equal to 1 ($R_{m/f\text{Al}^{3+}} = 1$). But, if there is an excess of network modifiers (mono- and bivalent network modifiers) $R > 1$, an increase in the formation of NBO occurs. The increase of NBO in the glass network renders the glass more alkaline and hence more vulnerable to acid attack and an increase in the dissolution rate is expected^{67,80}.

Oxygens in the glass network can exist as either BOs or NBOs. If the oxygen binds with one glass network former (a tetrahedron) and one or more network modifiers a NBO is created. In the case of BO, the oxygen is bonded with two glass network formers, two tetrahedra. The BO bonded to two network formers has a stronger bond in comparison to the NBO bond⁶⁸. The greater the number of BOs in the glass network, the higher the amount of crosslinkages and the tighter the glass structure and therefore the less ion diffusion. Generally, properties of the glass structure concomitantly determine the properties of the resulting cement⁶⁷.

Creating more NBOs in the glass structure weakens/disturbs the general stability of the glass network, this having been observed previously when introducing calcium fluoride (CaF_2)⁶⁹ (a strong network modifier) into an aluminosilicate glass network. The introduction of CaF_2 ions destabilises the glass network by reducing the crosslink density of the glass. All F^- ions form a complex with $[\text{SiO}_3\text{F}]$ and $[\text{AlO}_3\text{F}]$ tetrahedra which can result in the formation of NBF thereby increasing the reactivity of the glass towards acid attack⁶⁹.

Wang and Stamboulis¹⁶³ investigated the same glass compositions used here, but employed a different molar basis range of 25% - 100% regarding Ca^{2+} replacement

by Sr^{2+} and Ba^{2+} , respectively. In this project, Ca^{2+} substitution by Sr^{2+} and Ba^{2+} was based on a molar basis of 75%. The FTIR spectra of each of the three glass compositions investigated by Wang and Stamboulis¹⁶³ exhibited similar course curvatures to those obtained here. Moreover, Wang and Stamboulis¹⁶³ suggested that the displacement of FTIR bands towards lower wave numbers indicated the development of NBOs for the glass network modifiers Sr^{2+} and Ba^{2+} . Higher amounts of NBOs resulted in a shift to lower wave numbers for Si-O-Si stretching (Q^3) and Si-O-[NBO] and additionally increased absorbance intensity of Si-O-[NBO]. Wang and Stamboulis¹⁶³ concluded from those Si-O-Si and Si-O-[NBO] ratios that the amount of Si-O-[NBO] present in Ca-Glass < Ca-Sr-Glass < Ca-Ba-Glass.

Therefore it was expected that Ca-Ba-Glass would be more reactive towards the acidic proton of the PAA coupled with higher development/rise of metal polycarboxylate peak in the FTIR, and to lesser extents in Ca-Sr-Glass and Ca-Glass. However, it has to be noted that the experimental glasses used in this project were not pretreated (acid-washed) initially, therefore, a higher ion release upon acid attack might be expected, which settles down after some time. This could result in a faster saturation of the leached ions and the formation of metal carboxylates.

To activate the acid-base setting reaction, the PAA solution has to merge with the ion leachable glass powder. The acidic protons H^+ of the PAA $(\text{C}_3\text{H}_4\text{O}_2)_n$ attack the glass surface and cause dissolution of various ions from the glass structure, depending on the glass content^{53,57}. The dissolution process of the glass and the corresponding leaching process are dependent upon the reactivity of the glass. This reactivity in turn is determined by the number of NBOs (which in turn is determined by excess of network modifiers which render the glass more alkaline)^{67,80}. The migration of ions into the aqueous phase of the cement and their complex with the carboxylate anions COO^- of the PAA leads to the formation of a polysalt matrix. This setting reaction of

GIC has been extensively studied via a number of analytical methods including FTIR^{47,48,49}.

An ATR attachment to an FTIR spectrometer was used in this project because it is more suitable for short term studies of C-GICs, as it prevents dehydration¹⁸⁷. The FTIR spectroscopy makes it possible to distinguish between the symmetric and asymmetric Ca- and Al-carboxylate salt stretching bands along the setting reaction⁵⁷. However, Young⁴⁸ pointed out that significant variations in the polycarboxylate salt peaks occur in the FTIR because of its high sensitivity towards the C=O.

The most important change regarding the acid-base neutralisation can be followed by observing the decrease of the carboxylic acid groups of the PAA peak at around 1700 cm^{-1} with a simultaneous increase of the metal salts ($\frac{1}{2}\text{Ca}^{2+}\text{-COO}^- + \frac{1}{3}\text{Al}^{3+}\text{-COO}^-$) at around 1550 cm^{-1} . The formation of metal salts is an indication of early cement setting¹⁸⁸. Both the symmetric and asymmetric stretching vibration bands in the FTIR are strong and visible⁴⁶, this finding being consistent with the results achieved here. The asymmetric Ca- and Al-carboxylates were significantly higher in intensity from 1 to 60 minutes compared with the symmetric Ca- and Al-carboxylates. The peaks for Ca- and Al-carboxylates (asymmetric stretching vibrations for $\frac{1}{2}\text{Ca}^{2+}\text{-COO}^-$ around 1550 cm^{-1} , symmetric stretching vibrations for $\frac{1}{2}\text{Ca}^{2+}\text{-COO}^-$ around 1410 cm^{-1} , asymmetric stretching vibrations of $\frac{1}{3}\text{Al}^{3+}\text{-COO}^-$ around 1638 cm^{-1} and symmetric stretching vibrations of $\frac{1}{3}\text{Al}^{3+}\text{-COO}^-$ around 1450 cm^{-1}) increased from 1 to 60 minutes at the expense of the narrow peak around 1700 cm^{-1} , due to C=O stretching vibrations of the PAA¹⁸⁸. The peak at 1700 cm^{-1} , at 1 minute, was an indication of the initial amount of free carboxylic acid, which decreased during the setting reaction (over 60 minutes), because of the formation of metal polycarboxylates ($\frac{1}{2}\text{Ca}^{2+}\text{-COO}^-$, $\frac{1}{3}\text{Al}^{3+}\text{-COO}^-$).

PAA is a weak acid and therefore will hardly ionise in water to COO^- and H^+ (in contrast to a strong acid, which would completely ionise)¹⁸⁸. Young *et al.*^{46,188} suggested that the initial acid-base reaction involves the ion release of the glass structure upon the acidic proton attack. This first step is strongly dependent upon the glass surface and composition. This step can be partially controlled by pre-treating the glass surface either by adding a hydrophobic silane coating or by an acid wash¹⁸⁸.

As the medium for the acid-base reaction is water, lack of water can retard the acid-base reaction or even stop the acid-base reaction¹⁸⁷. Young *et al.*⁴⁶ studied the acid-base reaction in GICs with Raman spectroscopy. They observed that the spectrum of a dehydrated two-day old GIC is equal to the Raman spectra of a mixture of PAA and its salts. By adding water to the cement, the water level increased and neutralisation continued. They suggested that a decrease of the carboxylic acid groups of the PAA that is located around 1700 cm^{-1} is probably an indication for water loss, which is needed for the acid-base reaction to progress or for the development of metal salts around 1550 cm^{-1} .

Zainuddin *et al.*¹⁸⁸ investigated the long-term cement setting reaction of three experimental glasses (ART10, LG125 and LG26Sr) with ^{27}Al MAS-NMR. In these experimental glasses, 100% of the Ca^{2+} was replaced by Sr^{2+} . The LG26Sr corresponds to the experimental glass Ca-Sr-Glass (Table 2-1) used here. However, in this project the Sr^{2+} replaced Ca^{2+} on a molar basis of 75% instead of 100%. Zainuddin *et al.*¹⁸⁶ suggested that on the basis of the LG125 and LG26Sr analyses, the bivalent Ca^{2+} and Sr^{2+} ions were initially released into the aqueous phase followed by Al^{3+} and F^- ions. This conclusion was calculated on the basis of the $\text{Al(IV)} / (\text{Al(V)} + \text{Al(VI)})$ ratios and the Al(IV, V, VI) peaks in the spectroscopy. Al^{3+} ions exist in a four-fold coordination in a tetrahedra silica network. However, during

the formation of GIC the Al(IV) transforms to Al six-fold coordination (Al(VI)). Therefore, during the setting reaction the Al(IV) peak reduces, while the Al(VI) increases. This transformation of Al from a four-fold coordination to a six-fold coordination is an indication for cement setting. The initial release of the bivalent cations (Ca^{2+} and Sr^{2+}) was explained by Zainuddin *et al.*¹⁸⁶ as being an attribute of the high phosphorus (PO_4^{3-}) content in the glass, hence the formation of Al-O-P complexes. PO_4^{3-} is actually a network former, but adapts to act as a network modifier in the glasses which were used to investigate GIC in this work. Formation of complexes of Si-O-Al-O-P was observed by Wang and Stamboulis¹⁶³ and Zainuddin *et al.*¹⁸⁶ in the experimental glasses (Table 2-2) used to form GIC. Linkages of Al-O-Al and P-O-P were thought to be unlikely, but linkages of Si-O-Al, Si-O-Si and Al-O-P were reported previously¹⁸⁹. During acid attack, protons preferably attack the Si instead of the P moiety of the Si-O-Al-O-P complex, since Si is more susceptible¹⁸⁹. Therefore, more Al^{3+} ions would still be retained within complexes such as Al-O-P, the result being delayed leaching action of Al ions into the aqueous phase.

In this work, the absorbance intensity between $900 - 1000 \text{ cm}^{-1}$ for Ca-GIC and Ca-Ba-GIC, compared with Ca-Sr-GIC, is markedly higher, which is in keeping with the suggestions of Young *et al.*¹⁸⁸ that with decreased PS, higher absorbance intensity appears around 1000 cm^{-1} . The PS listed in Table 2-1 shows that Ca-Sr-GIC exhibits the largest PS of $8.87 \pm 0.22 \mu\text{m}$ which accounts for its low absorbance intensity.

Matsuya *et al.*¹⁵⁷ analyzed in extensive research with ^{27}Al MAS-NMR, FTIR and CS the change of the silicate structure and the corresponding resulting strength of the cement. The resultant hardening of the GIC corresponded to the degree of poly salt crosslinkages, due to gelation of Ca^{2+} and Al^{3+} polycarboxylates to form the cement network⁵³. An increase in the peak of the metal salts ($\frac{1}{2}\text{Ca}^{2+}\text{-COO}^-$, $\frac{1}{3}\text{Al}^{3+}\text{-COO}^-$) at around 1550 cm^{-1} was at the expense of the carboxylic acid peak

(around 1700 cm^{-1}). The FTIR results of Matsuya *et al.*¹⁵⁷ indicated structural change in the silicate network.

An increase of a broad shallow peak around 1050 cm^{-1} over time was an indication of silica gel formation. An increase in the formation of silica gel in all three GIC compositions was observed from 1 to 60 minutes. Ca-Sr-GIC exhibited the highest silica gel formation of 18% from 1 to 60 minutes, followed by Ca-GIC with 16%. The least formation of silica gel was observed by Ca-Ba-GIC with 5%.

The setting reaction in all three experimental GICs employed here occurred during 60 minutes (FTIR graphs). This is mainly observed by metal salt formation in the range of 1350 cm^{-1} to 1750 cm^{-1} and is caused by the carboxylic acid groups around 1700 cm^{-1} and the simultaneous growth of the metal carboxylates at around 1550 cm^{-1} . Table 4-1 illustrates the mean ratio of polycarboxylate salt development and the silica gel formation over 60 minutes for each GIC composition.

Ca-Ba-GIC exhibited 26% in metal polycarboxylate crosslinkages, whereas the silica gel formation, namely 5%, was considerably quantitatively reduced. Contrary to Ca-Ba-GIC, Ca-Sr-GIC and Ca-GIC respective metal polycarboxylate crosslinkages and silica gel formation were Sr^{2+} 24% and 18% and Ca^{2+} 14% and 16%, respectively (Table 4-1).

In this study, minor errors were observed. Generally, a decrease in the intensity of absorbance can be due to the tendency of the setting cement to detach from the crystal of the Golden Gate¹⁸⁷. A strong broad peak at 3300 cm^{-1} is associated with inter- and intralayer H-bonded O-H stretching vibrations¹⁸⁰. Peaks and troughs in this range can be due to water absorption⁴⁸. However, in the FTIR results water evaporation during the 60 minute experiment is likely to be a factor (due to the rubber ring used not forming a perfect seal). Moreover, the strong absorbance band at

1640 cm⁻¹¹⁸⁴, associated with bending vibrations of water, can overlap with the important metal carboxylate peak specific to asymmetric Al-carboxylate peak around 1640 cm⁻¹.

Real time spectra for all three GIC compositions over a duration of 60 minutes were investigated by following the chemical setting reaction of GICs. The setting reaction for all three GIC compositions was observed via the FTIR spectrum. It is believed that the development of the crosslinked matrix of Ca- and Al-carboxylates, which occur within several minutes, contribute to the resulting strength of the GIC. Additionally, the resulting properties of the GICs are determined by the extent to which the acid-base reaction between the basic glass powder and acidic polymeric solution occur.

Table 4-1: Percentage ratio of polycarboxylate salt development and the silica gel formation over 60 minutes for each GIC composition.

GIC composition	Ratio in the absorbance change over 60 minutes (%)															Mean ratio for metal salt development (%)		
	Symmetric Ca-carboxylate			Symmetric Al-carboxylate			Asymmetric Ca-carboxylate			Asymmetric Al-carboxylate			Silica gel formation (%)					
	Ca-GIC	Ca-Sr-GIC	Ca-Ba-GIC	Ca-GIC	Ca-Sr-GIC	Ca-Ba-GIC	Ca-GIC	Ca-Sr-GIC	Ca-Ba-GIC	Ca-GIC	Ca-Sr-GIC	Ca-Ba-GIC	Ca-GIC	Ca-Sr-GIC	Ca-Ba-GIC	Ca-GIC	Ca-Sr-GIC	Ca-Ba-GIC
A/C	11	28	30	11	21	21	26	44	47	7	2	6	16	18	5	14	24	26

A/C: 1 minute/60 minutes

4.2 Fluoride release of GICs in artificial saliva and deionized water

Among other important characteristics of GICs is its ability to release fluoride – one of the major characteristics that is associated with anticariogenic action. Despite the large amount of studies of fluoride release in GICs, the amount of fluoride required to inhibit caries formation has not been determined. However, Matz and Emilson¹⁰² demonstrated in an *in vitro* experiment that the growth of *Streptococci* can be prevented by an amount of fluoride release ranging from 0.16 to 0.31 mol/l. Several other studies have confirmed that the F⁻ release of a restorative dental material has an inhibitory effect on the development of tooth decay at the margins of the dental restoration^{103,121}. The obtained results in this work suggested that an amount of 0.1 – 1.5 ppm F⁻ ions, reduced the growth of *S. mutans*. As Rothwell *et al.*¹¹¹ mentioned, it is more significant for a restorative material to have the capacity to recharge, if exposed to a F⁻ ion source, than to have a high initial inherent F⁻ amount.

In general, less fluoride release has been observed in AS and saliva than in deionized water. The results shown in Figure 3-27 – Figure 3-34 are consistent with the existing literature^{112,113,114}. The reason for decreased F⁻ release in saliva or AS is that both contain a high number of ions, as does the restorative material (GIC), in contrast with deionized water. It is the similar ion distribution, as between AS, saliva and GIC, which causes a low diffusion gradient. Conversely, the dissimilar ion distribution, as between deionized water and GIC, causes a higher diffusion gradient¹²⁶. Therefore, more ion exchange from the dental restorative material into the deionized water is expected because of the unequal ion distribution and the corresponding high diffusion gradient. In addition, Bell *et al.*¹²⁶ demonstrated that the ion layer formed by the ions of the saliva on the tooth structure might prevent the release of ions, including fluoride ions, into the mouth.

The F⁻ release in GICs and hybrids has been extensively researched¹¹⁵. Generally, two mechanisms are involved; the initial burst from the surface of the restorative material and the second long lasting ion diffusion from the bulk of the material¹¹⁶. The cumulative F⁻ release observed in this study is similar to reported studies¹¹⁵. The initial F⁻ ion burst is clinically significant in reducing secondary caries after dental work is carried out as residual bacteria may be present in the cavity underneath the restoration work¹⁵⁴. After the initial burst, the amount of F⁻ ions released decreases and controlled ion diffusion occurs¹¹⁷. This finding is consistent with the existing literature¹¹⁵. In this project a high F⁻ release in the initial phase occurred between 6 and 8 hours in the case of deionized water. It has been reported that the above usually occurs in deionised water during the first 24 to 72 hours^{119,126,154}. However, fluoride release reached a plateau in the period of time between 18 and 35 days in deionized water and 18 and 28 days in AS. Generally, a constant level of fluoride release could be achieved between 10 and 20 days¹¹⁸. The *in vitro* results presented in this project demonstrated that the initial short term release occurred faster than expected. Usually, commercially available GICs and hybrids release a high amount of fluoride (15 – 115 ppm first stage; 1 – 4 ppm second stage¹¹⁹). However, experimental GICs are expected to release less fluoride as compared to commercially available GICs¹²⁰. The obtained results in this work presented a lower amount of F⁻ ion release and a delayed plateau in comparison to the commercially available GICs. It is important to note though that all characteristics regarding fluoride release in AS and deionized water have been observed, such as:

- maximum F⁻ ion release in the first hours, due to initial burst;
- followed by plateau, due to bulk diffusion;
- less F⁻ ion release in AS, due to the similar ion distribution and the low diffusion gradient;

- high F⁻ ion release in deionized water, due to unequal ion distribution and the high diffusion gradient;
- uptake of F⁻ ions from external source, which was released over time.

Rothwell *et al.*¹¹¹ monitored the F⁻ release after exposing four GICs and modified GICs to a F⁻ containing toothpaste. Fuji IX, a C-GIC, exhibited a low amount of F⁻ release; this was explained by the low soluble glass, which is a component of Fuji IX. Fuji IX is a highly viscous cement used in Atraumatic Restorative Technique (ART), therefore it is less sensitive to moisture in comparison to other C-GICs¹⁹⁰. Rothwell *et al.*¹¹¹ explained that the glass network component for Fuji IX has fewer alkali metals. The Fuji IX cement matrix would appear to have a high DCL and consequently less ion diffusion (including F⁻ ions) through the tightly bonded cement matrix.

The degree of crosslinking in the cement matrix determines the amount of ion diffusion. Therefore, a dense crosslinked cement matrix would result in a low diffusion of ions¹⁰³, including F⁻ ions. In this study it was therefore expected that a higher amount of F⁻ ion release should occur in the following order Ca-GIC > Ca-Sr-GIC > Ca-Ba-GIC; this assumption is in accordance with the achieved results. As Wang and Stamboulis¹⁶³ previously concluded from the Si-O-Si and Si-O-[NBO] ratio, the amount of Si-O-[NBO] is in ascending order Ca-Glass < Ca-Sr-Glass < Ca-Ba-Glass. Therefore, the highest number of NBO formation in all the glasses was expected for Ca-Ba-Glass. Triggering the setting reaction to form cement, the highest diffusion of cations into the aqueous phase would be expected for Ca-Ba-GIC, because of the high disturbance in the glass network. The high number of cations released into the aqueous form would result in a high DCL in the cement matrix. The diffusion of ions in a dense cement matrix is impeded, resulting in a low diffusion of ions, including F⁻ ions. Therefore the least diffusion of ions was expected for Ca-Ba-GIC, while the highest diffusion of ions in Ca-GIC was expected.

The setting reaction of GICs continues over a few years. During the setting time the crosslinkage in the cement matrix is continued¹⁹². This entails that a mature cement has less F⁻ release or uptake, because the diffusion process is impeded, due to the tight crosslinked cement matrix¹¹¹. This explains also why the 40 days mature cement in this project released fewer F⁻ ions after exposure to a F⁻ source.

GICs have the ability to act as a F⁻ reservoir. Increasing the time during which the GIC is exposed to a F⁻ source would increase the F⁻ release. The longer the cement was exposed to a F⁻ source, the more time the F⁻ ions have to diffuse in the inner of the cement. The finding in this experiment is consistent with Xu and Burgess¹⁵⁴. Diaz-Arnold *et al.*¹²⁸ suggested that the fluoride release after exposing the specimens to a fluoride source is just a superficial absorption and not bulk absorption, due to the rapid discharge of the F⁻ ions. This observation is consistent with the findings in this experiment. After exposing the mature GICs in AS for 12 hours to a fluoride containing mouthwash, there was almost no F⁻ release after 90 minutes. This view is shared by Hardley *et al.*¹⁹¹, who were using Secondary Ion Mass Spectroscopy (SIMS) to measure fluoride concentrations in the bulk of the cements and reported that the highest fluoride amount was observed on the surface of cements. Additional hindrance of fluoride release is caused by the maturity of cements. This has an important clinical advantage; the cement develops more strength over time. This is explained by the increased number of ionic matrix crosslinkages, and therefore less diffusion of water and fluoride ions¹⁹². Dhondt *et al.*¹²⁹ corroborated this conclusion that the decrease of fluoride release in a mature cement is due to the strong interaction of ions with the organic crosslinked matrix and a reduced permeability of the matrix. Additionally, it is important to consider the morphological difference of the material; porosity may have an impact on the total ion release¹⁹³. The low amount of fluoride release for all three experimental GICs could result in low water diffusion.

The microstructure of GIC, with its voids and cracks, promotes water diffusion into the deeper or even superficial area of the specimens. The higher the porosity, the easier for F^- ions to diffuse from the bulk of the restorative cement¹⁹⁴. Itota *et al.*¹⁹⁵ suggested that the recharge properties of a material depend upon the diffusion and absorption ability of the material. Therefore, a high amount of porosity would contribute and promote diffusion and absorption properties. However, the F^- release of a mature cement is expected to be less, hence a more crosslinked matrix or a tight polymer chain matrix would inhibit the diffusion process substantially^{111,115,154}.

The ion diffusion process in the cement matrix is dependent upon the density of the ionic crosslinking and the cement porosity. Neglecting the porosity and focusing on the ionic crosslinkage, it can be predicted that the glass network with the highest formation of NBO is releasing the highest amount of cations into the aqueous phase upon the setting reaction and therefore a higher DCL in the resulting cement matrix can be expected. This leads to an impeding of the diffusion process and therefore fewer ions, including F^- ions, diffuse out of the inner cement matrix to the outer environment or vice versa.

Other attributes regarding F^- release for GICs could not be ascribed to the experimental GICs used in this work. For example, the recharge capability. Generally, the restorative dental material with the highest initial F^- release has also the highest recharge capability¹⁵⁴. But this was not the case. It was expected that the 40 days mature Ca-GIC would exhibit the highest recharge capability, as it had the highest F^- ion release initially. But, the mature Ca-GIC did not have the highest amount of released F^- ions in deionized water. In fact, it was the lowest. However, it exhibited the highest amount of F^- ions in AS. Therefore, this assumption is not applicable.

Furthermore, one very important factor should not be neglected; the P/L ratio used to form Ca-GIC was just 2:1 in comparison to Ca-Sr-GIC and Ca-Ba-GIC with 3:1. Glass filler component is a very important factor since the fluoroaluminosilicate glass particles are the main source for the F⁻ ions¹⁵⁴. The fewer glass particles used, the less F⁻ ion release was expected. However, this conclusion is not supported by this work, since Ca-GIC had the highest F⁻ release after 40 days. But, it was previously reported that reducing the P/L ratio would result in higher solubility of the GIC, which results in higher F⁻ ion release¹⁹⁶. This conclusion would support the findings in this study.

The high content of F⁻ release for Ca-GIC could be the result of high formation of metal fluoride in Ca-Sr-GIC and Ca-Ba-GIC. These complexes would bind the F⁻ ions to the cement and would be therefore not detectable for F⁻ measurements. However, Wang and Stamboulis¹⁶³ analysed the glass compositions previously with magic angle spinning nuclear magnetic resonance (MAS-NMR) conducted of ¹⁹F. They concluded that F⁻ is present in Ca-Glass as F-Ca(n) and Al-F-Ca(n) in Ca-Sr-Glass as F-Sr(n) and Al-F-Sr(n) and in Ca-Ba-Glass as F-Ba(n) and Al-F-Ba(n), respectively. With decreasing the cation size Ba < Sr < Ca an increase in the formation of F-M(n) (where M stands of Ca, Sr and Ba) species was observed and reported previously from Stamboulis *et al.*¹⁷⁴. Therefore, a high amount of F⁻ formation was expected in the order F-Ba < F-Sr < F-Ca followed by Al-F-Ba < Al-F-Sr < Al-F-Ca. Therefore, the assumption of higher fluoride metal formation in Ca-Sr-GIC and Ca-Ba-GIC does not apply. On the contrary, the highest formation of fluoride metals is present in Ca-GIC.

F⁻ measurement in this work was not conducted with a fluoride ion selective electrode, as it is generally done. In this project a photometer Nanocolor 500D was used to measure the activity of free F⁻ ions in the solution. To date, there is no

published paper where F^- measurements were conducted with 500D. Initially it was planned to perform F^- measurement with inductively coupled plasma mass spectrometry (ICP-MS). However, this was not possible as a residue of silica layer became stuck in the concentric glass tubes of the ICP and adversely affected the measurements. Therefore, an alternative measurement for the F^- ion release had to be found.

The F^- release measurements demonstrated all the previously observed characteristics regarding fluoride release in AS and deionized water. From the obtained results it can be predicted that a high number of NBO formation in the glass component causes a high amount of cations to be released into the aqueous phase (upon the setting reaction) and therefore a higher DCL in the resulting cement matrix can be expected. These factors lead to a lower diffusion of ions, including F^- ions, through the dense cement matrix. However, lower glass powder volume (2:1) was expected to release less F^- ions, since the glass powder is the F^- source. But, this can be compensated for by the fact that a low P/L ratio results in higher solubility of the GIC, which in turn results in higher F^- ion release.

To validate these results, additional F^- ion measurements have to be performed.

4.3 Antimicrobial effectiveness of glass ionomer cements

The bacteria playing a main role in cariogenesis are *S. mutans* and *S. sobrinus*¹³⁶. *Streptococci* are able to produce organic acids such as lactate and undergo anaerobic glycolysis with production of lactate¹³⁶. The resulting dissociation products, which are H^+ ions, are transferred out from the bacteria cells leading to pH reductions within the plaque matrix and subsequent damage to enamel¹³⁶. *S. mutans* forms multicellular aggregates that are water-insoluble, highly branched, fibrillar and resistant to enzymes produced by other bacteria and therefore act as a very good substrate for initial formation of plaque, which in turn allows other pathogenic bacteria

to attach and grow¹⁹⁷. Materials with antibacterial characteristics are well known and widely used to prevent plaque formation. High concentrations of silver (Ag) species in dental material have been shown to be bacteriostatic against oral *Streptococci*¹⁹⁸. A further species with caries-inhibitory effect is fluoride. Fluoride's antimicrobial effect is thought to occur via several mechanisms including decrease of demineralisation, improvement of remineralisation, interference with pellicle and plaque development and the inhibition of microbial growth and metabolism¹²³. Previous investigations have validated the ability of GICs, compomers and RM-GICs to inhibit bacterial growth via an agar plate diffusion method¹³⁹. Koch and Hatibović-Kofman¹⁴⁰ have also conducted an *in vivo* experiment with 3 C-GICs in 36 children. Before and after the restorative replacement, the numbers of *S. mutans* were analysed. They reported that fluoride concentration in saliva increased significantly after replacement and thereafter consistently increased. After 6 weeks the F⁻ amount was 6 times higher. The quantity of *S. mutans* decreased after replacement. Svanberg *et al.*¹⁴¹ stated that the percentage of *S. mutans* in the plaque from the margins of Class II GICs is significantly less in comparison to amalgam and composites. In the same year Svanberg *et al.*¹²³ demonstrated that the occurrence of *S. mutans* in interproximal plaque in adult teeth with GICs was significantly lower than for amalgam alone. The bacteriostatic effectiveness of GICs rests upon its ability to release fluoride in the oral environment; this has been verified by several studies¹⁹⁹. However, Sr²⁺ is also believed to contribute to the bacteriostatic effect of GICs. Guida *et al.*²⁰⁰ analysed the antibacterial effectiveness of Sr²⁺ in several experimental glass compositions. The antibacterial activity of the experimental GICs was analysed by the agar plate diffusion method against *Streptococcus* and *Actinomyces*. They suggested that Sr²⁺ ions have a more important role in the bactericidal properties than F⁻ ions and that the antibacterial effect is based upon the contribution of Sr²⁺ ions, or Sr²⁺ and F⁻ ions

together. The results for the antimicrobial activity in this project suggest that substitution of Sr^{2+} for Ca^{2+} in the glass composition of the GIC component is not necessarily more effective, in contrast to the results of Guida *et al.*²⁰⁰. Guida *et al.*²⁰⁰ identified an antibacterial activity of the cements made of glass components close to the composition of glass used in this study. Recently, more investigations regarding the antibacterial role of strontium have been published in the literature. Thuy *et al.*²⁰¹ suggested in an extensive study of sixty human enamels that Sr^{2+} ions are involved in enhancing remineralization. Dabsie *et al.*²⁰² investigated the bacteriostatic effect of strontium ions from RM-GICs on young patients' premolars and reported that strontium ions have a weak bacteriostatic effect but the inhibition of tooth decay is based on strontium ions' ability to enhance remineralization of the tooth substance. However, the synergistic effect of strontium and fluorine ions could have an advantageous role in the restitution of enamel in orthodontic treatment, but further research is necessary. In this work it is clear that all GICs show a significant antibacterial activity, from 15 minutes to 24 hours, and what is known is that fluorine release occurs for all three GIC compositions. The obtained results in this work suggested that an amount of 0.1 – 1.5 ppm F^- ions, from 30 minutes to 48 hours reduced the growth of *S. mutans*. It is clear that the strontium cements, compared to calcium cements, do not show any material difference in their antibacterial behaviour and it is very difficult to say that there is one cement significantly better than the other. Therefore, it must be concluded that all cements are antibacterial most likely because they all release an effective amount of fluorine that contributes towards the GICs' antibacterial behaviour. In this study there was no evidence for any synergistic effect of strontium, barium or calcium with fluorine however some of the authors in the literature claim that such a synergistic effect could be one of the reasons for the antibacterial behaviour of glass ionomer cements in general²⁰⁰.

4.4 Calculation of cement setting time

Rheology is originated from two Greek words; rheo meaning flow and –logy meaning study. An ideal restorative dental material has to be viscous enough to be mixed easily followed by a sudden raise in viscosity, so that the restorative dental material preserves and maintains its intended purpose²⁰³.

Resistance to penetration used for the calculation of cement setting time is a convenient method used widely in industry. The extrusion-style capillary rheometer²⁰⁴, cone and plate rheometer⁶⁵ and ram and piston penetrometer²⁰⁵ are examples of techniques which have been suggested in the past for measuring the change in cement viscosity with time. Each technique has its advantages and disadvantages, the extrusion capillary rheometer being subjected to a range of shear rates²⁰⁴, the cone and plate rheometer being subjected solely to constant shear rate⁶⁵ and the ram and piston penetrometer not being appropriate for fundamental rheological studies because of its sophisticated geometry²⁰⁵.

An important factor in cement setting time is the glass filler surface area component where an increase in the glass powder to liquid (P/L) ratio results in a decrease in setting time²⁰³. Lowering the amount of glass fillers, lowers the ion source and ion diffusion and results in a lowered viscosity, an increased setting time a decreased reaction rate²⁰³ and a reduced extent of crosslinkages¹⁵⁴, which is in keeping with the results obtained here.

Cook²⁰³ pointed out that the viscosity of a material was a result of the interaction between two independent factors; the degree of crosslinkage of the Ca- and Al-carboxylates in the cement matrix and the effect of the glass PS on the viscosity of the paste.

The experimental glass powder hand-mixed easily with the polymeric liquid at the P/L ratio of 2:1. In general, ideal restorative dental material should have a low viscosity at

the beginning, to make for easy hand-mixing and for placing the restorative material in the cavity of the tooth after which the viscosity should increase rapidly²⁰³. All experimental GICs employed here were close to being ideal restorative material apart from Ca-GIC with the 2:1 ratio. However, the exception in setting time of Ca-GIC may have been due to the ambient RT or the temperature of the instruments used during the preparation of this cement.

Once the glass powder and the polymeric solution are mixed together the acid-base reaction takes place. The acidic protons attack the basic glass powder surface, resulting in dissolution of the glass powder. Cations, such as Ca^{2+} and Al^{3+} ions diffuse/leach into the aqueous phase and form Ca- and Al-carboxylates, with the free carboxyl anions, which results in a crosslinked polysalt matrix^{53,57}. Less ion diffusion during the formation of the metal salt matrix brings about a decrease in its viscosity²⁰³.

The rheological properties of these restorative materials are very important, since they affect their behaviour in clinical practice. The viscosity of a material bears an inverse relationship with temperature; viscosity usually increasing with temperature decrease and viscosity decreasing with temperature increase²⁰⁶. Pearson and Atkinson⁷⁰ investigated the influence of temperature change on the working and setting times of 5 different cements (4 water-based polyacrylates and 1 zinc phosphate), the results of which showed that all five cements exhibited longer setting and working times in a chilled state. Extensive increases of 200% for working and 130% for setting times were observed in all four water-based polyacrylate cements, whereas such extensive increases in working and setting times were not evident in the zinc phosphate cement when chilled⁷⁰.

The dissolution process of the glass and the corresponding leaching or diffusion process of the cations in the aqueous phase is strongly dependent upon the reactivity

of the glass. This reactivity is in turn determined by the number of NBOs, which in turn is determined by an excess of network modifiers that renders the glass network more alkaline and increase the dissolution rate^{67,80}. The greater the number of NBOs formed in the glass component of the GIC, the greater the facility for the cations to diffuse, through the expanded glass network¹⁶³ into the aqueous solution and collide with carboxylate anions thereby forming a polysalt matrix.

Therefore, the shortest setting time would be expected to be associated with those cements whose glass component contained the highest number of NBOs. In this case, the glass network that exhibited the highest number of NBOs and lowered the oxygen density and increased expansion of the glass network was Ca-Ba-Glass, used for make barium glass ionomer cements. The least expanded glass network was Ca based whereas, the Sr based glass network was more expanded due to the presence of a larger amount of NBOs in the case of Ca alone¹⁶³. On the basis of the above, the Ba glass ionomer cement would be expected to exhibit a shorter setting time compared with both Ca-Sr-GIC and Ca-GIC, the slowest setting time occurring in the Ca-GIC.

The glass ionomer cement setting reaction is not a diffusion controlled process²⁰³, for during the acid attack, the cations spread out into the aqueous phase. On the basis of FTIR setting time results: only 5% silica gel formation was evident in the Ca-Ba-GIC, whereas Ca-GIC and Ca-Sr-GIC exhibited 13% and 18% silica gel formation, respectively, within a 1 to 30 minute test period. Moreover, the FTIR results demonstrate the high degree of metal salt crosslinkages occurring in the cement matrices from 1 minute to 30 minutes, namely, 13%, 21% and 25% for Ca-GIC, Ca-Sr-GIC and Ca-Ba-GIC, respectively. The high degree of metal salt development during the first 30 minutes for Ca-Sr-GIC and Ca-Ba-GIC lends support for hypothesis of higher ion diffusion from the expanded glass network into the liquid

phase. However, it is still unclear why the high degree of crosslinkage, in the case of Ca-Ba-GIC, did not lead to the shortest setting time of the three GICs. One conclusion could be related to the process of silica gel formation and the extent to which the silica gel formation has occurred. The inorganic glass core being surrounded by a silica gel, possibly hinders or slows down ion diffusion over long distances into the liquid phase. The initial diffusion of cations into the aqueous phase slightly increases the cement viscosity, but has a minimal effect on the overall viscosity of the cement, whereas the cement viscosity increases by the degree of crosslinkages in the cement matrix²⁰³. However, if cations diffuse over a longer distance into the aqueous phase, this would reduce the reaction rate, resulting in a delay of setting time and the corresponding lesser degree of crosslinkage. Therefore, the greater the diffusion distance of the ion the slower the diffusion rate²⁰⁷, resulting in a delay in the setting time, hence the crosslinkage rate being decreased.

However, this hypothesis has to be further investigated. It was assumed that the rheological setting time of the resulting cement is strongly dependent upon the amount of NBO in the glass component. It was thought that the greater the vulnerability of the glass network to acid attack, the greater the amount of leachable cations into the aqueous phase. This necessitates a greater degree of crosslinkage in the cement matrix thereby resulting in an increase in viscosity. However, the diffusion distance of the ions was not taken into the account. The more the diffusion rate is reduced, the greater the diffusion distance²⁰⁷ and this fact could delay the rate of crosslinkage and the corresponding setting time.

Rheology is an interdisciplinary science that includes the chemistry, physics and mechanism of a continuum of molecules. Therefore, several factors need to be considered in order to be able to predict within reason the setting time of cements. As Cook²⁰³ summarized, the viscosity is dependent upon two factors – the surface of the

filler particles and the degree of crosslinkage in the aqueous phase. However, several other factors, such as the molecular physics, thermodynamics, and intermolecular interactions have also to be taken into account.

4.5 Vickers Hardness

The hardness of a material demonstrates the ability to resist the force before plastic deformation occurs via penetration. Generally, a hardness value is composed of several factors, such as the indentation shape, the indentation depth and the force that was applied for a specific time²⁰⁸.

Generally, the hardness of a material gives an indication of the wear resistance of the material. The two most important surface characteristics of a dental material are its ability to be polished and its resistance to wear¹⁵¹. Rabinowicz²⁰⁹ suggested that three parameters are important – Ra, PS and hardness for surface analysis. Generally, the restorative material should mimic the tooth in all categories.

In 1922 Willems *et al.*²¹⁰ indicated that the microhardness of a real human enamel is 4002 ± 323 MPa. Gladys *et al.*⁶ measured among other things the HV of 2 commercial available C-GICs (HIFI Master Palette and Ketac-Fil) after 1 month storage in deionized water. Both GICs exhibit a HV value at ca. 1000 MPa (HIFI Master Palette 1020 ± 137 MPa and Ketac-Fil 1138 ± 461 MPa). The hardness values presented in this work (Figure 3-37) at 1 month storage in deionized water are lower (Ca-Ba-GIC: 580 ± 70 MPa, Ca-Sr-GIC: 652 ± 49 MPa and Ca-GIC: 526 ± 38 MPa) compared to the existing literature; this was expected, since the GICs used for this project are experimental GICs, therefore reduced strength values were expected.

Behr *et al.*⁷¹ stated in an extensive experiment, with varied GICs and RM-GICs, that the HV of a C-GIC was significantly influenced and dependent on its powder content. The three GIC compositions in this project were prepared according to Table 2-2.

The powder content differed because it was not possible to obtain a homogeneous paste with Ca-GIC with a P/L ratio of 3:1. Therefore, Ca-GIC was prepared with a P/L ratio of 2:1, while Ca-Sr-GIC and Ca-Ba-GIC were prepared with a P/L ratio of 3:1, respectively. However, the results in Figure 3-37 demonstrate that Ca-GIC (550 MPa at 1 month) with a P/L ratio of 2:1 exhibits the lowest HV value at 1 month in comparison to Ca-Ba-GIC and Ca-Sr-GIC (580 MPa and 650 MPa, respectively), therefore the obtained results in this project are in agreement with Behr *et al.*⁷¹. The higher the amount of glass powder component, thus an increase in the surface area, and an increased rate in the chemical reaction is given. This results in a larger amount of ion diffusion from the glass matrix in the aqueous phase⁶.

The resistance relationship between the maxillary and mandibular teeth can be determined when masticating by the hardness and the elastic modulus of the restorative material. The former is defined as the resistance to penetration force and the latter describes the stiffness of a restorative dental material²¹¹.

Generally, an increase in the surface microhardness of the three GIC compositions was expected from 1 h to 1 month of ageing time. The hardening of the GICs is based on the formation of an infinite metal salt carboxylate network²¹², which progresses over a few years^{149,150}. This is consistent with the obtained results in this project. The microhardness values of the three experimental GICs increased from 1 hour to 1 month.

Ellakuria *et al.*¹⁵⁵ observed the micro-HV of C-GICs and RM-GICs stored in distilled water over one year. RM-GICs have the same components as the C-GICs with an addition of photopolymerizable monomers²¹³. Ellakuria *et al.*¹⁵⁵ reported that the C-GICs exhibit a higher HV than the RM-GICs. This observation was explained with the general two reaction mechanisms that are involved in RM-GICs. In RM-GICs a free-radical polymerisation and an acid-base reaction are occurring²¹⁴. Ellakuria *et*

*al.*¹⁵⁵ suggested that the addition of 2-hydroxyethyl methacrylate (HEMA) might prevent the acid-base reaction from proceeding, therefore less metal crosslinking formation occurs in the cement matrix, resulting in less strength. Generally, the light curing process, which is needed to activate the photopolymerizable monomers, decreases the formation of metal salt crosslinking in the cement matrix in the early setting progress^{215,216}. Ellakuria *et al.*¹⁵⁵ reported that the HV values increased over a 1 year period for C-GICs, however this was not the case for RM-GICs.

In the literature, several factors were mentioned that are responsible for the initial resistance of GICs:

- P/L ratio⁶⁶,
- Mw of PAA and the concentration of PAA^{73,74} and
- the chemical composition and the microstructure of the glass¹⁰⁹.

Cattani-Lorente *et al.*¹⁴⁹ suggested that all the above points can contribute to the enhancement or decline of the mechanical properties in the resulting GICs over time.

Xie *et al.*²⁷ investigated the mechanical properties and the microstructure of several GICs and hybrids. The hardness of the specimens was determined using a Knoop hardness (KH). They suggested that there is a relationship between the hardness of the specimens and their microstructure. Xie *et al.*²⁷ concluded the tighter and denser the micro surface structure of the cement is, the higher the hardness values are. Furthermore, Xie *et al.*²⁷ suggested that higher hardness values can be achieved if different PSs and shapes are present in the microstructure of the resulting cement.

Crisp *et al.*²¹ investigated the long-term hardness of the first ever commercial GIC, named ASPA. The surface hardness was determined using two approaches, the Wallace indentation and Woxen hardness (WH). Crisp *et al.*²¹ concluded that the

number of metal salt crosslinking formations can explain the hardness of the resulting cement. This conclusion is in good agreement with the our results.

From the obtained FTIR results in this project in Chapter 3.1.3, the ratio of the change in intensity against time for metal salt crosslinking formation (symmetric and asymmetric of $\frac{1}{2}\text{Ca}^{2+}\text{-COO}^-$ and $\frac{1}{3}\text{Al}^{3+}\text{-COO}^-$) of each experimental GIC from 1 minute to 60 minutes was obtained. Ca-Ba-GIC exhibits the highest degree of metal salt development from 1 minute to 60 minutes with 35% followed by Ca-Sr-GIC and Ca-GIC with 24% and 14%, respectively. And since the hardness of the cement is determined by the degree of metal salt crosslinking formation²¹², it can be assumed that the GIC composition with the highest degree of metal salt crosslinking exhibits the highest hardness. This assumption is in conclusion, with the obtained results of the HV for all experimental GICs at 1 hour. As mentioned previously by Wang and Stamboulis¹⁶³ from the Si-O-Si and Si-O-[NBO] ratio, the highest amount of Si-O-[NBO] is in Ca-Ba-Glass, followed by Ca-Sr-Glass and Ca-Glass. Upon the acid attack, in the more disrupted glass a higher amount of cations would diffuse from the glass network into the aqueous phase. This would result in a high degree of metal salt crosslinkage in the cement matrix. This conclusion is in good agreement with the finding in this project. The progression in metal salt crosslinking determined the strength of the three GIC compositions at 60 minutes. The number of metal salt crosslinking formations and hardness were increasing simultaneously. Therefore, it can be expected that using a glass component with high number of NBO to form GIC, a faster diffusion of bivalent and trivalent cations from the very first moment of the setting reaction, from the glass network, into and through the cement matrix would favour a higher DCL ions. The findings of this work were consistent with that expectation.

4.6 Nano-indentation

Two main surface characteristics of restorative dental materials can be determined from the nano-indentation: the hardness and the creep characteristics of the restorative material^{152,160,217,218,219}. The former is a statement about the wear resistance but generally hardness is defined as the resistance of a material to penetration²²⁰. Creep gives an indication of the DCL of the polysalt matrix or the viscosity of the restorative dental material^{152,220}. Generally, the stiffness of a material and the adhesive properties of a restorative material are believed to be preventative measures regarding secondary caries and microleakages²²⁰.

Yap *et al.*²¹¹ reported that nano-indentation is not an ideal technique to measure hardness especially when the material consists of two phases - in our case an inorganic and an organic phase. It was suggested that if the glass particles are bigger than the indenter head then the measurements are not accurate and therefore it is likely that only the mechanical properties of one phase can be measured by nano-indentation. Yap *et al.*²¹¹ investigated the hardness and the modulus of 6 tooth coloured restorative materials (e.g. C-GIC, RM-GIC, giomers, compomers and composite) via depth-sensing microindentation. Yap *et al.*²¹¹ reported that further physical and mechanical tests, in addition to hardness and Young's modulus of a restorative dental material, have to be performed for a restorative material in posterior area.

Towler *et al.*¹⁵² compared the hardness and creep properties of Fuji IX chemically cured and ultrasonically cured GIC. They reported that the hardness of the ultrasonically cured GIC was significantly higher than the chemically cured GIC. The ultrasonically cured GIC showed no creep, which was an indication that the ionic crosslinking was completed, while still a significant amount of uncured polymer was

present in the chemically cured GIC. Generally, the creep decreased the more the ionic crosslinking in the cement matrix proceeded.

The creep of all the three experimental GIC compositions decreased after ca. 40 seconds. A decrease in the creep displacement would be expected if the ionic crosslinking in the matrix increases over time¹⁵². In this work the creep response in Chapter 3.6 indicated that the polysalt crosslinking was still taking place. It can be assumed that a respective amount of unreacted polymer in the cement matrix was present at the time when the measurements were taken.

The force/displacement curve of the three GIC compositions in Chapter 3.6 corresponded to a typical force/displacement C-GIC curve¹⁵².

Generally, the mechanical properties of a conventional glass ionomer dental restorative material improved with increasing the P/L ratio²²⁰. This is in good agreement with Behr *et al.*⁷¹ investigated in an extensive experiment, with several GICs and hybrids, the hardness, FS and three body abrasion of a C-GIC was significantly influenced and dependent on the powder content. The three GIC compositions in this project were prepared according to Table 2-2. The powder content differed since it was not possible to obtain a homogeneous paste with Ca-GIC. Therefore the powder content in Ca-GIC was lower in comparison to Ca-Sr-GIC and Ca-Ba-GIC. The results in Figure 3-38 support the findings of Behr *et al.*⁷¹. The glass particles are the source for the cations. If a higher amount of glass powder is present, a higher amount of cations will diffuse from the glass matrix in the aqueous phase, resulting in a higher amount of metal salt crosslinking in the cement matrix²²¹.

Al-Haik *et al.*²²² measured, in an extensive investigation of mechanical properties of enamel, the hardness and the corresponding modulus of the human enamel. The hardness that was identified was around 5 GPa and the corresponding modulus was

around 112 GPa. Additionally, the hardness of a C-GIC and its modulus was measured ($H_{GIC} = 1.93$ GPa; $E_{GIC} = 37.36$ GPa). Comparing the above values with the hardness and the corresponding modulus measured in this work, the values obtained were much lower. This was expected since an experimental GIC was used in this project.

The results obtained from the nano-indentation in this project exhibit a decline from 1 hour ageing time to 1 month ageing time. Generally, an increase in strength was expected, since the polysalt crosslinking progresses²¹², over a few years^{149,150} and determines the hardness/strength of a GIC restorative material. The limitation of using nano-indentation for two phase materials has been previously mentioned by Yap *et al.*²²⁰. The development in hardness over 1 month ageing time can decrease if the indenter head is measuring the hardness of the organic phase, with less strength in comparison to the inorganic phase.

The nano-indentation as a surface characterisation method of two phase dental restorative materials is not ideal.

4.7 Wear behavior of glass ionomer cements

Wear is a very important factor in dentistry since this process occurs continuously in the mouth cavity²²³.

Generally, C-GICs are well known for their high surface wear in molar areas²²⁴. Pearson and Atkins¹⁵⁰ reported that their initial low strength is a disadvantage but the strength develops over a long-term period and reaches an acceptable level. Gee *et al.*¹⁵⁶ investigated the early (8 hours) and long-term (1 year) wear of several GICs and hybrids. All GICs exhibited an increase in wear resistance over time and this was explained by the continuation of acid-base reaction. Wear is caused by eating, chewing, biting etc. or even by chemical interaction. Hard food particles can cause

high wear rate between the maxillary and mandibular teeth¹⁵⁶. Wear can be divided into two categories, depending on the forces that are present on the opposing materials; the fatigue wear and the abrasive wear. Wear due to fatigue is caused by repeatable movements, such as mastication, on the material's surface. This results in crack progression. Wear due to abrasion can be subdivided into 2 categories; 2-body wear and 3-body wear. A hard or sharp material causing rills on the antagonist's surface is defined as the 2-body wear. The 3-body wear is when a third abrasive medium is located between the two opposing surfaces such as food²²⁵.

Gee *et al.*¹⁵⁶ reported a decrease in the wear rate of GICs and hybrids over 1 year of ageing time due to continuous acid-base reaction and continuous increase in the DCL in the polysalt matrix. Generally, the mechanical properties of GICs are believed to increase over time therefore they are expected to have higher wear resistance with time. However, in long-term studies a decrease in FS¹⁵⁰, CS and DTS¹⁴⁷ with ageing time was reported¹⁴⁹. The decline in strength was mainly explained because of water storage¹⁴⁹ or surface cracks²²⁶. Generally, water hardening cements, if exposed to water, absorb water and act as a plasticizer⁹³, resulting in a decline in strength of the GIC. However, Gee *et al.*¹⁵⁶ also reported that microcracks on the dental restorative surface were negligible since the wear apparatus removes the outer surface of the restorative dental material continuously.

Two different wear values were obtained in this project, the wear volume and the wear depth. Generally, volume is made of the wear depth and the wear area²²⁷. The wear depth is not an accurate parameter, as it depends on the direction and the location where the wear depth is measured. The wear depth was originally measured to give a vertical reference of wear between the cavosurface and the restorative material's surface²²⁸. The wear area is not time consistent and the wear facet does

not necessary represent the active wear area. Therefore, the wear volume is the most important factor expressing the loss of volume of dental material²²⁷.

In this project the wear volume was used in order to interpret the wear behavior of GICs. Ca-Ba-GIC was expected to exhibit the highest wear resistance compared to the rest of the GIC samples measured, as the DCL in this cement seems to be higher from the early stages of setting. This was proven to be accurate as the wear resistance was highest for Ca-Ba-GIC followed by Ca-GIC and Ca-Sr-GIC.

4.8 Mechanical testing

GICs are well known for their advantages (F⁻ release, antimicrobial behaviour etc.); however a major drawback is their low mechanical properties²⁷. Therefore, Class I, II or III molar restorations are not performed with the use of C-GICs, as high forces are present²⁷. It is worth noticing here that usually experimental glass ionomer cements exhibit inferior mechanical properties compared to commercially available materials. One of the reasons is the mixing technique which for experimental glass ionomer cements is usually hand mixing compared to commercially available cements that are supplied in small capsules whereby the mixing can be completed mechanically with the use of a special mixing apparatus. Encapsulate restorative materials ensure precise metering of the two compounds enabling better mechanical properties for the cement. Mixing with the mixing apparatus decreases the development of air voids resulting in better mechanical properties¹⁴⁹.

Initially, all three GIC compositions were mixed with a P/L ratio of 3:1. In the case of Ca-GIC, however, the P/L ratio of 3:1 was not appropriate as the viscosity of the paste was too high for homogeneous mixing. Therefore, a lower P/L of 2:1 (Table 2-2) was used. For the CS measurements, in order to be able to compare all three GIC compositions together, strontium and barium substituted GICs with a P/L ratio of 2:1 had also to be prepared.

The CS is an important indication for mastication forces¹⁴⁷. This test method is able to compare brittle materials, which would generally exhibit low strength values, if exposed to tension forces¹⁴⁸. As it is not feasible to determine the tensile strength of brittle materials directly, the British Standards Institution adopted the DTS¹⁴⁶. In the DTS testing, the specimens are placed across the diameter (Figure 2-17) on the Instron plate and compressive forces are applied on the specimens¹⁴⁸. In contrast, in the CS testing, the specimens are placed vertically on the Instron plates and forces are applied along the axial axis¹⁴⁸. Generally, the tensile strength of brittle materials is significantly lower than their CS. Brittle materials, such as GICs, break down due to crack propagation. Crack propagation occurs mainly by tensile loading than compression loading²⁷. Usually, the occurrence of shear failure in the middle of the specimens occurs before tensile failure. Shear stresses are present just at the contact area between the specimens and the Instron plates¹⁴⁸. However, Prosser *et al.*¹⁰⁹ stated that the CS measurements have no fundamental meaning, since either a tensile or shear failure occurs, due to either atom separation or polymer chain slipping. Generally, the direct tensile measurements are more accurate than the CS measurements. However, measuring the direct tensile of brittle materials entails technical errors. Therefore, the direct measurement of DTS has to fulfil certain prerequisites, in order for the DTS measurements to be valid. These certain prerequisites include no plastic deformation before fracture, otherwise the DTS measurements are invalid and therefore not representative. Therefore, Prosser *et al.*¹⁰⁹ suggested that FS measurements are more convenient and reliable to evaluate the tensile strength of a brittle material such as cement. A dental material requires high FS in order to withstand the repeated chewing forces²²⁹. However, many studies reported for CS and DTS data^{6,27,149}, whereas FS data are rarely reported^{70,150,109}, due to the time consuming specimen preparation.

None of the GIC compositions showed a decrease in the mean strength values for all three test methods or the corresponding moduli after 1 month storage in water. This is in consistent with published literature^{6,158}. The results illustrate that the DTS and FS are distinctly lower than the CS values, which is in agreement with the literature^{27,147,149}.

The P/L ratio affects the strength of the resulting GICs. Increasing the glass powder content at a constant polymer level, an increase in strength should be expected²³⁰. Fleming *et al.*¹⁵⁹ investigated the influence of powder reduction with a constant liquid volume on the compressive performance of ChemFil®. The reduction in the amount of reinforced glass particles caused a decrease in the mean CS values. Generally, lowering the powder amount results in the reduction of resistance against compressive forces. This finding is consistent with the demonstrated results. The Ca-Sr-GIC and Ca-Ba-GIC with a P/L ratio of 2:1 (Figure 3-44) exhibited lower CS values in comparison to a P/L ratio of 3:1 (Figure 3-43).

Generally, reducing the PS of the glass powder component simplifies the polishability and results in a smoother restorative surface after polishing²³⁰. Smaller particles provide a bigger surface area, which results in a larger total surface of reactive glass that can be attacked from the acidic polymeric solution²³⁰. Gladys *et al.*⁶ investigated the PSD of commercial available hybrids, C-GICs and resin composites. They stated that the hybrids offer a high diversity in glass particle distribution, while the resin composites have a small PS and the C-GICs the largest PS. In the case of hybrids, the manufacturer added either larger glass particles to smaller glass particles or vice versa or an equal distribution of small and/or large glass particles was present. However, the PSD is a factor that influences the surface characteristics of the restorative material, such as wear and polishability²⁰⁹. Furthermore, the glass particles

do not enhance the physico-mechanical properties of C-GICs, but participate in the acid-base reaction⁶.

Xie *et al.*²⁷ stated that the CS of GICs results from the reinforced glass particles, which resist against the compression forces and not the crosslinked matrix. Xie *et al.*²⁷ suggested from the SEM microstructure that small glass particles might be responsible for high CS values. But further research is needed to confirm this hypothesis. Regarding the glass PS, Gladys *et al.*⁶ stated that the smaller the PS, the higher are the kinetics of the acid-base reaction, hence a larger surface area is provided.

One of the common characteristics of C-GICs is the brittleness of these materials. Mitra and Kedrowski¹⁴⁷ investigated the properties of 8 C-GICs, RM-GICs and metal reinforced GICs (MR-GICs) in a long-term *in vitro* study. They reported that high E-Modulus values in CS in combination with low DTS and FS would indicate the tendency of the material to brittle fracture. This conclusion shows similarities to the findings in this work. The E-modulus of a material is an indication of the stiffness of a material and is calculated from the stress-strain curve as illustrated in Chapter 2.2.9.4. The E-modulus is influenced by the degree of ionic crosslinking in the cement matrix. A rise in the E-modulus can be an indication for a rise in the degree of ionic crosslinking of the polymer chains¹⁰⁵. If a high DCL in the cement matrix occurs, the restorative material can become rigid or glassy. This would have the reverse effect on the strength of GIC¹⁴⁹. The E-modulus for Ca-Ba-GIC for CS and DTS with a P/L ratio of 3:1 from 1 week to 1 month increased, while the strength value decreased. The decrease in the strength value could be due to the high DCL of the polymer chains, which make the cement rigid.

Cattani-Lorent *et al.*¹⁴⁹ investigated the effect of water storage on long-term mechanical properties of several GICs and hybrids. CS, DTS and FS measurements

from 24 hours to 24 months were taken. The mechanical properties of the GICs did not continuously increase over 1 year ageing time. As previously mentioned, Cattani-Lorente *et al.*¹⁴⁹ believed that several factors such as P/L ratio²⁰⁰, Mw of PAA⁷³ and the concentration of PAA⁷⁴ and the chemical composition and the microstructure of the glass¹⁰⁹ contribute to the enhancement or decline of the mechanical properties in the resulting GICs over time.

An additional factor, which might cause a decrease in strength of GICs, is the long-term storage in deionized water. GICs absorb water; this water absorption from the cement can increase the fluidity of the material, resulting in a decrease in strength¹⁴⁹. Furthermore, hydrolysis with GIC compounds can result in degradation of the cement and a decrease in strength²³¹. The hydrolysis can take place by one of two mechanisms: it can replace the carboxylate anions (COO⁻) by hydroxide anion (OH⁻) ligands that disrupt the ion-linking of the metal ion or water (H₂O) ligands may displace carboxylate anions, reducing the strength of ionic binding¹⁵⁸. Tang and Xu¹⁵⁸ studied the short-term mechanical properties (CS) of GICs stored in silicone oil, distilled water and in air at different temperatures (37 ± 1°C and 20 ± 1°C). The highest CS values were obtained, with specimens kept in air, followed by specimens stored in silicone oil. The specimens in distilled water exhibited the lowest strength value, that increased gradually over 120 days.

Wang and Stamboulis¹⁶³ investigated the impact of substituting bigger cations in the glass structure, such as Sr²⁺ and Ba²⁺ for Ca²⁺. They proved with FTIR spectroscopy and MAS-NMR that the quantity of NBO increases with growth of the ionic radius. Barium with an ionic radius of 0.135 nm²³² exhibits a larger amount of NBOs (extended glass network) compared to strontium with an ionic radius of 0.118 nm²³² or calcium with an ionic radius of 0.1 nm²³². The hypothesis that larger cations disrupt more effectively the glass network resulting in the formation of more NBOs is

supported by the fact that larger cations lead to a decrease in oxygen density in the glass network (expanded glass network) and allow a higher amount of cation diffusion through the glass network¹⁶³. Therefore, it is expected that since the mechanical properties of the cements depend on the degree of ionic crosslinking that takes place from the very first stages of the setting reaction, a faster diffusion of bivalent and trivalent cations from the glass network into and through the cement matrix would favour a higher DCL and consequently an increase in mechanical properties from the very first stages of the setting reaction. This would result in the conclusion that the Ca-Ba-Glass, because of the expanded glass network hypothesis, would allow the greater diffusion of cations in the aqueous phase compared to Ca-Sr-Glass and Ca-Glass. The least affected would be the Ca-GIC, once attacked by the protons of the polymeric solution.

This hypothesis of higher degree of ionic crosslinking resulting in higher strength values is consistent with the obtained results. Ca-Ba-GIC with a P/L ratio of 3:1 exhibits higher strength values up to 1 day for CS and DTS and up to 1 week for FS, in comparison with Ca-Sr-GIC. However, Ca-Sr-GIC (P/L ratio 3:1) exhibits higher strength values at 1 month for all three mechanical tests compared to Ca-Ba-GIC (P/L ratio 3:1). Similarities in the progression of strength with the ageing time for Ca-Sr-GIC and Ca-Ba-GIC with a P/L ratio of 3:1 for all three mechanical tests can be observed. While strength values continued to increase for Ca-Sr-GIC during 1 month, a decrease in strength values was observed for Ca-Ba-GIC from 1 week to 1 month, whereas an increase was observed for 1 hour to 1 week for the same cement. The decrease in strength for Ca-Ba-GIC could be related to the higher DCL in the cement matrix. Cattani-Lorent *et al.*¹⁴⁹ stated that crosslinking of bivalent and trivalent carboxylates in the resulting cement in deionized water over a long period increases up to the point where the matrix becomes rigid. Gladys *et al.*⁶ investigated the

physico-mechanical properties of several C-GICs, composites and hybrids including the Young's modulus over 6 months. Gladys *et al.*⁶ stated that the increase of the E-modulus of C-GIC over 6 months is an indication that the acid-base reaction is still occurring.

Crisp *et al.*²¹ investigated different generations of ASPAs. They investigated the long-term hardness and CS of these raw materials. Regarding the CS, the materials developed half of the 1 day CS value within 1 hour, and a further increase of the strength values was observed up to one year. This was explained through the development of Al-polycarboxylate crosslinks in the resulting cement matrix, which enhances the mechanical properties. From the FTIR results in Chapter 3.1 the percentage ratio in the intensity against time was plotted through the 2D Figures. Percentage changes from 1 minute to 30 minutes or 60 minutes can be obtained, if the FTIR peak and its association is known. The Al-polycarboxylates (symmetric and asymmetric) peaks are located at ca. 1450 cm^{-1} and 1640 cm^{-1} . Transferring the above conclusion to the obtained results in this project, one noticed that the degree of Al-polycarboxylates (symmetric and asymmetric) crosslinking is 9%, 4% and 38.5% for Ca-GIC (P/L=2:1), Ca-Sr-GIC (P/L=3:1) and Ca-Ba-GIC (P/L=3:1) from 1 minute to 60 minutes, respectively. The percentage ratio of intensity plotted against time is significantly higher for Ca-Ba-GIC (P/L=3:1) in comparison to Ca-Sr-GIC (P/L=3:1) and Ca-GIC (P/L=2:1). This is an indication that the degree of crosslinked metal salts during 60 minutes for Ca-Ba-GIC is ca. five times higher than for Ca-GIC and ca. 10 times higher than for Ca-Sr-GIC. This conclusion could explain the initial high strength values for Ca-Ba-GIC and supports the fact that the hardening of the GIC depends on the degree of ionic crosslinks in the cement matrix²¹².

Pearson and Atkinson¹⁵⁰ examined the change of FS of 5 commercially available GICs with ageing time. An initial peak in FS values for all GICs was reached within

24 hours after mixing, which continued to slowly rise up to three months. The increase in the FS values is correlated with the development of Al-polycarboxylate in the GIC, which occurs within 24 hour after mixing. From the 3 measurements obtained in this project, the initial peak for FS measurements for all three GIC compositions was at 1 week for Ca-GIC and Ca-Ba-GIC.

Generally, it is to date not established if continued increase or decrease of strength over a long period of time is a feature of GICs, since major variation in strength is present^{149,158}. This conclusion is in consistent with the obtained results. Ca-Sr-GIC and Ca-Ba-GIC with a P/L ratio of 3:1 show similarities in progression for CS and DTS. However, the mechanical testing results for all three GIC compositions and all three test methods do not show a consistent change. Furthermore, an increase in strength for all test methods from 1 hour to 1 month was observed. Additionally, it can be concluded that a high number of NBOs in the glass component of the GIC have a short term effect on the mechanical strength. The expanded glass network allows a higher diffusion rate of ions into the aqueous phase, upon acid attack, resulting in a higher DCL earlier on during setting. For all three test methods at a P/L ratio of 3:1 for Ca-Sr-GIC and Ca-Ba-GIC higher strength values were observed at 1 hour. However, Ca-Sr-GIC overtook Ca-Ba-GIC over a duration of 1 month. It can be concluded that the high degree of NBO in the glass compound has a short term effect on the resulting mechanical strength. It can be assumed that the initially higher mechanical strength initially will decrease in the long-term, due to the high degree of ionic crosslinking, which might have a reverse effect on the mechanical properties (increased brittleness).

5 Conclusions

The chief aim of this project was to investigate if the substitution of bigger cations for smaller cations has an effect on the setting reaction and the resulting mechanical properties of the experimental GICs. Furthermore, the focus of the observation was to investigate if the substitution may overcome the inferior mechanical properties of the GICs and extend their clinical applications. The obtained results demonstrated that substituting bigger cations for proportionally smaller cations has an effect (up to 1 hour) on the resulting strength (DTS, CS and FS). However, the increase in strength endures only up to 1 hour.

The properties of the substituted glasses were compared as follows:

- real time fourier transform infrared (FTIR) was used to follow the progress of the setting reactions of the cements.
- Setting time, fluoride release and the antibacterial behaviour of the three experimental GICs were evaluated.
- Nano-indentation, Vickers hardness (HV) and wear rate (or wear resistance) were calculated.
- Compressive strength (CS), diametral tensile strength (DTS), flexural strength (FS) and modulus of elasticity were also measured.

5.1 FTIR

The FTIR spectroscopies demonstrated that the obtained results are consistent with the hypothesis that larger cations disrupt effectively the glass network and facilitate a higher amount of cation diffusion from the glass structure into the aqueous phase. The released ions complex with the carboxylate anions of the PAA to form metal salts. The glass with the highest amount of NBOs, which is Ca-Ba-GIC, has the

highest metal salt development, followed by Ca-Sr-GIC and Ca-GIC over 60 minutes. The real time FTIR measurements showed clearly the formation of polysalt matrix during a setting time of 60 minutes. This can be mainly observed by the metal salt formation indicated by significant intensity changes in the range of 1350 cm^{-1} to 1750 cm^{-1} and formation of metal carboxylates observed with the appearance of a strong peak around 1550 cm^{-1} (Table 3-3). Furthermore, from the FTIR results in this project the ratio of the change in intensity against time for metal salt crosslinking formation (symmetric and asymmetric of $\frac{1}{2}\text{Ca}^{2+}\text{-COO}^-$ and $\frac{1}{3}\text{Al}^{3+}\text{-COO}^-$) of each experimental GIC from 1 minute to 60 minutes was obtained. Ca-Ba-GIC exhibits the highest degree of metal salt development from 1 minute to 60 minutes with 35% followed by Ca-Sr-GIC and Ca-GIC with 24% and 14%, respectively.

5.2 Fluoride release of GICs in deionized water and AS

The fluoride release and recharge ability of all the experimental GICs in deionized water and AS showed similar characteristics. A maximum of F^- ion release in the first hours, due to an initial burst, was observed, followed by a plateau, due to bulk diffusion. Generally, less F^- ion release in AS was observed due to the similar ion distribution. On the other hand, high F^- ion release in deionized water was observed due to unequal ion distribution. Finally, the uptake of F^- ions from a commercially available mouth wash, showed that increasing the time during which the GIC is exposed to a F^- source would consequently increase the F^- release.

5.3 Antimicrobial effectiveness of glass ionomer cements

All the experimental GICs exhibited antibacterial behaviour over 48 hours duration, most likely because they all released an effective amount of fluorine that contributed towards the GICs' antibacterial behaviour. There was no evidence that strontium or barium contributed to the antibacterial effect of GICs, as the three cements, , did not show any significant difference in their antibacterial behaviour compared to the

control without cement. The obtained results in this work suggested that an amount of 0.6 – 1.5 ppm of F⁻ ions in ionised water and 0.2 – 0.9 ppm of F⁻ ions in AS prevent the growth of *S. mutans*.

5.4 Calculation of cement setting time

The setting time was calculated using a resistance to penetration test method. It was expected that the shortest setting time should be measured for the cements with the glass component that exhibits higher NBOs. But this was not the case as Ca-Sr-GIC exhibited a shorter setting time compared to Ca-Ba-GIC and Ca-GIC. Furthermore, it was observed that at a lower amount of powder content and at a constant liquid volume an increase in the setting time was observed for all cements.

5.5 Vickers hardness

The Vickers hardness values of the three experimental GICs increased from 1 hour to 1 month. This was explained with the formation of an infinite metal salt carboxylate network.

5.6 Nano-indentation

The nano-indentation hardness, depending on the ageing time, slightly decreased from 1 hour to 1 month for all three GIC compositions. The use of nano-indentation was proved to be problematic as all the glass ionomer cements consisted of two phases - the organic and the inorganic. The inorganic phase consisted of remaining glass particles that could be larger than the indenter itself. This results in inaccuracies in the measurements as the glass particles should be stiffer than the glass ionomer cement.

5.7 Wear behaviour of GICs

The wear behaviour of the experimental GICs was observed via a reciprocating wear test. Ca-Ba-GIC exhibited the highest wear resistance compared to the rest of the

GIC samples measured, as the DCL in this cement was higher from the early stages of setting.

5.8 Mechanical properties of GICs

The compressive, diametral tensile and flexural strength of Ca-Ba-GIC gave the highest measurements at 1 hour after setting, followed by Ca-Sr-GIC and Ca-GIC. Furthermore, from the FTIR results in this project the ratio of the change in intensity against time for metal salt crosslinking formation (symmetric and asymmetric of $\frac{1}{2}\text{Ca}^{2+}\text{-COO}^-$ and $\frac{1}{3}\text{Al}^{3+}\text{-COO}^-$) of each experimental GIC from 1 minute to 60 minutes was obtained. Ca-Ba-GIC exhibits the highest degree of metal salt development from 1 minute to 60 minutes with 35% followed by Ca-Sr-GIC and Ca-GIC with 24% and 14%, respectively. This observation is consistent with the hypothesis. The high amount of metal salt development would have consequently an effect on the resulting mechanical properties of the experimental cements. Therefore, following the metal salt development from the obtained FTIR results, the mechanical strength can be predicted for the experimental GIC over 60 minutes. And the prediction is in keeping with the obtained mechanical strength of the experimental GICs over 1 hour.

However, over a duration of 1 month Ca-Sr-GIC had higher mechanical properties than Ca-Ba-GIC whereas Ca-GIC exhibited always lower mechanical properties. The above was explained considering that at early setting time the barium substituted glass network exhibiting a higher number of NBOs and being expanded, it would release easier barium, calcium and aluminium cations resulting in the formation of a higher DCL in the polysalt matrix and therefore initially better mechanical properties. Therefore Ca-Ba-GIC performed better after 1 hour of setting compared to Ca-Sr-GIC and Ca-GIC.

On the other hand, at later setting times Ca-Ba-GIC did not continue to show better mechanical properties. Although the modulus of elasticity continued to increase, a decrease in compressive, diametral tensile and flexural strength was observed.

6 Future work

In this project the cation substitution in the glass component was investigated and the effect on the properties of the resulting glass ionomer cements. The ideal restorative material, which mimics the tooth material as closely as possible, still does not exist on the market. The current project can be used as a basis for the development of a commercially novel GIC system.

The following points for future work can be suggested:

- Pre treating the glass composition, either with acid-wash or heat, to achieve a controlled ion release upon acid attack.
- FTIR studies should be carried out over a long-term period.
- Trying to find a correlation between the metal salt development and the obtained strength values.
- The reciprocating wear test should be conducted over a long-term period.
- Long-term mechanical testing (1 year) should be conducted to observe the development of the experimental GICs.
- In this project the acidic polymer solution component was excluded from consideration. In the future, a higher concentration/Mw of PAA (or copolymers of acrylic acid and maleic acid) can be used, and/or TA can be added.

Although the research with GICs has been ongoing since 1972, several procedures are still not entirely understood. For example, the precise amount of fluoride ions which are needed to have a cariostatic effect, or whether the inorganic matrix in the cement matrix contributes to the strength value. Working with GICs, entails a consideration of various factors; therefore, the direction of development for any future project has to be clearly established at its inception. If, for example, a future project

focuses upon the antimicrobial effect of the GICs, the following points can be suggested:

- To prepare fluoride free glass,
- to prepare fluoride free glass with addition of strontium and
- to prepare a combined fluoride/strontium glass.

All these glasses have to be prepared and mixed with the polymeric solution to form GIC. Antimicrobial tests have to be conducted to see if there is evidence that there is a synergistic effect between the strontium and fluoride ions.

7 References

-
- ¹ K. J. Anusavice, R. W. Phillips, C. Shen, H. R. Rawls. 2013. Philip's science of dental materials. Elsevier Saunders, Missouri. pp7.
- ² J. L. Ferracane. 2001. Materials in Dentistry: Principles and Applications, 2nd Edition. Lippincott Williams & Wilkins, Maryland. pp2.
- ³ W. K. Roentgen. 1896. Ueber eine neue Art von Strahlen. Sitzungsberichte der Physikalisch-Medizinischen Gesellschaft, Wuerzburg. p11-19.
- ⁴ B. Reitemeier, N. Schwenzer, M. Ehrenfeld. 2006. Zahn-Mund-Kiefer-Heilkunde. Lehrbuchreihe zur Aus- und Weiterbildung: Einführung in die Zahnmedizin. Georg Thieme Verlag, Stuttgart. pp2.
- ⁵ A. D. Wilson, B. E. Kent. 1971. The glass-ionomer cement, a new translucent dental filling material. Journal of Applied Chemistry and Biotechnology, 21;11:13.
- ⁶ S. Gladys, B. Vanmeerbeek, M. Braem, P. Lambrechts, G. Vanherle. 1997. Comparative physico-mechanical characterization of new hybrid restorative materials with conventional glass-ionomer and resin composite restorative materials. Journal of Dental research, 76;4:883-894.
- ⁷ G. Schmalz, D. Arenholt-Bindslev. 2009. Biocompatibility of dental Materials. Springer, Berlin-Heidelberg. p149-159.
- ⁸ T. P. Croll, J. W. Nicholson. 2008. Glass-Ionomer Cements: History and Current Status. Inside Dentistry, 4;3:7-14.
- ⁹ A. D. Wilson, J. W. Mclean. 1988. Setting reaction and its clinical consequences. Glass-ionomer cement. Quintessence, Chicago. p43-55.
- ¹⁰ N. Garg, A. Garg. 2013. Textbook of Operative Dentistry, 2nd Edition. Jaypee Brothers Medical Publishers (P) Ltd., New Dehli. pp428.
- ¹¹ H. F. Albers. 2002. Tooth-colored restoratives: principles and techniques. 9th Edition. BC Beckers Inc., Ontario. pp44.
- ¹² C. H. Pierce. 1870. Discussion, Pennsylvania Association of Dental Surgery. 21:696-697.

-
- ¹³ W. V. B. Ames. 1892. A new oxyphosphate for crown setting. *Dental Cosmos*, 34:392-394.
- ¹⁴ D. J. Fleck. 1902. The chemistry of oxyphosphates. *Dent Items Interest*, 24:906.
- ¹⁵ P. Steenbock. 1954. Improvements in and relating to the manufacture of a material designed for the production of cement. UK Patents Nos. 15176, 15181.
- ¹⁶ F. Schoenbeck. 1908. Process for the production of tooth material. US Patent No. 897160.
- ¹⁷ A. W. G. Walls. 1986. Glass polyalkenoate (glass-ionomer) cements: a review. *Journal of Dentistry*, 14:231-246.
- ¹⁸ A. D. Wilson, B. E. Kent. 1972. A New translucent Cement for Dentistry: the Glass-ionomer Cement. *British Dental Journal*, 132;4:133-135.
- ¹⁹ P. U. Nagaraja, G. Kishore. 2005. Glass-ionomer Cement-The Different Generations. *Trends in Biomaterials and Artificial Organs*, 18;2:158-165.
- ²⁰ B. M. Culbertson. 2001. Glass-ionomer dental restoratives. *Progress in Polymer Science*, 26:577-604.
- ²¹ S. Crisp, B. G. Lewis, A. D Wilson. 1976. Characterization of glass-ionomer cements 1. Long term hardness and compressive strength. *Journal of Dentistry*, 4;4:162-166.
- ²² A. D. Wilson, S. Crisp, A. J. Ferner. 1976. Reactions in glass ionomer cements, IV Effect of chelating comonomers on setting behaviour. *Journal of Dental Research*, 55:489-495.
- ²³ J. W. McLean, A. D. Wilson. 1977. The clinical development of glass ionomer cements: I Formulations and properties. *Australian Dental Journal*, 22:33-36.
- ²⁴ G. J. Mount. 2002. *An atlas of glass-ionomer cements: a clinician's guide*. 3rd Edition. Thieme, New York. p1-6.
- ²⁵ J. W. McLean, A. D. Wilson, M. J. Prosser. 1984. Development and use of water-hardening glass ionomer luting cements. *Journal of Prosthetic Dentistry*, 52:175-181.
- ²⁶ M. A. Naasan, T. F. Watson. 1998. Conventional glass-ionomers as posterior restorations: A status report for the American Journal of Dentistry. *American Journal of Dentistry*, 11:36-45.
- ²⁷ D. Xie, W. A. Brantley, B. M. Culbertson, G. Wang. 2000. Mechanical properties and microstructures of glass-ionomer cements. *Dental Materials*, 16:129-138.

-
- ²⁸ M. Pelka, J. Ebert, H. Schneider, N. Krämer, A. Petschelt. 1996. Comparison of two- and three-body wear of glass-ionomers and composites. *European Journal of Oral Sciences*, 104:132-137.
- ²⁹ M. Massler, D. S. Berman, V. E. James. 1957. Pulp capping and pulp amputation. *Dental Clinics of North America*, 797.
- ³⁰ D. B. Mahler, G. K. Armen. 1962. Addition of amalgam alloy to zinc phosphate cement. *The Journal of Prosthetic Dentistry*, 12:157-164.
- ³¹ J. W. McLean, O. Gasser. 1985. Glass-cermet cements. *Quintessence International*. 16;5:333-343.
- ³² I. A. Al-Badry, F. M. Kamel. 1994. Clinical use of glass-ionomer cement: a literature review. *The Saudi Dental Journal*, 6;2:107-116.
- ³³ J. M. Antonucci, J. E. McKinney, J. W. Stansbury. 1988. Resin- modified glass-ionomer cement. *US Patent Application*, 160:856.
- ³⁴ R. Van Noort. 2007. *Introduction to dental materials 3rd edition*. Mosby Elsevier, London. p124-140.
- ³⁵ S. B. Mitra. 1989. Photocurable ionomer cement systems. *European Patent Application No. 0 323 120 A2*.
- ³⁶ S. B. Mitra. 1991. Adhesion to Dentin and Physical Properties of a Light-cured Glass-ionomer Liner/Base. *Journal of Dental Research*, 70;1:72-74.
- ³⁷ R. J. Smales, H. Yip. 2000. The atraumatic restorative treatment (ART) approach for primary teeth: review of literature. *American Academy of Pediatric Dentistry*, 22;4:294-298.
- ³⁸ T. S. Carvalho, T. R. Ribeiro, M. Boenecker, E.C. Pinheiro, V. Colares. 2009. The Atraumatic Restorative Treatment approach: an "atraumatic" alternative. *Medicina Oral, Patología Oral y Cirugía Bucal*, 14:668-673.
- ³⁹ A. U. Yap, Y. S. Pek, P. Cheang. 2003. Physico-mechanical properties of a fast-set highly viscous GIC restorative. *Journal of Oral Rehabilitation*, 30:1-8.

-
- ⁴⁰ 3M ESPE. Ketac™ Molar Easymix Glass-ionomer Filling Material.
<http://multimedia.mmm.com/mws/mediawebserver.dyn?6666660Zjcf6IVs6EVs66S3IzCOrrrr>
Q-. 30.09.2010.
- ⁴¹ K. M. Y. Hse, S. K. Leung, S. H. Y. Wei. 1999. Resin-ionomer restorative materials for children: A review. *Australian Dental Journal*, 44;1:1-11.
- ⁴² USAF Dental Evaluation & Consultation Service.
http://airforcemedicine.afms.mil/idc/groups/public/documents/afms/ctb_109841.pdf .
01.10.2010.
- ⁴³ A. Stamboulis, R. V. Law, R. G. Hill. 2004. Characterisation of commercial ionomer glasses using magic angle nuclear magnetic resonance (MAS-NMR). *Biomaterials*, 25:3907-3913.
- ⁴⁴ R. G. Hill, A. Stamboulis, R. V. Law, 2006. Characterisation of fluorine containing glasses by ¹⁹F, ²⁷Al, ²⁹Si and ³¹P MAS-NMR spectroscopy. *Journal of Dentistry*, 34:525-532.
- ⁴⁵ A. Santini, V. Miletic. 2008. Comparison of the hybrid layer formed by Silorane adhesive, one-step self-etch and etch and rinse systems using confocal micro-Raman spectroscopy and SEM. *Journal of Dentistry*, 36:683-691.
- ⁴⁶ A. M. Young, A. Sherpa, G. Pearson, B. Schottlander, D. N. Waters. 2000. Use of Raman spectroscopy in the characterisation of the acid-base reaction in glass-ionomer cements. *Biomaterials*, 21:1971-9.
- ⁴⁷ J. W. Nicholson, P. J. Brookman, O. M. Lacy, A. D. Wilson. 1988. Fourier transform infrared spectroscopic study of the role of tartaric acid in glass-ionomer dental cements. *Journal of Dental research*, 67;12:1451-1454.
- ⁴⁸ A. M. Young. 2002. FTIR investigation of polymerisation and polyacid neutralisation kinetics in resin-modified glass-ionomer dental cements. *Biomaterials*, 23:3289-3295.
- ⁴⁹ H. K. Yip, W. M. To. 2005. An FTIR study of the effects of artificial saliva on the physical characteristics of the glass ionomer cements used for art. *Dental Materials*, 21:695-703.
- ⁵⁰ E. A. Wasson, J. W. Nicholson. 1993. Change in pH during setting of polyelectrolyte dental materials. *Journal of Dental Research*, 21;2:122-126.

-
- ⁵¹ P. V. Hatton, I. M. Brook. 1992. Characterisation of the ultrastructure of glass-ionomer (poly-alkenoate) cement. *British Dental Journal*, 173:275-277.
- ⁵² S. Crisp, A. D. Wilson. 1974. Reactions in glass ionomer cements. I Decomposition of the powder. *Journal of Dental Research*, 53:1408-1413.
- ⁵³ S. Crisp, A. D. Wilson 1974. Reactions in glass ionomer cements. III The precipitation reaction. *Journal of Dental Research*, 53:1420-1424.
- ⁵⁴ S. Crisp, A. D. Wilson. 1976. Reactions in glass ionomer cements. V Effect of incorporating tartaric acid in the cement liquid. *Journal of Dental Research*, 55:1023-1031.
- ⁵⁵ S. G. Griffin, R. G. Hill. 1999. Influence of glass composition on the properties of glass polyalkenoate cements. Part I: Influence of aluminium to silicon ratio. *Biomaterials*, 20:1579-1586.
- ⁵⁶ T. I. Barry, D. J. Clinton, A. D. Wilson. 1979. The structure of a glass-ionomer cement and its relationship to the setting process. *Journal of Dental Research*, 58:1072-1079.
- ⁵⁷ J. W. Nicholson. 1998. Chemistry of glass-ionomer cements: a review. *Biomaterials*, 19:485-494.
- ⁵⁸ R. A. Pires, T. G. Nunes, I. Abrahams, G. E. Hawkes. 2008. The role of aluminium and silicon in the setting chemistry of glass ionomer cements. *Journal of Materials Science: Materials in Medicine*, 19:1687-1692.
- ⁵⁹ E. A. Wasson, J. W. Nicholson. 1991. Studies on the setting chemistry of glass-ionomer cements. *Clinical Materials*, 7;4:289-293.
- ⁶⁰ E. A. Wasson, J. W. Nicholson. 1993. New Aspects of the setting chemistry of glass-ionomer cements. *Journal of Dental Research*, 72: 481-483.
- ⁶¹ A. Sullivan, R. G. Hill. 2000. Influence of poly(acrylic acid) molar mass on the fracture properties of glass polyalkenoate cements based on waste gasifier slags. *Journal of Materials Science*, 35:1125-1134.
- ⁶² S. G. Griffin, R. G. Hill. 1998. Influence of poly(acrylic acid) molar mass on the fracture properties of glass polyalkenoate cements. *Journal of Materials Science*, 33:5383-5396.

-
- ⁶³ S. G. Griffin, R. G. Hill. 2000. Influence of glass composition on the properties of glass polyalkenoate cements. Part IV: Influence of fluorine content. *Biomaterials*, 21:693-698.
- ⁶⁴ R. Nomoto, J. F. McCabe. 2001. Effect of mixing methods on the compressive strength of glass ionomer cements. *Journal of Dentistry*, 29:205-210.
- ⁶⁵ W. D. Cook. 1983. Dental polyelectrolyte cements. II Effect of powder/liquid ratio on their rheology. *Biomaterials*, 4:21-24.
- ⁶⁶ S. Crisp, B. G. Lewis, A. D. Wilson. 1976. Characterisation of glass ionomer cements 2: effect of the powder:liquid ratio on the physical properties. *Journal of Dentistry*, 4:287-290.
- ⁶⁷ E. A. P. De Maeyer, R. M. H. Verbeek, C. W. J. Vercruysse. 1998. Reactivity of Fluoride-containing Calcium Aluminosilicate Glasses Used in Dental Glass-ionomer Cements. *Journal of Dental Research*, 77;12:2005-2011.
- ⁶⁸ J. F. Stebbins, Z. Xu. 1997. NMR evidence for excess non-bridging oxygen in an aluminosilicate glass. *Nature*, 390:60-62.
- ⁶⁹ D. Wood, R. G. Hill. 1990. Glass ceramic approach to controlling the properties of a glass-ionomer bone cement. *Biomaterials*, 12:164-170.
- ⁷⁰ G. J. Pearson, A. S. Atkinson. 1987. Effects of temperature change on the working and setting characteristics of water-based dental cements. *Dental Materials*, 3:275-279.
- ⁷¹ M. Behr, M. Rosentritt, H. Loher, C. Kolbeck, C. Trempler, B. Stemplinger, V. Kopzon, G. Handel. 2008. Changes of cement properties caused by mixing errors: The therapeutic range of different cement types. *Dental Materials*, 24;9: 1187-1193.
- ⁷² A. D. Wilson, R. G. Hill, C. P. Warrens, B. G. Lewis. 1989. The influence of polyacid molecular weight on some properties of glass-ionomer cements. *Journal of Dental Research*, 68:89-94.
- ⁷³ A. D. Wilson, S. Crisp, G. Abel. 1977. Characterization of glass-ionomer cements: 4: Effect of molecular weight on physical properties. *Journal of Dental Research*, 5:117-120.
- ⁷⁴ S. Crisp, B. G. Lewis, A. D. Wilson. 1977. Characterization of glass-ionomer cements: 3: Effect of polyacid concentration on the physical properties. *Journal of Dental Research*, 5:51-56.

-
- ⁷⁵ ISO 9917-1:2007 Dentistry - water-based cements - part 1: powder/liquid acid- base cements. International Organization for Standardization 2009.
- ⁷⁶ A. Cifford, A. Rafferty, R. Hill, P. Mooney, D. Wood, B. Samuneva, S. Matsuya. 2001. The influence of calcium to phosphate ratio on the nucleation and crystallization of apatite glass-ceramics. *Journal of Materials Science: Materials in Medicine*, 12:461-469.
- ⁷⁷ ASTM C162 - 05(2010) C162-05(2010). Standard Terminology of Glass and Glass Products.
- ⁷⁸ W. H. Zachariasen. 1932. The atomic arrangements in glass. *Journal of the American Chemical Society*, 54:3841-3851.
- ⁷⁹ W. Lowenstein. 1954. The distribution of aluminium in the tetrahedra of silicates and aluminates. *American Mineralogist*, 39:92-96.
- ⁸⁰ A. D. Wilson, S. Crisp, H. J. Prosser, B. G. Lewis, S. A. Merson. 1980. Aluminosilicate Glasses for Polyelectrolyte Cements. *Industrial & Engineering Chemistry Product Research and Development*, 19:263-270.
- ⁸¹ S. Likitvanichkal, W. C. Lacourse. 1995. The effect of fluorine content on the crystallisation of canasite, glass-ceramics. *Journal of Materials Science*, 3;30:6151-6155.
- ⁸² R. G. Hill, D. Wood. 1995. Apatite-mullite glass-ceramics. *The Journal of Materials Science: Materials in Medicine*, 5;6:311-318.
- ⁸³ F. T. Wall, S. W. Drenan. 1951. Gelation of polyacrylic acid by divalent cations. *Journal of Polymer Science*, 1;7:83-90.
- ⁸⁴ D. Smith. 1994. Development of glass-ionomer cement systems. In *Glass-ionomers: The Next Generation. 2nd International Symposium on Glass-ionomers*. Hunt. P.R. Ed.: International Symposia in Dentistry: Philadelphia, USA.
- ⁸⁵ H. Hosoda. 1993. The composition and setting reaction of glass ionomer cement. In: Katsuyama S, Ishikawa T, Fujii B. *Glass ionomer dental cement*. Ishiyaku EuroAmerican Inc.. p16-24.
- ⁸⁶ A. D. Wilson, B. E. Kent. 1970. Dental cements: Dental silicate cements IX. Decomposition of the powder. *Journal of Dental Research*, 49:7-13.

-
- ⁸⁷ D. Wood, R. G. Hill. 1991. Structure-Property Relationships in Ionomer Glasses. *Clinical Materials*, 7:301-312.
- ⁸⁸ K. Greene, M. J. Pomeroy, S. Hampshire, R. G. Hill. 2003. Effect of composition on the properties of glasses in the K_2O -BaO-MgO-SiO₂-Al₂O₃-B₂O₃-MgF₂ system. *Journal of Non-Crystalline Solids*, 325:193-205.
- ⁸⁹ B. E. Kent, B. G. Lewis, A. D. Wilson. 1979. Glass-ionomer cement formulations: I. The preparation of novel fluoroaluminosilicate glasses high in fluorine. *Journal of Dental Research*, 58:1607-1619.
- ⁹⁰ M. Darling, R. G. Hill. 1994. Novel polyalkenoate (glass-ionomer) dental cements based on zinc silicate glasses. *Biomaterials*, 15:299-306.
- ⁹¹ A. D. Neve, V. Piddock, E. C. Combe. 1992. Development of Novel Dental Cements. I. Formulation of Aluminoborate Glasses. *Clinical Materials*, 9:7-12.
- ⁹² A. D. Neve, V. Piddock, E. C. Combe. 1992. Development of Novel Dental Cements. II. Cement properties. *Clinical Materials*, 9:13-20.
- ⁹³ H. J. Prosser, D. R. Powis, P. Brant, A. D. Wilson. 1984. Characterisation of glass ionomer cements 7. The physical properties of current materials. *Journal of Dental Research*, 12:231-240.
- ⁹⁴ S. M. Abo-Naf, F. H. El Batal, M. A. Azooz. 2003. Characterisation of some glasses in the system SiO₂ Na₂O·RO by infrared spectroscopy. *Materials Chemistry and Physics*, 77:846-852.
- ⁹⁵ Y. Masayoshi. 1998. Role of zinc in bone formation and bone resorption. *The journal of Trace Elements in Experimental Medicine*, 11:119-135.
- ⁹⁶ Y-H. Cho, S-J. Lee, J. Y. Lee, S. W. Kim, C. B. Lee, W. Y. Lee, M. S. Yoon. 2002. Antibacterial effect of intraprostatic zinc injection in a rat model of chronic bacterial prostatitis. *International Journal of Antimicrobial Agents*, 19:576-582.
- ⁹⁷ S.G. Griffin, R.G. Hill. 2000. Influence of glass composition on the properties of glass polyalkenoate cements. Part II: influence of phosphate content. *Biomaterials*, 21:399-403.
- ⁹⁸ N. H. Ray. 1978. *Inorganic polymers*. Academic Press, Inc. London. pp16.

-
- ⁹⁹ A. D. Wilson, J. W. McClean. 1988. Glass-ionomer cement. Quintessence Publishing Co. Inc., Chicago. pp18.
- ¹⁰⁰ E. De Barra, R.G. Hill. 2000. Influence of glass composition on the properties of glass polyalkenoate cements. Part III: influence of fluorite content. *Biomaterials*, 21:563-569.
- ¹⁰¹ R. G. Hill, A. D. Wilson. 1988. Some structural aspects of glasses used in ionomer cements. *Glass Technology: European Journal of Glass Science and Technology*, 29:150-157.
- ¹⁰² M. Maltz, C. G. Emilson. 1982. Susceptibility of oral bacteria to various fluoride salts. *Journal of Dental Research*, 61:786-790.
- ¹⁰³ E. Griffin, K. J. Donly, R. Erickson. 1992. Caries inhibition by fluoride releasing liners. *American Journal of Dentistry*, 5:293-295.
- ¹⁰⁴ B. E. Kent, B. G. Lewis, A. D. Wilson. 1979. Glass Ionomer Cement Formulations: I. The Preparation of Novel Fluoroaluminosilicate Glasses High in Fluorine. *Journal of Dental Research*, 58:1607-1619.
- ¹⁰⁵ E. De Barra, R. G. Hill. 1998. Influence of alkali metal ions on the fracture properties of glass polyalkenoate (ionomer) cements. *Biomaterials*, 19:495-502.
- ¹⁰⁶ D. A. G. Brune. 1982. Heat treatment of glass ionomer, silicate, zinc phosphate and zinc polycarboxylate cements. *European Journal of Oral Sciences*, 90;5:409-412.
- ¹⁰⁷ D. Neve, V. Piddock, E. C. Combe. 1993. The Effect of Glass Heat Treatment on the Properties of a Novel Polyalkenoate Cement. *Clinical Materials*, 12:113-115.
- ¹⁰⁸ C. M. Crowley, J. Doyle, M. R. Towler, N. Rushe, S. Hampshire. 2007. Influence of acid washing on the surface morphology of ionomer glasses and handling properties of glass ionomer cements. *The Journal of Materials Science: Materials in Medicine*, 18:1497-1506.
- ¹⁰⁹ H. J. Prosser, D. R. Powis, A. D, Wilson. 1986. Glass-ionomer Cements of Improved Flexural Strength. *Journal of Dental Research*, 65;2:146-148.
- ¹¹⁰ H. L. Prentice, M. J. Tyas, M. F. Burrow. 2005. The effect of particle size distribution on an experimental glass-ionomer cement. *Dental Materials*, 21:505-510.

-
- ¹¹¹ M. Rothwell, H. M. Anstice, G. J. Pearson. 1998. The uptake and release of fluoride by ion-leaching cements after exposure to toothpaste. *Journal of Dentistry*, 26:591-597.
- ¹¹² J. J. M. Damen, M. J. Buijs, J. M. Ten Cate. 1996. Uptake and release of fluoride by saliva-coated glass ionomer cement. *Caries Research*, 30;6:454-457.
- ¹¹³ P. Karantakis, M. Helvatjoglou-Antoniades, S. Theodoridou-Pahini, Y. Papadogiannis. 2000. Fluoride release from three glass ionomers, a compomer, and a composite resin in water, artificial saliva, and lactic acid. *Operative Dentistry*, 25;1:20-25.
- ¹¹⁴ L. A. Marks, R. M. Verbeeck, E. A. De Maeyer, L. C. Martens. 2000. Effect of a neutral citrate solution on the fluoride release of resin-modified glass ionomer and polyacid-modified composite resin cements. *Biomaterials*, 21;19:2011-2016.
- ¹¹⁵ A. Wiegand, W. Buchalla, T. Attin. 2007. Review on fluoride-releasing restorative materials-Fluoride release and uptake characteristics, antibacterial activity and influence on caries formation. *Dental Materials*, 23:343-362.
- ¹¹⁶ R. M. Verbeeck, E. A. De Maeyer, L. A. Marks, R. J. De Moor, A. M. De Witte, L. M. Trimpeneers. 1998. Fluoride release process of (resin-modified) glass-ionomer cements versus (polyacid-modified) composite resins. *Biomaterials*, 19;6:509-519.
- ¹¹⁷ A. Guida, R. G. Hill, M. R. Towler, S. Eramo. 2002. Fluoride release from model glass ionomer cements. *The Journal of Materials Science: Materials in Medicine*, 13:645-649.
- ¹¹⁸ J. A. Williams, R. W. Billington, G. J. Pearson. 2001. A long study of fluoride release from metal-containing conventional and resin-modified glass-ionomer cements. *Journal of Oral Rehabilitation*, 28:41-47.
- ¹¹⁹ S. L. Creanor, L. M. Carruthers, W. P. Saunders, R. Strang, R. H. Foye. 1994. Fluoride uptake and release characteristics of glass ionomer cements. *Caries Research*, 28:322-328.
- ¹²⁰ A. Moshaverinia, S. Ansari, N. Roohpour, M. Reshad. S. R. Schricker, W. L. Chee. 2011. Effects of N-vinylcaprolactam containing polyelectrolytes on hardness, fluoride release and water sorption of conventional glass ionomers. *The Journal of Prosthetic Dentistry*, 105;5:323-331.

-
- ¹²¹ H. Fross, L. Seppa. 1990. Prevention of enamel demineralization adjacent to glass ionomer filling materials. *Scandinavian Journal of Dental Research*, 98;2:173-178.
- ¹²² J. M. Ten Cate, J. D. M. Featherstone. 1996. Physicochemical aspects of fluoride-enamel interactions. In: O. Fejerskov, J. Ekstrand, B. A. Burt. Chapter 14, Fluoride in dentistry. Blackwell Munksgaard, Copenhagen. 252-272.
- ¹²³ M. Svanberg, B. Krasse, H. O. Ornerfeldt. 1990. Mutans streptococci in interproximal plaque from amalgam and glass ionomer restorations. *Caries Research*, 24;2:133-136.
- ¹²⁴ S. Crisp, B. G. Lewis, A. D. Wilson. 1980. Characterization of glass ionomer cement. 6. A study of erosion and water absorption in both neutral and acidic media. *Journal of Dental Research*, 8:68-74.
- ¹²⁵ J. A. Williams, E. Briggs, R. W. Billington, G. J. Pearson. 2003. The effects of adding fluoride compounds to a fluoride-free glass ionomer cement on subsequent fluoride and sodium release. *Biomaterials*, 24:1301-1308.
- ¹²⁶ A. Bell, S. L. Creanor, R. H. Foye, W. P. Saunders. 1999. The effect of saliva on fluoride release by a glass-ionomer filling material. *Journal of Oral Rehabilitation*, 26:407-412.
- ¹²⁷ A. J. Preston, S. M. Higham, E. A. Agalamanyi, L. H. Mair. 1999. Fluoride recharge of aesthetic dental materials. *Journal of Oral Rehabilitation*, 26:936-940.
- ¹²⁸ A. M. Diaz-Arnold, D. C. Holmes, D. W. Wistrom, E. J. Swift. 1995. Short-term fluoride release/uptake of glass ionomer restoratives. *Dental Materials*, 11:96-101.
- ¹²⁹ C. L. Dhondt, E. A. P. De Maeyer, R. M. H. Verbeeck. 2001. Fluoride release from Glass Ionomer activated with Fluoride Solutions. *Journal of Dental Research*, 80;5:1402-1406.
- ¹³⁰ H. Koo. 2008. Strategies to enhance the biological effects of fluoride on dental biofilms. *Advances in dental Research*, 1;20:17-21.
- ¹³¹ R. E. Marquis. 1995. Antimicrobial actions of fluoride for oral bacteria. *Canadian Journal of Microbiology*, 41;11:955-964.
- ¹³² J. M. ten Cate, C. van Loveren. 1999. Fluoride mechanisms. *Dental Clinics of North America*, 43;4:713-742.

-
- ¹³³ M. R. Nouri, K. C. Titley. 2003. Paediatrics: A Review of the Antibacterial Effect of Fluoride. Oralhealthgroup, 1-7.
- ¹³⁴ R. E. Marquis, S. A. Clock, M. Mota-Meira. 2003. Fluoride and organic weak acids as modulators of microbial physiology. *FEMS Microbiology Review*, 26;5:493-510.
- ¹³⁵ K. Nakajo, S. Imazato, Y. Takahashi, W. Kiba, S. Ebisu, N. Takahashi. 2009. Fluoride released from glass-ionomer cement is responsible to inhibit the acid production of caries-related oral streptococci. *Dental Materials* 25;6:703-708.
- ¹³⁶ O. Fejerskov, E. Kidd. 2008. *Dental Caries. The disease and its Clinical Management*, 2nd Edition. Blackwell Munksgaard, Oxford. pp8.
- ¹³⁷ R. K. Rose, S. J. Turner. 1998. Fluoride-induced enhancement of diffusion in streptococcal model plaque biofilms. *Caries Research*, 32;3:227-232.
- ¹³⁸ K. M. Lehmann, E. Hellwig, H. J. Wenz. 2011. *Zahnaerztliche Propaedeutik. Einfuehrung in die Zahnheilkunde*. 12. Auflage. Deutsche Zanaerzte Verlag, Koeln. pp15.
- ¹³⁹ M. Herrera, A. Castillo, M. Bravo, J. Liébana, P. Carrión. 2000. Antibacterial activity of resin adhesives, glass ionomer and resin-modified glass ionomer cements and a compomer in contact with dentin caries samples. *Operative Dentistry*, 25;4:265-269.
- ¹⁴⁰ G. Koch, S. Hatibović-Kofman. 1990. Glass ionomer cements as a fluoride release system in vivo. *Swedish Dental Journal*, 14;6:267-273.
- ¹⁴¹ M. Svanberg, I.A. Mjör, D. Ørstavik. 1990. Mutans Streptococci in Plaque from Margins of Amalgam, Composite, and Glass-ionomer Restorations. *Journal of Dental Research*, 69;3:861-864.
- ¹⁴² S. Spets-Happonen, L. Seppa, A. Korhonen, P. Alakujala. 1998. Accumulation of strontium and fluoride in approximal dental plaque and changes in plaque microflora after rinsing with chlorhexidine-fluoride-strontium solution. *Oral Diseases*, 4;2:114-119.
- ¹⁴³ A. D. Wilson, J. W. McLean. 1988. *Glass ionomer cements*. Quintessence Publishing Co., Chicago.

-
- ¹⁴⁴ J. M. Ten Cate, M. J. Buijs, J. J. M. Damen. 1995. The effects of GIC restorations on enamel and dentin demineralization and remineralization. *Advances in Dental Research*, 9;4:384-388.
- ¹⁴⁵ G. Rolla, E. Saxegaard. 1990. Critical evaluation of the composition and use of topical fluorides with emphasis on the role of calcium fluoride in caries inhibition. *Journal of Dental Research*, 69:780-785.
- ¹⁴⁶ British Standards Institution. 1981. British Standards Specification for Dental Glass Ionomer Cement BS 6039:4.
- ¹⁴⁷ S. B. Mitra, B. L. Kedrowski. 1994. Long-term mechanical properties of glass ionomers. *Dental Materials*, 10:78-82.
- ¹⁴⁸ E. Bresciani, T. E. Barata, T. C. Fagundes, A. Adachi, M. M. Terrin, M. F. Navarro. 2004. Compressive and diametral tensile strength of glass ionomer cements. *Journal of Applied Oral Science*, 12;4:344-348.
- ¹⁴⁹ M. A. Cattani-Lorente, C. Godin, J. M. Meyer. 1994. Mechanical behavior of glass ionomer cements affected by long-term storage in water. *Dental Materials*, 10:37-44.
- ¹⁵⁰ G. J. Pearson, A. S. Atkinson. 1991. Long-term flexural strength of glass-ionomer cements. *Biomaterials*, 12:658-660.
- ¹⁵¹ K. C. Ludema. 1996. *Friction, Lubrication, Wear, Lubrication Technology. A Textbook in Tribology*. C. R. C. Press, Florida. pp13.
- ¹⁵² M. R. Towler, A. J. Bushby, R. W. Billington. 1999. Nano-Indentation of the Glass Ionomer / Enamel Interface in a Tooth. 15th European Conference on Biomaterials: Conference Proceedings; Arcachon, France.
- ¹⁵³ J. ,R. Triana, N. Minguenza, I. Soler, G. Ibaseta, J. Maza, F. García-Godoy. 2003. Effect of one-year water storage on the surface microhardness of resin-modified versus conventional glass-ionomer cements. *Dental Materials*, 19;4:286-290.
- ¹⁵⁴ X. Xu, J. O. Burgess. 2003. Compressive strength, fluoride release and recharge of fluoride-releasing materials. *Biomaterials*, 24:2451-2461.

-
- ¹⁵⁵ J. Ellakuria, R. Triana, N. Mingueza, I. Soler, G. Ibaseta, J. Maza, F. Garcia-Godoy. 2003. Effect of one-year water storage on the surface microhardness of resin-modified versus conventional glass-ionomer cements. *Dental Materials*, 19;4:286-290.
- ¹⁵⁶ A. J. de Gee, R. N. B. van Duinen, A. Werner, C. L. Davidson. 1996. Early and Long-term Wear of Conventional and Resin-modified Glass Ionomers. *Journal of Dental Research*, 75;8:1613-1619.
- ¹⁵⁷ S. Matsuya, T. Maeda, M. Ohta. 1996. IR and NMR analyses of hardening and maturation of glass-ionomer cement. *Journal of Dental Research*, 75:1920-1927.
- ¹⁵⁸ S. Tang, D. Xu. 2009. Short-term Mechanical Properties of Glass Ionomer Cements. *Journal of Wuhan University of Technology-Material Science*, 24;3:494-496.
- ¹⁵⁹ G. J. P. Fleming, A. A. Farooq, L. E. Barralet. 2003. Influence of powder/liquid mixing ratio on the performance of a restorative glass-ionomer dental cement. *Biomaterials*, 24:4173-4179.
- ¹⁶⁰ M. R. Towler, A. J. Bushby, R. W. Billington, R. G. Hill. 2001. A preliminary comparison of the mechanical properties of chemically cured and ultrasonically cured glass ionomer cements, using nano-indentation techniques. *Biomaterials*, 22:1401-1406.
- ¹⁶¹ C. C. Bonifacio, C. J. Kleverlaan, D. P. Raggio, A. Werner, R. C. R. de Carvalho, W. E. van Amerongen. 2009. Physical-mechanical properties of glass ionomer cements indicated for atraumatic restorative treatment. *Australian Dental Journal*, 54:233-237.
- ¹⁶² C. J. Kleverlaan, R. N. B. van Duinen, A. J. Feilzer. 2004. Mechanical properties of glass ionomer cements affected by curing methods. *Dental Materials*, 20:45-50.
- ¹⁶³ F. Wang. 2009. Cation substitution in ionomer glasses: Effect on glass structure and crystallization. A thesis submitted to the School of Metallurgy and Materials of University of Birmingham.
- ¹⁶⁴ W. Lei, K. Fujiwara, K. Fuwa. 1986. Application of Total Reflection Long Capillary Cell to determination of Fluoride in Drinking water. *Analytical Science*, 2:213-217.
- ¹⁶⁵ ASTM C1327-08 Standard test method for Vickers indentation hardness of advanced ceramics. ASTM international 2008.

-
- ¹⁶⁶ J. Bowen. 2012. *Indentations; Measurement Techniques*. University of Birmingham.
- ¹⁶⁷ W. C. Oliver, G. M. Pharr. 1992. An improved technique for determining hardness and elastic modulus using load and displacement sensing indentation experiments. *Journal of Material Research*, 7;6:1564-1583.
- ¹⁶⁸ A. C. Fischer-Cripps. 2004. *Nanoindentation 2nd Edition*. Springer, New York. p6.
- ¹⁶⁹ ASTM G133 Standard test method for linearly reciprocating ball-on-flat sliding wear. ASTM international 2002.
- ¹⁷⁰ American Dental Association. 1989. Council on Dental Materials and Devices. American National Standard. Specification n. 66 for dental glass ionomer cements. *Journal of the American Dental Association*, 119;1:205.
- ¹⁷¹ L. Stoch, M. Środa. 1999. Infrared spectroscopy in the investigation of oxide glasses structure. *Journal of Molecular Structure*, 512:77-84.
- ¹⁷² C. Huang, E. C. Behrman. 1991. Structure and properties of calcium aluminosilicate glasses. *Journal of Non-Crystalline Solids*, 128;3:310-321.
- ¹⁷³ L. G. Hwa, S. L. Hwanga, L. C. Liub. 1998. Infrared and Raman spectra of calcium alumino-silicate glasses. *Journal of Non-Crystalline Solids*, 238;3:193-197.
- ¹⁷⁴ A. Stamboulis, R. G. Hill, R. V. Law. 2005. Structural characterization of fluorine containing glasses by F-19 Al-27 Si-29 and P-31 MAS-NMR spectroscopy. *Journal of Non-Crystalline Solids*, 351:3289-3295.
- ¹⁷⁵ N. J. Clayden, S. Esposito, A. Aronne P. Pernice. 1999. Solid state Al-27 NMR and FTIR study of lanthanum aluminosilicate glasses. *Journal of Non-Crystalline Solids*, 258:11-19.
- ¹⁷⁶ S. A. MacDonald, C. R. Schardt, D. J. Masiello, J. H. Simmons. 2000. Dispersion analysis of FTIR reflection measurements in silicate glasses. *Journal of Non-Crystalline Solids*, 275:72-82.
- ¹⁷⁷ J. Serra, G. Gonzalez, S. Liste, C. Serra. S. Chiussi, B. Leon, M. Perez-Amor, H. O. Ylanen, M. Hupa. 2003. FTIR and XPS studies of bioactive silica based glasses. *Journal of Non-Crystalline Solids*, 332:20-27.

-
- ¹⁷⁸ V. C. Farmer, A. R. Fraser, J. M. Tait. 1979. Characterization of the chemical structures of natural and synthetic aluminosilicate gels and sols by infrared spectroscopy. *Geoch et Cosmoch Acta*, 43:1417-1420.
- ¹⁷⁹ D. Gao, R. B. Heimann. 1993. Structure and mechanical properties of superabsorbent poly(acrylamide)-montmorillonite composite hydrogels. *Polymer Gels and Networks*, 1:225-246.
- ¹⁸⁰ J. Billingham, C. Breen, J. Yarwood. 1997. Adsorption of polyamine, polyacrylic acid and polyethylene glycol on montmorillonite: An in situ study using ATR-FTIR. *Vibrational Spectroscopy*, 14:19-34.
- ¹⁸¹ A. M. Efimov. 1996. Quantitative IR spectroscopy: applications to studying glass structure and properties. *Journal of Non-Crystalline Solids*, 203:1-11.
- ¹⁸² J. M. Miller, L. J. Lakshmi. 1998. Spectroscopic characterization of sol-gel-derived mixed oxides. *The Journal of Physical Chemistry, B*;102:6465-6470.
- ¹⁸³ S. Matsuya, Y. Matsuya, Y. Yamamoto, M. Yamane. 1984. Erosion process of a glass-ionomer cement in organic acids. *Dental Materials Journal*, 3:210-219.
- ¹⁸⁴ K. M. Davis, M. Tomozawa. 1996. An infrared spectroscopic study of water-related species in silica glasses. *Journal of Non-Crystalline Solids*, 201:177-198.
- ¹⁸⁵ E. A. P. De Maeyer, R. M. H. Verbeeck, C. W. J. Vercruyse. 2002. Infrared Spectrometric Study of Acid-degradable Glasses. *Journal of Dental Research*, 81;8:552-555.
- ¹⁸⁶ N. Zainuddin, N. Karpukhina, R. G. Hill. 2009. A long-term study on the setting reaction of glass ionomer cements by ²⁷Al MAS-NMR spectroscopy. *Dental Materials*, 25:290-295.
- ¹⁸⁷ A. C. A. Wan, A. U. J. Yap, G. W. Hastings. 1999. Acid-Base Complex Reactions in Resin-Modified and Conventional Glass Ionomer Cements. *Journal of Biomedical Materials Research*, 48;5:700-704.
- ¹⁸⁸ A. M. Young, S. A. Rafeeka, J. A. Howlett. 2004. FTIR investigation of monomer polymerization and polyacid neutralization kinetics and mechanisms in various aesthetic dental restorative materials. *Biomaterials*, 25:823-833.

-
- ¹⁸⁹ J. Yu, R. Xu. 2006. Insight into the construction of open-framework aluminophosphates. *The Royal Society of Chemistry*, 35:593–604.
- ¹⁹⁰ J. E. Frencken, Y. Songpaisen, P. Phantumvanit, T. Pilot. 1994. An atraumatic restorative treatment (ART) technique; evaluation after one year. *International Journal of Dentistry*, 44:460-464.
- ¹⁹¹ P.C. Hardley, E. Milella, C. Cerardi, R. G. Hill, R. W. Bilington. 2001. Distribution of fluoride in glass-ionomer cement determined using SIMS. *Biomaterials*, 22:1563-1569.
- ¹⁹² A. D. Wilson, D. M. Groffman, A T. Kuhn. 1985. The release of fluoride and their chemical species from a glass ionomer cement. *Biomaterials*, 6:431-433.
- ¹⁹³ S. M. Mousavinasab, I. Meyers. 2009. Fluoride Release and Uptake by Glass Ionomer Cements, Compomers and Giomers. *Research Journal of Biological Sciences*, 4;5:609-616.
- ¹⁹⁴ A. T. Kuhn, A. D. Wilson. 1985. The dissolution mechanisms of silicate and glass ionomer dental cements. *Biomaterials*, 6:378-382.
- ¹⁹⁵ T. Itota, T. E. Carrick, S. Rusby, O. T. Al-Naimi, M. Yoshiyama, J. F. McCabe. 2004. Determination of fluoride ions released from resin-based dental materials using ion-selective electrode and ion chromatograph. *Journal of Dentistry*, 32;2:117-122.
- ¹⁹⁶ M. R. Hadi, S. S. Rahmatallah, S. S. Al-Ameer. 2010. Fluoride release from newly formulated resin-modified and conventional glass ionomer cements. *Journal of College of Dentistry of University of Baghdad*, 22;4:32-35.
- ¹⁹⁷ N. Shetty, J. W. Tang, J. Andrews. 2009. *Infectious Disease: Pathogenesis, Prevention and Case Studies*. Wiley-Blackwell, Oxford pp 66.
- ¹⁹⁸ K. Yoshida, M. Tanagawa, S. Matsumoto, T. Yamada, M. Atsuta. 1999. Antibacterial activity of resin composites with silver-containing materials. *European Journal of Oral Sciences*, 107;4:290-296.
- ¹⁹⁹ T. Itota, T. E. Carrick, M. Yoshiyama, J. F. McCabe. 2004. Fluoride release and recharge in giomer, compomer and resin composite. *Dental Materials*, 20;9:789-795.

-
- ²⁰⁰ A. Guida, M. R. Towler, J. G. Wall, R. G. Hill, S. Eramo. 2003. Preliminary work on the antibacterial effect of strontium in glass ionomer cements. *Journal of Material Science*, 22:1401-1403.
- ²⁰¹ T. T. Thuy, H. Nakagaki, K. Kato, P. A. Hung, J. Inukai, S. Tsuboi, H. Nakagaki, M. N. Hirose, S. Igarashi, C. Robinson. 2008. Effect of strontium in combination with fluoride on enamel remineralization in vitro. *Archives of Oral Biology*, 53;11:1017-1022.
- ²⁰² F. Dabsie, G. Gregoire, M. Sixou, P. Sharrock. 2009. Does strontium play a role in the cariostatic activity of glass ionomers? Strontium diffusion and antibacterial activity. *Journal of Dentistry*, 37:554-559.
- ²⁰³ W. D. Cook. 1984. Rheological studies of the setting of water-based cements. *Australian Dental Journal*, 29;1:44-49.
- ²⁰⁴ D. C. Watts, E. C. Combe, E. H. Greener. 1981. The rheological properties of polyelectrolyte cements. II Glass Ionomers. *Journal of Rehabilitation*, 8:61-67.
- ²⁰⁵ L. Lorton, B. K. Moore, L. Swartz Marjorie, R. W. Phillips. 1980. Rheology of luting cements. *Journal of Dental Research*, 59:1486-1492.
- ²⁰⁶ J. F. McCabe, A. W. G. Walls. 2008. *Applied Dental Materials 9th Edition*. Wiley Blackwell, Oxford. pp19.
- ²⁰⁷ M. Roberts, M. Reiss, G. Monger. 2000. *Advanced Biology*. Nelson, London. pp104.
- ²⁰⁸ H. Chandler. 1999. *Hardness Testing, 2nd Edition*. ASM International. pp51.
- ²⁰⁹ E. Rabinowicz. 1965. *Friction and wear of materials. 2nd Edition*. John Wiley & Sons, Inc.. p167-198.
- ²¹⁰ G. Willems, P. Lambrechts, M. Braem, J. P. Celis, G. Vanherle. 1992. A classification on dental composites according to their morphological and mechanical characteristics. *Dental Materials*, 8:310-319.
- ²¹¹ A. U. J. Yap, X. Wang, X. Wu, S. M. Chung. 2004. Comparative hardness and modulus of tooth-colored restoratives: A depth-sensing microindentation study. *Biomaterials*, 25:2179-2185.

-
- ²¹² S. Crisp, A. D. Wilson. 1974. Reaction in glass-ionomer cements: III. The precipitation reaction. *Journal of Dental Research*, 53:1420-1424.
- ²¹³ J. F. McCabe. 1998. Resin-modified glass-ionomers. *Biomaterials*, 19:521-527.
- ²¹⁴ A. D. Wilson. 1990. Resin-modified glass ionomer cements. *The International Journal of Prosthodontics*, 3:425-429.
- ²¹⁵ J. W. McLean. 1992. Clinical applications of glass ionomer cements. *Journal of Operative Dentistry*, 5:184-190.
- ²¹⁶ G. Eliades, G. Palaghias. 1993. In vitro characterization of visible light-cured glass liners. *Journal of Dental Materials*, 9:198-203.
- ²¹⁷ G. Willems, J. P. Celis, P. Lambrechts, M. Braem, G. Vanherle, 1993. Hardness and Young's modulus determined by nanoindentation technique of filler particles of dental restorative materials compared with human enamel. *Journal of Biomedical Materials Research*, 27:747-755.
- ²¹⁸ J. Alcala, A. E. Giannakopoulos, S. Suresh. 1998. Continuous measure affect the modulus of materials, the hardness of thements of load-penetration curves with spherical micro-indenters and the estimation of mechanical properties. *Journal of Materials Research*, 13:1390-1400.
- ²¹⁹ F. Lippert, D. M. Parker, K. D. Jandt. 2004. In vitro demineralization/remineralization cycles at human tooth enamel surfaces investigated by AFM and nanoindentation. *Journal of Colloid and Interface Science*, 280;2:442-448.
- ²²⁰ A. U. J. Yap, S. Mudambi, C. L. Chew, C. L. Neo. 2001. Mechanical properties of an improved visible light-cured resin-modified glass ionomer cement. *Operative Dentistry*, 26:295-301.
- ²²¹ X. Xu, J. O. Burgess. 2003. Compressive strength, fluoride release and recharge of fluoride-releasing materials. *Biomaterials*, 24:2451-2461.
- ²²² M. S. Al-Haik, S. Trinkle, D. Garcia, F. Yang. 2009. Investigation of the nanomechanical and tribological properties of dental materials. *International Journal of Theoretical and Applied Multiscale Mechanics*, 1;1:1-15.

-
- ²²³ J. McKinney, W. Wu. 1982. Relationship between subsurface damage and wear of dental composites. *Journal of Dental Research*, 61:1083-1088.
- ²²⁴ L. Forsten, S. Karjalainen. 1990. Glass ionomers in proximal cavities of primary molars. *Scandinavian Journal of Dental Research*, 98:70-73.
- ²²⁵ J. Powers, L. Allen, R. G. Craig. 1974. Two-body abrasion of commercial and experimental restorative and coating resins and an amalgam. *The Journal of the American Dental Association*, 89:1118-1122.
- ²²⁶ U. Soltész, M. Leupolz. 1993. Abriebverhalten von Glasionomerzementen. *Deutsche Zahnärztliche Zeitung*, 48:379-382.
- ²²⁷ R. DeLong. 2006. Intra-oral restorative materials wear: Rethinking the current approaches: How to measure wear. *Dental Materials*, 22:702-711.
- ²²⁸ K. F. Leinfelder, D. R. Taylor, W. W. Barkmeier, A. J. Goldberg. 1986. Quantitative wear measurements of posterior composite resins. *Dental Materials*, 2:198-201.
- ²²⁹ L. Wang, P. H. P. D'alpino, L. G. Lopes, J. C. Pereira. 2003. Mechanical properties of dental restorative materials: relative contribution of laboratory tests. *Journal of Applied Oral Science*, 11;3:162-167.
- ²³⁰ A. Mitsuhashi, K. Hanaoka, T. Teranaka. 2003. Fracture toughness of resin-modified glass ionomer restorative materials: effect of powder/liquid ratio and powder particle size reduction on fracture toughness. *Dental Materials*, 19:747-757.
- ²³¹ S. Crisp, B. G. Lewis, A. D. Wilson. 1975. Glass ionomer cements: Chemistry of erosion. *Journal of Dental Research*, 55:1932-1041.
- ²³² R. D. Shannon. 1976. Revised effective ionic radii and systematic studies of interatomic distances in halides and chalcogenides. *Acta Crystallographica Section A*, 32:751-767.